The Development and Characterisation of Peptides to Image αvβ6 in Cancer

Antonio Saha

A thesis submitted for the degree of
Doctor of Philosophy
University of London

January 2011

Tumour Biology Laboratory
The Barts Cancer Institute,
Queen Mary,
University of London.

Statement of Originality

The work described in this thesis was carried out in the Cancer Research UK Tumour Biology Laboratory, Queen Mary, University of London. Unless stated otherwise, the author performed the experiments described.

I hereby declare that the thesis entitled 'The Development and Characterisation of Peptides to Image αvβ6 in Cancer' has not been submitted for a degree or any other qualification at any other university.

Acknowledgements

This project took four years to complete and inevitably involved the help and collaboration of many groups and individuals. Unfortunately, I cannot name all of those who have helped in the space provided. I have tried to thank everyone, in person, at the time of their assistance. The following text, however, tries to name a small number of people whose assistance proved invaluable during my training and therefore I would especially like to thank them for their involvement:-

I am deeply grateful to my colleagues in the Departments of Tumour Biology and Cancer Imaging, Queen Mary, who have contributed to my education and enjoyment during this project.

I recognise that I have not been the easiest student to supervise and thus I am especially indebted to my supervisors, Professor Ian Hart and Dr. John Marshall, whose experience, knowledge and patience were all appreciated. This project was based on the work of a previous member of the laboratory, Dr. Dani Di Cara, and her initial help proved invaluable. Indeed without the foundations of Dani's work, this project could not have started. Additionally, Sabrinath Vallath provided support, friendship and expertise for this project and is now progressing some of the research in this field. Furthermore, I would like to acknowledge Nicola O'Reilly, and her team at the Cancer Research UK Peptide Synthesis Laboratory, for providing high quality peptides and for their technical advice during this project.

This project took place jointly in Professor Mather's Imaging laboratory. Thus, I am also deeply grateful to Professor Stephen Mather, David Ellison, Dr. Jane Sosabowski, Dr. Torkjel Matzow, Dr. Julie Foster and Ciara Finucane for their help, friendship and advice on experimental design and analysis.

Many of the experiments could not have succeeded without the assistance of the Biological Service Units, at Queen Mary (University Of London) and Clare Hall (Cancer Research UK). Therefore, I would like to thank Arif Mustafa, Sandra Peak and their teams for their cooperation throughout this project.

I am grateful to Cancer Research UK for funding this project.

I would, of course, like to acknowledge my parents for their continuing encouragement and resources throughout this degree and my whole career.

Finally, I would like to acknowledge Elaine Margaret Stewart, who has supported me through the highs and lows of my training. These words do not give suitable justice to the level of assistance she has given, but I am truly grateful for all her help, encouragement and kindness.

List of Abbreviations

αvβ6	Integrin alpha v beta 6
ADMIDAS	Adjacent to MIDAS
ANOVA	Analysis Of Variance Between Groups
ARSAC	Administration of Radioactive Substance Advisory Committee
BFCA	Bifunctional Chelating Agent
BSA	Bovine Serum Albumin
Bq	Becquerel
BrdU	5'-bromo-2'-deoxyuridine
CA	California
cDNA	Complementary DNA
CDR	Complementarity-determining Region
CR-UK	Cancer Research UK
CT	Computed Tomography
Da	Dalton
D.C.	District of Columbia
DCIS	Ductal carcinoma in situ
DMEM	Dulbecco's Modification of Eagle's Medium
DMSO	Dimethyl sulfoxide
DTPA	Diethylenetriaminepentaacetic acid
DOTA	1,4,7,10-tetraazacyclododecane-1,4,7,10-tetraacetic acid
DNA	Deoxyribonucleic Acid

E4	Enrichment 4
ECG	Electrocardiogram
ECM	Extracellular Matrix
ECOG	Eastern Cooperative Oncology Group
EDTA	Ethylenediaminetetraacetate
EGF	Epidermal Growth Factor
ELISA	Enzyme-linked Immunosorbent Assay
EMT	Epithelial-Mesenchymal Transition
eV	Electron Volt
F	Fluorine
FACS	Fluorescently Activated Cell Sorting
FAK	Focal Adhesion Kinase
FBA	Fluorobenzoic Acid
FBC	Full Blood Count
FCS	Foetal Calf Serum
FDA	Food and Drug Administration
FDG	Fludeoxyglucose
FMDV	Foot-and-Mouth Disease Virus
Ga	Gallium
GCP	Good Clinical Practice
GI tract	Gastrointestinal tract
GTP	Guanosine-5'-triphosphate
HAHA	Human Anti-human Antibodies

HAMA	Human Anti-mouse Antibody
HBTU	2-(1H-benzotriazol-lyl)-1, 1, 3, 3-tetramethylironium hexafluorophosphate
HCl	Hydrochloric Acid
HEPES	4-(2-hydroxyethyl)-1-piperazineethanesulfonic acid
HGF	Hepatocyte Growth Factor
HNSCC	Head And Neck Squamous Cell Carcinoma
HYNIC	Hydrazino nicotinamide
% I.D./g	Percentage Injected Dose per Gram
Ig	Immunoglobulin
In	Indium
i.v.	Intravenous
Kd	Dissociation constant
KGM	Keratinocyte Growth Medium
Ki	Binding Affinity
LAP	Latency Associated Peptide
LIBS	Ligand-induced Binding Site
LIMBS	Ligand-induced Metal-binding Site
LLC	Large Latent Complex
LTBP	Latent TGF-β Binding Protein
µg	Microgram
µL	Microlitre
M	Molar

MA	Massachusetts
mAbs	Monoclonal Antibodies
MAPK	Mitogen-activated Protein Kinase
MCF	Michigan Cancer Foundation
MDA	MD Anderson
MEM	Minimum Essential Medium
MET	Mesenchyme-to-Epithelium Transition
MHRA	Medicines and Healthcare products Regulatory Agency
MIDAS	Metal Ion-dependent Adhesion Site
Min	Multiple Intestinal Neoplasia
MIP	Maximal Intensity Projection
MMP	Matrix Metalloproteinase
MO	Missouri
M.O.M.	Mouse-on-Mouse
MRI	Magnetic Resonance Imaging
MRT	Mean Residence Time
mRNA	Messenger Ribonucleic Acid
MT1	Membrane Type 1
NIH	National Institutes of Health
NFκβ	Nuclear Factor Kappa-light-chain-enhancer of activated B cells
NMR	Nuclear Magnetic Resonance
NS	Non-specific
nu/nu	Nude

NY	New York
PEG	Polyethylene Glycol
PET	Positron Emission Tomography
p.i.	Post-injection
PBS	Phosphate Buffered Saline
PI 3 Kinase	Phosphatidylinositol 3-kinase
Puro	Puromycin
PK	Protein Kinase
RGD	Arginine-Glycine-Aspartate
RNA	Ribonucleic acid
RP-HPLC	Reverse Phase High-performance Liquid Chromatography
RTK	Receptor Tyrosine Kinases
RT-PCR	Reverse transcription Polymerase Chain Reaction
SB	Specific-binding
scFv	Single Chain Variable Fragment
SLC	Small Latent Complex
SPECT	Single Photon Computed Tomography
SPPS	Solid-Phase Peptide Synthesis
SRE	Serum Response Element
SUV	Standardised Uptake Value
TB	Total Binding
TBS	Tris Buffered Saline
Tc	Technetium

TETA	Triethylenetetramine
TFA	Trifluoroacetic acid
TGF-β	Transforming Growth Factor-β
TIMP	Tissue Inhibitor of Metalloproteinase
TLC	Thin-Layer Chromatography
TNF-α	Tumour Necrosis Factor-α
TRIS	Tris(hydroxymethyl)aminomethane
TSS	Transcription Start Site
TSTU	O-(N-succinimidyl)-N,N,N',N'-tetramethyluronium tetrafluoroborate
UCSF	University of California, San Francisco
UHP	Ultra High Purity
UK	United Kingdom
USA	United States of America
UV/Vis	Ultraviolet–visible
uPA	Urokinase Plasminogen Activator
uPAR	Urokinase Plasminogen Activator Receptor
% v/v	Percentage solution: volume/volume
% w/v	Percentage solution: mass/volume
VEGF	Vascular endothelial growth factor

Abstract

Introduction The epithelial-specific integrin αvβ6 usually is undetectable on normal, adult, human tissue but is upregulated during tissue re-modelling and carcinogenesis.

Objective To develop and characterise agents for targeting αvβ6 in cancer.

Methods A series of peptides was generated from known high-affinity αvβ6 ligands. These peptides were then assessed for their ability to inhibit αvβ6-dependent cell adhesion. The lead 20 mer peptide, A20FMDV2, was identified. Flow cytometry, with two genetically identical cell lines that differed only in their expression of αvβ6 – A375P puro(negative) and A375Pβ6(positive)-, confirmed specificity for binding of A20FMDV2 to αvβ6. The A20FMDV2 sequence was synthesised with both a biotin and DTPA-chelator group added. This was radiolabelled with Indium-111 and purity and structural integrity analysed by HPLC.

Prior to *in vivo* experiments the endogenous expression of αvβ6 in nu/nu athymic mice was determined by examining 20 different organs (in triplicate) by immunohistochemistry. For *in vivo* experiments, athymic mice were inoculated subcutaneously with A375Pβ6 (right shoulder) and A375P puro (left shoulder**).** A radiolabelled variant of A20FMDV2 (^{111}In-DTPA-A20FMDV2) was injected into xenografted mice. Some mice were imaged on a NanoSPECT/CT imager and biodistribution confirmed by determining the radioactivity associated with excised organs.

Results Immunohistochemistry of mouse tissues revealed, as expected, strong expression of αvβ6 in the A375Pβ6 tumour but none in the A375Ppuro tumour. In addition, expression of αvβ6 was found in normal murine hair follicles, gallbladder, urinary bladder, secretory endometrium, the stomach and along the GI tract.

Flow cytometry with A375Ppuro and A375Pβ6 cells confirmed that DTPA-chelate addition to A20FMDV2 did not affect its specificity or affinity for αvβ6. HPLC confirmed that DTPA-biotinylated-A20FMDV2 was labelled successfully with Indium-111 resulting in a single radiolabelled peak. *Ex-vivo* gamma counts revealed seven-fold higher uptake of the radiolabelled-peptide in the A375Pβ6 tumour compared with the A375Ppuro tumour. Biodistribution data were consistent with the endogenous αvβ6 expression as determined by immunohistochemistry. NanoSPECT/CT imaging clearly identified that the A375Pβ6 tumour retained more radioactive peptide than the A375Ppuro tumour at 30, 60 and 120 minutes after injection. Images also showed uptake in the GI tract.

Conclusion We have determined that the peptide DTPA-A20FMDV2 is specific for αvβ6, can be labelled with Indium-111 and selectively localises *in vivo* to αvβ6-positive tissues, including human cancer. This is the first peptide described for the successful imaging, by SPECT, of αvβ6-positive cancers.

Table of Contents

STATEMENT OF ORIGINALITY **2**

ACKNOWLEDGEMENTS **3**

LIST OF ABBREVIATIONS **5**

ABSTRACT **11**

CHAPTER I: INTRODUCTION TO CANCER **26**

1.1 CANCER 26

1.2 INTEGRINS 32

1.2.1 Integrin Structure 33

1.2.2 Integrin Function 37

1.2.2.1 Outside-In Signalling 40

1.2.2.2 Inside-Out Signalling 43

1.2.2.3 Cation-Dependent Integrin Regulation 47

1.3 INTEGRINS AND CANCER 48

1.3.1 Proliferation 49

1.3.2 Invasion 51

1.3.3 Migration 56

1.3.4 Dissemination 59

1.3.5 Survival mechanisms during Invasion and Metastasis 62

1.4 αvβ6 64

1.4.1 Transcriptional Regulation of αvβ6 64

1.4.2 αvβ6 Ligands 67

1.4.2.1 Transforming Growth Factor- β (TGF-β) 67

1.4.2.2 Foot-And-Mouth Disease Virus (FMDV) 72

1.4.2.3 Fibronectin 72

1.4.2.4 Vitronectin 73

1.4.2.5 Tenascin-C 73

1.5 αvβ6 AND CANCER 74

1.5.1 Proliferation 76

1.5.2 Invasion *76*

1.5.3 Migration *78*

1.5.4 Dissemination *79*

1.5.5 Survival mechanisms during Invasion and Metastasis *81*

CHAPTER II: INTRODUCTION TO IMAGING 83

2.1 MEDICAL IMAGING 83

2.1.1 Radiography: X-rays and Computed Tomography 83

2.1.2 Ultrasonography 87

2.1.3 Magnetic Resonance Imaging (MRI) 88

2.1.4 Nuclear Medicine 90

2.1.4.1 Scintigraphy and Single Photon Computed Tomography (SPECT) 91

2.1.4.2 Positron Emission Tomography (PET) 93

2.2 MOLECULAR IMAGING 96

2.2.1 Probe Design 98

2.2.1.1 ^{18}F-FDG substrate 101

2.2.1.2 Antibody vs. Peptide 103

2.2.2 Radiolabelling Techniques 107

2.2.2.1 Pre-labelling vs. Post-labelling 112

2.2.3 Bifunctional chelating agents (BFCAs) 113

2.2.4 Combined Functional and Anatomical Imaging 117

2.3 αvβ6 AS A BIOLOGICAL MARKER 123

2.4 OVERVIEW OF PROJECT 127

2.5 PROJECT OBJECTIVES 128

CHAPTER III: MATERIALS AND METHODS 129

3.1 SALINE AND MEDIA FORMULATIONS 129

3.2 ANTIBODIES 129

3.3 RADIOISOTOPES 130

3.4 HPLC SOLVENTS 130

3.5 CELL LINES 130

3.5.1 Melanoma cell line as a model for β6 targeting 131

3.5.2 Breast Cell Lines 132

3.5.3 Mouse Keratinocyte cell line 136

3.5.4 Maintenance of cell lines 137

3.5.5 Long-term Storage of Cell Lines in Liquid Nitrogen 138

3.6 PEPTIDES 139

3.7 FLOW CYTOMETRY EXPERIMENTS 141

3.7.1 Analysis Of Integrin Expression Using Flow Cytometry 141

3.7.2 Confirmation of Biotinylated Peptide binding to Cells by Flow Cytometric Analysis 142

3.7.3 Anti- αvβ6 Competition Assay to Confirm Binding Specificity of Peptide 143

3.8 TRANSWELL® INVASION ASSAYS 144

3.9 RADIOLABELLED PEPTIDE STUDIES 145

3.9.1 Peptide Radiolabelling 145

3.9.2 Radioligand binding studies: Saturation Assays 146

3.9.3 Radioligand binding studies: Cell Internalisation Assay 147

3.9.3.1 Optimisation of Cell Internalisation Assay 149

3.9.3.2 Cell Viability Check 150

3.9.3.3 Correlation of Cell Protein with Cell Number 150

3.10 IN VIVO STUDIES 151

3.10.1 Plasma Stability Studies 152

3.10.2 Biodistribution 152

3.10.2.1 Peptide Mass Studies 153

3.10.2.2 Co-injection Studies in vivo 154

3.10.2.3 NanoSPECT /CT 154

3.11 IMMUNOHISTOCHEMICAL STAINING AND EVALUATION 155

CHAPTER IV **157**

RESULTS: CHARACTERISATION AND OPTIMISATION OF αVβ6 TARGETING AGENTS **157**

4.1 MELANOMA CELL MODEL FOR TARGETING αvβ6 157

4.2 ASSESSMENT OF PEPTIDE SENSITIVITY AND SPECIFICITY BY FLOW CYTOMETRY 158

4.3 PEPTIDE DERIVATISATION AND EFFECTS ON AFFINITY AND SPECIFICITY 160

4.4 COMPETITION WITH αvβ6-FUNCTION BLOCKING ANTIBODY IN THE A375P B6 CELL LINE 163

4.5 COMPETITION WITH αvβ6-FUNCTION BLOCKING ANTIBODY IN MOUSE KERATINOCYTES 164

4.6 IMMUNOHISTOCHEMICAL STAINING AND EVALUATION OF MURINE TISSUES. 166

4.6.1 Skin 166

4.6.2 Uterus 167

4.6.3 Gallbladder 168

4.6.4 Urinary Bladder 168

4.6.5 Stomach 169

4.6.6 Duodenum 169

4.6.7 Ileum 170

4.6.8 Colon 171

4.6.9 Xenografts 172

4.7 PEPTIDE RADIOLABELLING AND QUALITY CONTROL 175

4.8 RADIOLOIGAND BINDING STUDIES 177

4.8.1 Saturation Binding Assays 177

4.8.2 Internalisation Assays 178

4.8.2.1 Optimisation of Cell Internalisation Assay 179

4.8.2.2 Internalisation Assay with ^{111}In-DTPA-A20FMDV2 on A375P β6 cells, using E4/HCl (pH 4) 180

4.9 IN VIVO STUDIES 183

4.9.1 Plasma Stability Studies 183

4.9.2 Biodistribution 185

4.9.2.1 Post-Injection Interval Studies 185

4.9.2.2 Peptide Mass Studies 186

4.9.2.3 Species Generalisation Experiments 186

4.9.2.4 Whole body biodistribution 190

4.9.2.5 Co-injection Studies in vivo 192

4.9.2.6 Non-Biotinylated ^{111}In-DTPA-A20FMDV2 198

4.9.3 NanoSPECT/CT Small Animal Imaging 200

CHAPTER V 203

RESULTS: VALIDATION OF *αVβ6* TARGETING ON OTHER MODELS AND THE STUDY OF OTHER PEPTIDE VARIANTS 203

5.1 BREAST CANCER MODEL FOR TARGETING αVβ6. 203

5.1.1 Integrin Expression Profile on Breast Cell Lines. 203

5.1.2 Invasive Activity of an αvβ6-expressing Breast Cancer Cancer Cell Line 205

5.1.3 Maintenance of αvβ6 expression within Tumour Xenografts 206

5.1.4 Biodistribution Experiments using CD1 mice bearing MCF-10 DCIS.com / Matrigel Xenografts 207

5.1.5 Biodistribution Experiments using CD1 mice bearing either MCF-10 DCIS.com or MCF-10A.CA1a Xenografts (No Matrigel) 209

5.1.6 NanoSPECT/CT Small Animal Imaging of Breast Cancer Models 211

5.2 COLON CANCER MODEL FOR TARGETING αVβ6. 213

5.3PEPTIDE VARIANTS AND PROBE STABILISATION METHODS 217

5.3.1 Cyclisation: A Method of Inhibiting Proteolysis of Peptides 217

5.3.1.1 Assessment of Cyclic Peptides' Sensitivity and Specificity by Flow Cytometry 217

5.3.1.2 DTPA-DBD2 Radiolabelling and Quality Control 219

5.3.1.3 Plasma Stability Studies of ^{111}In-DTPA-DBD2 220

5.3.1.4 Biodistribution of ^{111}In-DTPA-DBD2 222

5.3.2 The DOTA Chelator Variant of A20FMDV2 225

5.3.2.1 DOTA-A20FMDV2 Radiolabelling and Quality Control 225

5.3.2.2 Biodistribution of ^{111}In- DOTA-A20FMDV2 226

5.3.2.3 DOTA-A20FMDV2ran Radiolabelling and Quality Control 229

5.3.2.4 Biodistribution of ^{111}In- DOTA-A20FMDV2ran 230

5.3.2.5 NanoSPECT/CT Small Animal Imaging 232

CHAPTER VI: DISCUSSION 234

6.1 The αvβ6 Receptor and Peptide Pharmacology 235

6.1.1 Limitations of Peptide Pharmacology Experiments 246

6.2 Tumour Xenograft Model in Mice 249

6.2.1 Limitations of the Tumour Xenograft Model in Mice 253

6.3 Immunohistochemical Correlation with Flow Cytometry and Biodistribution 256

6.3.1 Limitations of Immunohistochemistry 260

6.4 Peptide Excretory Experiments 261

6.4.1 Limitations of Peptide Excretory Experiments 264

6.5 In vivo Imaging 266

6.5.1 Limitations of NanoSPECT/CT Experiments 267

6.6 Summary 269

CHAPTER VII: POTENTIAL HUMAN TRIALS **271**

7.1 PROPOSED PHASE I TRIAL SCHEMA: ^{68}GA-DOTA-A20FMDV2 271

7.2 PROPOSED PHASE II / III TRIAL SCHEMA: A20FMDV2 277

7.3 DIAGNOSTIC, THERAPEUTIC AND HEALTH IMPACT 281

7.4 POSSIBLE BARRIERS TO THE TRANSLATION OF A20FMDV2 INTO A SUCCESSFUL CLINICAL IMAGING AGENT 282

7.4.1 Adverse Effects 282

7.4.2 Potential Immunogenicity of A20FMDV2 283

7.4.3 The Gastrointestinal Tract and the αvβ6 Integrin 284

7.4.4 Peptide Therapeutics 287

7.4.5 Cancer Cell Plasticity 288

CHAPTER VIII: REFERENCES **289**

APPENDIX A **311**

LIST OF FIGURES

FIGURE 1 THE TWENTY MOST COMMONLY DIAGNOSED CANCERS IN UK (2004), EXCLUDING NON-MELANOMA SKIN CANCERS. *TAKEN FROM CANCER STATISTICS REGISTRATIONS, GREAT BRITAIN [4]*. 27

FIGURE 2 AGE-STANDARDISED (EUROPEAN) INCIDENCE RATES, ALL CANCERS EXCLUDING NON-MELANOMA SKIN CANCERS, GB, 1975-2004. *TAKEN FROM MORTALITY STATISTICS, GREAT BRITAIN [6]*. 28

FIGURE 3 THE DEVELOPMENT AND EVOLUTION OF A TARGETED PROBE FOR A BIOLOGICAL MARKER OF CANCER 31

FIGURE 4 THE INTEGRIN RECEPTOR FAMILY. *TAKEN FROM HYNES RO [13]*. 32

FIGURE 5 SIMPLIFIED DIAGRAM OF THE INTEGRIN RECEPTOR AND ITS RELATION TO THE CELL MEMBRANE. *TAKEN FROM ALBERTS B ET AL [18]*. 33

FIGURE 6 SCHEMATIC REPRESENTATION OF THE αvβ3 INTEGRIN STRUCTURE. (A) BENT IMAGE OF αvβ3 INTEGRIN. (B) STRAIGHTENED IMAGE OF αvβ3 INTEGRIN. *TAKEN FROM HUMPHRIES MJ ET AL [24]*. 35

FIGURE 7 INTEGRINS AND THE ACTIN CYTOSKELETAL SYSTEM. *TAKEN FROM MIRANTI CK ET AL [30]*.. 39

FIGURE 8 REGULATION OF INTRACELLULAR SIGNALLING BY INTEGRINS. *TAKEN FROM GUO AND GIANCOTTI [16]* 42

FIGURE 9 INSIDE OUT SIGNALLING AND INTEGRIN MODULATION. *TAKEN FROM HUGHES AND PFAFF [41]*. 44

FIGURE 10 PROPOSED QUARTERNARY STRUCTURAL REARRANGEMENTS IN INTEGRIN ACTIVATION. *TAKEN AND ADAPTED FROM TAGAKI ET AL [46]* 46

FIGURE 11 THE MAIN STEPS IN THE FORMATION OF A METASTASIS. *TAKEN FROM FIDLER IJ[53]*. 49

FIGURE 12 INTEGRINS, MATRIX DEGRADATION AND REMODELLING. *TAKEN FROM GUO AND GIANCOTTI [16]* 54

FIGURE 13 CELL MIGRATION, INTEGRINS AND RHO-FAMILY GTPASES. *TAKEN AND ADAPTED FROM RAFTOPOULOU AND HALL [78]*. 58

FIGURE 14 HOMING OF NEOPLASTIC CELLS TO TARGET ORGANS. *TAKEN FROM GUO AND GIANCOTTI* [16]. 60

FIGURE 15 GENOMIC LOCI OF THE αvβ6 SUBUNITS. *TAKEN AND ADAPTED FROM HTTP://WWW.GENECARDS.ORG.* 64

FIGURE 16 SCHEMATIC OF THE HUMAN INTEGRIN β6 PROMOTER. *TAKEN FROM BATES ET AL [101].* 65

FIGURE 17 SCHEMATIC OF THE HUMAN INTEGRIN β6 PROMOTER. *TAKEN FROM AZARE ET AL [105].* 66

FIGURE 18 SCHEMATIC REPRESENTATION OF ORGANISATION OF LATENT COMPLEXES OF TRANSFORMING GROWTH FACTOR-β (TGF- β). *TAKEN AND ADAPTED FROM SHEPPARD D [115].* 69

FIGURE 19 SMAD PROTEIN AND SIGNALLING. *TAKEN FROM HELDIN, MIYAZONO AND TEN DIJKE [109].* 71

FIGURE 20 EPITHELIAL TO MESENCHYMAL TRANSITION AND A PROPOSED MECHANISM FOR CARCINOMA PROGRESSION. *TAKEN FROM THIERY JP* [140] 80

FIGURE 21 PLAIN CHEST RADIOGRAPH SHOWING A LESION IN THE APEX OF THE RIGHT LUNG, LATER CONFIRMED TO BE AN ADENOCARCINOMA. 84

FIGURE 22 A CROSS-SECTIONAL CT IMAGE DELINEATING A LESION IN THE UPPER ZONE OF THE RIGHT LUNG, SUBSEQUENTLY CONFIRMED TO BE CANCER. 86

FIGURE 23 A SAGITTAL MRI IMAGE OF A HEAD, WITH EXCELLENT SOFT-TISSUE DIFFERENTIATION 89

FIGURE 24 SCHEMATIC OF IMAGING WITH POSITRON EMISSION TOMOGRAPHY (PET). *TAKEN FROM SHOKEEN M AND ANDERSON CJ [167].* 93

FIGURE 25 *IN VIVO* SCINTIGRAM WITH ^{18}F-FDG AT 2 HOURS POST INJECTION (1); AND EXCISED TUMOUR (2), IN A DOG WITH SPONTANEOUS SEMINOMA. *TAKEN FROM SOM ET AL [190].* 102

FIGURE 26 A GENERAL SCHEME FOR THE PREPARATION OF ^{18}F-LABELLED PEPTIDES VIA N-SUCCINIMIDYL-4-[^{18}F]-FLUOROBENZOATE (O-(N-SUCCINIMIDYL)-N,N,N',N'-TETRAMETHYLURONIUM TETRAFLUOROBORATE)-MEDIATED ESTERIFICATION OF 4-[^{18}F]-FLUOROBENZOIC ACID. *TAKEN FROM OKARVI [185].* 112

FIGURE 27 CHEMICAL STRUCTURE OF DTPA-TETRA (T-BU ESTER) 114

FIGURE 28 CHEMICAL STRUCTURE OF DOTA-TRIS (T-BU ESTER) 114

FIGURE 29 AVB6 AMINO ACID HOMOLOGY BETWEEN MICE AND HUMANS. 121

FIGURE 30 AVB6 AMINO ACID HOMOLOGY BETWEEN MICE AND HUMANS. 122

FIGURE 31 THE MCF-10A CELL SERIES 133
FIGURE 32 THE MCF-10ANEOT CELL SERIES. 134
FIGURE 33 THE MCF-10CA1 CELL SERIES. 135
FIGURE 34 INTEGRIN EXPRESSION PROFILES OF A375P PURO AND A375PB6, USING FLOW CYTOMETRY 157
FIGURE 35 PEPTIDE AFFINITY TO THE A375PΒ6 CELL LINE, USING FLOW CYTOMETRY 158
FIGURE 36 PEPTIDE SPECIFICITY USING A375P PURO (NON-Β6 EXPRESSING) CELL LINE AND FLOW CYTOMETRY 159
FIGURE 37 COMPARING THE AFFINITY AND SPECIFICITY OF A20FMDV2 WITH DTPA-A20FMDV2, USING FLOW CYTOMETRY. 161
FIGURE 38 COMPARING THE AFFINITY AND SPECIFICITY OF A20FMDV2RAN WITH DTPA-A20FMDV2RAN, USING FLOW CYTOMETRY 162
FIGURE 39 ΑVΒ6-DEPENDENT ADHESION OF A20FMDV2 TO A375P Β6 CELLS, USING FLOW CYTOMETRY 164
FIGURE 40 ΑVΒ6-DEPENDENT ADHESION OF A20FMDV2 TO MOUSE KERATINOCYTES, USING FLOW CYTOMETRY 165
FIGURE 41 MURINE SKIN STAINING FOR ΑVΒ6 167
FIGURE 42 MURINE UTERINE STAINING FOR ΑVΒ6.. 167
FIGURE 43 MURINE GALLBLADDER STAINING FOR ΑVΒ6. 168
FIGURE 44 MURINE URINARY BLADDER STAINING FOR ΑVΒ6. 168
FIGURE 45 MURINE GASTRIC STAINING FOR ΑVΒ6.. 169
FIGURE 46 MURINE DUODENAL STAINING FOR ΑVΒ6.. 170
FIGURE 47 MURINE ILEAL STAINING FOR ΑVΒ6. 170
FIGURE 48 MURINE COLONIC STAINING FOR ΑVΒ6. 171
FIGURE 49 MURINE A375P Β6 XENOGRAFT STAINING FOR ΑVΒ6. 172
FIGURE 50 MURINE A375P PURO XENOGRAFT STAINING FOR ΑVΒ6 172
FIGURE 51 REVERSE PHASE HPLC TRACE MEASURING ^{111}IN-DTPA-A20FMDV2 RADIOLABELLING EFFICIENCY. 175

Figure 52 Reverse phase HPLC trace measuring ^{111}In-DTPA-A20FMDV2ran radiolabelling efficiency 176
Figure 53 Saturation binding assay of ^{111}In-DTPA-A20FMDV2 to adherent A375P β6 cells.
Figure 54 Internalisation Assay:..... 181
Figure 55 Internalisation Assay:..... 182
Figure 56 Internalisation Assay:..... 182
Figure 57 Plasma Stability Study:..... 184
Figure 58 Determining the optimal parameters for pre-clinical imaging studies of αvβ6. 187
Figure 59 Determining the optimal parameters for pre-clinical imaging studies of αvβ6. 188
Figure 60 A375Pβ6 and A375Ppuro xenografts..... 189
Figure 61 ^{111}In-DTPA-A20FMDV2 tissue biodistribution..... 191
Figure 62 100-fold excess of non-radiolabelled DTPA-A20FMDV2 was co-injected with 4μg/1MBq of ^{111}In-DTPA-A20FMDV2.. 193
Figure 63 Biodistribution of ^{111}In-DTPA-A20FMDV2ran (scrambled peptide).. 195
Figure 64 100-fold excess of non-radiolabelled scrambled peptide (DTPA-A20FMDV2ran) co-injected with 4μg/1MBq of ^{111}In-DTPA-A20FMDV2..... 197
Figure 65 Biodistribution of biotinylated peptide vs. non-biotinylated peptide. 199
Figure 66 Non-invasive imaging of αvβ6-expressing tumour with ^{111}In-DTPA-A20FMDV2. 202
Figure 67 Transwell Invasion Assay with MCF-10A.CA1a cells, in the presence of αvβ6-blocking (63G9) and non-blocking antibodies (7.2). 205
Figure 68 Murine MCF-10 DCIS.com / Matrigel xenograft staining for αvβ6.. 207
Figure 69 ^{111}In-DTPA-A20FMDV2 biodistribution in Matrigel xenografts, with or without MCF-10 DCIS.com cells.. 208
Figure 70 ^{111}In-DTPA-A20FMDV2 biodistribution in mice bearing either MCF-10 DCIS.com or MCF-10A.CA1a xenografts.. 210

FIGURE 71 ^{111}IN-DTPA-A20FMDV2 INJECTED I.V. INTO MICE BEARING EITHER MCF-10 DCIS.COM OR MCF-10A.CA1A BREAST TUMOURS. 212
FIGURE 72 MIN MOUSE: NORMAL COLON STAINING FOR AVB6 (X100).. 214
FIGURE 73 MIN MOUSE: ADENOMA STAINING FOR αVβ6. 215
FIGURE 74 APC $^{F/+}$; PTEN $^{F/F}$ MOUSE: ADENOCARCINOMA STAINING FOR αVβ6.. 215
FIGURE 75 APC $^{F/+}$; PTEN $^{F/F}$ MOUSE: ADENOCARCINOMA STAINING FORαVβ6..... 216
FIGURE 76 COMPARING THE AFFINITY AND SPECIFICITY OF A20FMDV2 WITH DTPA-A20FMDV2, USING FLOW CYTOMETRY. 218
FIGURE 77 RP- HPLC TRACE MEASURING ^{111}IN-DTPA-DBD2 RADIOLABELLING EFFICIENCY. 220
FIGURE 78 PLASMA STABILITY STUDY:..... 221
FIGURE 79 ^{111}IN-DTPA-DBD2 (1 MBQ / 2μG) INJECTED INTO GROUPS OF TUMOUR-BEARING MICE. . 223
FIGURE 80 ^{111}IN-DTPA-DBD2 TISSUE BIODISTRIBUTION..... 224
FIGURE 81 REVERSE PHASE HPLC TRACE MEASURING ^{111}IN-DOTA-A20FMDV2 RADIOLABELLING EFFICIENCY. 226
FIGURE 82 ^{111}IN-DOTA-A20FMDV2 (1 MBQ / 4μG) INJECTED INTO GROUPS OF TUMOUR-BEARING MICE. 227
FIGURE 83 ^{111}IN-DOTA-A20FMDV2 TISSUE BIODISTRIBUTION.. 228
FIGURE 84 REVERSE PHASE HPLC TRACE MEASURING ^{111}IN-DOTA-A20FMDV2 RADIOLABELLING EFFICIENCY. 230
FIGURE 85 BIODISTRIBUTION OF ^{111}IN-DOTA-A20FMDV2RAN (SCRAMBLED PEPTIDE). 231
FIGURE 86 NANOSPECT/CT IMAGING OF αVβ6-EXPRESSING TUMOUR WITH ^{111}IN-DOTA-A20FMDV2: 233
FIGURE 87 COLONIC TISSUE SAMPLES FROM TWO 'NORMAL' HUMAN DONORS. 285

LIST OF TABLES

TABLE 1 THE MAJOR EXTRACELLULAR LIGANDS OF INTEGRINS. *ADAPTED FROM PLOW, EF ET AL [17]* . 38

TABLE 2 αvβ6 EXPRESSION IN CARCINOMAS. *ADAPTED FROM [104]*. 75

TABLE 3 PHYSICAL PROPERTIES OF SPECT RADIOISOTOPES 92

TABLE 4 PHYSICAL PROPERTIES OF PET RADIOISOTOPES 95

TABLE 5 CHARACTERISTICS OF DIFFERENT RADIONUCLIDES USED FOR RADIOLABELLING. *ADAPTED FROM OKARVI S.M. [185]*. 99

TABLE 6 METHODS OF INHIBITING PROTEOLYSIS OF PEPTIDES. *ADAPTED FROM OKARVI [185].* 105

TABLE 7 COMPLEXING AGENTS AND CORRESPONDING RADIONUCLIDES 116

TABLE 8 OVERVIEW OF IMAGING TECHNOLOGIES. *ADAPTED FROM WEISSLEDER R AND PITTET MJ [183]*. 118

TABLE 9 SUMMARY OF CELL LINES TESTED WITHIN THIS PROJECT. 131

TABLE 10 PATTERN OF αvβ6 EXPRESSION IN MURINE TISSUES, AS DETECTED BY IMMUNOHISTOCHEMISTRY. 174

TABLE 11 COMPARISON OF DIFFERENT ACID WASH BUFFER EFFICIENCIES 180

TABLE 12 SURFACE INTEGRIN EXPRESSION BY BREAST CANCER CELL LINES IN COMPARISON WITH THE A375P β6 MELANOMA LINE. 204

Chapter I: Introduction to Cancer

1.1 Cancer

Cancer is a term that encompasses many diseases which involve dynamic changes within the genome [1]; leading to the genomes of incipient cancer cells acquiring mutant alleles of proto-oncogenes, tumour-suppressor genes, and other genes that control, directly or indirectly, cell proliferation [2]. Consequently cancer cells have the ability to divide without control, to form tumour masses and to 'invade' other normal tissues. Cancer is propagated by possible 'seeding' into the blood and lymphatic systems, resulting in dissemination of the malignant tissue to other parts of the body (metastasis).

Cancer is a major cause of morbidity and mortality in the United Kingdom (UK). In the UK, 297,991 persons were diagnosed with cancer in 2007; while 156,723 individuals died from this constellation of diseases in 2008 [3]. There are more than 200 different types of cancer; however, breast, lung, colorectal and prostate account for over half of all new cases of cancer [4]. Overall it is estimated that approximately 2% of the population of the UK are alive having received a diagnosis of cancer: that is, around 1.2 million people [5]. The 20 most commonly diagnosed cancers in the UK are shown in **Figure 1**.

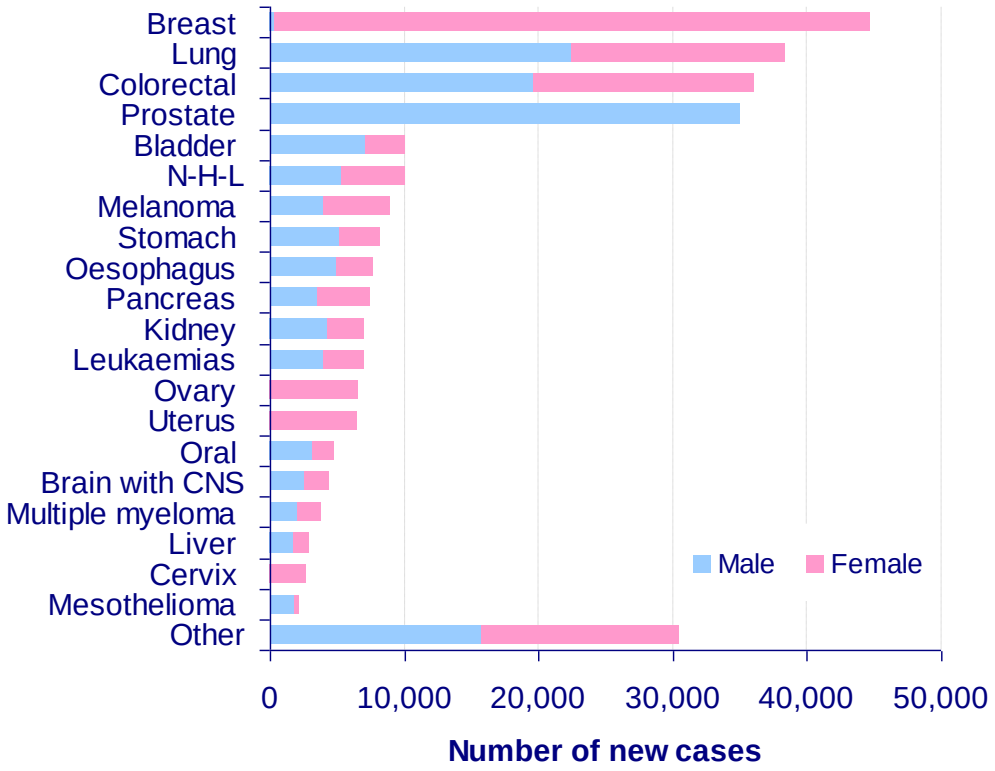

Figure 1 The Twenty Most Commonly Diagnosed Cancers in UK (2004), excluding non-melanoma skin cancers. *Taken from Cancer statistics registrations, Great Britain [4].*

Furthermore, in the 30-year period 1975 to 2004, the overall age-standardised incidence rate for cancer has increased in Great Britain, by 25%, with a 15% increase in men and a 32% increase in women [4].

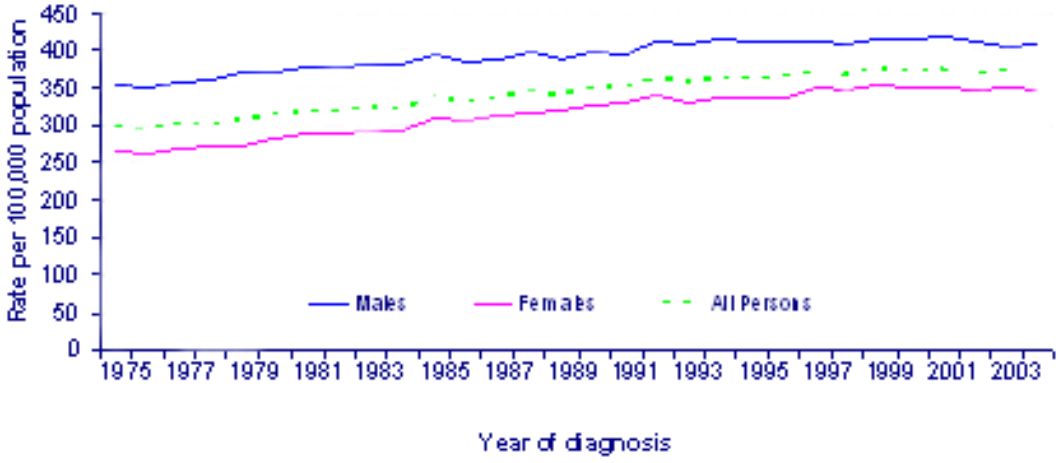

Figure 2 Age-standardised (European) incidence rates, all cancers excluding non-melanoma skin cancers, GB, 1975-2004. *Taken from Mortality statistics, Great Britain [6]*.

In spite of better preventive strategies, screening programmes and improving therapeutic interventions, there still were 153,491 deaths from cancer, in the UK during 2005; when cancer was responsible for 26% of all deaths [6]. While lung cancer remains the greatest killer, breast cancer has the greatest incidence, largest prevalence and is the third most common cause of cancer death in all persons. The most frequent cause of death in breast cancer patients can be attributed to metastasis of tumour cells and their growth at distant regions rather than the *in situ* effects of the malignancy at the primary site.

The diagnosis of malignancy usually involves history taking and clinical examination of the patient, blood tests, non-invasive imaging, biopsy and histology [7]. Furthermore, modern therapeutic interventions rely primarily on non-invasive imaging techniques to guide the intensity and duration of therapy. Therefore imaging is crucial to early diagnosis and monitoring of cancer. That is, improvements in imaging technologies have the potential to diagnose cancer at earlier stages (non-metastatic) and guide treatments to make them more effective; thereby improving survival and reducing toxicity. However, many of the current imaging modalities, such as computed tomography (CT) and magnetic resonance imaging (MRI), crudely rely on reduction in tumour size as an indicator of response to therapy. Anatomical or structural imaging is fraught with issues around interpretation, since it analyses over a single timepoint and is only reliable in assessing well-defined lesions larger than 10mm [8]. Furthermore, tumour size reduction is not always a surrogate marker for response to therapy. Reduction in the viable cancer cell fraction of a tumour does not always result in a volume reduction, since cancerous tissue can be replaced by necrotic, fibrotic or cystic changes and morphological images may be unable to differentiate between these different tissue types [9]. Furthermore, the newer anti-vascular and cytostatic targeted agents aim at tumour growth stabilisation, rather than tumour shrinkage, and thus no major volume changes are to be expected. This difficulty, potentially, could result in the incorrect withdrawal of effective therapy and thus impact adversely on patient survival. Moreover, anatomical imaging gives no information on biological markers, which could help in the selection of the most efficient therapy and indicate prognosis. These issues are tackled by the relatively newer functional or molecular imaging modalities, such as positron emission

tomography (P.E.T.) and single photon emission computed tomography (S.P.E.C.T.). In these modalities, biological markers can be targeted using radiolabelled small molecules which, therefore, can be traced in the body. This technique could, potentially, evaluate small volume disease (lesions less then 10 mm), which is classed as ‘indeterminate’ by conventional anatomical scanning [8]. A recent study showed that quantitative FDG-PET was significantly more accurate than CT size-based criteria at assessing histopathologic response to chemotherapy, in high-grade soft-tissue sarcomas [10]. Furthermore, if the biological marker is present, it would allow appropriate selection of targeted therapy and a means to monitor response of minimal residual disease. However, before a biological marker can be applied in the aforementioned roles, it must be selected using *in vitro* characterisation and validated in pre-clinical models. A flow plan for how an imaging probe could be taken through to clinical evaluation is outlined in **Figure 3**.

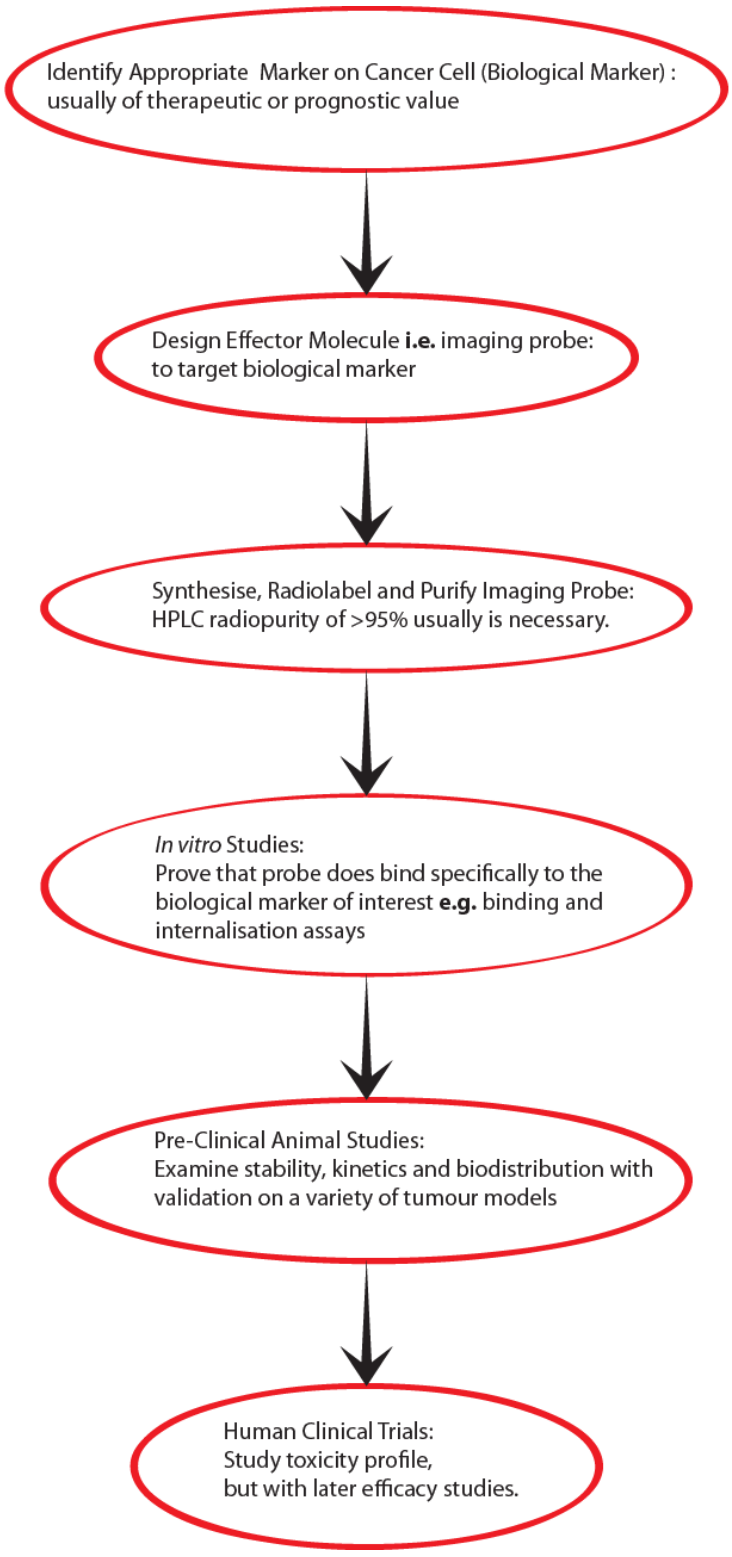

Figure 3 The development and evolution of a targeted probe for a biological marker of cancer.

1.2 Integrins

The "integrin" terminology first was applied in a 1987 review article [11]. Integrins are a superfamily of trans-membrane, heterodimeric, cell adhesion glycoproteins. They comprise a pair of non-covalently linked α and β subunits [12]. The different combinations of α and β subunits result in more than twenty different integrin receptors (**Figure 4**) and this variability in heterodimer composition determines ligand binding specificity [13]. Integrin variants also have been characterised which result from differential splicing and post-translational modifications [14]. Integrins recognise specific amino acid sequences in their ligands and at least eight of the possible subunit combinations recognise the RGD (Arg-Gly-Asp) motif [15].

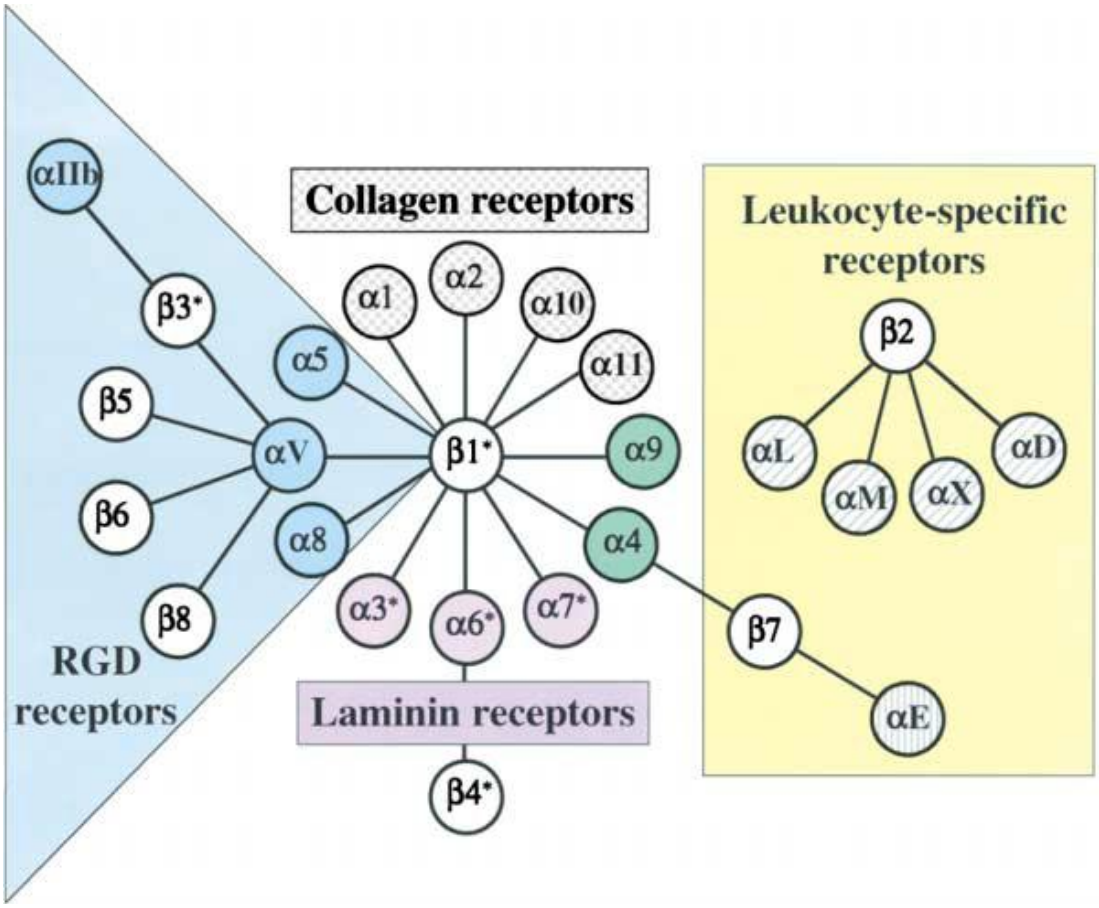

Figure 4 The Integrin Receptor Family. *Taken from Hynes RO [13].*

1.2.1 Integrin Structure

Cells continually secrete, assemble and remodel an insoluble network of proteins - the extracellular matrix (ECM). The ECM provides a pliable, but resistant, scaffold for the organisation of cells in tissues and exerts control on the behaviour of cells. The effects of the ECM on cells are mediated mainly by integrins [16]. Integrin-binding ECM ligands include fibronectin, vitronectin, collagen, laminin and tenascin-C [17] (see **Table 1**, page 38). Integrins link their ECM ligands to the actin-based microfilament system; with the exception of α6β4, which links through the cytokeratin microfilament system [13].

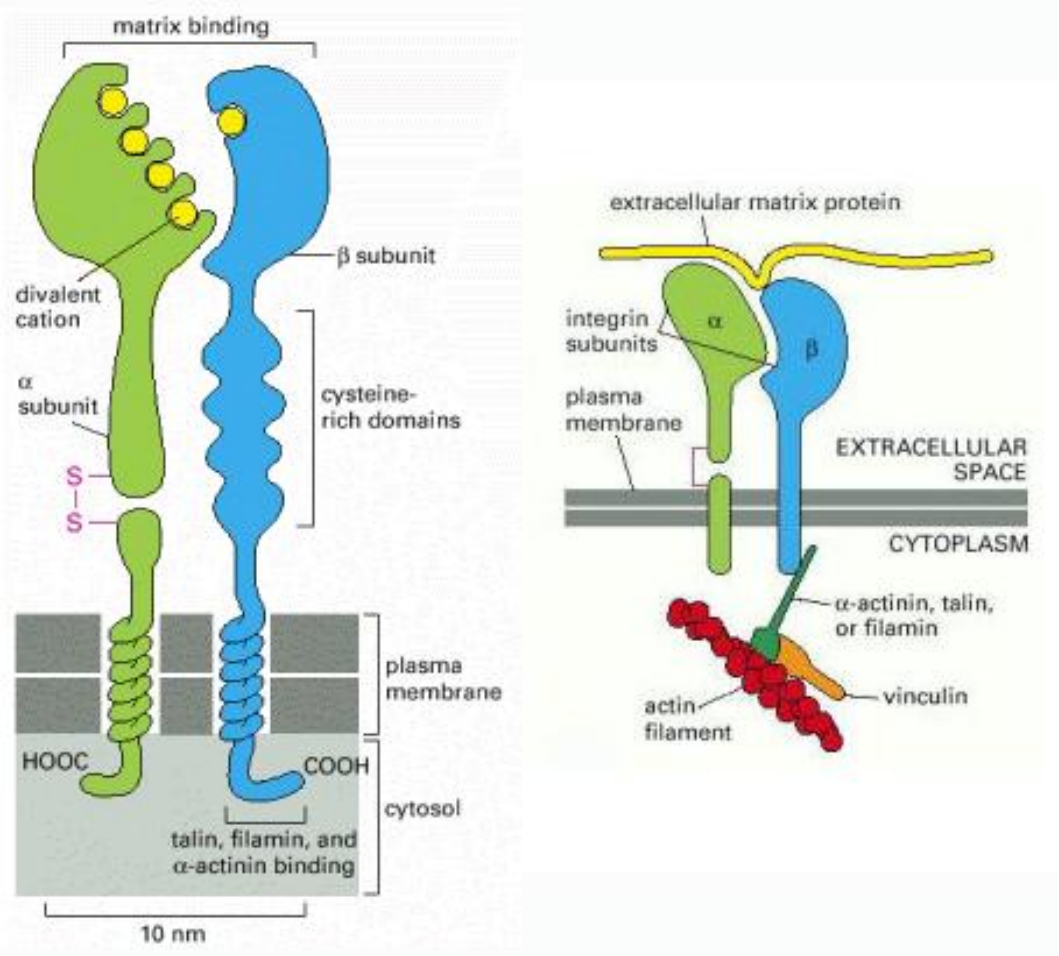

Figure 5 Simplified diagram of the Integrin Receptor and its relation to the Cell Membrane. *Taken from Alberts B et al [18].*

Each integrin subunit is a type I transmembrane protein [19], composed of a large extracellular domain, a single transmembrane region and, in most cases, a short non-catalytic cytoplasmic tail (**Figure 5)**. All integrin dimers are dissociated by ionic detergents, indicating that the subunits are held together by non-covalent interactions [20].

The x-ray crystal structure of the extracellular domain of αvβ3 has been determined [21]. The extracellular domains of both subunits represent the interface for the 'ligand binding pocket'. Electron microscopic integrin images reveal a globular head, approximately 70–100 Å in diameter. With the aid of primary sequence analysis, the N-terminal region of all α subunits was discovered to be made up of seven repeats; each of which contains approximately 60 amino acids. The seven repeats are quite similar in sequence, with the exception of the final three or four. These final repeats contain inserted sequences that are similar to the EF-hand; a 13-residue bivalent-cation-binding motif found in proteins such as calmodulin and parvalbumin [20]. These repeats form the basis of a seven-bladed β-propeller fold in the α subunit. Furthermore, a subset of nine α subunits also contain an approximate 200-amino-acid insert that is homologous to the A domain of von Willebrand factor [20]. The additional insert seems to bestow a different mode of integrin activation and ligand binding on those integrins which express this structure.

The extracellular domain of the β-subunit also has been predicted to contain an A-domain-like polypeptide segment. The major contact between the two subunits is with this βA-domain and the β-propeller fold of the α subunit. Furthermore, the location of the ligand-binding pocket is at the junction of the β propeller and the βA domain, in the integrin head. The β-subunit also contains a plexin-semaphorin-

integrin (PSI) domain [22], an immunoglobulin fold, termed the hybrid domain, a novel cystatin-like fold and four cysteine-rich epidermal growth factor (EGF)-like repeats (stabilising the large extracellular amino terminal loop[23]). This is finally followed by a β-tail domain (see **Figure 6**).

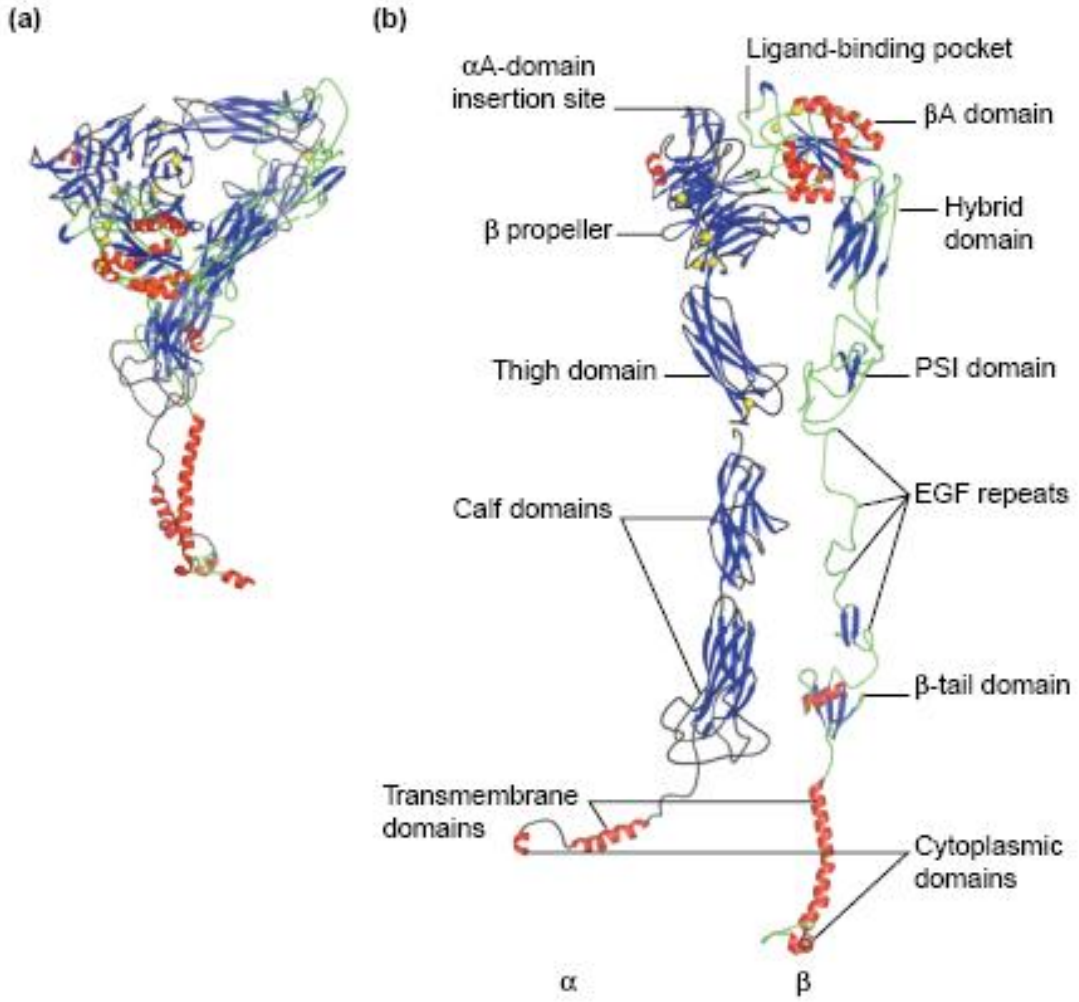

Figure 6 Schematic representation of the αvβ3 integrin structure. (a) Bent image of αvβ3 integrin. (b) Straightened image of αvβ3 integrin. *Taken from Humphries MJ et al [24]*.

The short β-cytoplasmic tail contains regions which bind and link integrins to the actin cytoskeletal system (e.g. α-actinin [25]). However, the cytoplasmic tail domains of integrins also can recruit signalling proteins, which regulate integrin adhesiveness to the extracellular matrix (ECM) [26]. For instance, the α-chain cytoplasmic domain is able to bind to calreticulin, via its highly conserved K*X*GFFKR sequence motif [27]. Calreticulin is a highly conserved, ubiquitously expressed intracellular protein, which regulates calcium transmembrane channel influx, and has been implicated in the regulation integrin conformation and thus its affinity [27, 28]. This represents one of the components of 'inside-out' signalling associated with integrins (see later).

1.2.2 Integrin Function

Integrins dynamically *integrate* the extracellular matrix with the intracellular cytoskeleton, and transmit both mechanical and chemical signals. They impart polarity to the cell and organise its cytoskeleton during adhesion and migration. Integrin signalling exerts a rigorous control on cell proliferation, migration and cell survival [16].

Integrins are able to recognise multiple ligands. **Table 1** (page 38) includes some of the major extracellular ligands of integrins. The list broadly comprises extracellular matrix proteins (bone matrix proteins, collagens, fibronectins, fibrinogen, laminins, thrombospondins, vitronectin, and von Willebrand factor), 'counter-receptors' (cross-talk) and numerous micro-organisms (using integrins for cell entry). Most integrins recognise relatively short peptide motifs and ligand specificities rely on both subunits of a given αβ heterodimer [13]. Furthermore, the preference of any given integrin for any particular substrate (from among its ligands) is determined by relative affinity, availability within a specific microenvironment, and the conformational state of the ligand, which controls exposure of its integrin recognition sequence [17].

Ligand	Integrin
Adenovirus penton base protein	αvβ3, αvβ5
Bone sialoprotein	αvβ3, αvβ5
Borrelia burgdorferi	αIIbβ3
Candida albicans	αMβ2
Collagens	α1β1, α2β1, α11β1, αIbβ3
Denatured collagen	α5β1, αvβ3, αIIbβ3
Cytotactin/tenascin-C	α8β1, α9β1, αvβ3, αvβ6
Decorsin	αIIbβ3
Disintegrins	αvβ3, αIIbβ3
E cadherin	αEβ7
Echovirus 1	α2β1
Epiligrin	α3β1
Factor X	αMβ2
Fibronectin	α2β1, α3β1, α4β1, α4β7, α5β1, α8β1,
Fibrinogen	α5β1, αMβ2, αvβ3, α*x*β2, αIIbβ3
HIV Tat protein	αvβ3, αvβ5
iC3b	αMβ2, α*x*β2
ICAM-1	αLβ2, αMβ2
ICAM-2,3,4,5	αLβ2
Invasin	α3β1, α4β1, α5β1, α6β1
Laminin	α1β1, α2β1, α6β1, α7β1, α6β4, αvβ3
MAdCAM-1	α4β7
Matrix metalloproteinase-2	αvβ3
Neutrophil inhibitory factor	αMβ2
Osteopontin	αvβ3
Plasminogen	αIIbβ3
Prothrombin	αvβ3, αIIbβ3
Sperm fertilin	α6β1
Thrombospondin	α3β1, αvβ3, αIIbβ3
VCAM-1	α4β1, α4β7
Vitronectin	αvβ1, αvβ3, αvβ5, αIIbβ3
von Willebrand factor	αvβ3, αIIbβ3

Table 1 The major extracellular ligands of integrins. *Adapted from Plow, EF et al [17]*

Following ligand binding, integrins cluster into supramolecular complexes, termed focal contacts, which link integrins to the cytoskeleton (**Figure 7**). These focal contacts serve to transmit force or tension at adhesion sites to maintain strong anchoring attachments to the underlying ECM and to act as signalling centres [29].

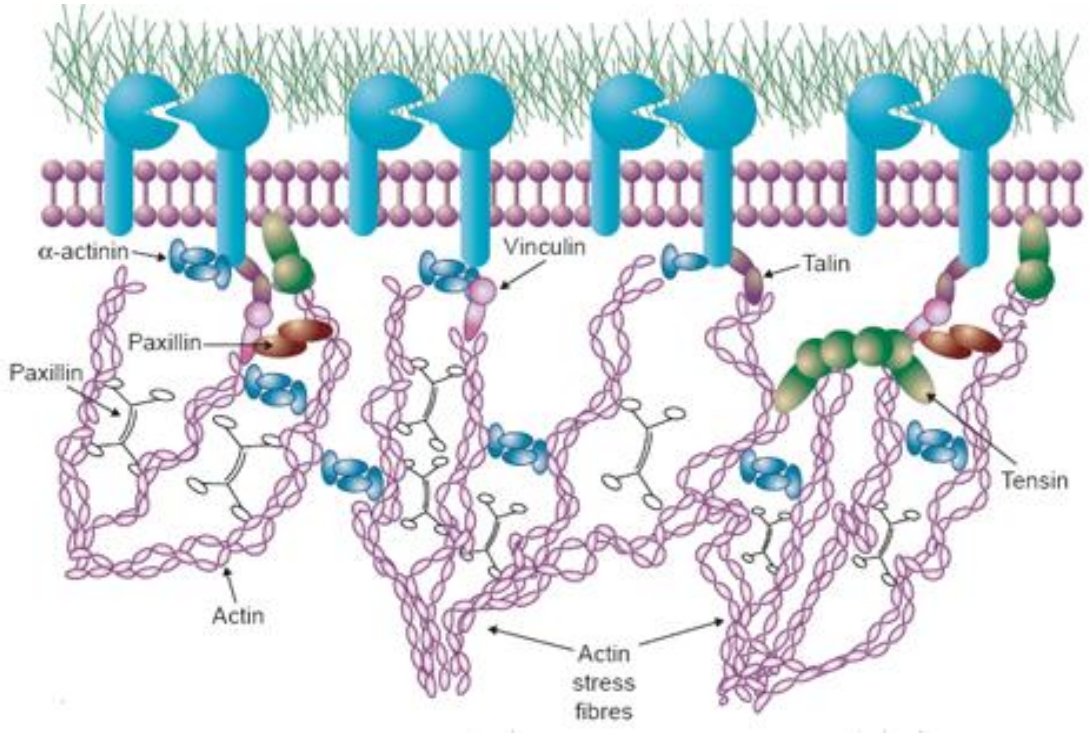

Figure 7 Integrins and the Actin cytoskeletal system. *Taken from Miranti CK et al [30]*.

The aggregation of integrins juxtaposes many signalling and structural molecules, which are associated with their cytoplasmic tails, allowing them to interact. Adherent normal cells must be anchored to an appropriate ECM to survive. Normal epithelial cells often undergo inappropriate apoptosis when deprived of the ECM – 'anchorage dependence' [31]. Indeed, the apoptosis resulting from lack of anchorage has been

termed ‘anoikis’[32]. Control of anchorage dependence appears to be reliant on various integrin-related signalling pathways [33]. It should be noted that these integrin-associated apoptotic cues do not seem to function properly in certain cancer cells and represent a characteristic of neoplastic transformation (see later).

Integrins can signal through the cell membrane in either direction – ‘bidirectional signalling’. Unlike other receptors, ligand binding with integrins generally is not constitutive but is regulated to reflect the activation state of the cell. Specifically, high affinity binding of integrins to ligands is elicited in response to cell "activation" signals (so-called "inside-out signalling”) that alter the tertiary and quaternary structure of the extracellular region, making the integrin ligand-competent. Ligand binding in turn induces structural rearrangements in integrins that trigger "outside-in" signalling. Therefore, the extracellular binding activity of integrins is regulated from the inside of the cell, while the binding of the ECM elicits signals that are transmitted into the cell [34].

1.2.2.1 Outside-In Signalling

Integrin-mediated ‘outside-in’ signalling occurs when ligand binding activates intracellular signalling pathways [34]. Outside-in signalling can be divided, broadly, into two descriptive categories (**Figure 8)**. The first is 'direct signalling', in which ligand binding and resultant clustering of integrins is the *only* extracellular stimulus. In this way, adhesion to ECM proteins can activate cytoplasmic tyrosine kinases (e.g. focal adhesion kinase [FAK]) and serine/threonine kinases (e.g. mitogen-activated protein kinase [MAPK] cascade), produce ionic flux (e.g. Ca^{2+}, Na^{+}/H^{+}) and initiate small GTPases, recruit adaptor proteins and induce lipid metabolism [35].

The second category of integrin signalling is 'collaborative signalling', in which integrin-mediated cell adhesion *modulates* signalling events initiated through *other* types of receptors; particularly receptor tyrosine kinases (RTKs) that are activated by polypeptide growth factors [35]. These kinases can phosphorylate cytoskeletal proteins and regulate stress-fibre formation, cell shape and migration. For example, ECM binding to α6β4 or α6β1, seems to increase the activation of ErbB-2, in carcinoma cells [36]. Indeed, Falconi *et al* demonstrated that concomitant over-expression of ErbB-2 and β4 proteins confers proliferative and invasive advantages to transformed cells and strongly suggest that the interaction of α6β4 and ErbB-2 receptors has a role in malignant progression [36].

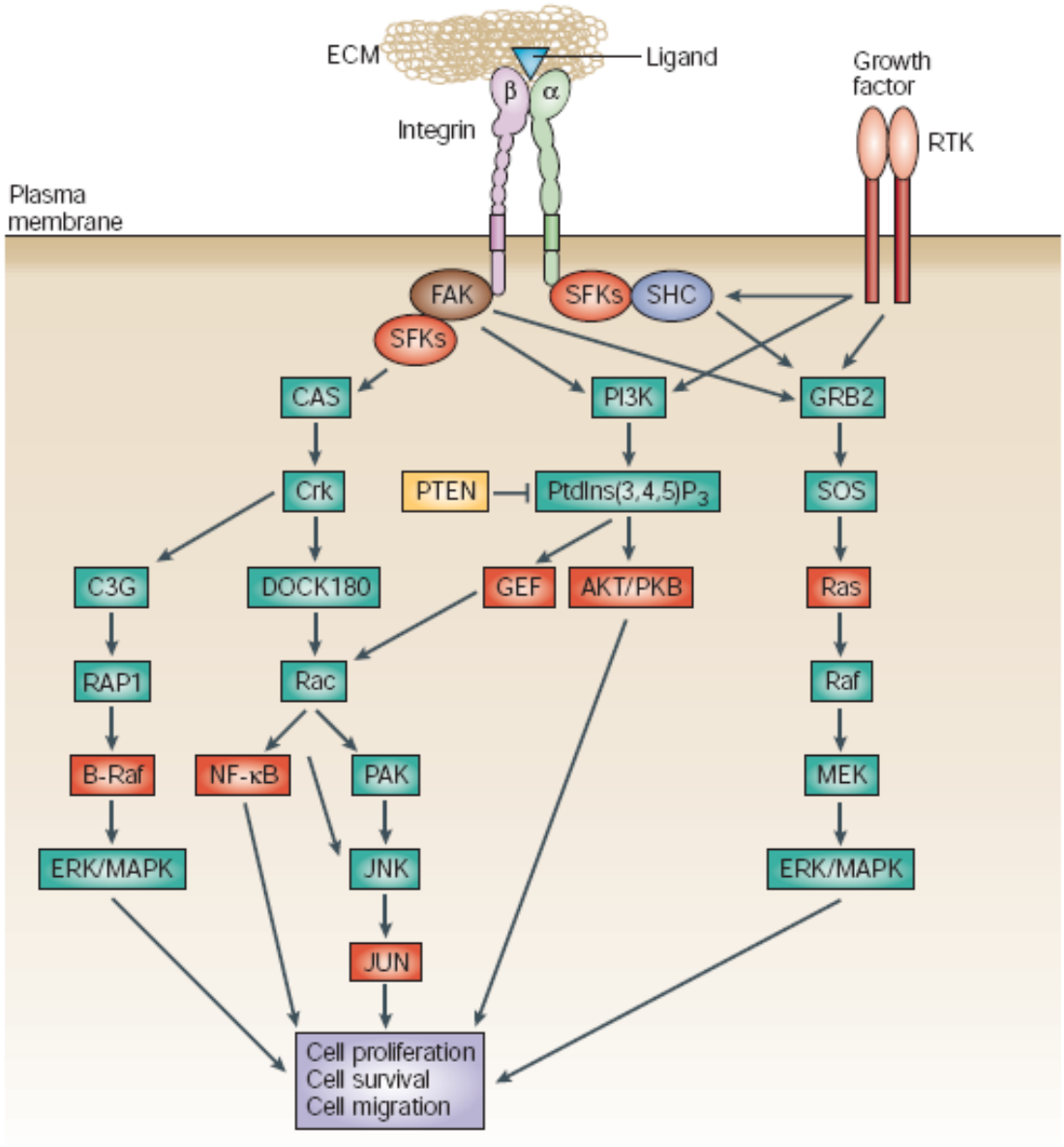

Figure 8 Regulation of Intracellular Signalling by Integrins. *Taken from Guo and Giancotti [16].*

1.2.2.2 Inside-Out Signalling

Inside-out signalling occurs when signals are received *by other receptors* and this activates various intracellular signalling pathways. These intracellular cues interact with integrin cytoplasmic domains, propagate conformational changes and, thereby, alter the way in which their extracellular domains associate with the extracellular environment [37]. That is, alteration of the extracellular domain (described later) can modulate the *affinity* of integrins for their ECM and regulate integrin adhesiveness to their ligands. Furthermore, intracellular cues also affect receptor clustering (*avidity* modulation), which also regulates ligand binding. The mechanism of regulation for integrin clustering can be via intracellular signalling events that remodel the cytoskeletal-integrin complexes or alter receptor diffusion rates within the cell membrane [38, 39]. Therefore, integrins are also involved in bi-directional signalling, regulated by affinity and avidity modulation, to control cell invasion and migration [35, 40, 41].

One such intracellular cue is the activity of small GTPases (proteins that bind and hydrolyse GTP), of the Rho and Ras families. The activation of these GTPases is under the control of integrins themselves, as well as other cell-surface receptors (see **Figure 9)**. It has been shown that the activation of R-Ras leads to enhancement of integrin *affinity* to ECM substrates [42]; in contrast, H-Ras activation inhibited integrin *affinity* (no substrate binding)[43]. Similarly, activation of the small GTP-binding proteins RAC and cdc42 (and subsequent protein kinase C (PKC) induction) can lead to integrin clustering and thus an increase in integrin *avidity* [26, 44]. Therefore, meticulous regulation of these signalling events is necessary for efficient cell adhesion and migration (see **Figure 13)**.

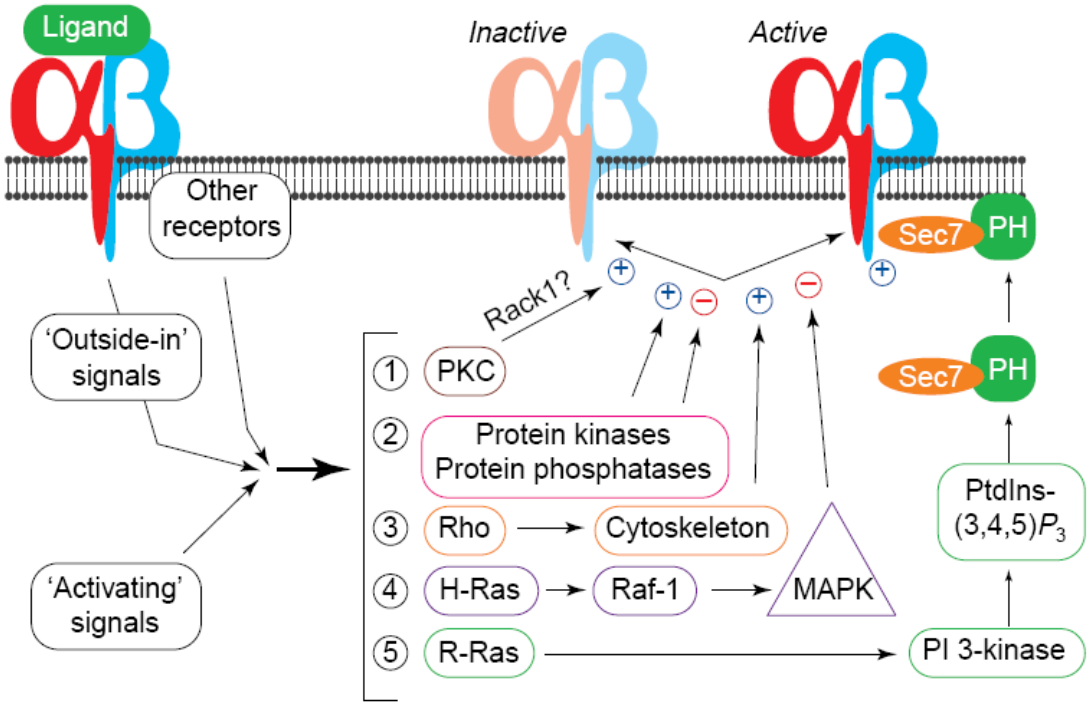

Figure 9 Inside Out Signalling and Integrin Modulation. *Taken from Hughes and Pfaff [41].*

A Mechanism for Affinity Modulation

Although, each cell type can control its adhesive interactions partly by synthesising specific subsets of integrins at different stages of differentiation, this is a relatively slow process. Integrins must be controlled so as to undergo rapid adhesion and binding to the ECM, at certain times e.g. clot formation during bleeding. Equally important, integrins must then be inactivated to avoid cell adhesion and ECM binding at inopportune times and locations - adherent cells need to detach to undergo mitosis or during physiological migration [45]. That is, it may cause harm if normally motile cells suddenly became immobilised. Therefore, integrin signalling has to be controlled in a dynamic manner with a rapid mechanism for switching

between ‘inactive’ to ‘active’ states. Researchers in the integrin field use the term ‘activation’ or ‘priming’ to denote the switch from an inactive to an active state [24]. The active, or primed state, correlates with the acquisition of ligand binding ability by integrins. Steric regulation or conformational switches seems to be important in regulating integrin activation and affinity regulation. Specifically, an initial ‘physiological’ highly bent integrin can transform (via a switchblade-like opening) into an extended structure, and the ligand binding pocket and the αA domain are able, as a consequence, to modify their orientation [20]. The extended structure of the integrin results in the head groups becoming ‘open’, with the exposure of concealed epitopes (see later), and this lends itself to ligand binding. Electron microscopic images of recombinant integrins, in the presence of calcium (non-supportive for ligand binding) and manganese (promotes ligand binding), confirmed predominantly bent and extended forms, respectively [46]. It is this change in the integrin conformation that allows strict control of ligand binding and subsequent adhesion. However, it is more than likely that this is a simplified view, with several intermediate steps and conformations involved (See **Figure 10)**.

The hypothesis for exposure of concealed epitopes was first proposed by Ginsberg *et al*, in 1988 [47]. The authors described the appearance of ligand-induced binding site (LIBS) epitopes, on αIIbβ3, in response to ligand or ligand-mimetic binding. However, intracellular cues can also expose neo-epitopes and therefore the term activation-dependent binding site probably is more appropriate [46]. These neo-epitopes are recognised by a subset of anti-integrin monoclonal antibodies and are located primarily on the β-subunit at a series of sites along the whole length of the

polypeptide [46, 48]. Furthermore, an NMR structure of β2 integrin domains confirmed that epitopes become exposed when integrins are activated [49].

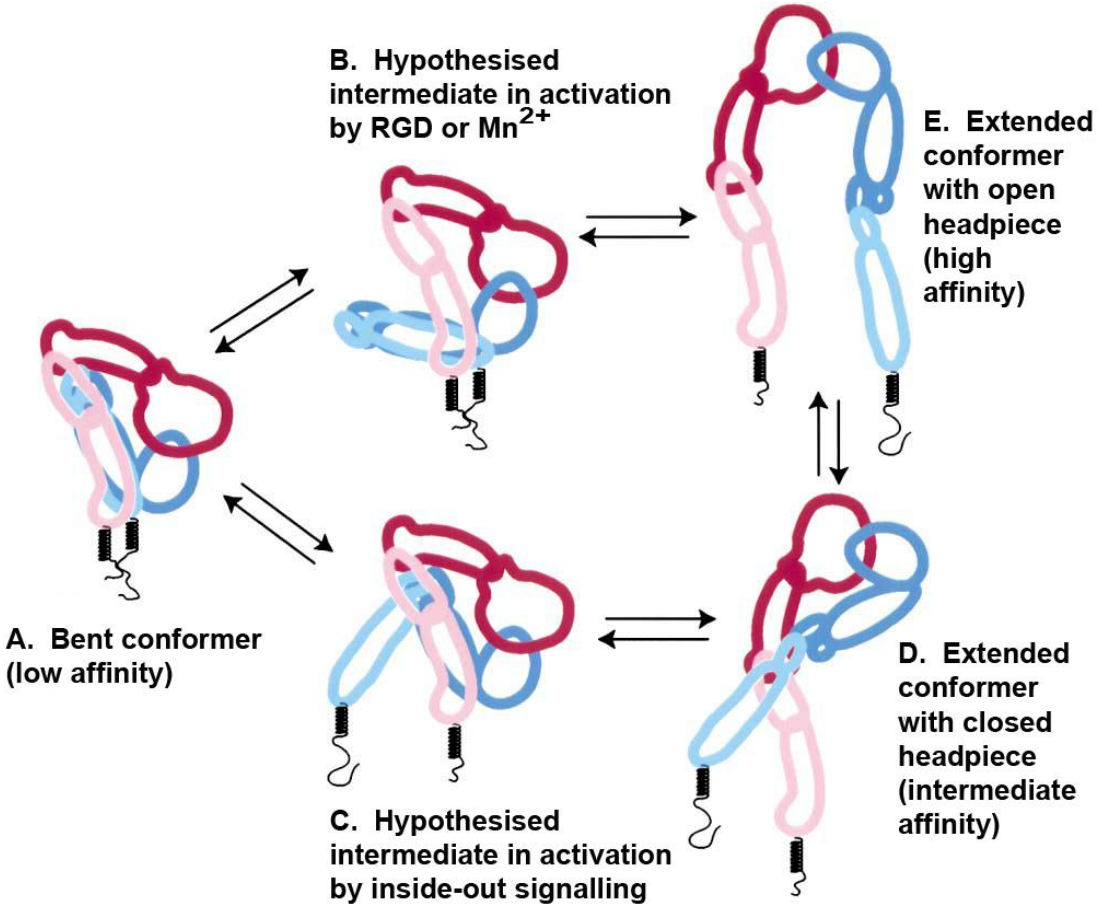

Figure 10 Proposed Quarternary Structural Rearrangements in Integrin Activation. *Taken and adapted from Tagaki et al [46]*

.

1.2.2.3 Cation-Dependent Integrin Regulation

All integrins bind their ligands in a divalent cation-dependent manner with manganese and magnesium generally promoting binding, and calcium having the opposite effect [50]. Each integrin heterodimer contains several divalent cation-binding sites of relatively low affinity and the bound cations exert profound effects on integrin function [17]. Additionally, the presence of divalent cations can maintain the integrity, and form the interface, of the ligand binding pocket: The αA(when present) and βA-domains of integrins are intricately involved with the β-propeller fold (of the α subunit) to form the ligand binding pocket [24]. Lee et al [51] demonstrated a magnesium / manganese co-ordination site on the surface of the αA-domain, which plays an important role in protein ligand binding. The authors termed this co-ordination site - 'the metal ion-dependent adhesion site' (MIDAS). Disruption of the MIDAS, using mutagenesis experiments, reduced protein ligand binding [51]. The authors also proposed that the β subunits of integrins contain a MIDAS motif, within their modified A domains. Subsequent crystal structure experiments on αvβ3 have confirmed this MIDAS, but it also is flanked by two other cation-binding sites within the ligand-binding pocket of the βA-domain; termed ADMIDAS (adjacent to MIDAS) and LIMBS (ligand-induced metal-binding site) [24]. The MIDAS phenomenon explains the cation dependence of ligand binding, and thus cell adhesion. Therefore, collectively, divalent ions and cation binding sites can act as effectors, promoting ligand binding; as antagonists, inhibiting ligand binding; and as selectors, changing the ligand binding specificity.

In summary, integrins have been shown to be involved in bi-directional signalling and their affinity and avidity are under tight control. This strict modulation is necessary for gene transcription, cell differentiation, cell survival, cell proliferation and migration [52].

1.3 Integrins and Cancer

Cancer primarily causes death through spread to different organs from that in which the primary tumour arose (metastasis). In order for tumours to metastasise and grow, neoplastic and endothelial cells must *proliferate, invade and remodel their surrounding environment, migrate through surrounding tissues, disseminate, survive and differentiate* [2, 53]. As cancer cells become metastatic, they develop altered affinity and avidity for their extracellular matrix (ECM). The phenotypic change initially is mediated by alterations in the expression of integrins, release of proteases that remodel the ECM and the deposition of new ECM molecules. These activate signalling cascades that regulate gene expression, cytoskeletal organisation, cell adhesion and cell survival. These cascades promote cancer cell passage through to the stroma, entrance into new tissues and survival within different microenvironments [26]. The following is a description of how integrins are vital to neoplastic cell growth, dissemination and survival:-

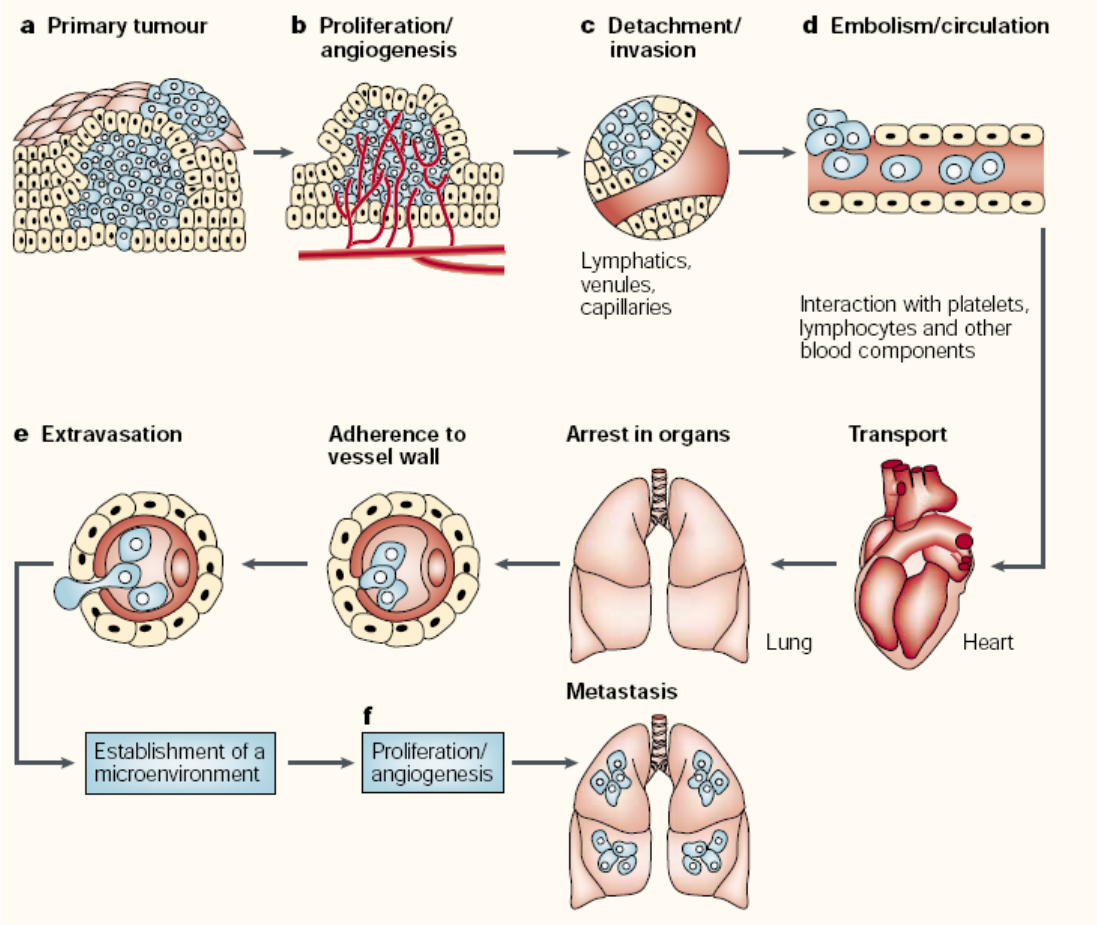

Figure 11 The Main Steps in the Formation of a Metastasis. *Taken from Fidler IJ[53]*.

1.3.1 Proliferation

Proliferation without limits ('immortalisation') is necessary for tumours to have expansive growth in both primary and metastatic sites [2]. Mainiero *et al* have linked the integrin, α6β4, with the control of proliferation of basal keratinocytes [54]. The authors used primary human keratinocytes which adhere to laminin 5, via α6β4 and α3β1 [55]. Mainiero and colleagues [54] used immunoblotting experiments to display that adherence of these keratinocytes, via the β4 subunit, resulted in tyrosine phosphorylation of Shc isoforms and subsequent recruitment of Grb2.

[^{32}P]orthophosphate labelling of (serum and phosphate starved) keratinocytes, consecutive immunoprecipitation of Ras, successive nucleotide elution and separation by Thin-Layer Chromatography (TLC) permitted phosphorimaging quantification of the guanine nucleotides bound to Ras [56]. Mainiero incorporated this 'Ras-GTP loading assay' and showed that α6β4-mediated cell adhesion causes activation of Ras, probably through Grb2's association with the Ras-GTP exchange factor mSOS. Furthermore, the authors used immunoprecipitation and *in vitro* kinase assays to show that mitogen-activated protein kinase Erk is activated, via Ras and RhoA proteins, upon β4 ligation. Erk is known to regulate transcription from the Fos serum response element (SRE) by phosphorylation and cooperation with the Rho family proteins [57]. Luciferase assays demonstrated that ligation of α6β4 is required for optimal induction of Fos SRE-dependent transcription, in response to EGF. Furthermore, 5'-bromo-2'-deoxyuridine (BrdU) incorporation illustrated that ligation of α6β4 allows progression through G_1 and entry into S phase, in keratinocytes which have been treated with EGF. Indeed, Mainiero et al suggested that ligation of α6β4 is required and sufficient to promote keratinocyte proliferation, in response to laminin 5 [54].

As well as direct transcriptional control, integrins can complex and cross-talk with other receptors to control proliferation. The collaborative signalling between ErbB-2 and the β4 subunit, and its proliferative and invasive advantages to transformed cells, already has been mentioned above [36].

1.3.2 Invasion

The transition from a benign to an invasive cell is driven by a discrete series of adhesive changes and the partial degradation and extensive remodelling of the local ECM. Integrins cooperate with various oncogenic signals to promote the many phases of this process [16].

Cancer cells can assume a more invasive and migratory phenotype by modulating their adhesive capacity and intracellular signalling activities by altering their integrin expression and affinity profiles:-

Neoplastic cells can undergo dramatic alterations in levels of integrin expression for ECM substrates. Some integrins are either overexpressed or no longer expressed whereas others become phosphorylated, affecting their cytoskeletal and extracellular ligand binding properties [23]. The changes in integrin expression and the cell surface distribution seem to be specific to the tumour cell type. These changes in certain types of integrin levels aim to promote neoplastic cell proliferation, migration and cell survival [16]. It has been shown that inducing expression of the αv integrin subunit in a melanoma cell line increases its tumourigenicity [58]. Furthermore, Shaw et al demonstrated that neo-expression of α6β4 increases the invasiveness of MDA-MB-435 cells through Matrigel, in standard chemoinvasion assays [59]. Using experimental combinations of immunoprecipitation, kinase assays, a dominant-negative PI3K subunit and a PI3K inhibitor, the authors proposed that the increased invasiveness is dependent on PI3K signalling [59].

In addition, there is increasing evidence indicating that dysregulated joint integrin–RTK signalling contributes to the disruption of cell–cell adhesion and the

promotion of invasion, in cancer cells [16]. Numerous studies have demonstrated that the progression to invasive carcinoma involves loss of function of adhesion molecules involved in maintenance of the epithelial phenotype, namely, cadherins [60, 61] and catenins [62-64]. Classic cadherins, such as E-cadherin, have a key role in epithelial cell–cell adhesion. E-cadherin has been shown to be modulated by integrin-RTK signalling, through transcriptional repression (via SNAIL/SLUG transcriptional factors) and endocytosis of receptor complexes [65].

Matrix Degradation And Remodelling

Tumour invasion requires partial degradation of the ECM at the invasion front. In particular, neoplastic cells have to induce local degradation of basement membranes, because these structures are not permeable to cells under physiological conditions [16]. However, ECM degradation must occur in a controlled fashion. Sufficient ECM must remain, after degradation, so that neoplastic cells still have the ability to adhere and generate the traction required for migration.

Integrins are involved in the regulation of proteolytic enzymes that degrade the basement membrane and thereby facilitate invasion [16, 26]. The matrix metalloproteinases (MMPs) are the main proteases that are involved in remodelling of the ECM [66]. Stromal cells close to the invasive front of metastatic breast tumours have elevated levels of matrix metalloproteinase activity compared with non-malignant control cells [67]. MMPs are secreted as inactive zymogens (pro-MMPs) that require proteolytic activation by extracellular proteases. This mechanism of activation permits precise regulation and localisation of MMPs, and integrins have

been shown to play a central role: MMP-2 is activated on the cell surface by a multimeric complex that is composed of MMP-2, membrane type 1 MMP (MT1-MMP) and tissue inhibitor of metalloproteinase 2 (TIMP2) [26, 66]. Zymography, competitive adhesion assays and immunohistochemical co-localisation experiments, on melanoma and glioma cell lines, indicate that this multimeric MMP-activating complex also includes the integrin αvβ3 [68, 69]. MMP-2 initially binds to TIMP2, which sequentially combines with the *transmembrane* metalloproteinase MT1-MMP. Following this, MT1-MMP cleaves the amino-terminal pro-domain of MMP-2, resulting in an intermediate, partially active form. This intermediate form is capable of binding integrin αvβ3, at the leading edge of the cell surface. This interaction fully activates MMP-2 and thereby *localises* its proteolytic activity to the invasive front of cells [26].

I have mentioned already that ECM degradation must occur in a controlled fashion. ECM degradation must allow passage of the neoplastic cell through impermeable basement membranes to promote migration; but excessive ECM degradation would reduce potential cellular traction and inhibit migration [70]. A negative-feedback regulation of ECM degradation has been proposed in the regulation of integrin and protease interactions [26, 71]. An auto-proteolytic fragment of MMP2 (haemopexin-like domain), termed PEX, is one such regulatory mechanism. PEX can compete with MMP-2 for αvβ3 combination and thereby block full protease activation [72]. In addition to these effects upon the motile behaviour of tumour cells it also is recognised that growth factors, sequestered in the extracellular matrix, are liberated by MMP activity leading to increased cancer cell proliferation; an aid to invasive activity [73].

Therefore, αvβ3's role in tumour invasion and metastasis seems partly to involve MMP-2 control and might explain the αvβ3-facilitated transition from radial to vertical phase of growth, in melanomas [74]. This vertical growth assists in penetration of the basement membrane and thus invasion of the underlying stroma. αvβ3 also associates with the urokinase plasminogen activator (uPA) receptor, uPAR [75]. Activated uPA converts plasminogen to plasmin. Plasmin, a broad-spectrum protease, is able to degrade ECM components both directly and through the activation of MMPs. Therefore, this integrin association provides a further mechanism to recruit proteolytic activity to the leading edge of migrating cancer cells (see **Figure 12**).

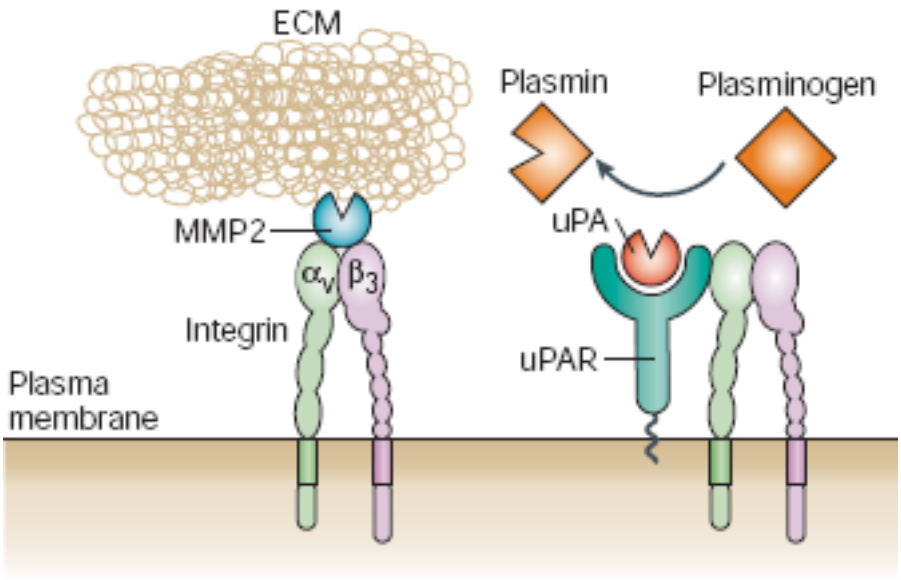

Figure 12 Integrins, Matrix Degradation And Remodelling. *Taken from Guo and Giancotti [16]*

Integrins also regulate matrix degradation and MMP expression through signalling mechanisms (i.e. not just by physical association and thus recruitment of protease to the cell surface). As described in the **Outside-In Signalling** section, integrins can signal through FAK and transient recruitment of Src-family protein tyrosine kinases. Hauck et al examined FAK signalling outcomes by performing experiments on Rous sarcoma virus-transformed NIH-3T3 fibroblasts and transfecting FRNK (a dominant negative protein of FAK) [76]. The authors used immunoprecipitation, *in vitro* kinase assays and semi-quantitative RT-PCR to show that FAK-mediated activation of ERK2 and JNK enhances gene transcription of MMP2 and MMP9. Zymography confirmed increased secretion of MMP2 and MMP9, as a result of FAK signalling. Hauck hypothesised that this is an important mechanism for integrins to enhance tumour invasion and metastasis, as seen in their *in vitro* invasion assays and *in vivo* models [76].

Furthermore, remodelling the ECM exposes new cell-binding sites, which promotes the migration of tumour cells. For example, cleavage of collagen IV by MMPs exposes a cryptic αvβ3-binding site, which is important for the migration of αvβ3-expressing endothelial cells and impacts on tumour angiogenesis [16]. Therefore, αvβ3-aided activation of MMP2 encourages local matrix degradation and invasion, but also contributes to the generation of new αvβ3-binding sites, and thus promotes migration.

1.3.3 Migration

Cell migration is a complex multi-step process that requires the continuous, coordinated formation and disassembly of adhesions [77]. Integrin-dependent modifications of the actin cytoskeleton are necessary for cell migration, via the Rho-family GTPases [78].

Initially, cells project filopodia. A filopodium is a long, thin membrane projection at the leading edge of the cell in the direction of movement. They are composed of F-actin bundles and merge into lamellipodia. Actin polymerisation (through Rac) induces extension of filopodia / lamellipodia and this process is facilitated by a localised decrease in membrane tension [79]. Lamellipodia attach to the ECM and simultaneously the cells break existing ECM contacts at their trailing edge.

The interaction of integrins with the extracellular matrix stabilises this attachment / adhesion, by recruiting FAK signalling, phosphorylation of cytoskeletal proteins and alterations in gene expression [77]. It has become evident that cell direction and motility are dependent on integrin-mediated Cdc42, ERK/MAPK and JNK signalling [80].

At the rear of migrating cells, the release of adhesions results in retraction of the cell (‘rear retraction’) and a net movement of the cell forward. Rho stimulates the congregation of actin-myosin fibres, and their subsequent contraction, which contributes to rear retraction [16, 78]. Retraction of the trailing cell edge is dependent on the adhesive environment and occurs either by intracellular fracture of cytoskeleton-integrin bonds in highly adhesive environments (during slow migration), or by simple extracellular dissociation of integrin–extracellular matrix

linkages, in less adhesive environments (during fast migration) [77, 81, 82]. Therefore, integrins carry out essential roles during cell migration (normal and neoplastic).

Alterations in the expression of integrins also can promote migration. Certain neoplastic cells lose the integrins that secure their adhesion to the basement membrane and maintain or overexpress the integrins that foster their migration. Alternatively, other integrins become phosphorylated, affecting their cytoskeletal and extracellular ligand binding properties [23]. As mentioned already, the changes in integrin expression and the alteration in their cell surface distribution seem to be specific to the tumour cell type.

In addition, there is evidence indicating that integrin receptors associate with other receptors to promote migration, through collaborative signalling. Both EGF [83] and Met [84] receptors induce tyrosine phosphorylation of the β4 cytoplasmic tail. This action converts α6β4 from a pro-adhesive to a pro-migratory receptor, through disassembly of hemidesmosomes, activation of kinase signalling cascades and recruitment of adaptor molecules e.g. PI3K and SHC [16, 84].

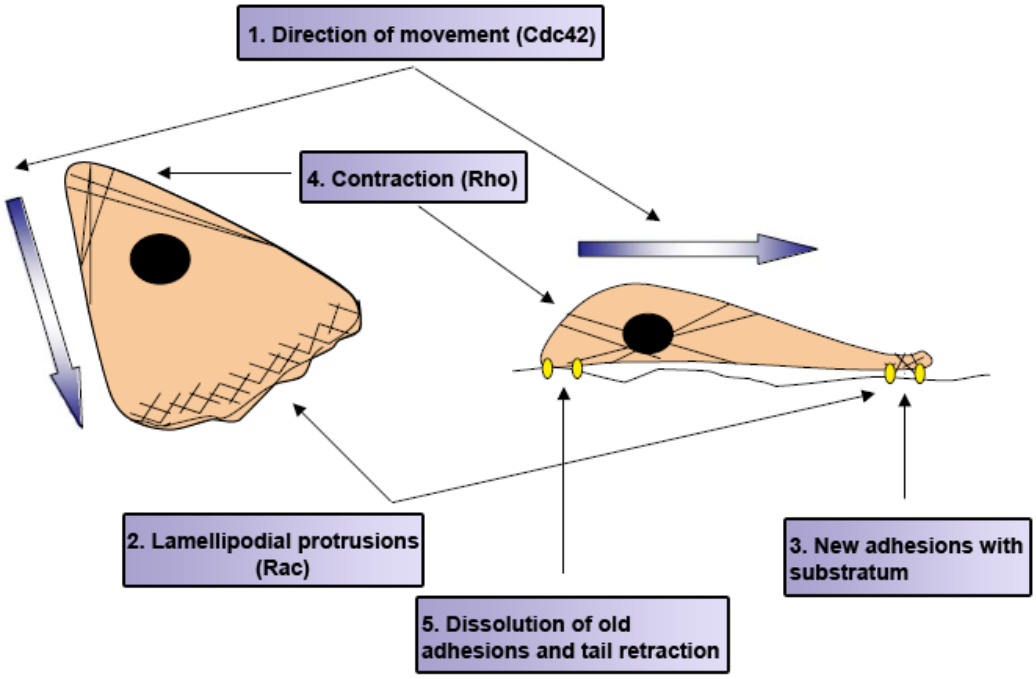

Figure 13 Cell Migration, Integrins and Rho-family GTPases. *Taken and adapted from Raftopoulou and Hall [78].*

Furthermore, neoplastic cells can increase their migratory potential, through altering their adhesiveness, in a manner which increases the affinity of their integrins. Selective blocking of 'high-affinity αvβ3', for example, has been reported to impair the directed migration of endothelial cells [85].

1.3.4 Dissemination

The process of metastasis involves cells breaking away from their primary tumours in the tissue of origin. It necessitates all of the processes described above and therefore is likely to involve dependence on integrin manipulation. Furthermore, metastatic cells must induce angiogenesis to escape the limits that passive diffusion of nutrients and oxygen impose on expansive tumour growth [86]. The vicious cycle is completed by the fact that neovascularisation provides a further gateway for tumour cells to enter the circulation and 're-seed'. Integrins have a well-documented role in tumour angiogenesis [87]. It seems that integrins are targets of both angiogenic activators (e.g. VEGF) and inhibitors (e.g. endostatin). The combination of integrins and these factors influences angiogenesis. However, the extensive literature research in integrins and angiogenesis [88] or lymphangiogenesis is beyond the scope of this review. Instead, this section will continue with survival and homing mechanisms during dissemination. Tumour cells are subjected to tremendous shear forces on entering a turbulent vascular system. Integrins and other adhesion molecules permit adhesion of neoplastic cells to leukocytes and platelets [89]. This potentially protects the tumour cells from the shear forces and fashions small tumour emboli, promoting dissemination.

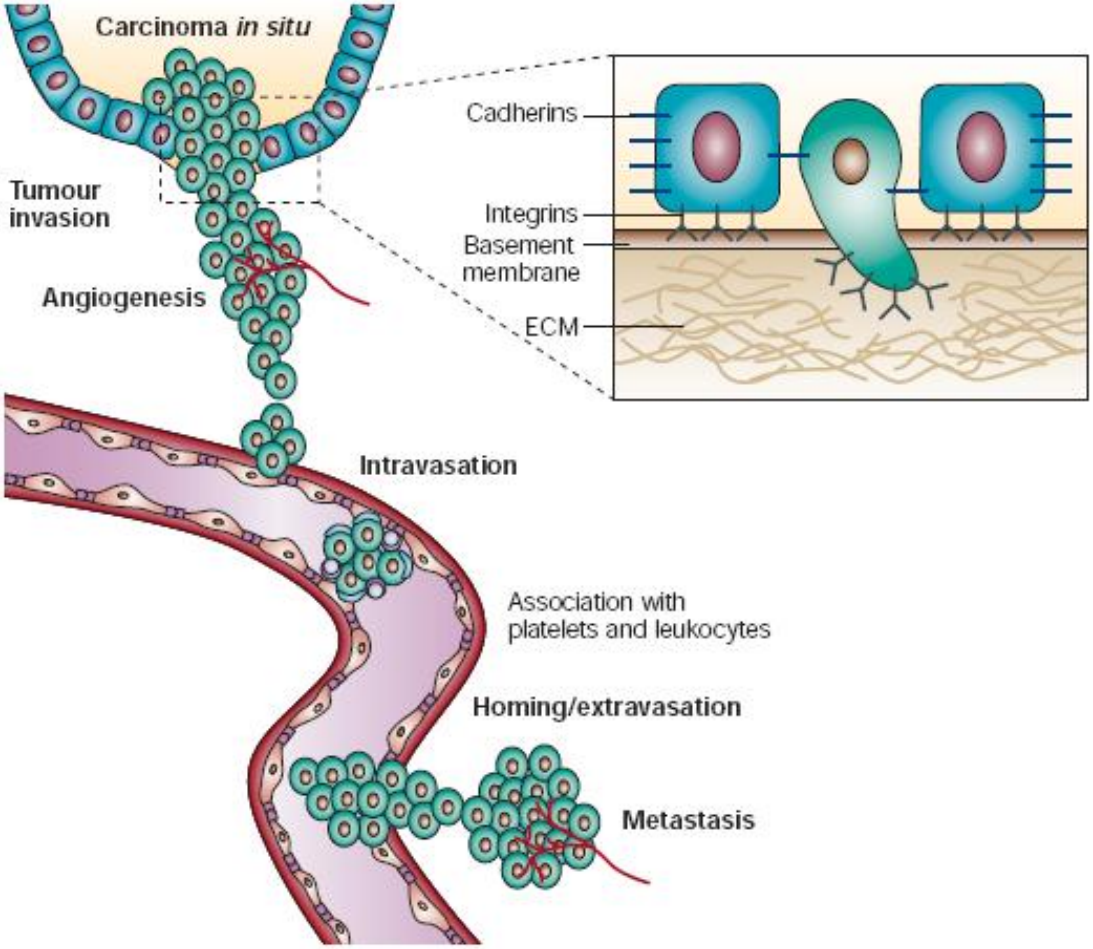

Figure 14 Homing of Neoplastic cells to Target Organs. *Taken from Guo and Giancotti [16]*.

Most cancers have a characteristic dissemination pattern, with a predilection to metastasise to certain organs [90]. For instance, breast cancer tends to have a predilection to metastasise to the liver, bone and lungs; and rarely to the kidneys and spleen, despite the good blood supply of these organs. Stephen Paget first proposed the existence of this non-random pattern to metastasis and introduced his 'seed and soil' theory, in 1889 [91]. That is, some organs provide a more fertile milieu, compared to others, for the growth of certain metastases. This suggests that metastasis depends on cross-talk between selected cancer cells (the 'seeds') and

specific organ microenvironments (the 'soil'). This is in direct contrast to James Ewing's theory, which suggested that dissemination occurs by purely anatomic pathways and mechanical mechanisms e.g. calibre of capillaries [92]. It was only in the 1980s, that Paget's original theory was proven. Ian Hart and Isaiah Fidler used a C57BL/6 mouse model, in which kidneys, ovaries and $1mm^3$ lung fragments were transplanted into the quadriceps femoris muscle of syngeneic mice. After a 2- to 3-week recovery period (to allow wound repair and organ vascularisation), these mice bearing transplants had intravenous injections of 5×10^4 viable B16 melanoma cells. Three weeks following injection, the mice were killed and autopsied. Metastases in the *in situ* organs and grafted organs were determined under a dissecting microscope. Furthermore, metastases in the grafted organ sites were confirmed histologically. Results revealed that metastatic lesions developed in lungs and ovaries and this was reflected in the grafts of pulmonary or ovarian tissue, whereas they failed to develop in control grafts of similarly implanted renal tissue or at the site of a surgical trauma. Since renal grafts appeared to survive and vascularise as well as lung or ovarian grafts, it seemed that there was a distinct organ preference for tumour growth [93]. The authors also illustrated that radiolabelled tumour cells may indeed reach and be arrested in the microvasculature of many organs and were equally likely to be trapped in the kidney tissue as in either of the other transplants. Nevertheless, tumour cell proliferation into visible metastases still only occurred in some but not all organs [93, 94]. This indicates that sites of metastasis are determined not solely by the characteristics of the neoplastic cells but also by the microenvironment of the host tissue.

‘Homing’ to target organs requires adhesion within the vasculature of the arresting tissue. This adhesion will need to arrest the tumour cell during blood flow, and may protect cells from its shear forces, and permit extravasation. Integrins, and their adhesive capacity, have been implicated in this cell arrest. The site of tumour cell metastasis is influenced by the composition of the extracellular matrix (ECM) and the integrins expressed by the tumour cells [95] (see **Figure 14**). Furthermore, the complex of tumour cells, leukocytes or platelets provides additional adhesive mechanisms. That is, the integrins expressed on leukocytes and platelets can home the complexed tumour cell embolus to the target organ. Therefore, the various activated integrins expressed on the tumour cell complex will have a predilection to bind to certain ligands in the extracellular matrix. The distribution of these extracellular ligands, in the capillary beds of visceral organs, may help account for the characteristic metastatic pattern of certain cancers.

1.3.5 Survival mechanisms during Invasion and Metastasis

Neoplastic cells require various survival mechanisms to promote continued existence within the different microenvironments of metastatic sites. Lack of extracellular adhesion (a feature during parts of the metastatic cascade) induces normal cells to undergo anoikis. This anchorage dependence survival of cells, and its reliance on various integrin-related signalling pathways, has already been mentioned. Cells that have undergone neoplastic transformation are much less dependent on ECM adhesion for their survival and proliferation [34]. One mechanism of anchorage independence may lie with the formation of constitutive complexes between integrins and RTKs. Trusolino *et al* have reported that Met forms a selective

complex with the α6β4 integrin, using immunoprecipitation, immunoblotting and immuno-histochemistry studies to establish the existence of this interaction [84]. Upon HGF stimulation of Met, α6β4 is tyrosine phosphorylated and Shc and PI3K recruitment occurs. This signalling recruitment provides an additional signalling platform that amplifies HGF-triggered activation of Ras- and PI3K-dependent pathways. Interestingly, the authors also looked at the necessity for integrin ligation to provide HGF-potentiation. A β4 mutant subunit was produced, which was devoid of most of the normal extracellular domain and thus incapable of binding laminins. Remarkably, HGF activation could still be potentiated, in the presence of the mutant subunit, as efficiently and durably as with wild-type β4. The fact that α6β4 signals are independent of cell adhesion but contingent on tyrosine kinase activation suggests that neoplastic cells might evade matrix dependence by turning integrins from adhesive devices into non-adhesive integrators of oncogenic signalling pathways [84].

Nevertheless, despite their relative anchorage independence, neoplastic cells still benefit from integrin signals, during tumourigenesis. Integrin binding to ECM ligands initiates several pro-survival mechanisms to prevent apoptosis. Multiple mechanisms have been proposed which include FAK signalling mediated inhibition of caspase-8 [96], fibronectin binding to α5β1 with resultant *bcl-2* up-regulation [97], or NFκβ activation after laminin-induced ligation of β4 integrin [98]. These studies reveal that ligation of integrins can protect against exogenous apoptotic insults in cancer cells that are *already* capable of anchorage-independent survival.

1.4 αvβ6

In this study I have chosen to concentrate on only one integrin associated with tumour progression: αvβ6. The gene for the αv subunit is coded at chromosome 2q31-q32 and the protein is 150kDa [99]. The β6 subunit was first identified in cultured epithelial cells as part of the αvβ6 heterodimer [100] and its human gene regional localisation is chromosome 2q24-q31 (see **Figure 15**). The β6 subunit is 100 – 110 kDa [99] and its cytoplasmic domain is required for linking integrins to the cytoskeleton [12].

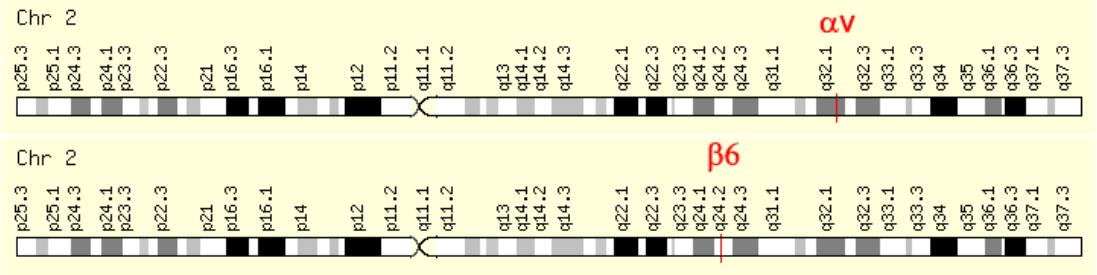

Figure 15 Genomic loci of the αvβ6 subunits. *Taken and adapted from http://www.genecards.org.*

1.4.1 Transcriptional Regulation of αvβ6

Bates *et al* first described Ets-1 as a transcription regulator of the β6 integrin, using luciferase assays [101]. The authors identified 4 potential consensus Ets-binding sites in the first 1 kb of the human β6 promoter (see **Figure 16**). However, gel shift assays and site-directed mutagenesis revealed that Ets-1 only bound strongly

to site 1. Furthermore, Scott et al used Tumour Necrosis Factor-α-deficient (TNFα-/-) mice to demonstrate that αvβ6 is upregulated by TNFα [102]. A GEArray™ Original series kit was incorporated to expression profile the TNFα-/- keratinocytes and compare them to wild-type keratinocytes. TNFα-/- keratinocytes expressed significantly less αvβ6 mRNA than wild-type keratinocytes, and this correlated with reduced β6 protein as assessed by immunoblot. Scott showed that administration of exogenous TNFα to TNFα-/- keratinocytes upregulated αvβ6 protein, in a dose-dependent manner [102]. In an earlier paper, Bates and Mercurio reported that Transforming Growth Factor-β worked synergistically with TNFα to increase levels of αvβ6 [103]. It has been suggested that both these cytokines work via the Ets-1 transcription factor [104], however further research is required before confirmation of this relationship is achieved.

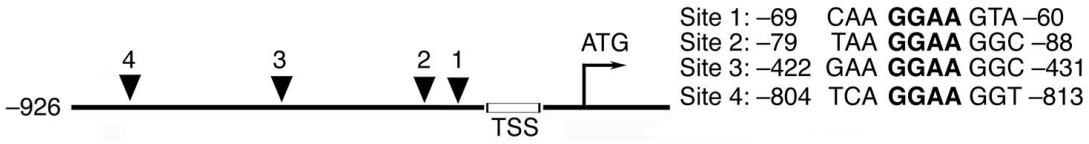

Figure 16 Schematic of the human integrin β6 promoter. The transcription start site (TSS) and translation start site (ATG) are indicated. Putative Ets-binding sites are shown (triangles), and the 4 corresponding sequences are listed, including location detail. The consensus DNA-binding sequence (GGAA) is shown in bold. *Taken from Bates et al [101]*.

Azare et al used Affymetrix analysis, quantitative PCR, luciferase assays and short hairpin RNA experiments to show that signal transducer and activator of transcription 3 (STAT3) mediates transcriptional regulation of β6 [105]. The authors examined the β6 promoter and discovered numerous STAT3 binding recognition sites (see **Figure 17**) and confirmed this with cross-linking immunoprecipitation assays. Indeed, Azare established upregulated β6 protein translation, as a result of this increased transcription, using immunoblotting, flow-cytometric and immuno-histochemical experiments. Functionally, the resultant increased β6 protein expression led to increased cell migration and anchorage independent growth [105]. Interestingly, the same paper revealed that STAT3 also transcriptionally regulates fibronectin and Tenascin C (known αvβ6 ligands, described in the next section).

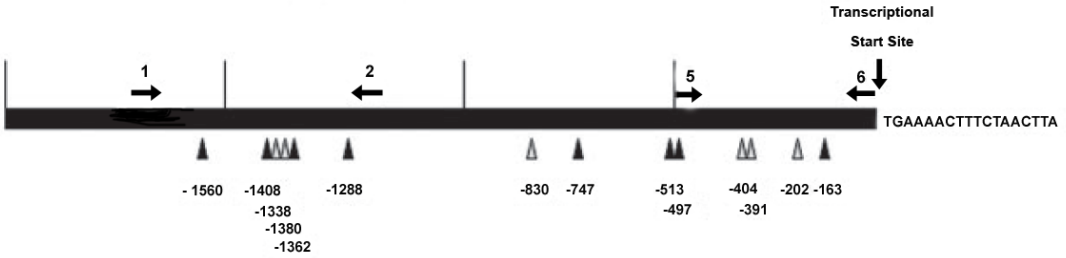

Figure 17 Schematic of the human integrin β6 promoter. Potential Stat3 binding sites are indicated as triangles; those marked by dark triangles are optimal (TTN_5AA) and those marked by light triangles have either a TTN_4AA or a TTN_6AA sequence or an AT-rich region at the N positions on the β6 promoter. Arrows indicate the directions of transcription, and nucleotide positions are shown below the diagram. *Taken from Azare et al [105]*.

1.4.2 αvβ6 Ligands

αvβ6 binds to a number of ECM proteins, including fibronectin, tenascin-C, vitronectin, all via their tripeptide recognition sequence arginine-glycine-aspartic acid (RGD). In addition, TGF-β LAP isoforms 1 [106] and 3 [107] are ligands for αvβ6 and binding can lead to latent TGF-β activation. Furthermore, αvβ6 also mediates virus binding, internalisation and, thus, infection of foot-and-mouth disease, via its RGD-containing capsid protein [108]. The αvβ6 ligands will be described briefly in the following section:-

1.4.2.1 Transforming Growth Factor- β (TGF-β)

In mammals, there are three isoforms of TGF- β; TGF- β 1, 2 and 3, each of which is the product of a separate gene. The TGF-β cytokine family is involved in the regulation of cell proliferation, differentiation, migration, survival, extracellular matrix synthesis, angiogenesis and apoptosis [109]. In normal circumstances, TGF- β is anti-mitogenic and thereby inhibits epithelial cell proliferation with induction of extracellular matrix component production. Excessive TGF-β activity will lead to exaggerated scar formation / granulation and subsequent loss of function [110]. Conversely, reduced TGF- β activity will lead to increased epithelial cell proliferation, and this may include cancerous cells. TGF-β has been implicated in normal embryonal development, tissue repair and modulation of the immune system. Therefore, the location and concentration of TGF- β needs to be controlled tightly for these processes to function appropriately.

One mechanism involved in the rigid control of TGF-β is that the isoforms initially are secreted in an inactive or latent form [111]. The latent form arises from their synthesis in union with latency associated peptide (LAP). This product is cleaved in the endoplasmic reticulum (by the endoprotease furin) and assembled into a double homodimer (non-covalent) association of TGF-β with LAP, termed the small latent complex (SLC). In this latent form, TGF-β cannot interact with its receptors. However, LAP enhances proper folding and secretion of TGF-β [112]. If LAP is disulphide linked to another protein family, latent TGF-β binding proteins (LTBPs), the resulting complex is termed the large latent complex (LLC). The LTBPs are usually directly cross-linked to fibronectin in the extracellular matrix (see **Figure 18**). Thus, this protein targets latent TGF-β to the extracellular matrix and thereby can exert a degree of control on its location. Investigators have shown that latent TGF-β can be released from the matrix by limited proteolysis of LTBP, by proteases such as thrombin, mast cell chymase, neutrophil elastase and plasmin [111]. These molecules suggest the processes of matrix remodelling or inflammation are indirectly linked with TGF-β activation. Structural features of LAP and/or LTBP allow the latent complex to associate with the cell surface and potentially become activated – 'latent activation of TGF-β'. Two mechanisms of TGF-β activation have been shown definitively to be important *in vivo*: interaction with the secreted protein thrombospondin 1 [113] and activation by the integrin αvβ6 [106]. LAP is a high affinity ligand for αvβ6, but requires an intact cytoskeleton for TGF- β activation. However, because mice lacking both thrombospondin 1 and αvβ6 are born alive and manifest phenotypes considerably more mild than the phenotypes of mice

homozygous for null mutations of TGF-β 1, 2, or 3, it is clear that additional mechanisms of TGF-β activation must play important roles *in vivo* [114].

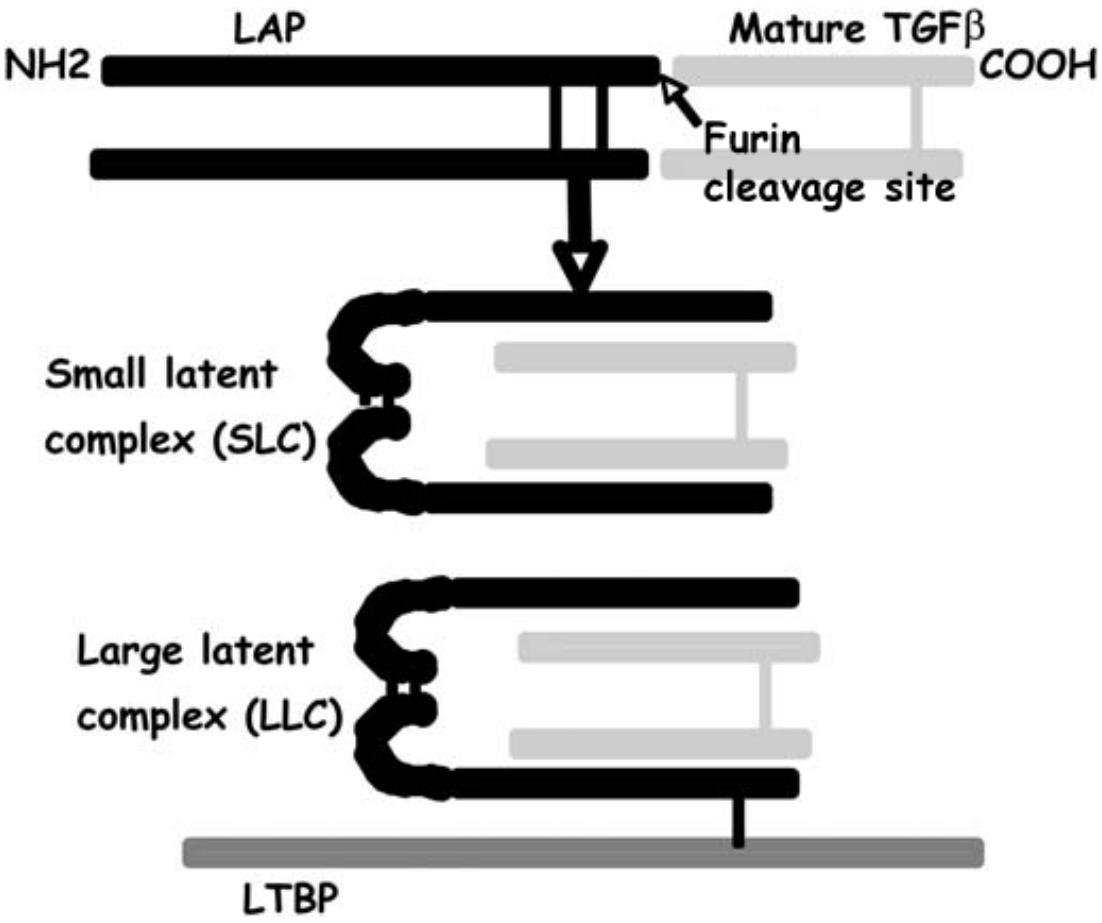

Figure 18 Schematic representation of organisation of latent complexes of transforming growth factor-β (TGF- β). *Taken and adapted from Sheppard D [115].*

Once activated, all TGF-β isoforms have the ability to bind to transmembrane serine / threonine kinase receptors (TβR) [116]. The binding initiates a cascade of cytosolic kinase phosphorylation and involves signal transduction though the activation of the SMAD family of proteins. In mammalian cells, SMAD4 forms complexes with SMAD2 and SMAD3 after activation with TGF-β [117]. In the resting cell, SMADs are localised in the cytoplasm. Stimulation with TGF-β leads to translocation of SMADs to the nucleus, binding (indirectly or directly) to DNA and thus can affect transcription of various genes [118]. However, SMAD6 and SMAD7 function as inhibitors of TGF-β – 'Inhibitory SMADs'. They bind to TβRs and interfere with the phosphorylation of the pathway-restricted SMADs (see **Figure 19**). Consequently, active heteromeric SMAD complexes are not formed. Inhibitory SMADs may act as autoregulatory negative-feedback signals in the signal transduction of the TGF- β family.

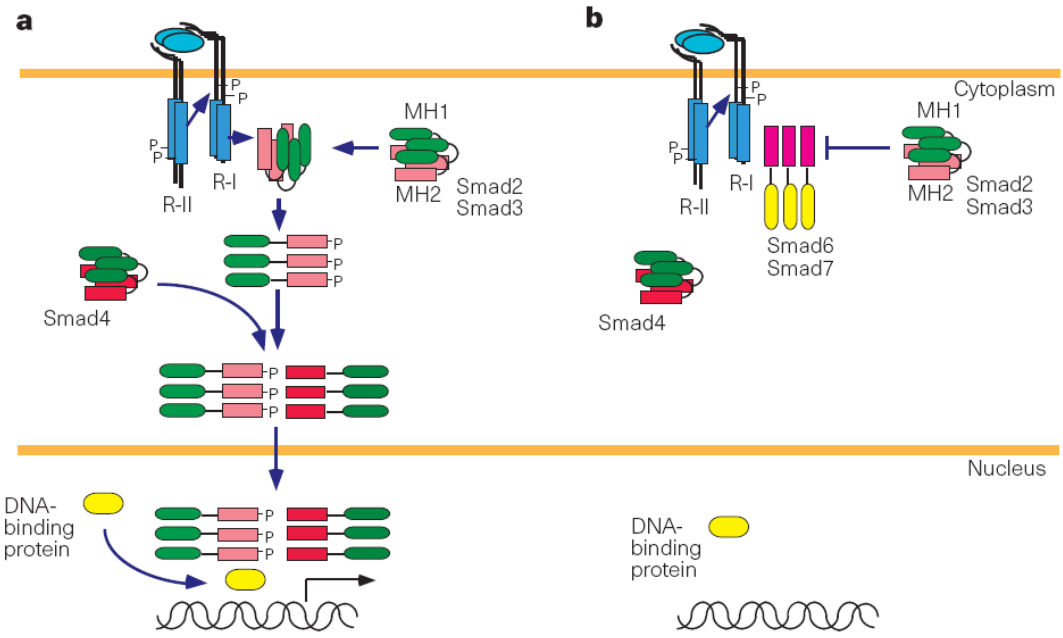

Figure 19 SMAD Protein and Signalling. Agonistic and antagonistic SMAD proteins in TGF-β signalling. **a**, A hypothetical signal transduction pathway for TGF-β. TGF-β binding leads to the assembly of a heterotetrameric receptor complex in which the type II receptor phosphorylates and activates the type I receptor. Pathway restricted SMADs (Smad2 and Smad3), which may be anchored in the cytoplasm in homotrimeric forms, are phosphorylated, which leads to heteromerisation with Smad4, a common-mediator SMAD. The hetero-oligomeric complex is then translocated to the nucleus, where it binds, directly or in complex with other component(s), to DNA and affects transcription of specific genes. Note that it is not known if the hetero-oligomer between Smad2, Smad3 and Smad4 is a hexamer or has another stoichiometry. **b**, Inhibitory SMADs (Smad6 and Smad7) bind to the receptors, and prevent the phosphorylation and signalling activity of pathway-restricted SMADs. Whether inhibitory SMADs occur as monomers or multimers is not known**.** *Taken from Heldin, Miyazono and ten Dijke [109].*

1.4.2.2 Foot-And-Mouth Disease Virus (FMDV)

Foot-And-Mouth Disease Virus is a member of the Aphthovirus genus in the Picornaviridae family. It is a highly contagious, and sometimes fatal, viral disease which commonly affects cloven-hoofed animals [119]. Foot-and-mouth virus has been shown to infect cells, in culture, via αvβ1 [120], αvβ3 [121], αvβ6 [108] and αvβ8 [122]. However, Monaghan *et al* provided evidence that αvβ6 is the major FMDV receptor, *in vivo* [123]. Berryman *et al* showed that αvβ6-mediated infection of SW480 cells by FMDV is dependent on an RGD interaction [108], a clathrin-dependent endocytosis and active endosomal acidification [124].

1.4.2.3 Fibronectin

Fibronectin is a high-molecular-weight glycoprotein and is a major component of the ECM. It binds cell surfaces (via integrins) and various ECM compounds including collagen, fibrin, and heparan sulphate [125]. Fibronectin has several isoforms and has been implicated in cell adhesion, cell migration [99], opsonisation, wound healing, and maintenance of cell shape. Fibronectin is an important ligand for αvβ6, and therefore their interaction can influence a wide variety of essential functions. Busk *et al* described the formation of 'focal contacts', upon interaction of αvβ6 with fibronectin [99]. The authors performed immunoprecipitation and affinity chromatography on pancreatic cancer cell line lysates and showed that fibronectin binding was cation-dependent.

1.4.2.4 Vitronectin

Vitronectin is an extracellular glycoprotein and is a member of the pexin family. Vitronectin is found abundantly in serum and the extracellular matrix; promoting cell adhesion and spreading, inhibiting the membrane-damaging effect of the terminal cytolytic complement pathway, and binding to several serpin serine protease inhibitors [126]. These functions have implicated vitronectin to be important in homeostasis regulation and tumourigenesis. Vitronectin contains an RGD sequence and is thus recognized by certain members of the integrin family. Huang *et al* initially described keratinocyte migration to vitronectin [127]. Huang utilized keratinocytes expressing a null mutation in the β6 subunit, 'β*6-/-*'. Both adhesion and migration of these keratinocytes to vitronectin-coated membranes were reduced dramatically, as compared to cells from wild-type mice. Furthermore, adhesion and migration of keratinocytes from wild-type mice was decreased to the same extent, when in the presence of antibody 10D5 (function-blocking monoclonal to αvβ6). Their data suggest that αvβ6 plays a critical role in keratinocyte adhesion and migration on vitronectin, probably though the protein kinase C pathway [127].

1.4.2.5 Tenascin-C

Tenascins are a highly conserved family of ECM glycoproteins, in vertebrate organisms [128]. Tenascin-C is one of at least five members of the tenascin family, and currently is the best understood [129]. Tenascin-C is detectable only in small amounts in normal adult tissues, but is abundantly detected during embryogenesis and in tissue re-modelling processes (e.g. wound healing, neovascularisation and

tumourigenesis) [129]. Tenascin-C has been implicated in foetal lung development [129], the guidance of migrating neurons during embryogenesis, synaptic plasticity as well as neuronal regeneration [128, 130]. Many of these proposed functions of tenascin-C may be via its modulation of cellular adhesion and migration. Indeed, Prieto *et al* demonstrated that tenascin-C is able to mediate cellular attachment through αvβ6, using monoclonal antibodies and RGD-sequence-containing peptide experiments [131].

1.5 αvβ6 and Cancer

The epithelial-specific integrin αvβ6 is not usually detectable on normal, human, adult tissue but is upregulated during inflammation, development and on many different types of carcinoma [101, 132-138]. Indeed, Breuss *et al* reported that expression is strongest at the invasive edge of such expressing cancers [134]. Data from this and other laboratories have shown αvβ6 promotes carcinoma migration and invasion *in vitro* and *in vivo*. This may explain the data of Bates and colleagues [101] who reported that the hazard of dying was 60% higher in colon cancer patients with strong expression of αvβ6. Together these data could suggest that αvβ6 actively promotes cancer progression, possibly explaining the poor prognosis associated with expression.

Overexpression of αvβ6 has been reported in a broad spectrum of epithelial cancers. Oral, cutaneous, lung, breast, ovarian, pancreatic and other gastrointestinal cancers have all been associated with increased αvβ6 expression (see **Table 2**, page 75).

Carcinoma	Reference	Numbers of Carcinomas	% of Positive Tumours	Evidence	Comment
Oral Squamous Cell Cancer	Breuss et al (1995)	30	90	ISH	Absent αvβ6 expression in normal oral mucosa from same patients
	Jones et al (1997)	17	100	IHC	
	Hamidi et al (2000)	5	80	IHC	41% expression in oral leukoplakia peri-tumoural dysplasia also αvβ6 +ve
	Impola et al (2004)	11	100	ISH	Expression maintained in LN mets
	Regezi et al (2002)	40	100	IHC	αvβ6 expression colocalised with TN-C peri-tumoural dysplasia also αvβ6 +ve
Colon	Bates et al (2005)	488	37	IHC	Poor prognostic marker, avb6 expression maintained in mets
Pancreas	Sipos et al (2004)	34	100	IHC	Well differentiated tumours expressed more than poorly differentiated
Gastric	Kawashima et al (2003)	38	47	IHC , RT-PCR	94% αvβ6 +ve carcinomas had LN mets
NSCLC	Smythe et al (1995)	51	50	IHC	αvβ6 +ve carcinomas well-differentiate and node negative; ? Good prognostic marker
Breast	Arihiro et al. (2000)	90	18	IHC, WB	No grade 1 tumours αvβ6 +ve
Ovary	Ahmed et al (2002)	45	100	IHC	Staining correlated with grade; Benign mucinous tumours also αvβ6 +ve

Table 2 αvβ6 expression in carcinomas. *Adapted from [104].*

αvβ6 seems to be implicated in playing a key role in all parts of the metastatic cascade:-

1.5.1 Proliferation

Agrez *et al* revealed evidence that αvβ6 enhances the proliferative capacity of cancer cells [139]. The human colon carcinoma cell line, SW480, normally does not express the β6 subunit. The authors transfected the cell line with cDNA encoding for wild-type or truncated forms of β6, or the expression plasmid only. Cells were plated onto collagen-coated, three-dimensional culture systems with thymidine incorporation utilised as a means of quantifying proliferation at pre-arranged time-points. Results revealed that αvβ6 augments cell proliferation; at least when recipient cells were cultured in three dimensional collagen gels. Furthermore, this promotion of proliferation correlated with the presence of the unique 11 amino acid carboxy-terminal extension of the β6 tail [139]. Agrez *et al* showed that the proliferative advantage of wild-type β6-transfected cells was not simply a function of clonal variation, but related directly to the expression of this integrin sub-unit.

1.5.2 Invasion

Thomas *et al* [140] created a panel of squamous cell carcinoma (SCC) cell lines expressing various levels of αvβ6. Cells were resuspended in α-MEM and added to Matrigel-coated Transwell filters. Keratinocyte Growth Medium (KGM) was placed in the lower chamber and invasion measured after 72 hours. Results indicated that

increased expression of αvβ6 in malignant keratinocytes promoted invasion towards fibronectin [140]. This increased invasion was not due to differences in growth rates of cells in Matrigel, which were similar for all the SCC cell lines. Furthermore, invasion by the high αvβ6-expressing cell lines could be reduced dramatically using anti-αv or anti-αvβ6 antibodies.

The mechanisms for the increased invasion, seen with αvβ6-expressing cancer cell lines, involve increased protease secretion.

Thomas *et al* also demonstrated that increased expression of αvβ6, in the aforementioned panel of malignant keratinocytes, upregulates the type IV collagenases (MMP-9 and MMP-2), as shown by zymographic examination and ELISA [141]. Both MMP-9 and MMP-2 expression were reduced when high αvβ6-expressing SCC lines were incubated with αv or αvβ6 blocking antibodies. Furthermore, high αvβ6-expressing SCC invasiveness could be reduced significantly by anti-MMP-9 antibody, suggesting that MMP-9-dependent activities were the main drivers of invasion. Additionally, indirect immunochemistry revealed that MMP-9 localises to the terminal aspect of αvβ6-positive filopodia, suggesting a cellular mechanism for targeting MMP activity.

Similarly, Niu *et al* performed gelatin zymography experiments on SW480 colon carcinoma cells transfected with wild-type or truncated forms of β6, or the expression plasmid only [142]. The authors reported that neo-expression of αvβ6 in the cell line induces MMP (gelatinase B) secretion through the C-terminal cytoplasmic extension unique to the β6 integrin subunit, and that this ligand-independent event involves activation of the protein-kinase-C pathway. Furthermore,

this effect could not simply be explained by the relative amounts of αvβ6 present on cells expressing full-length β6 compared with truncated β6 transfectants [142].

Furthermore, Li *et al* studied a different β6-transfected SCC line [143]. Immunoprecipitation and *in vitro* kinase assays were performed. Upon fibronectin stimulation, Fyn (a member of Src family kinases) was activated and formed a complex with FAK and β6. A cascade of activation occurred involving FAK and the Shc adaptor protein. Thus Shc recruited the Grb2-mSOS complex and thereby activated the Raf-MAPK pathway. Luciferase assays revealed that β6-mediated Fyn signalling up-regulates the expression of the MMP-3 gene, via MAPK [143].

1.5.3 Migration

Huang *et al* apparently demonstrated a critical role for αvβ6 in cell migration (comparing murine wild-type keratinocytes with mouse β6-/- keratinocytes) on both fibronectin and vitronectin [127]. However, Thomas *et al* looked specifically at carcinoma cell migration and αvβ6 expression [140]. Haptotactic SCC migration assays were performed using fibronectin-coated Transwell filters. The results indicated that increased expression of αvβ6 promoted migration towards fibronectin. Again, for these cell lines, differing proliferation rates did not seem to confound the results. Furthermore, antibodies against αvβ6 could significantly inhibit migration towards fibronectin. This implies that high αvβ6 expression is associated with a more migratory phenotype.

Li *et al's* experiments (described above [143]) also demonstrated increased SCC migration towards fibronectin, *in vitro*. The authors showed that Fyn activation, by β6 adhesion to fibronectin, correlated with this increased migration [143].

1.5.4 Dissemination

Mutations in the various TGF-β signalling components have been implicated in the spread of cancer. TGF-β has a bi-phasic role in tumourigenesis. At early stages, when cells still respond to its anti-mitogenic effect, TGF-β may act as a tumour suppressor. However, during malignant progression, when cells acquire insensitivity to growth inhibition by TGF-β, it may function as a tumour promoter by stimulation of angiogenesis, immunosuppression and synthesis of extracellular matrix, which provides an appropriate microenvironment for rapid tumour growth and metastasis [144].

The transition of epithelia into mesenchyme occurs during embryogenesis, tissue remodelling and wound repair by a process known as the epithelial-mesenchymal transition (EMT) [145]. This multi-step process has also been hypothesised to occur during neoplasia and tumour progression (see **Figure 20**) [146]. The mechanism involves loss of cell-to-cell junctions and reorganisation of the cytoskeleton, which together result in the loss of apical-basal cell polarity and the acquisition of spindle-shaped morphology [146]. Accordingly, it is associated with a decrease in epithelial-specific gene expression, notably E-cadherin, and the accrual of a mesenchymal-specific gene expression. The transition permits epithelial neoplastic cells to acquire a more migratory and aggressive phenotype. Eventually the mesenchymal cells may regain their epithelial phenotype, allowing settlement at a secondary site, through a mesenchyme-to-epithelium transition (MET). TGF-β has been proposed as an inducer of EMT [147, 148]. Therefore TGF-β, and its αvβ6-mediated latent activation, could play a central role in tumour progression. However, there is not a consensus agreement on the theory of EMT, since it

primarily has been inferred from highly artificial, two-dimensional, *in vitro* environments [149, 150]; with no dynamic vascular, endocrine or neurological contribution [151]. These studies presume that epithelial cells acquire spindle-cell morphology and neo-express mesenchymal markers, but the morphology of these cells is histologically indistinguishable from normal stromal cells. Furthermore, direct *in vivo* evidence for EMT in cancer is lacking and hence the occurrence of EMT in cancer remains speculative.

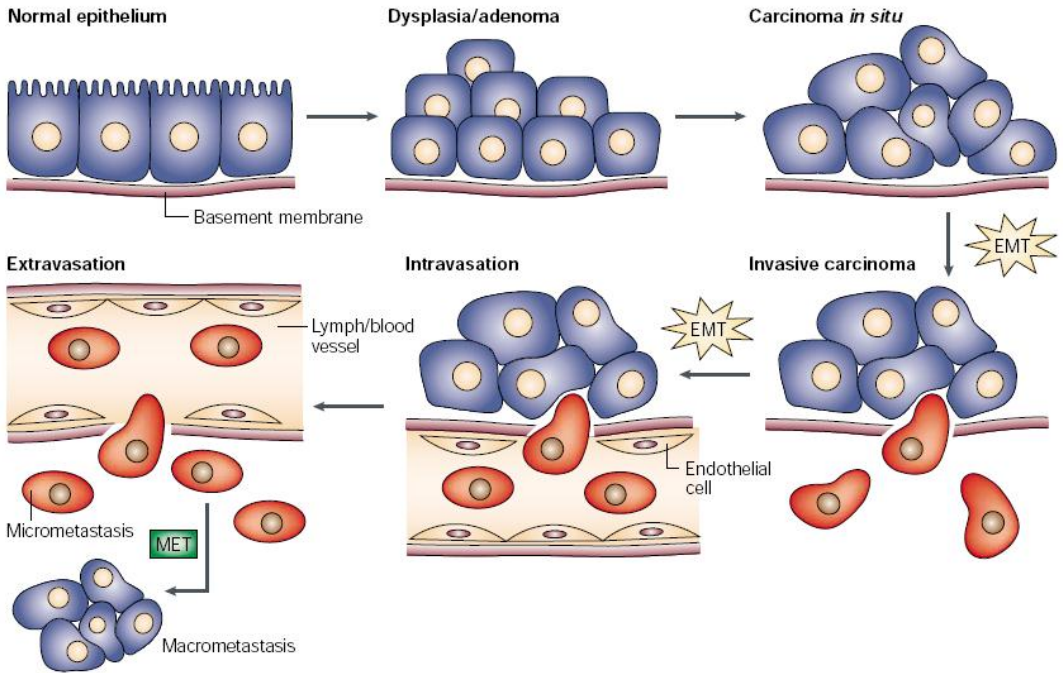

Figure 20 Epithelial to Mesenchymal Transition and a proposed mechanism for carcinoma progression. *Taken from Thiery JP [146].*

1.5.5 Survival mechanisms during Invasion and Metastasis

Oral keratinocytes naturally switch from αvβ5 to αvβ6 expression, at their cell surface, when they transform from normal to malignant phenotypes [133]. Jones and Watt initially transduced an αv-negative human SCC line with a retroviral vector containing the cDNA encoding the αv integrin subunit; and later created a further cell line by infecting with a second vector that contained cDNA which encoded the β6 subunit. β6 was weakly detectable in cells transduced with αv alone and was strongly expressed in cells transduced with both αv and β6, using Western Blot analysis [133]. Conversely, cells transduced with both αv and β6 no longer expressed surface αvβ5 (αvβ5 previously was readily detectable in cells transduced with αv alone). Flow cytometry indicated that all of the αv on the cell surface was now in an heterodimer with the β6 subunit. Western blot on proteins isolated from the double-transduced line was consistent with intracellular accumulation of β5 and incomplete glycosylation. Interestingly, the authors reported that *de novo* expression of αvβ6 seems to protect oral SCC from suspension-induced anoikis and that resistance to anoikis correlated with PKB/Akt activation [152]. The authors proposed that upregulation of αvβ6 in SCCs allows growth of tumour cells in the absence of a basement membrane [152].

In summary, αvβ6 has the potential to influence *in vivo* tumour growth in a variety of ways. Agrez *et al* showed that the β6 cytoplasmic domain (specifically an 11-amino acid region at the COOH terminus) is required for *in vivo* tumour xenograft growth, for the αvβ6-neo-expressing SW480 cancer cell line, within athymic mice [139]. Ahmed *et al* reported that the β6 cytoplasmic domain binds directly to ERK, and deletion of the ERK2 binding site on this domain inhibits tumour growth [153]. Li *et al* confirmed that expression of β6 promotes oral SCC tumour growth in nude mice. However, they also retrovirally over-expressed, KD-Fyn in β6-expressing SCC cell lines. KD-Fyn is a specific competitor for endogenous Fyn (Src family kinase). These murine experiments revealed that both local and metastatic tumour growth is dependent on Fyn activation, for β6-positive oral SCC cells [143].

Chapter II: Introduction to Imaging

2.1 Medical Imaging

Medical imaging is the scientific field in which non-invasive techniques are used to create internal and external images of the (human) body. There are a variety of imaging techniques, each with certain advantages and disadvantages over each other:-

2.1.1 Radiography: X-rays and Computed Tomography

Plain film radiography is the process of creating two-dimensional images using x-ray radiation. X-rays (a.k.a. Röntgen radiation) are a form of electromagnetic radiation, discovered by the Nobel prize-winning physicist, Wilhelm Conrad Röntgen, in 1895 [154, 155]. X-rays are emitted by electrons from outside of the nucleus and are forms of ionising radiation; that is, there is sufficient energy to potentially remove electrons from an atom, thus giving it a charge and making it an 'ion'. Ionising radiation has sufficient energy to penetrate human tissue and will be absorbed differentially according to its energy and to the density of the object [156]. If a 'cassette' is placed behind the object, which contains photographic film and two fluorescent intensifying screens, penetrating x-rays can produce a photochemical reaction [157]. However, areas of the object which have completely absorbed the x-rays will not permit a photochemical reaction in the corresponding area of the cassette. Therefore, the developed film will be a representation of the absorption pattern of the x-rays, and

thus a reflection of the different densities within the object (see **Figure 21**). This property of x-rays is used to differentiate areas of bone and soft-tissues within the human body. Consequently, plain film radiography can detect fractures and tumours, owing to differences in density from the surrounding tissue.

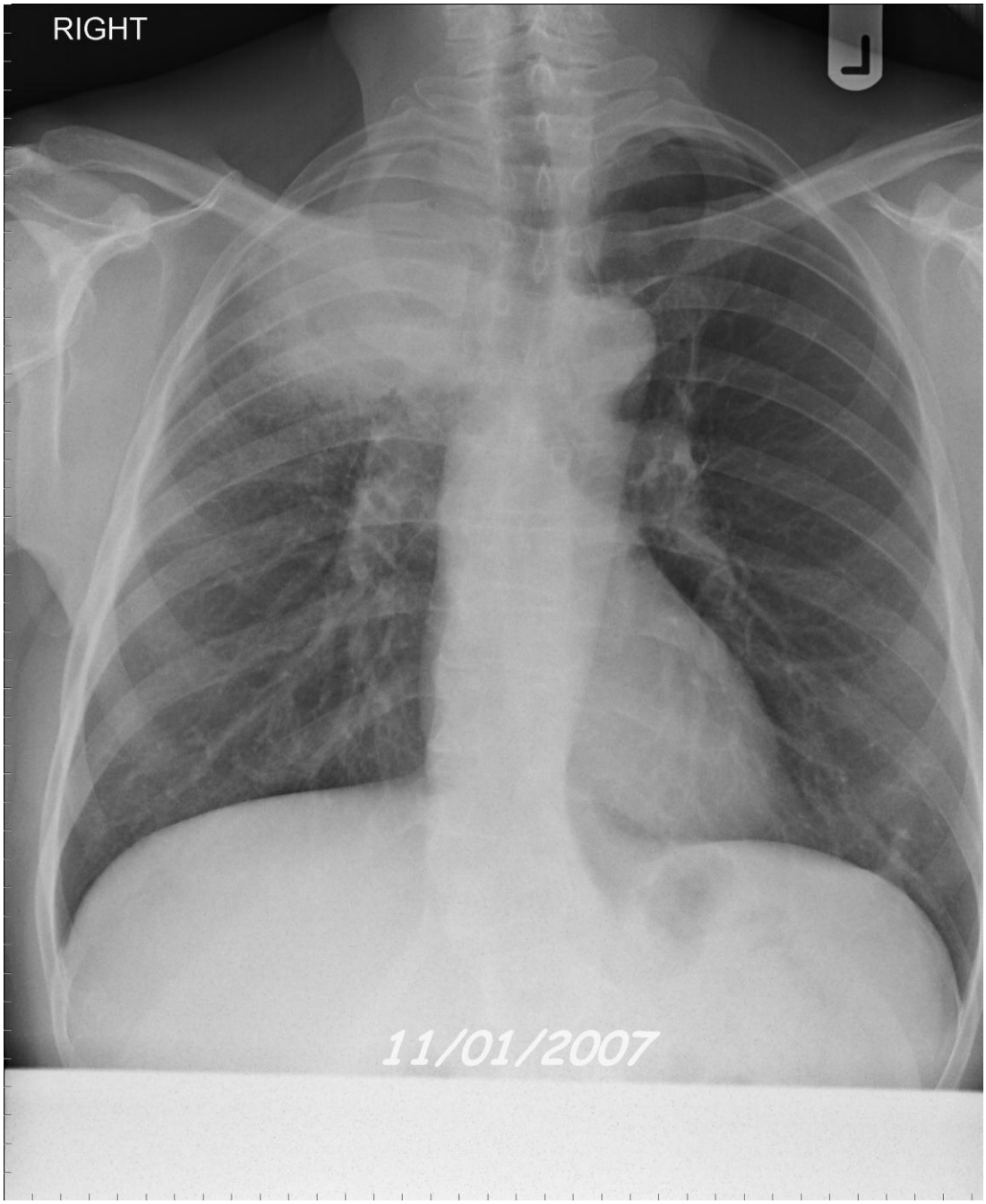

Figure 21 Plain chest radiograph showing a lesion in the apex of the right lung, later confirmed to be an adenocarcinoma.

One disadvantage of a plain radiograph is that it results from an image which presents x-ray absorption in one plane only. That is, structures that are in the same plane as the x-ray beam will be superimposed; thereby creating problems in differentiating these mono-planar entities. Therefore, the solution is to create a radiograph in a different plane, so that these structures no longer are in the same plane and thus not superimposed. Computed Tomography (CT) involves moving the x-ray source around the patient to create multiple radiographs at different angles, and replacing photographic films with digital images. Computers help reconstruct the multitude of radiographic absorption information into detailed cross-sectional images (see **Figure 22**). In other words, the pictorial arrangement of x-ray absorption values constructs the final CT image. Sir Godfrey Hounsfield conceived this idea of CT scanning in 1967 [158], and shared the Nobel Prize with Allan McLeod Cormack for their work on the conception and implementation of this approach [159]; to this day its scale for radiodensity (absorption values) is expressed in Hounsfield units. This technology enables a detailed study of closely-related structures within the body. Furthermore, the use of intravenous or oral contrast agents also facilitates distinction of anatomical boundaries and differentiation of tissue densities. Modern scanners allow absorption data to be reformatted into volumetric (3D) representations of structures [160]; giving highly detailed and several views of complex structures e.g. tumour deposits within organs. These detailed views can help guide surgeons with pre-operative decisions i.e. whether successful tumour resection is possible or potentially hazardous. However, this superior image quality and detail is at the expense of increased radiation exposure.

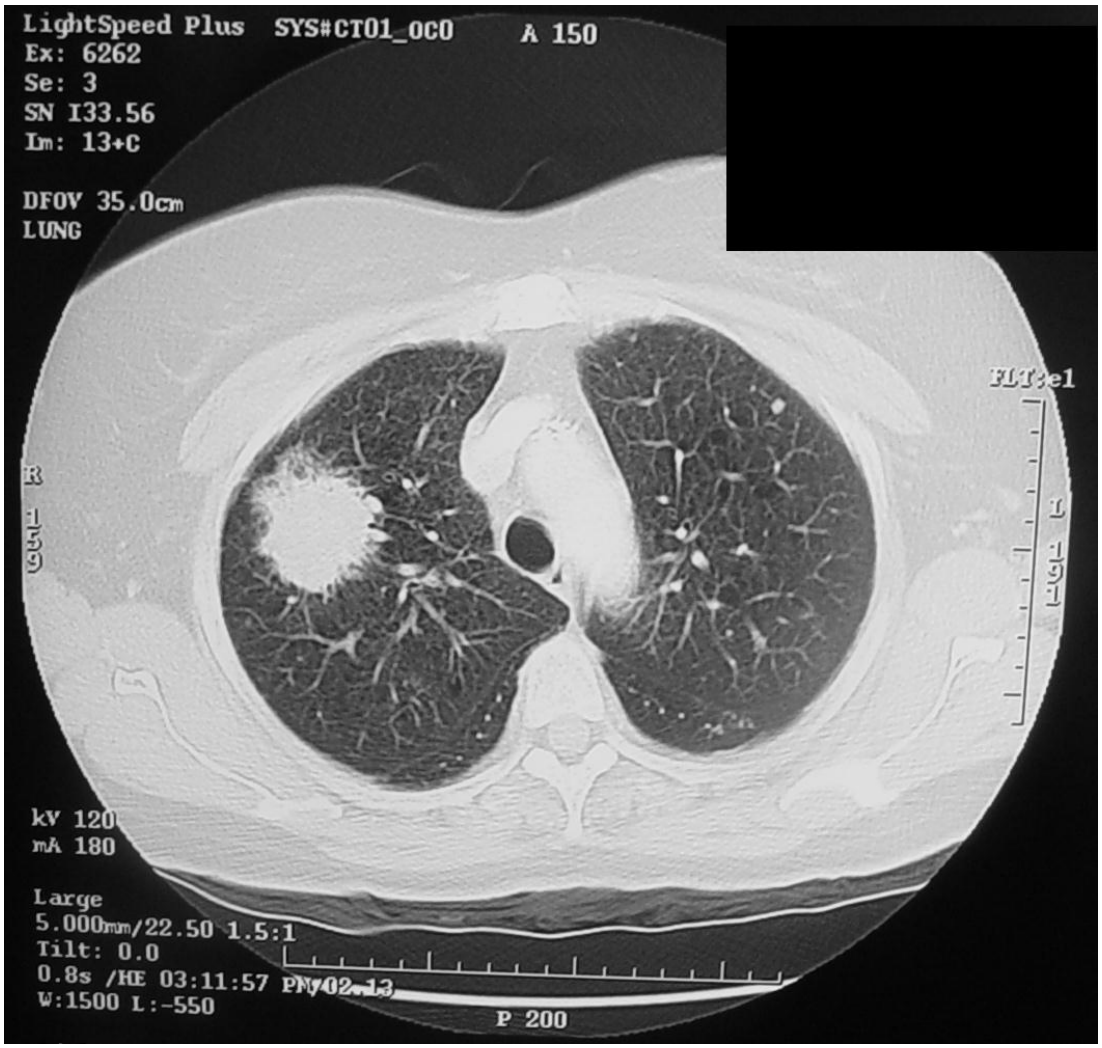

Figure 22 A cross-sectional CT image delineating a lesion in the upper zone of the right lung, subsequently confirmed to be cancer.

2.1.2 Ultrasonography

This procedure creates an internal image of the body, by analysing the manner in which high frequency sound waves are reflected back from organs [161]. Sound 'echoes' are produced whenever there is a mismatch between densities in two adjacent tissues; a phenomenon termed 'acoustical impedance' [161], e.g. interfaces between fluid-filled cysts and solid parenchymal tissue within an organ. Part of the sound wave usually is reflected back as 'echoes' to a transducer, whereas the residual wave will continue to penetrate tissues beyond the interface (with the potential for later reflection) [161]. Analysis of the time it takes for an echo to return to the source of the sound wave helps with the calculation of the depth of an interface, and measurement of the strength of the returning echo determines the mismatch in density of the interface [162]. These data are analysed by a computer and digitised into grey-scale images. Therefore, solid organs materialise as white, echogenic structures since they consist of tissues with multiple acoustic interfaces; while fluids emerge as black, anechoic areas owing to their absence of internal acoustic reflectors.

Ultrasonography does not utilise ionising radiation and thus minimises the potential for biological injury. Ultrasound scanners tend to be less expensive than CT and are more mobile. This portability enables the ultrasound machine to be taken to patients, who are too unwell to be moved from their clinical area. Furthermore, the use of the Doppler Effect helps with the real-time visualisation of moving objects e.g. blood and estimates its speed and direction. However, the clarity and detail of the image is inferior to that of CT. Indeed the quality of the image is much more dependent on the

ultrasound operator than for CT. Additionally, ultrasonography may take longer to acquire than CT scanning, depending on the difficulty of the examination.

2.1.3 Magnetic Resonance Imaging (MRI)

Paul Lauterbur and Sir Peter Mansfield were awarded the 2003 Nobel Prize for their "discoveries concerning magnetic resonance imaging". Lauterbur published the first MR image in 1973 [163]; however Mansfield pioneered the mathematical analysis and techniques required for fast imaging. Magnetic resonance imaging (a.k.a. Nuclear Magnetic Resonance) employs powerful magnets to polarise hydrogen nuclei (single proton) in fat and water molecules, within human tissue. When a further radiofrequency magnetic field is applied, it 'excites' the protons and alters their alignment. However, removal of this radiofrequency signal will allow the protons to return to their previous equilibrium, with emission of the absorbed radiofrequency wave. These emitted radiofrequency waves can be detected by antennae and hence computers are able to determine the spatial localisation of protons within the body. Furthermore, tissues of differing molecular composition (e.g. tumours) may also be distinguished from each other, since protons of differing tissues return to their equilibrium state at dissimilar rates [164]. These data enable a grey-scale (2D or 3D) image of the body to be constructed (see **Figure 23**). Intravenous contrast agents (e.g. gadolinium) may also be injected to enhance the appearance of blood vessels and tumours [165].

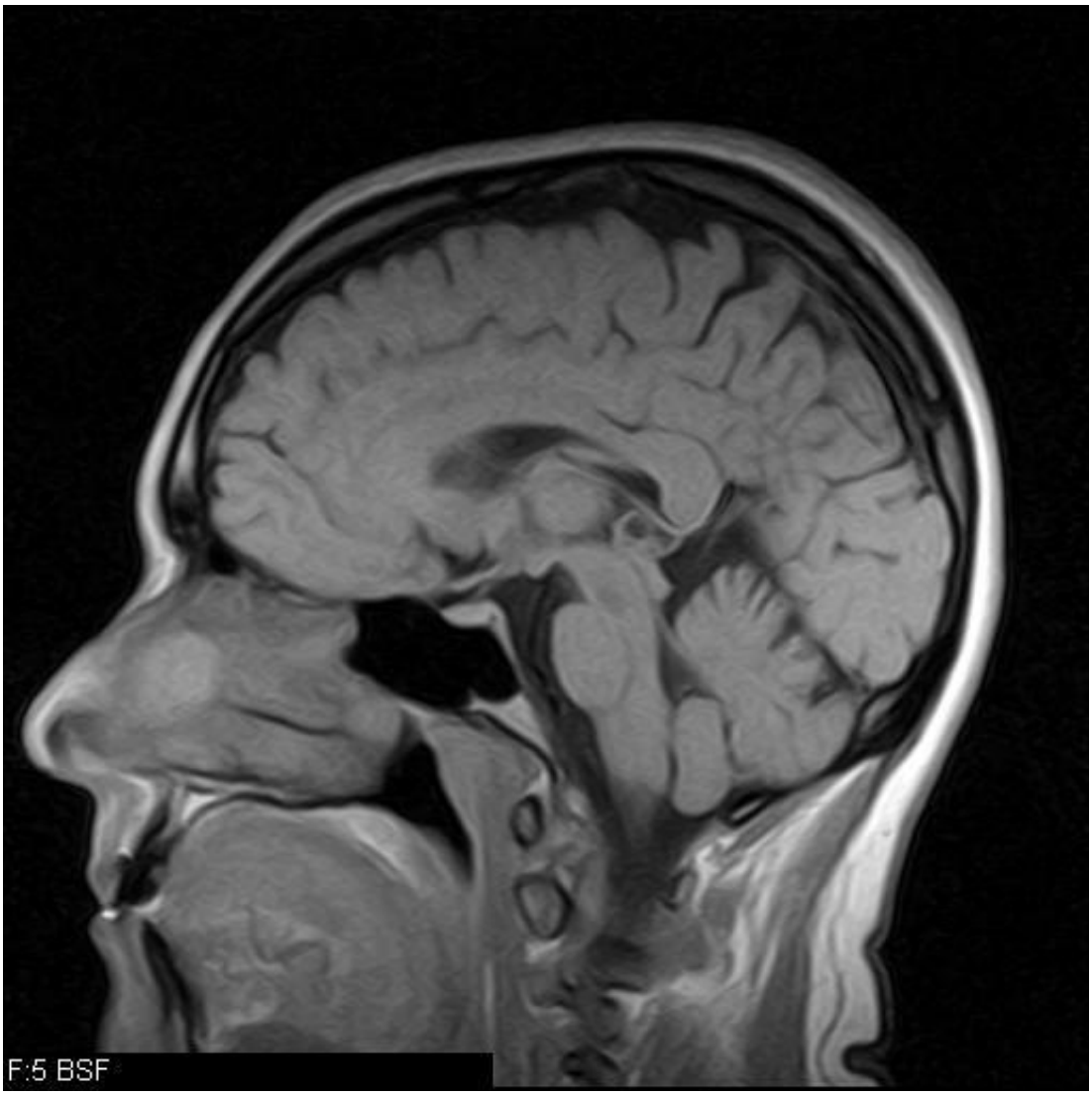

Figure 23 A sagittal MRI image of a head, with excellent soft-tissue differentiation.

The MRI technique gives greater soft-tissue differentiation than CT scanning and, unlike plain film radiography and CT, MRI does not use ionising radiation. However, MRI does have some disadvantages: Patients with implants, made from ferromagnetic metals, must not be in close proximity to an operational MRI instrument. The powerful magnets of the MRI machine would impose on these

implants; potentially causing significant harm. Furthermore the magnetic field and radiofrequency pulses, generated by an MRI scanner, can alter *programmable* implants e.g. cardiac pacemakers or attached infusion pumps. Consequently, all of the aforementioned patient groups cannot be examined by an MRI instrument. Furthermore, owing to the construction of some MRI scanners, the scanning procedure may be unpleasant for the patient. Older models of MRI scanners have a long and narrow tunnel, in which the patient must lie still for up to 40 minutes. This scanning setting, together with the noisy procedure, may precipitate claustrophobia and is intolerable for some patients. Consequently there is a higher risk of motion artefact, compared with a 90-second CT scan. Additionally, motion artefact inhibits the image quality of thorax and abdominal MRI scans, owing to respiratory and cardiac movements. Finally, CT currently is more widely available and less expensive than MRI.

2.1.4 Nuclear Medicine

Nuclear imaging uses specific radioactive isotopes (radionuclides) to visualise organs, through exploitation of the tissue's metabolism, blood supply or protein expression. The radionuclide is administered internally (orally, intravenously or inhaled) to the subject and a time interval is permitted to allow it to reach its target organ. Since these radionuclides decay with resultant emission of gamma rays, the location of the radionuclide within the body can be calculated using external gamma cameras and computer analysis.

The isotopes chosen for nuclear medicine are those that have half-lives of hours or days. Consequently the emission of gamma rays will be limited in time and thus

minimise the patient's radiation exposure. Usually the isotopes are 'tagged' to another molecule (radiopharmaceutical), and it is the property of this molecule that is exploited to image the organ.

2.1.4.1 Scintigraphy and Single Photon Computed Tomography (SPECT)

Technetium diphosphonates can be used to image bone turnover and are usually displayed as a planar representation of the skeleton (scintigram). The data used to create the scintigram usually are obtained from a single gamma camera and at one projection angle. This 2D image can help identify bone metastases; but areas of positive uptake are not cancer-specific and sometimes may represent diseases or entities of non-malignant aetiology e.g. arthritis.

However Single Photon Computed Tomography (SPECT) uses data, taken from multiple gamma cameras at several projections, to construct a 3D tomographic representation of the radionuclide's biological distribution within the body. Positional information is obtained through the placement of collimators in front of the gamma cameras, which only permit detection of γ-rays travelling in certain directions. Consequently, detailed images can be obtained using this technique and this has advantages over other nuclear medicine techniques in certain situations [166]. SPECT and the radiopharmaceutical, ^{99m}Tc-sestamibi, can be important in the clinical assessment of left ventricular volume and function, following an ischaemic cardiac event [167]. The accuracy of the measurements obtained from SPECT analysis is sufficient to risk-stratify patients and guide further interventions.

Many different gamma-emitting radioisotopes could be used for SPECT or scintigraphy. However, ideally, the isotope should be a pure γ-emitter with

negligible particulate emissions and minimal toxicity. Furthermore, it should have a suitable emission-energy (100-300-keV) for *in vivo* studies i.e. an energy level appropriate for photoelectric absorption by NaI crystals (gamma camera), but also appropriate to have minimal interaction with human tissue [168]. Additionally, the isotope should be chemically reactive, permitting combination with other molecules and thus forming a radiopharmaceutical. However, this reactive combination ideally should not change the pharmaceutical's ability to recognise its target. Additionally, if the isotope's location is to be used as a surrogate for the location of the radiopharmaceutical, the biological half-life of the radioisotope should be comparable or less than the half-life of the radiopharmaceutical, and the isotope should also be 'carrier free'. That is, a radiopharmaceutical, with the correct physical properties, should be able to represent the pharmaceutical's (not combined to the radioisotope) biological property accurately, in position and time. Technetium-99m is a frequently used isotope, since it can easily be manufactured using portable generators, has a 6-hour half-life and is relatively inexpensive. **Table 3** (below) lists the properties of radioisotopes commonly applied in SPECT:-

ISOTOPE	HALF-LIFE ($T_{½}$) IN HOURS	GAMMA EMISSION ENERGY (KEV)	MANUFACTURE
^{99M}TC	6	140	PORTABLE GENERATOR [169]
^{123}I	13	159	CYCLOTRON [170]
^{111}IN	67	172 & 247	CYCLOTRON [171]

Table 3 Physical properties of SPECT radioisotopes

2.1.4.2 Positron Emission Tomography (PET)

This nuclear medicine technique employs the internal administration of radioisotopes, which possess proton rich nuclei. These types of radioisotopes decay to form a daughter product with the conversion of the proton into a neutron; the ejection of a positron (beta plus decay) and a neutrino. A positron is a positively charged electron (i.e. the anti-matter counterpart of an electron), which moves a short distance (0.6 - 5 mm) before colliding with an electron. It is this collision which results in their annihilation, the conversion of mass to energy with the emission of two simultaneous gamma rays (180^{o} to each other and both 511 keV). These simultaneous rays are able to be 'coincidence detected', using opposing gamma cameras (see **Figure 24**). Consequently, computers are able to use time of flight data to determine the location of the annihilation; *approximating* the source of the radioisotope within the body and generating images which represent this location.

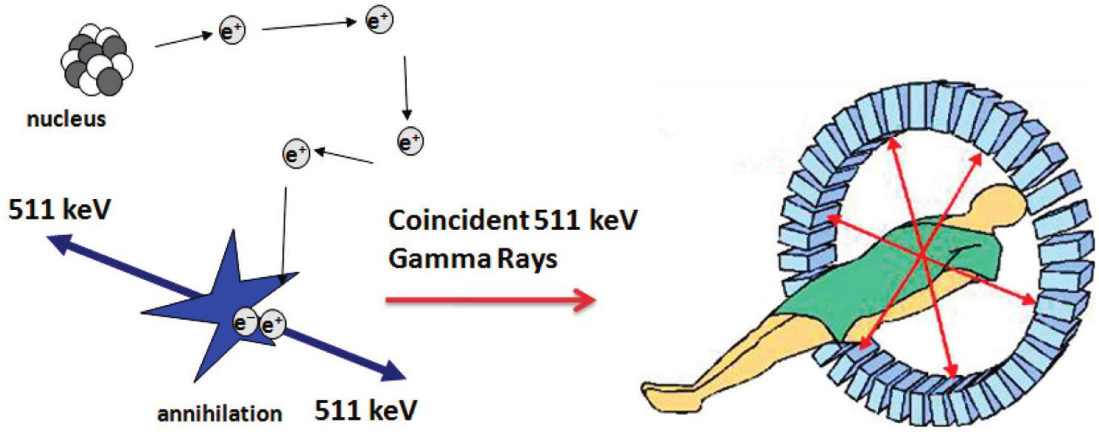

Figure 24 Schematic of imaging with positron emission tomography (PET). *Taken from Shokeen M and Anderson CJ [172].*

Since the positron has to travel a short distance before annihilation, and it is the location of the annihilation which is calculated (rather than the source of the positron), it is this short distance which limits the accuracy / resolution of PET imaging. Although the 0.6 – 5 mm 'blur' usually is not clinically significant to humans, it is a factor for smaller species (e.g. rodents) with tumours under 1 cm. In this situation, the higher resolution offered by the SPECT technology may be more appropriate. However, since time of flight (instead of collimator-limited) data are used for location calculation, more events potentially can be measured using PET in a shorter period of time. That is, the collimators in SPECT are necessary to calculate source, but also reduce the data / events travelling to the gamma cameras. Clearly, more events are preferable to improve statistical accuracy and ensure a valid representation of the radiopharmaceutical's biological distribution.

A range of positron-emitting radioisotopes could be used for PET. However an ideal PET isotope shares many of the same properties listed above for an ideal SPECT isotope; with the exception that a pure positron-emitting substance is desirable. Unfortunately these ideal radionuclides are difficult to obtain, have short half-lives and thus mostly are expensive to manufacture, owing to the requirement for an on-site cyclotron. **Table 4** (page 95) lists the properties of radioisotopes commonly applied to PET.

Isotope	Half-life ($T_{½}$) in hours	Electron-Positron Annihilation Energy (keV)	Manufacture
^{15}O	0.03 (or 2 mins)	511	Cyclotron [173]
^{13}N	0.17 (or 10 mins)	511	Cyclotron [174]
^{11}C	0.33 (or 20 mins)	511	Cyclotron [175]
^{68}Ga	1.13 (or 68 mins)	511	Generator[176]
^{18}F	1.82 (or 109 mins)	511	Cyclotron [177]
^{64}Cu	12.70 (or 762 mins)	511	Generator or Cyclotron [172]

Table 4 Physical properties of PET radioisotopes

Therefore, there are numerous advantages and disadvantages to both PET and SPECT technologies.

A number of the aforementioned imaging modalities are able to help with the diagnosis, staging, treatment assessment and follow-up of cancer patients. These modalities can be divided, broadly, into two groups: anatomical and functional. The anatomical group includes Computed Tomography (CT) and Magnetic Resonance Imaging (MRI) and gives structural and positional information of tumour masses. The functional group includes Positron Emission Tomography (P.E.T.) and Single Photon Emission Computed Tomography (S.P.E.C.T.) and has the potential to give information regarding metabolism, vascular supply and tissue viability, presence or absence of cell surface markers and response to particular treatments. The latter

group utilises biomarkers, probes and is part of a growing field of Molecular Imaging.

2.2 Molecular Imaging

Molecular imaging relies on the use of biological markers (biomarkers), which are molecules used as indicators of a biological state [178]. Biomarkers, in medicine, usually reflect a disease state [179], and so should be either absent or expressed in very low concentrations within normal cells. Many tumours, in humans and animals, express distinct cell surface molecules that distinguish them from non-malignant tissues [180]. Owing to the clonal nature of cancers [181], these cell surface molecules tend to be maintained from the primary site to their metastases; marking areas of malignant disease. Therefore, molecular imaging has the potential to detect minimal residual disease throughout the body, which presently cannot be resolved by conventional anatomical scanning [182]. That is, if a known marker of malignant cells can be targeted by a probe and its signal detected by a functional imager, then the presence of disease can be identified, even if morphologically undetectable. Furthermore, many of these distinct markers may be involved in the processes of maintaining and progressing malignancy [183]. Consequently, these biological markers have the potential to deliver prognostic information (prognostic / surrogate marker); be predictive in terms of tumour response and patients' side-effect profile to a given drug (predictive); and may also reveal if a given drug is activating a desirable molecular pathway (pharmacodynamic) [184]. Predictive markers are particularly important when using drugs with narrow 'therapuetic windows' and where there are

no acceptable or available surrogate markers for survival. This information could help in drug selection when alternative therapies are available [185]. Hence, the detection of these molecules, using radiolabelled ligands, allows tailored targeted therapy and response monitoring [184].

The use of radiolabelled small molecules (probes), to target biological markers, enables their tracing within the body scintigraphically. Radioactivity to label ligands, hence identifying biological markers, is ideal since low dose radiation has little effect on normal tissue [186]. Levine *et al* first described the use of monoclonal antibodies and Iodine-131 to image high density targets scintigraphically on tumour cells [187]. Consequently, P.E.T. and S.P.E.C.T. have the potential to track a given radiolabelled probe in four dimensions. New targeted radiolabelled ligands allow the sensitivity and specificity necessary for diagnosis and patient management. This improved diagnostic information has the potential to reduce the numbers of diagnostic biopsies and thereby reduce potential morbidity [184, 188]. Ideally the imaging technique would also identify distant metastases. Furthermore, future developments of targeted therapy and translation into clinical studies could be greatly facilitated by non-invasive techniques that allow serial studies of the proposed target [184, 188]. Molecular imaging has the potential to document target expression within tumours before the administration of prospective targeted antagonists, thus allowing appropriate selection of patients entering clinical trials [184].

2.2.1 Probe Design

For targeting, the affinity of the probe has to be high enough to generate a rapid and significant (i.e. easily measurable) signal to background ratio in order to discriminate the target tissue. A probe typically comprises three main components: a targeting ligand (such as antibody or peptide) that binds to the desired receptor; a radionuclide with an appropriate emission for the selected imaging modality; and in some cases, a chelating agent (such as diethylenetriamene pentaacetate (DTPA) and 1,4,7,10-tetraazacyclododecane-1,4,7,10-tetraacetic acid (DOTA)) and a spacer, which facilitates attachment of the radionuclide to the targeting moiety [189].

Correct radioisotope selection is essential for successful tumour imaging and this already has been discussed (**section 2.1.4**) with the associated imaging technique e.g. SPECT and PET. However, **Table 5** (page 99) further summarises the advantages and disadvantages of the common radionuclides, used for radiolabelling.

Advantages	Limitations
Technetium-99m	
• Easily available and low cost • Easy to handle • Reasonable $T_{½}$ of 6 hours • 140 keV γ-emission • Excellent imaging characteristics • Absence of α and β radiations • Favourable dosimetry	• Not suitable for delayed imaging studies
Iodine-123	
• 159 keV γ-emission • $T_{½}$ of 13 hours • Good imaging characteristics	• High cost • Limited availability • Cyclotron-produced radionuclide
Indium-111	
• 172 and 247 keV γ-emission • $T_{½}$ of 2.8 days • Useful for acquiring delayed imaging	• High cost • Limited availability • Cyclotron-produced radionuclide • Relatively high radiation burden to patients • Sub-optimal nuclear characteristics
Copper-64	
• Emissions of β^-(573 keV) and β^+(655 keV) • Suitable for both imaging and radiotherapy • $T_{½}$ of 12.7 days • Can be produced using a generator system or biomedical cyclotron	• Limited availability • Costly production and shipment • Sub-optimal characteristics for PET imaging due to low abundance of β^+ (19%)
Gallium-66/67/68	
• Suitable for γ-scintigraphy and PET imaging • $T_{½}$ of ^{66}Ga(9.5 hours), ^{67}Ga(78.3 hours) and ^{68}Ga(68 minutes) • Useful physical characteristics	• High cost • Limited availability • Cyclotron-produced radionuclides (^{66}Ga, ^{67}Ga)
Fluorine-18	
• Can be produced in high quantity (**i.e.** Ci) • Low positron energy of 0.635 MeV • High resolution and sensitivity • Low radiation dose to patients • $T_{½}$ of 110 minutes permits both radiophamaceutical preparation and imaging studies.	• High cost • Limited availability • Cyclotron-produced radionuclide

Table 5 Characteristics of Different Radionuclides Used for Radiolabelling.

Adapted from Okarvi S.M. [190].

Notably, when a choice of radioisotopes is available, it should not be assumed that the results of one tracer will be similar to another. That is, the spatial and chemical relationship of the radionuclide to the targeting ligand may influence the radiopharmaceutical's overall pharmacokinetics. Indeed, de Jong *et al* studied the binding of DOTATOC to somatostatin receptors and compared the biodistribution of **^{90}Y**-labelled DOTATOC to that of **^{111}In**-labelled DOTATOC, in rats bearing the CA 20948 tumour [191]. Interestingly, the authors discovered that uptake of ^{90}Y-labelled DOTATOC (into the somatostatin receptor-positive organs) was significantly higher than that of the ^{111}In-labelled compound. Marion de Jong *et al* suggested that the DOTA chelator was more appropriate for the complexation of ^{90}Y than for ^{111}In [191]. This phenomenon may be due to differing groups of the DOTATOC molecule interacting with the different radioisotopes. The relationship of the targeting ligand, chelator and radionuclide will be discussed further in **Section 2.2.3**.

There are many potential biopharmaceuticals which could be used as targeted ligands for imaging. However radiolytic resistance of the targeting ligand is an essential requirement, owing to its proximity with a radionuclide. That is, chemical stability can be a problem with certain radioisotopes, possibly resulting in diminished tumour targeting efficiency [192]. Although, free-radical scavenging may reduce radiolysis [193], this further step can complicate proceedings. Common targeting ligands include modified substrates for a cell's enzymatic processes, monoclonal antibodies, single chain Fv antibodies (scFv), peptides and viral vectors; each has advantages and disadvantages. Of note, probe-based imaging modalities also permit the targeting of cell surface markers, within tumours and associated 'normal' tissues [189]. That is, as well as targeting biological markers on cancer cells, biological markers can

also be sought out on tissues which are not themselves transformed but which are required for tumour growth. For example, new vessel formation is required to deliver blood nutrients to a growing tumour mass [194]. In order to achieve this need, tumours secrete a variety of factors to promote angiogenesis. Therefore, the receptors on newly-formed blood vessels can be targeted and used as a surrogate for tumour activity. The use of an RGD sequence-containing peptide [194] to image αvβ3 over-expression on neo-vascularisation will be described in **Section 2.3**.

2.2.1.1 ^{18}F-FDG substrate

In 1980, Som et al described a fluorinated glucose analogue, 2-fluoro-2-deoxy-D-glucose (^{18}F-FDG), and its potential for detecting transplanted and spontaneous tumours in animals [195]. Certain cancer cells have an increased metabolic demand compared to normal tissues, in part due to their increased cell division. In 1978, Monakhov *et al* showed that the hexokinase activity was raised significantly in certain malignant tumours, in contrast to normal tissues [196]. ^{18}F-FDG competes with glucose in the hexokinase reaction, in which glucose is phosphorylated at the 6-position to form glucose-6-phosphate. Once phosphorylated, FDG-6-phosphate escapes the usual glucose metabolism and is not released from the cell; trapping it within these cells after initial absorption. ^{18}F-FDG's tumour uptake was maximal at 30 minutes and remained relatively constant up to 60 minutes, post injection. Tumour-to-normal tissue and tumour-to-blood ratios ranged from 2.10-9.15 and 2.61-17.82, respectively, depending on the type of tumour [195]. However, it should be noted that the % dose / gram was quoted at just 0.43 ± 0.07 at 60 minutes post-injection, for a melanoma rabbit model. Nonetheless, the authors showed 60 minute

% dose / gram ranging from 0.4 – 18 in different tumour models, and published ^{18}F-FDG scintagrams in a dog with a seminoma (see **Figure 25**).

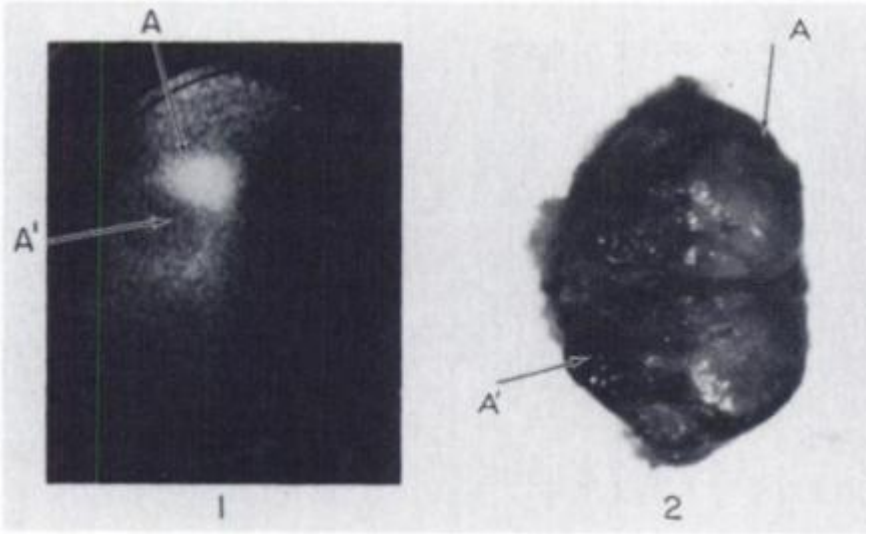

Figure 25 *In vivo* scintigram with ^{18}F-FDG 2 hours post injection (1); and excised tumour (2), in a dog with spontaneous seminoma. A = visible tumour; A' necrotic. *Taken from Som et al [195]*.

Tumour visualisation was described as 'excellent', owing to low blood and tissue background. Nevertheless, the dog required catheterisation in order to eliminate urinary activity; a considerable amount of ^{l8}F-FDG metabolite is excreted in the urine and thus could hinder image interpretation [197]. Toxicological studies in mice using 1000x human tracer dose per week (for 3 weeks) did not show any evidence of acute or chronic toxicity; determined by routine observations, changes in body weight, and gross and histopathology of the internal organs. This and subsequent studies have established ^{l8}F-FDG as a surrogate for tumour viability; through its accumulation in areas of high glycolytic activity [198]. Indeed the new staging criteria for Hodgkin's disease now incorporates P.E.T. and ^{l8}F-FDG analysis [199].

2.2.1.2 Antibody vs. Peptide

While monoclonal antibodies display high affinity and specificity, they suffer from clinical limitations when used as a targeting ligand.

Peptides can be synthesised in large quantities relatively inexpensively and are more amenable to 'derivatisation' [200]. Peptide synthesis techniques can be divided broadly into two main groups: solution-phase peptide synthesis and solid-phase peptide synthesis (SPPS) [190]. Although solution-phase synthesis is useful for large-scale peptide production and for specialised laboratory applications, it is time-consuming and requires complex purification procedures. Consequently, SPPS is the method of choice for small and medium-scale peptide synthesis. Furthermore, this method of synthesis permits relatively easy derivatisation. For example, biotinylation of the peptide is possible; this biotin 'tag' allows the peptide to be tracked and is useful in the analysis of certain cell binding assays. The addition of a bifunctional chelating agent (described later) may also be added to the peptide during SPPS, facilitating future radiolabelling.

Peptides seem to be *more* accessible to solid tumours. That is, the relatively larger antibodies (approximately 150 kDa) may penetrate tumour vasculature poorly, limiting delivery of the ligand to the tumour and thus slowing localisation and binding kinetics [201]. Other physiological barriers may also inhibit access of the larger antibody to its target e.g. blood-brain-barrier.

The binding of an ideal probe to its desired target would be stable and long-lived; possibly exhibiting receptor-mediated internalisation into tumour cells. Internalisation results in accumulation of the probe within the target tissues, providing an increased signal for imaging. Smaller molecules, such as short peptides,

may have the advantage in their potential to be internalised and, therefore, accumulated.

Integrins are known to bind some ligands more stably than others [202]. This property permits greater clearance of non-specifically bound probe, and is thus important for target-to-background ratio. Reduction of the background signal helps contrast the target signal. As well as more rapid localisation within the target tissue, low molecular weight peptides have the potential for faster blood clearance from blood and non-target tissues. Small peptides tend to be degraded quickly / metabolised *in vivo*, by e.g. proteases, and renally excreted; resulting in a relatively short biological half-life. These processes take longer for the 'bulkier' monoclonal antibody structures and therefore also permit non-specific binding to persist. Furthermore, this slower clearance (monoclonal antibodies) from the circulation results in greater radiation exposure to normal organs.

However, the targeting ligand must have sufficient stability to reach its biological target. Therefore, a fine balance is required between clearance (background signal) and target localisation (target signal) for maximal contrast. The relative ease of peptide modification can also help shift this balance for improved efficacy. That is, peptides can be modified, using certain techniques (see **Table 6**, page 105), to enhance resistance against proteolysis and hence improve *in vivo* stability. Conversely, knowledge of these techniques could be utilised to decrease *in vivo* stability, improving clearance and thus reduce background signal.

• Introduction of appropriate D-amino acids
• Substitution of peptide bonds
• Replacement of amino moieties with imino groups
• Use of unusual amino acids or side chains
• Use of non-peptide molecules with similar configurations
• Terminal capping process(by acetylating the N-terminus or by converting the C-terminus carboxylic acid into an amide)
• Cyclisation
• Introduction of non-cleavable isotere bonds
• Peptide mimetics (group reduction)

Table 6 Methods of Inhibiting Proteolysis of Peptides. *Adapted from Okarvi [190].*

Murine monoclonal antibodies are also immunogenic, generating human anti-mouse antibody (HAMA) responses [203]. These responses create allergic-like reactions to the mouse antibody and rapid removal of the mouse antibody from the body, thus limiting efficacy [204]. This problem can be minimised by immunosuppression, the use of chimeric antibodies or even 'humanising' the antibody in order to reduce the immunogenic components. However, immunosuppression may not be desirable in some patients, and could cause other troublesome side-effects [205]. Furthermore, the process of humanisation involves the mimicking of a protein sequence of a human antibody; producing an immunoglobulin framework in which non-human hypervariable complementarity-determining regions (CDRs) can be inserted. These CDRs potentially could contain inherently antigenic determinants, which would initiate an immune response – 'human anti-human antibodies (HAHA) production [206]. On the other hand, small peptide molecules tend to have low antigenicity and therefore minimise this issue [200].

Single-chain Fv recombinant proteins are prepared by connecting genes encoding heavy chain and light chain variable regions of immunoglobulins at the DNA level using an oligonucleotide linker. Since these fragments are approximately 25 kDa in size, they do have the potential for better tumour penetration and faster clearance compared to whole immunoglobulins [207]. However, owing to their monovalency, they do have lower avidity. This problem can be overcome by generating multivalent forms of scFv molecules and optimising their affinity. Nevertheless, scFv development is still in its infancy for clinical use.

All of the aforementioned properties must be accounted for in the design of an imaging probe; maximising target-to-background efficiency and safety. It, therefore, has been suggested that small synthetic receptor-binding peptides are the agents of choice for diagnostic imaging of cancers due to their favourable pharmacokinetics and flexibility in chemical modification facilitating radiolabelling [190].

Notwithstanding the above, monoclonal antibodies have been relatively successful, when incorporated within an imaging probe. Prostascint® is an ^{111}In-labelled monoclonal mouse antibody specific for the prostate-specific membrane antigen and has been FDA-approved for the detection of recurrence in prostate cancer patients [208]. Indeed Ellis *et al* have been able to detect cancer foci in the prostate, with 79% sensitivity and 80% specificity when correlated with histology, using this reagent [209]. Furthermore, an increasing body of evidence indicates that radiolabelled trastuzumab is able to identify HER2-positive tumours within advanced breast cancer patients [210].

However, the archetypal radiopharmaceutical is ^{111}In-DTPA-D-Phe^{1}-octreotide (OctreoScan, ^{111}In-pentetreotide) – a targeted cyclic radiopeptide. It was approved by the FDA in 1994 for scintigraphy of patients with neuroendocrine tumours [183]. Octreotide is an eight-amino acid, somatostatin-analogue and its DTPA-D-Phe^{1} modification transfers enhanced resistance to *in vivo* enzymatic degradation and reduced hepatobiliary excretion; thereby allowing good imaging of abdominal tumour sites. Somatostatin (a cyclic neuropeptide via a disulphide bond interaction) physiologically acts as a neurotransmitter in the brain with resultant inhibition of hormone release [211]. However, somatostatin receptors are expressed additionally in tumours of neuroendocrine origin e.g. carcinoids [211]. The over-expression of these receptors can serve as a potential target within the tumour for ^{111}In-DTPA-D-Phe^{1}-octreotide. Imaging is permissible within hours of injection of this radiolabelled peptide [212]. Furthermore, the availability of ^{68}Ga-labelled octreotide analogues now opens the field to PET imaging of neuroendocrine tumours [213].

2.2.2 Radiolabelling Techniques

Generally, radiolabelling techniques can be divided into either ‘direct’ or ‘indirect’ categories. Direct labelling usually involves a reaction with the radioisotope and the targeting ligand; whereas indirect labelling requires a conjugate or coupling method. The choice of labelling technique is determined by biological, chemical and structural consequences of the reaction and resulting radionuclide attachment.

Iodine (^{131}I and ^{125}I) labelling of proteins may be performed using electrophilic substitution, in which positively charged iodine attacks a system with high electron density e.g. an aromatic ring or a double bond; resulting in a covalent carbon-iodine bond formation. When hydrogen is replaced by a radioiodine atom (radioiodo-deprotonation) in an arene (activated for electrophilic substitution), direct radiolabelling occurs. However, this method involves strong oxidising conditions, which may be problematic for the native protein [214]. Consequently, the iodogen method™ is preferred for clinical applications. This technique involves a reaction vessel coated with 1,3,4,6-tetrachloro-3α, 6α-diphenylglycouril (iodogen), which 'mildly' oxidises iodine isotopes. If this oxidation occurs in the presence of a protein, which contains tyrosine, there is subsequent incorporation of the radioiodine into the tyrosine; that is, a substitution of iodine for hydrogen atoms (in the phenolic ring of tyrosine) within the protein [215]. Therefore, this direct labelling method is limited to proteins which contain an accessible tyrosine.

Alternatively, if a tyrosine residue is not available or if any oxidation is undesirable to the native protein, indirect radioiodination via prosthetic groups is possible. Here the protein is treated with an iodine-labelled acylating agent, e.g. iodinated 3-(4-hydroxyphenyl)propionic acid N-hydroxysuccinimide ester (iodine-labelled Bolton–Hunter reagent), which reacts with free amino groups in a protein molecule; attaching the iodine-labelled groups by amide bonds [216]. That is, an activated aromatic compound (Bolton–Hunter reagent) is first radioiodinated, and this subsequently is coupled to the native protein, via acylation of a free amino group e.g. lysine. In this way, the native protein escapes the harsh conditions required for iodination [216].

Technetium-99m (^{99m}Tc) is the most frequently used radioisotope in nuclear medicine [217]. Direct labelling involves the chelation of ^{99m}Tc to the reactive sulphide-groups within a compound. The direct labelling reaction usually involves a reducing agent which converts disulphide bridges into free thiols; the free thiols are able to chelate with ^{99m}Tc [218]. However, direct ^{99m}Tc labelling methods are limited to compounds containing disulphide bonds and the resultant products also have poor *in vivo* stability; the radiometal can dissociate during imaging [217]. Therefore different approaches are required to provide a range of stable radiolabelled compounds with minimal toxicity. One such approach is via an indirect method, using a bifunctional chelating agent (BFCA). The BFCA initially is attached to the peptide to form a BFCA-peptide conjugate. The attachment can occur to the C, or N terminus, or to a branch chain or even to the peptide backbone. However, since the attachment of any molecule has the potential to affect the targeting ligand's affinity for its receptor, the choice of attachment site is not only dependent on ease of attachment, but also on its resultant effect on the receptor binding affinity [219]. If necessary, 'spacers' can be used to increase the distance between the conjugation site and the receptor binding site. Once the conjugate has been selected, subsequent radiolabelling can be attained either by direct reduction of $^{99m}TcO_4^-$, or by ligand exchange using an intermediate ^{99m}Tc complex (e.g. [^{99m}Tc] glucoheptonate) [217]. This indirect labelling technique is the most practical approach for the development of peptide-based target-specific radiopharmaceuticals.

Indium-111 and gallium-67 are found in group 13 (post-transition metal category) of the periodic table. These trivalent metal radionuclides have physical properties suitable for radioisotope imaging. ^{111}In is produced by a charged particle accelerator (cyclotron) that creates proton-rich radionuclides by bombardment of a cadmium target with positively charged particles (proton irradiation). ^{111}In has a sixty-seven hour half-life and decays by electron capture; emitting γ-photons at 172 and 247 keV, with 55 to 72 percent yield factors for the two peaks [168, 171]. These characteristics are suitable for γ-scintigraphy and SPECT imaging. Gallium radionuclides have decay characteristics that are suitable for γ-scintigraphy, PET imaging, and receptor-mediated radiotherapy. However, to obtain an indium or gallium radiolabelled biomolecule (probe) with the required stability, a biomolecule-chelator conjugation also is required in order to complex the metal [219]. Furthermore, ^{111}In(III) does not cross the cell membrane readily and must first be chelated with a lipophilic chelating agent [168]. Chelators will be discussed further in **Section 2.2.3**.

At pH > 6, many metals form insoluble hydroxide complexes and thus become unavailable for binding to the chelator [219]. Therefore, radiolabelling with $^{111}InCl_3$ (dissolved in dilute HCl) requires buffering, at pH 4–6. Furthermore, the presence of weakly chelating ions in the buffer (such as acetate or citrate) will also reduce the likelihood of hydrolysis [219]. The radiolabelling mixture may also contain antioxidants (such as ascorbic or gentisic acid) to prevent radiolysis of the peptide [193]. To ensure that labelling will be almost 100% efficient, the peptide conjugate is usually in excess in comparison with the radionuclide. The most effective incubation

conditions are dependent on the chelator choice (see **Section 2.2.3)**, as well as on the peptide structure [219]. However, since chelators facilitate metal attachment, it is important to eliminate metal impurities from the indium radiolabelling mixture. The presence of other metals could lead to the chelation of impurities, rather than indium. Therefore, performing the radiolabelling reaction in polypropylene vessels (instead of glass), using polypropylene weighing spatulas, and acid-treating vials and pipette tips should all be considered [219].

Although direct electrophilic fluorination of peptides is possible, this method is unsuitable for medical applications [220]. Therefore, prosthetic groups are required for stable fluorine-18 radiolabelling [220], such as N-succinimidyl-4-[^{18}F]-fluorobenzoate ([^{18}F] SFB). However, there are usually three major steps involved in ([^{18}F] SFB synthesis: (i) [^{18}F]-fluorination of a suitable aromatic precursor, (ii) formation of 4-[^{18}F]-fluorobenzoic acid ([^{18}F] FBA), and (iii) activation of [^{18}F] FBA to form the [^{18}F] SFB reagent [220]. That is, peptides are usually radiolabelled with ^{18}F by first converting [^{18}F] FBA into a corresponding active ester, which is then isolated, purified, and coupled to a free amino group (via acylation) on the biomolecule e.g. lysine residue. The addition of O-(N-succinimidyl)-N,N,N',N'-tetramethyluronium tetrafluoroborate (TSTU) helps with the activation / esterification of [^{18}F] FBA (see **Figure 26)**, reduces synthesis time and achieves a higher yield of purity [220].

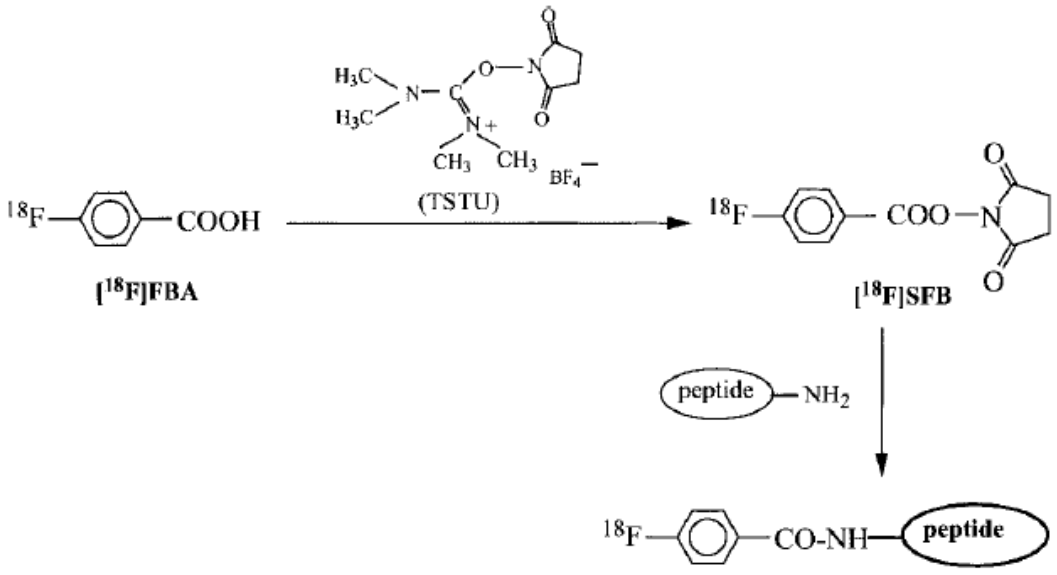

Figure 26 A general scheme for the preparation of ^{18}F-labelled peptides via N-succinimidyl-4-[^{18}F]-fluorobenzoate (O-(N-succinimidyl)-N,N,N',N'-tetramethyluronium tetrafluoroborate)-mediated esterification of 4-[^{18}F]-fluorobenzoic acid. *Taken from Okarvi [190]*.

2.2.2.1 Pre-labelling vs. Post-labelling

The previous section described some examples in which the radiometal was introduced to its chelator, after the chelator already had been attached to its targeting ligand; a process termed 'post-labelling'. 'Pre-labelling' occurs when the radionuclide-chelator complex is formed *prior* to activation and undergoes substitution into the targeting ligand. The choice of labelling strategy is influenced by a variety of considerations [221]. A direct one-step post-labelling may be appropriate if the radionuclide is not abundantly available, or if the labelling

efficiency is reduced with multiple stages of conjugation. However, if complex formation between the radionuclide and chelator can be achieved only under 'harsh' conditions (i.e. damaging to the targeting ligand), then clearly a pre-labelling strategy is indicated [221].

2.2.3 Bifunctional chelating agents (BFCAs)

If a metal radionuclide (e.g. ^{64}Cu) and targeting ligand have been selected for imaging, the subsequent step is to select a bifunctional chelating agent, consisting of a coordination site for metal complexation and a linking site for covalent coupling to an available functional group within the targeting ligand. The choice of complexation site not only is dependent on ease of attachment, but also on its resultant effect on the receptor binding affinity [219].

The first BFCAs to be described were analogues of ethylenediaminetetraacetate (EDTA) and diethylenetriaminepentaacetic acid (DTPA). The polyamino-polycarboxylic ligand, DTPA, provides linkage and coordination sites to "simple" aquo-ions, such as ^{111}In(III), without the necessity for derivatisation [221]. DTPA can be synthesised in a monoreactive state with regards to peptide conjugation: one free terminal carboxylic acid and four carboxylates protected with *tert*-butyl ester (see **Figure 27**). This DTPA derivative now affords a degree of site-specific attachment control to its biomolecule [222].

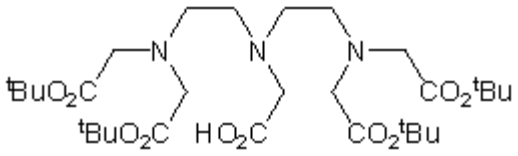

Figure 27 Chemical Structure of DTPA-tetra (t-Bu ester)

However, 1,4,7,10-tetraazacyclododecane-1,4,7,10-tetraacetic acid (DOTA) is a 12 member tetraaza macrocycle and is a modern BFCA (**Figure 28**) [223]. DOTA can complex a broad range of radioisotopes, suitable for use in nuclear medicine. DOTA complexes tend to be more thermodynamically and kinetically stable than the DTPA complexes [219]. An unstable complex may result in deposition of the radionuclide in normal tissue; producing false positive imaging data and unnecessary radiation exposure. Nevertheless, DOTA complexes require a degree of heating to aid their formation, whereas the less-stable DTPA complexes can form at room temperature (19–25 ^{o}C) [219].

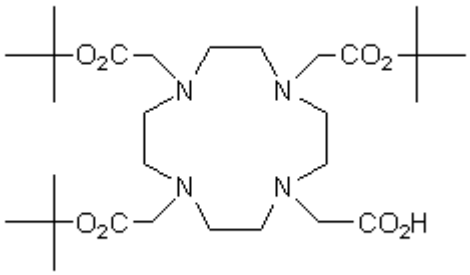

Figure 28 Chemical Structure of DOTA-tris (t-Bu ester)

Nevertheless, the choice of chelator for any given nuclide also may be influenced by the metabolic fate of the free radionuclide and its chelated form [221]. The ideal chelated radionuclide would be excreted rapidly via the urinary tract. Intact conjugate should accumulate and be retained intracellularly and selectively at tumour sites, but not in normal tissues [221]. However, this ideal is not always possible and persistent and unwanted non-target retention of metallic radionuclides (possibly still in their chelated forms) may occur.

Forrer *et al* compared the pharmacokinetics of somatostatin analogues (^{111}In-DOTATOC vs. ^{111}In-DOTATATE) in five patients with neuroendocrine tumours [224]. Both analogues showed high specific uptake in somatostatin receptor-positive tissue, although better visualisation of some liver metastases was found with ^{111}In-DOTATOC. Furthermore, dosimetry showed a significantly higher mean absorbed dose to the liver for ^{111}In-DOTATATE, and a favourable tumour-to-kidney ratio (P=0.065) for ^{111}In-DOTATOC. The amount of ^{111}In-DOTATOC excreted into the urine was significantly higher than for ^{111}In-DOTATATE. It was suggested that the difference in charge (positive overall charge of ^{111}In-DOTATOC and neutral charge of ^{111}In-DOTATATE) could lead to differing kidney absorbed doses.

Furthermore, chelator choice may alter the sensitivity and specificity of the targeting ligand. Marion de Jong *et al* studied the binding of ^{111}In-DOTATOC to somatostatin receptors and compared the biodistribution of ^{90}Y- and ^{111}In-labelled DOTATOC with that of ^{111}In-DTPAOC, in rats [191]. The authors found that the specific uptake of both ^{90}Y- and ^{111}In-labelled DOTATOC in octreotide receptor-expressing tissues was significantly (2 – 6 times) higher than that of ^{111}In-DTPAOC [191].

In addition, transferrin (the iron transport protein found in plasma) has a high affinity for ^{111}In(III) and may cause the ^{111}In(III) to detach from its chelate; thus de-stabilising the targeting ligand radiolabel. Therefore, Indium-peptide complexes (within radiopharmaceuticals) should not only be stable to proteolysis, but ideally should also be more stable than Indium-transferrin complexes [168]

Therefore, the spatial and chemical relationships of the chelator, radionuclide and targeting ligand are highly important to achieve maximal imaging efficiency. **Table 7** (below) lists some common radionuclides and their most favourable corresponding chelating agents.

Chelators	**Radionuclides**
Diethylenetriamine pentaacetic acid (DTPA)	Indium, Yttrium, Lutetium, Iodine
Tetraazacyclododecane tetraacetic acid (DOTA)	Gallium, Indium, Yttrium, Lutetium, Copper
Hydrazino nicotinamide (HYNIC)	Technetium
Tricarbonyl Core	Technetium, Rhenium
Triethylenetetramine (TETA)	Copper

Table 7 Complexing Agents and Corresponding Radionuclides

2.2.4 Combined Functional and Anatomical Imaging

Despite the advances in functional imaging and radiochemistry, conventional anatomical imaging still can add valuable positional information (see **Table 8**, page 118) to the data accrued from molecular imaging and biomarkers. Positional information is still necessary to guide certain treatments e.g. surgery. Therefore, SPECT data could be overlaid onto the corresponding CT images i.e. 'mapping' functional information onto anatomical imaging. This combined approach to imaging is increasing molecular imaging's profile in diagnostic medicine. Enhanced diagnostic and prognostic information can be achieved by this combined approach. It is for this reason that the experiments described in this thesis used Bioscan's combined NanoSPECT/CT.

Technique	Resolution	Depth	Time	Quantitative	Imaging agents	Target	Cost	Main small-animal use
MRI	10–100 µm	No limit	Minutes to hours	Yes	Paramagnetic chelates, magnetic particles	Anatomical, physiological, molecular	£££	Versatile imaging modality with high soft tissue contrast
CT	50 µm	No limit	Minutes	Yes	Iodinated molecules	Anatomical, physiological	££	Imaging lungs and bone
Ultrasound	50 µm	cm	Seconds to minutes	Yes	Microbubbles	Anatomical, physiological	££	Vascular and interventional imaging
PET	1–2 mm	No limit	Minutes to hours	Yes	**e.g.** ^{18}F-, ^{64}Cu- or ^{11}C-labelled compounds	Physiological, molecular	£££	Versatile imaging modality with Many tracers
SPECT	1–2 mm	No limit	Minutes to hours	Yes	**e.g.** ^{99m}Tc- or ^{111}In-labelled compounds	Physiological, molecular	££	Imaging labelled antibodies, proteins and peptides
Bioluminescence imaging	Several mm	cm	Minutes	No	Luciferins	Molecular	££	Gene expression, cell and bacterium tracking
Intravital microscopy	1 µm	<400–800 µm	Seconds to hours	No	Photoproteins, fluorochromes	Anatomical, physiological, molecular	£££	All of the above at higher resolutions but limited depths and coverage

Table 8 Overview of imaging technologies. *Adapted from Weissleder R and Pittet MJ [188].*

However, prior to use in humans, biological markers must be selected using *in vitro* characterisation and validated in pre-clinical models. These investigations will quantify non-specific binding, biodistribution, pharmacokinetics and pharmacodyamics as well as establish if tumour access of the targeted molecule is possible; that is, if the tumour is poorly perfused the targeted molecule may not be able to reach the biological marker and therefore may give false negative results. Furthermore, a concern of using cell lines for identification of potential biomarkers is that the cell surface expression profile in culture may not reflect the state of the cancer cells in a tumour. Therefore, pre-clinical models can answer many valuable questions prior to human trials. My analysis of αvβ6 expression suggests quite strongly that it could serve as an appropriate target for molecular imaging of a range of human carcinomas. Nevertheless, careful consideration should be made as to the choice of the most appropriate pre-clinical model.

The phylogenetic expression of cellular integrins and their tissue distribution appear to be universal from fungi to mammals. Indeed, the sequences and genes of the Drosophila integrins are about as closely related to chordates as are those which comprise the most divergent of the vertebrate subunits [12]. There is 92.33% αv similarity and 90.71% β6 similarity of the mouse to the human genes (comparison based on amino acids). This high degree of similarity is important, especially when dealing with mouse models which could spontaneously develop αvβ6-expressing tumours. However, integrin diversity varies widely among species; for example, in mammals, 19 alpha and 8 beta subunit genes encode polypeptides that combine to form 25 different receptors, whereas the Drosophila and Caenorhabditis genomes

encode only five and two integrin alpha subunits, respectively [20]. It should be noted that although the pattern of αvβ6 staining has been documented in primates [134], the baseline αvβ6 expression in mice has not been established. Therefore, this baseline expression must be ascertained prior to any targeting experiments.

αv Sequence Homology

```
Murine MAAPGRLLLRPRPGGLLLLLPGLLLPLADAFNLDVESPAEYAGPEGSYFGFAVDFFEPST 60
Human  MAFPPRRRLRLGPRGLPLLLSGLLLPLCRAFNLDVDSPAEYSGPEGSYFGFAVDFFVPSA 60
       ** * *  **  * ** ***.******. ******:*****:************** **:

Murine SSRMFLLVGAPKANTTQPGIVEGGQVLKCECSSSRRCQPIEFDSTGNRDYAKDDPLEFKS 120
Human  SSRMFLLVGAPKANTTQPGIVEGGQVLKCDWSSTRRCQPIEFDATGNRDYAKDDPLEFKS 120
       ******************************: **:*********:****************

Murine HQWFGASVRSKQDKILACAPLYHWRTEMKQEREPVGTCFLQDGTKTVEYAPCRSKNIDAD 180
Human  HQWFGASVRSKQDKILACAPLYHWRTEMKQEREPVGTCFLQDGTKTVEYAPCRSQDIDAD 180
       ************************************************************::****

Murine GQGFCQGGFSIDFTKADRVLLGGPGSFYWQGQLISDQVAEIISKYDPNVYSIKYNNQLAT 240
Human  GQGFCQGGFSIDFTKADRVLLGGPGSFYWQGQLISDQVAEIVSKYDPNVYSIKYNNQLAT 240
       ****************************************:*******************

Murine RTAQAIFDDSYLGYSVAVGDFNGDGIEDFVSGVPRAARTLGMVYIYDGKNMSSLHNFTGE 300
Human  RTAQAIFDDSYLGYSVAVGDFNGDGIDDFVSGVPRAARTLGMVYIYDGKNMSSLYNFTGE 300
       *************************:**************************:*****

Murine QMAAYFGFSVAATDINGDDYADVFIGAPLFMDRGSDGKLQEVGQVSVSLQRAVGDFQTTK 360
Human  QMAAYFGFSVAATDINGDDYADVFIGAPLFMDRGSDGKLQEVGQVSVSLQRASGDFQTTK 360
       ************************************************** *******

Murine LNGFEVFARFGSAIAPLGDLDQDGFNDIAIAAPYGGEDKKGLVYIFNGRSTGLNSVPSQI 420
Human  LNGFEVFARFGSAIAPLGDLDQDGFNDIAIAAPYGGEDKKGIVYIFNGRSTGLNAVPSQI 420
       ****************************************:************:*****

Murine LEGQWAAQSMPPSFGYSMKGATDVDRNGYPDLVVGAFGVDRAVLYRARPVVTVNAGLEVY 480
Human  LEGQWAARSMPPSFGYSMKGATDIDKNGYPDLIVGAFGVDRAILYRARPVITVNAGLEVY 480
       *******:***************:*:******:*********:*******:*********

Murine PSILNQDNKICPLPGTALKVSCFNVRFCLKADGKGTLPRKLHFQVDVLLDKLKQKGAIRR 540
Human  PSILNQDNKTCSLPGTALKVSCFNVRFCLKADGKGVLPRKLNFQVELLLDKLKQKGAIRR 540
       ********* *.**********************.*****:***::************** 

Murine ALFLHNRSPVHSKTMTVFRGGQMQCEELVAYLRDESEFRDKLTPITIFMEYRLDQRTAAD 600
Human  ALFLYSRSPSHSKNMTISRGGLMQCEELIAYLRDESEFRDKLTPITIFMEYRLDYRTAAD 600
       ****:.*** ***.**: *** ******:************************* *****

Murine ATGLQPILNQFTPANVSRQAHILLDCGEDNVCKPKLEVSVNSDQKKIYIGDDNPLTLTVK 660
Human  TTGLQPILNQFTPANISRQAHILLDCGEDNVCKPKLEVSVDSDQKKIYIGDDNPLTLIVK 660
       :***************:************************:**************** **

Murine AQNQGEGAYEAELIVSIPPQADFIGVVRNNEALARLSCAFKTENQTRQVVCDLGNPMKAG 720
Human  AQNQGEGAYEAELIVSIPLQADFIGVVRNNEALARLSCAFKTENQTRQVVCDLGNPMKAG 720
       ****************** ****************************************

Murine TQLLAGLRFSVHQQSEMDTSVKFDLKIQSSNSFDNVSPVVSYKVDLAEKAAVEIRGVSSP 780
Human  TQLLAGLRFSVHQQSEMDTSVKFDLQIQSSNLFDKVSPVVSHKVDLAVLAAVEIRGVSSP 780
       *************************:***** **:******:*****  ************

Murine DHIFLPIPNWEYKENPETEEDVGPIVQHIYELRNNGPSSFSKAILNLQWPYKYNNNTLLY 840
Human  DHIFLPIPNWEHKENPETEEDVGPVVQHIYELRNNGPSSFSKAMLHLQWPYKYNNNTLLY 840
       ***********:************:******************:*:***************

Murine ILHYDIDGPMNCTADTEINPLRIKTP-----EKNDTGAAGQGERSHLITKRGLTLREGDV 895
Human  ILHYDIDGPMNCTSDMEINPLRIKISSLQTTEKNDT-VAGQGERDHLITKRDLALSEGDI 899
       *************:* ******** .     ***** .******.******.*:* ***:

Murine HTLGCGIAKCLQITCQVGRLDRGKSAILYVKSLLWTETFMNKENQNHSYSLKSSASFNII 955
Human  HTLGCGVAQCLKIVCQVGRLDRGKSAILYVKSLLWTETFMNKENQNHSYSLKSSASFNVI 959
       ******:*:**:*.*************************************************:*

Murine EFPYKNLPIEDLFNSTLVTTNITWGIQPAPMPVPVWVIILAVLAGLLLLAVLVFVMYRMG 1015
Human  EFPYKNLPIEDITNSTLVTTNVTWGIQPAPMPVPVWVIILAVLAGLLLLAVLVFVMYRMG 1019
       ***********: ********:************************************

Murine FFKRVRPPQEEQEREQLQPHENGEGNSET 1044
Human  FFKRVRPPQEEQEREQLQPHENGEGNSET 1048
       ****************************
```

Figure 29 αvβ6 amino acid homology between mice and humans.

β6 Sequence Homology {Accession numbers NP_000879.2, human; NP_067334.1, murine}

```
Murine MGIELVCLFLLLLGRNDHVQGGCAWGGAESCSDCLLTGPHCAWCSQENFTHLSGAGERCD 60
Human  MGIELLCLFFLFLGRNDHVQGGCALGGAETCEDCLLIGPQCAWCAQENFTHPSGVGERCD 60
       *****:***:*:************ ****:*.**** **:****:****** **.*****

Murine TPANLLAKGCQLPFIENPVSRIEVLQNKPLSVGRQKNSSDIVQIAPQSLVLKLRPGREQT 120
Human  TPANLLAKGCQLNFIENPVSQVEILKNKPLSVGRQKNSSDIVQIAPQSLILKLRPGGAQT 120
       ************ *******::*:*:*********************:******  **

Murine LQVQVRQTEDYPVDLYYLMDLSASMDDDLNTIKELGSRLAKEMSKLTSNFRLGFGSFVEK 180
Human  LQVHVRQTEDYPVDLYYLMDLSASMDDDLNTIKELGSRLSKEMSKLTSNFRLGFGSFVEK 180
       ***:************************************:********************

Murine PVSPFMKTTPEEITNPCSSIPYFCLPTFGFKHILPLTDDAERFNEIVRKQKISANIDTPE 240
Human  PVSPFVKTTPEEIANPCSSIPYFCLPTFGFKHILPLTNDAERFNEIVKNQKISANIDTPE 240
       *****:*******:************************:*********::***********

Murine GGFDAIMQAAVCKEKIGWRNDSLHLLVFVSDADSHFGMDSKLAGIVIPNDGLCHLDHRNE 300
Human  GGFDAIMQAAVCKEKIGWRNDSLHLLVFVSDADSHFGMDSKLAGIVIPNDGLCHLDSKNE 300
       ********************************************************* :**

Murine YSMSTVLEYPTIGQLIDKLVQNNVLLIFAVTQEQVHLYENYAKLIPGATVGLLQKDSGNI 360
Human  YSMSTVLEYPTIGQLIDKLVQNNVLLIFAVTQEQVHLYENYAKLIPGATVGLLQKDSGNI 360
       ************************************************************

Murine LQLIISAYEELRSEVELEVLGDTEGLNLSFTALCNNGVLFPHQKKCSHMKVGDTASFNVT 420
Human  LQLIISAYEELRSEVELEVLGDTEGLNLSFTAICNNGTLFQHQKKCSHMKVGDTASFSVT 420
       *********************************:****.** ****************.**

Murine VSVSNCEKRSRNLIIKPVGLGDTLEILVSAECDCDCQREIETNSSKCHNGNGSFQCGVCT 480
Human  VNIPHCERRSRHIIIKPVGLGDALELLVSPECNCDCQKEVEVNSSKCHHGNGSFQCGVCA 480
       *.:.:**:***::**********:**:***.**:****:*:*.******:**********:

Murine CNPGHMGPHCECGEDMVSTDSCKESPGHPSCSGRGDCYCGQCICHLSPYGSIYGPYCQCD 540
Human  CHPGHMGPRCECGEDMLSTDSCKEAPDHPSCSGRGDCYCGQCICHLSPYGNIYGPYCQCD 540
       *:******:*******:*******:*.**********************.*********

Murine NFSCLRHKGLLCGDNGDCDCGECVCRDGWTGEYCNCTTNRDSCTSEDGVLCSGRGDCVCG 600
Human  NFSCVRHKGLLCGGNGDCDCGECVCRSGWTGEYCNCTTSTDSCVSEDGVLCSGRGDCVCG 600
       ****:********.************.***********. ***.****************

Murine KCVCRNPGASGPTCERCPTCGDPCNSKRSCIECYLSADGQAQEECADKCKAIGATISEE- 659
Human  KCVCTNPGASGPTCERCPTCGDPCNSKRSCIECHLSAAGQAREECVDKCKLAGATISEEE 660
       **** ****************************:*** ***:***.****  *******

Murine DFSKDTSVSCSLQGENECLITFLITTDNEGKTIIHNINEKDCPKPPNIPMIMLGVSLAIL 719
Human  DFSKDGSVSCSLQGENECLITFLITTDNEGKTIIHSINEKDCPKPPNIPMIMLGVSLAIL 720
       ***** ****************************.************************

Murine LIGVVLLCIWKLLVSFHDRKEVAKFEAERSKAKWQTGTNPLYRGSTSTFKNVTYKHREKH 779
Human  LIGVVLLCIWKLLVSFHDRKEVAKFEAERSKAKWQTGTNPLYRGSTSTFKNVTYKHREKQ 780
       ************************************************************:

Murine KAGLSSDG 787
Human  KVDLSTDC 788
       *..**:*
```

Figure 30 αvβ6 amino acid homology between mice and humans.

2.3 αvβ6 as a Biological Marker

Neoplastic cells are characterised by genetic, epigenetic, cytoplasmic, cell surface and extracellular matrix changes. During the stages of carcinogenesis, certain molecules may become expressed ectopically, whereas others may be down-regulated, on the cell surface of malignant cells. Such tumour markers often present a useful tool for cancer diagnosis and sometimes prognosis. The difference in the surface profile between cancerous cells and their non-malignant counterparts can serve as a molecular address for targeting reagents to deliver a molecule of choice to the desired cell type. As αvβ6 is 1) a cell surface molecule 2) expressed on cancers, but weak or absent on normal tissue and 3) associated with cancer progression, targeting αvβ6 represents a potential approach to detection and therapy of many types of cancer.

The concept of αv integrin targeting and imaging has been reported previously. For example, αvβ3 is found at much higher levels on activated, as opposed to resting, endothelial cells [225, 226]. It also is over-expressed in certain tumours, such as melanomas, and weakly expressed on most normal organ systems. Haubner *et al* [226] ^{18}F-labelled RGD-containing cyclo-glycopeptides to image αvβ3, using positron emission tomography (PET) *in vivo*. The authors used a melanoma xenograft model, M21, which expresses αvβ3, and M21-L which has weak expression and served as a negative control. Biodistribution studies were performed initially to prove that *in vivo* αvβ3 targeting had been achieved. Results revealed a tumour to blood ratio of 27.5 and a tumour to muscle ratio of 10.2, at 120 minutes post-injection (p.i.). At 120 minutes p.i. the % injected dose per gram (% I.D./g) in

the M21 xenograft was approximately 1.5. Higher % I.D./g for the tumour was achieved at earlier timepoints p.i., but this was at the expense of much smaller tumour to background ratios. Furthermore at 120 minutes p.i., the liver, colon and kidneys revealed a similar activity concentration to the αvβ3-expressing tumour. I also note that the lungs and spleen also had a relatively higher tracer uptake compared to blood and muscle. For their negative control M21-L xenograft mouse model the authors discovered a tracer uptake 3.8 times lower than that in the αvβ3-positive tumour, between 60 and 120 minutes p.i.. Although the study showed αvβ3-expressing tumour uptake of the radiolabelled peptide, it did not show that this specifically was αvβ3-dependent. Furthermore, αvβ3 receptor density was not determined quantitatively for the tumour models, e.g. immunohistochemistry or Western blot. Nonetheless the authors proceeded to PET studies and visualised the αvβ3-expressing tumour in the left flank of the mouse. This visualisation was in contrast to the negative control melanoma M21-L xenograft. Of note, only one mouse was imaged in each group. Haubner *et al* concluded that ^{18}F-labelled peptides were suitable compounds for the non-invasive determination of αvβ3 integrin status and could be used for monitoring of therapy [226].

In a later study, Haubner did correlate tracer uptake with αvβ3, as detected by immunohistochemistry and Western Blot [227]. At 90 min after tracer injection, their small-animal PET scanner showed increasing tracer uptake in the tumour corresponding with the percentage of receptor-positive cells. However, the full % I.D./g for each organ was not reported in this article. Furthermore, the % I.D./g for the M21 xenograft was now reported at only 1.07. Nevertheless, the authors proceeded to a human study and reported heterogeneous detection of αvβ3-

expressing tumours [227]. The authors have suggested many possible reasons for this heterogeneous result. These include poor vascular access (perfusion and permeability) to some of the tumours, potential necrotic areas within tumours and sampling error confounding correlation.

Hausner *et al* [228] have recently published initial results of our group's lead peptide (A20FMDV2) radiolabelled with 4-[^{18}F]fluorobenzoic acid and imaged on a PET scanner. *In vitro* sensitivity and specificity was documented for αvβ6. Male athymic nude mice were inoculated subcutaneously, on opposite shoulder areas, with either 3 x 10^6 αvβ6-expressing, or 3 x 10^6 αvβ6-non-expressing cells. Initially biodistribution experiments revealed uptake in the αvβ6-expressing tumour was 0.66% ID/g at 1 h, dropping to 0.28% and 0.06% ID/g at 2 and 4 h, respectively. In contrast, uptake in the control tumour stayed at less than one third of the αvβ6-expressing tumour at all time points (0.21%, 0.07%, and 0.02% ID/g at 1, 2, and 4 h, respectively). Other background measurements included blood (0.27%, 0.06%, and 0.03% ID/g at 1, 2, and 4 h, respectively) and muscle (0.56%, 0.22%, and 0.08% ID/g at 1, 2, and 4 h, respectively). Therefore, αvβ6-expressing tumour to blood and muscle ratios were around 3:1 and close to 1:1, respectively. Relative high levels of activity were also detected in the gall bladder (1 h, 15.1%I.D./g; 4 h, 1.97% ID/g) and stomach (1 h, 1.33% ID/g; 4 h, 0.22% ID/g). The uptake of the lungs was not published. Despite the disappointing tumour to background ratios, PET images with good positive tumour/negative tumour and positive tumour/background ratios generally were obtained 30 to 90 min after injection [228]. Based on PET volume-of-interest analysis, the ratio of accumulated activity in the αvβ6-expressing tumour versus background improved steadily over time (1 h, 2.2:1; 3 h, 3.5:1). The authors showed

that the differences in tumour uptake were not caused by differences in tumour viability; utilising the metabolic tracer [^{18}F]FDG as a surrogate for tissue viability. The similar uptake of the metabolic radiotracer in both tumours suggested comparable blood supplies and metabolic rates in both xenografts.

The above studies all serve as a proof-of-principle for targeting and imaging of integrins within cancers.

We therefore have developed αvβ6-specific peptides for *in vivo* targeting of αvβ6. This project will describe the coupling of these peptides to γ-emitting radioisotopes and the use of SPECT to localise the peptide-isotope complex, *in vivo*. The advantages of the NanoSPECT system, (e.g. improved resolution; relative ease of availabilty of the SPECT radionuclides - see **Table 8**, page 118) in comparison to microPET, lend the former system to be more favourable for murine experiments. Initially, the characterisation of linear peptides will be illustrated. However later studies will demonstrate the use of cyclic peptides. Cyclisation and use of D-amino acids can be used to stabilise peptides whilst maintaining (and sometimes improving) their biological activity [190]. This increased stability aims to retard protease degradation and increase serum viability. This allows greater time for the ligand to bind to its target.

2.4 Overview Of Project

Previous work in the Tumour Biology Laboratory synthesised a panel of short peptides, which contained the known tripeptide integrin–binding motif, RGD [12]. Linear peptides were generated, screened and selected on their ability to inhibit αvβ6-dependent adhesion competitively on known high affinity ligands e.g. LAP. Results revealed that the lead peptide was A20FMDV2 [229]. It was derived from the GH loop of the viral surface protein VP1 of Foot and Mouth Disease Virus (FMDV). The NMR solution structure of A20FMDV2 is consistent with the X-ray crystallography data of the reduced, stabilised sequence in the VP1 protein of FMDV O_1 BFS [230]. Nuclear Magnetic Resonance imaging demonstrated, and confirmed, that A20FMDV2 binds to αvβ6 via its RGDLXXL motif. Furthermore its extended carboxy α–helical structure is supportive to ligand binding.

Therefore, A20FMDV2 and other candidate peptides were selected to be radiolabelled for pre-clinical validation of their potential use as *in vivo* targeted agents for imaging.

2.5 Project Objectives

- To radiolabel A20FMDV2 and other candidate (αvβ6-specific) ligands
- To confirm *in vitro* specificity of the aforementioned probes and measure their affinity to αvβ6-expressing cells
- To establish whether the αvβ6-specific probes are internalised and retained within cells
- To examine the stability of αvβ6-specific probes upon purification
- To determine the biodistribution and kinetics of αvβ6-specific probes *in vivo*.
- To establish optimal conditions for SPECT imaging of αvβ6-expressing tumours *in vivo*.
- To validate the αvβ6-specific probes on other tumour models
- To compare the targeting capacity of different αvβ6-specific ligands as imaging modalities.
- To translate the benchwork into clinical benefit, by developing a potential human trial design.

Chapter III: Materials and Methods

3.1 Saline and Media Formulations

The following were supplied by Cancer Research UK (CR-UK) Media Services (South Mimms, Herts): Dulbecco's Modification of Eagle's Medium (DMEM), Ham's-F12 media and isotonic Phosphate Buffered Saline (PBS).

3.2 Antibodies

Several murine (unless stated otherwise) monoclonal antibodies (mAbs) were used in this study: FB12 (anti-α1 integrin subunit; Chemicon, Hampshire, UK), P1E6 (anti-α2 integrin subunit; Chemicon), P1B5 (anti-α3 integrin subunit; Chemicon), 7.2 (anti-α4 integrin subunit; CR-UK), P1D6 (anti-α5 integrin subunit; Chemicon), GOH3 (rat anti-α6 integrin subunit; Serotec), Y9A2 (anti-α9β1 integrin subunit; Chemicon), 3E1 (anti-β4 integrin subunit; Chemicon), LM609 (anti-αvβ3 integrin subunit; Chemicon), 10D5 (anti-αvβ6 integrin subunit, Chemicon), 14E5 (anti-β8 integrin subunit, kind gift of Dr. S. Nishimura, UCSF, San Francisco, USA). P1F6 (anti-αvβ5 integrin subunit, gift from Dr D. Sheppard, UCSF, San Francisco, USA) and AIIB2 (rat anti-β1 integrin subunit) were prepared in-house from hybridomas. 62G2, 68G6 and 63G9 were supplied by Biogen Idec (Cambridge, MA, USA) [231]. Control mouse and rat IgG1 was purchased from DAKO (DAKOCytomation Ltd., Ely, UK).

3.3 Radioisotopes

Indium chloride ($^{111}InCl_3$) was supplied by Tyco Healthcare UK Commercial Ltd. (Hampshire, UK).

3.4 HPLC solvents

HPLC solvents were sourced from Sigma-Aldrich (Dorset, UK) and were all 'HPLC grade'. Ultra High Purity (UHP) water was obtained from an Elga Purelab Maxima water purification system (Buckinghamshire, UK).

3.5 Cell Lines

Table 9 (page 131) lists the cell lines used in this study. All cells grew as adherent monolayers, in 100% humidified atmosphere of 8% (v/v) carbon dioxide / air at 37^{o}C (mouse keratinocytes at 33^{o}C). The tumour cell lines routinely were tested for and found free of *Mycoplasma* and were grown in Falcon tissue culture flasks.

Cell Line	Tissue of Origin	Growth Media[§]	Reference
A375P puro	Skin melanoma	DMEM	Generated in-house [232]
A375P β6	Skin melanoma	DMEM	Generated in-house [232]
Mouse Keratinocytes	Mouse Skin	KGM	DiPersio et al [233]
MCF-10A	Breast	DMEM/F12 (1:1)	DiPersio et al [233]
MCF-10AneoT	Breast	DMEM/F12 (1:1)	Santner et al [234]
AT1K.c12	Breast	DMEM/F12 (1:1)	Santner et al [234]
Ca1h	Breast	DMEM/F12 (1:1)	Santner et al [234]
CA1a	Breast	DMEM/F12 (1:1)	Santner et al [234]
MCF-10 DCIS.com	Breast	DMEM/F12 (1:1)	Santner et al [234]

Table 9 Summary of cell lines tested within this project.

[§] Media supplements are described within text.

3.5.1 Melanoma cell line as a model for β6 targeting

Human melanoma cancer cell lines were obtained from the CR-UK stocks and maintained according to standard protocols. The A375P β6 and A375P puro cells were generated in-house, as follows: The A375P human melanoma cell line [232] was retrovirally infected with the full-length gene for the human β6 integrin subunit and the puromycin resistance gene, or solely the puromycin resistance gene; generating A375P β6 and A375P puro, respectively [141, 229, 235]. Cells were selected in puromycin (1.25 μg/ml) and then αvβ6-expressing cells were selected by magnetic bead sorting, using 10D5 (anti-αvβ6; Chemicon International), according to

the manufacturer's instructions (Invitrogen). Clone 10D5 was also used in flow cytometry and function-blocking (see below).

Cells were maintained on DMEM supplemented with 10% foetal calf serum (FCS; Biowest, Nuaille, France), 4mM glutamine (CR-UK Media Services) and 1.25μg/ml of puromycin.

3.5.2 Breast Cell Lines

A panel of human breast cell lines, all derived from the immortal MCF-10A line, were provided by the Barbara Ann Karmonos Cancer Institute (Detroit, Michigan, USA). MCF-10A, MCF-10AneoT and AT1K.c12 belonged to the MCF-10A and MCF-10AneoT series. Ca1h, CA1a and MCF-10 DCIS.com belonged to the MCF-10CA1 series [234]. The culture medium for the MCF-10CA1 series of lines comprised DMEM/F12 with 5% horse serum (Invitrogen, Paisley, UK) and 4mM glutamine (CR-UK Media Services). The culture media for the MCF-10A and MCF-10AneoT lines is similar, but supplemented with 20 ng/ml epidermal growth factor (Upstate Biotechnology Inc, Lake Placid, NY), 10μg/ml insulin (Sigma Chemical, St Louis, MO), 100 ng/ml cholera enterotoxin (Sigma Chemical), and 0.5μg/ml hydrocortisone (Sigma Chemical).

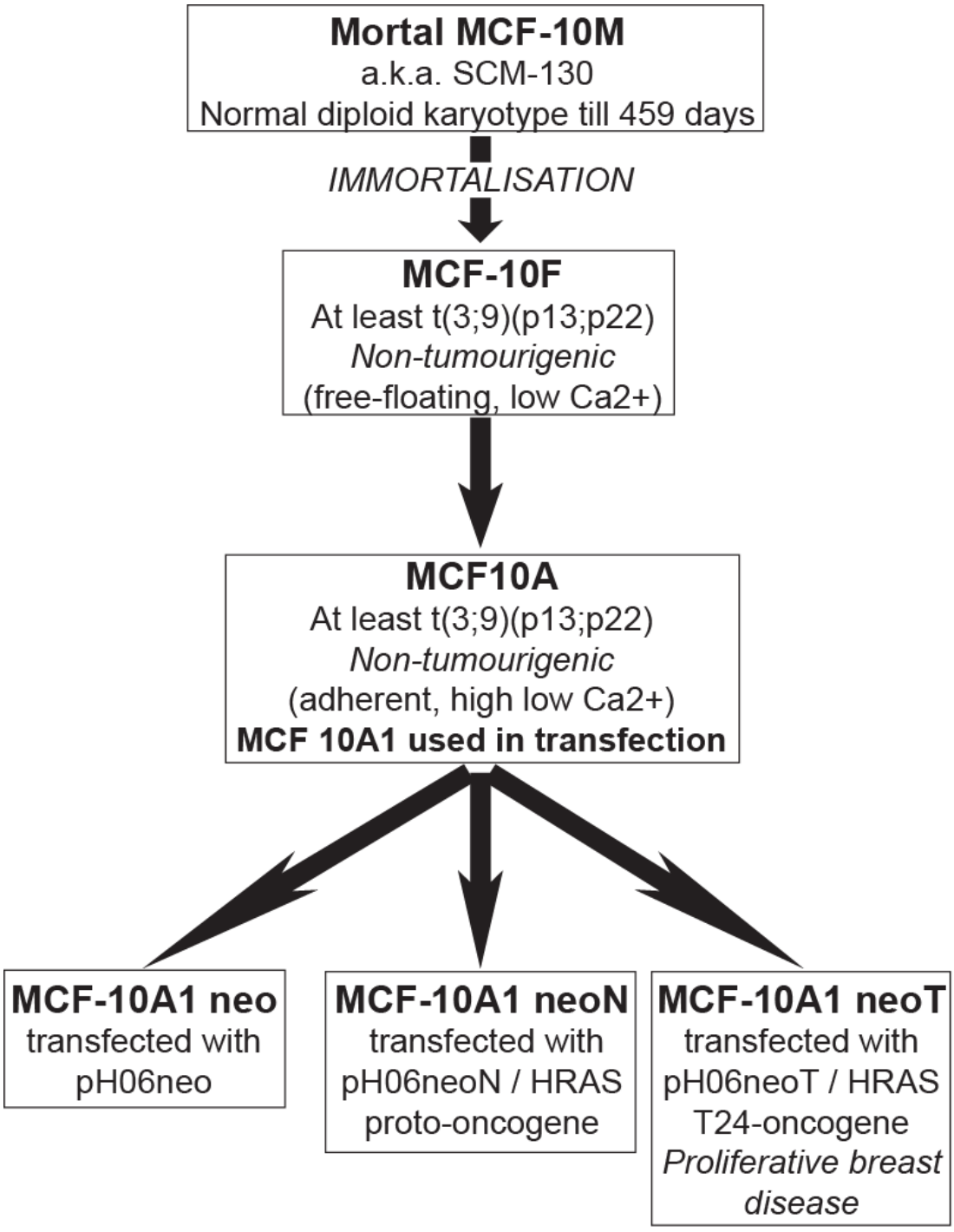

Figure 31 The MCF-10A cell series [234]

.

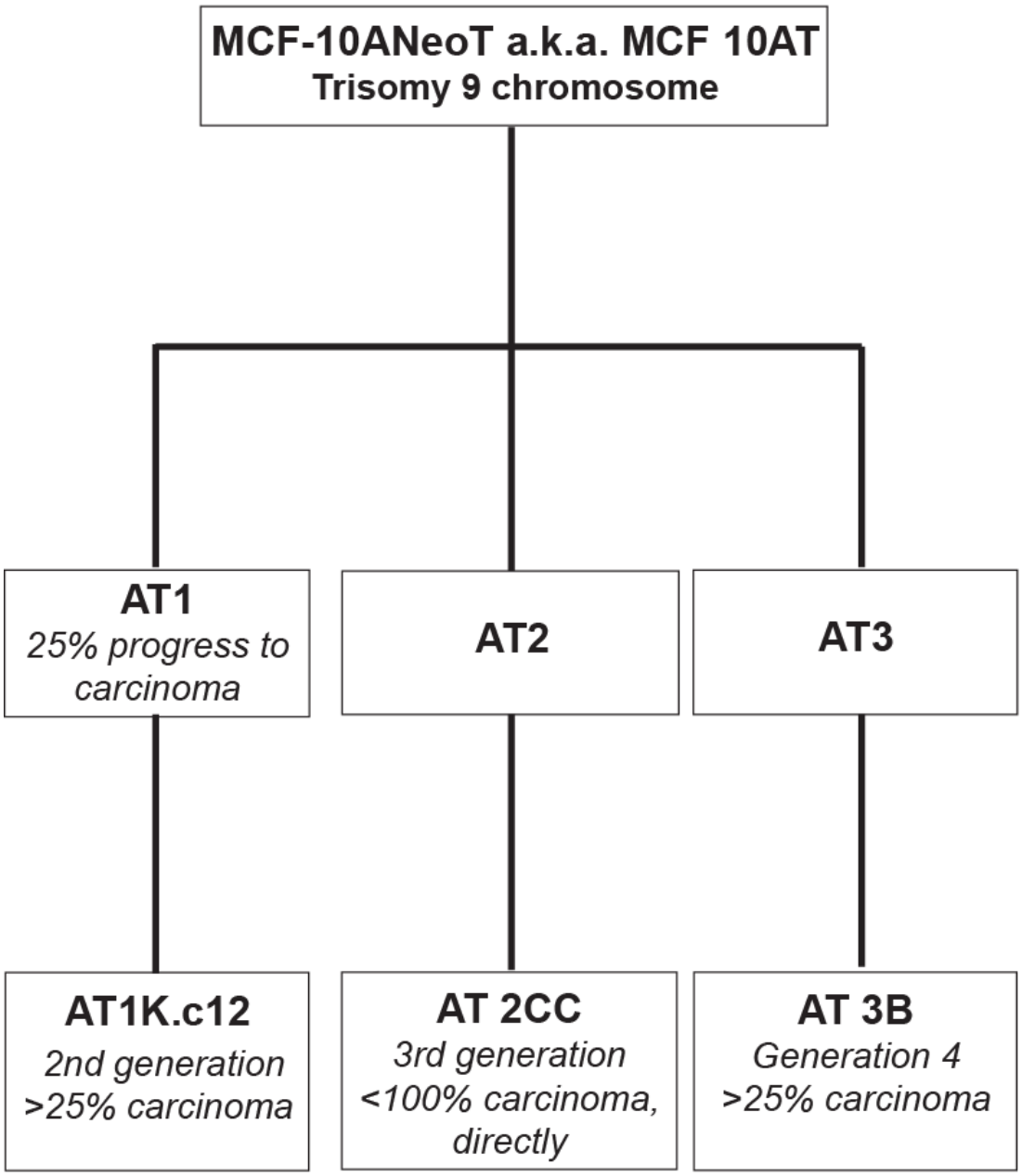

Figure 32 The MCF-10AneoT cell series [228].

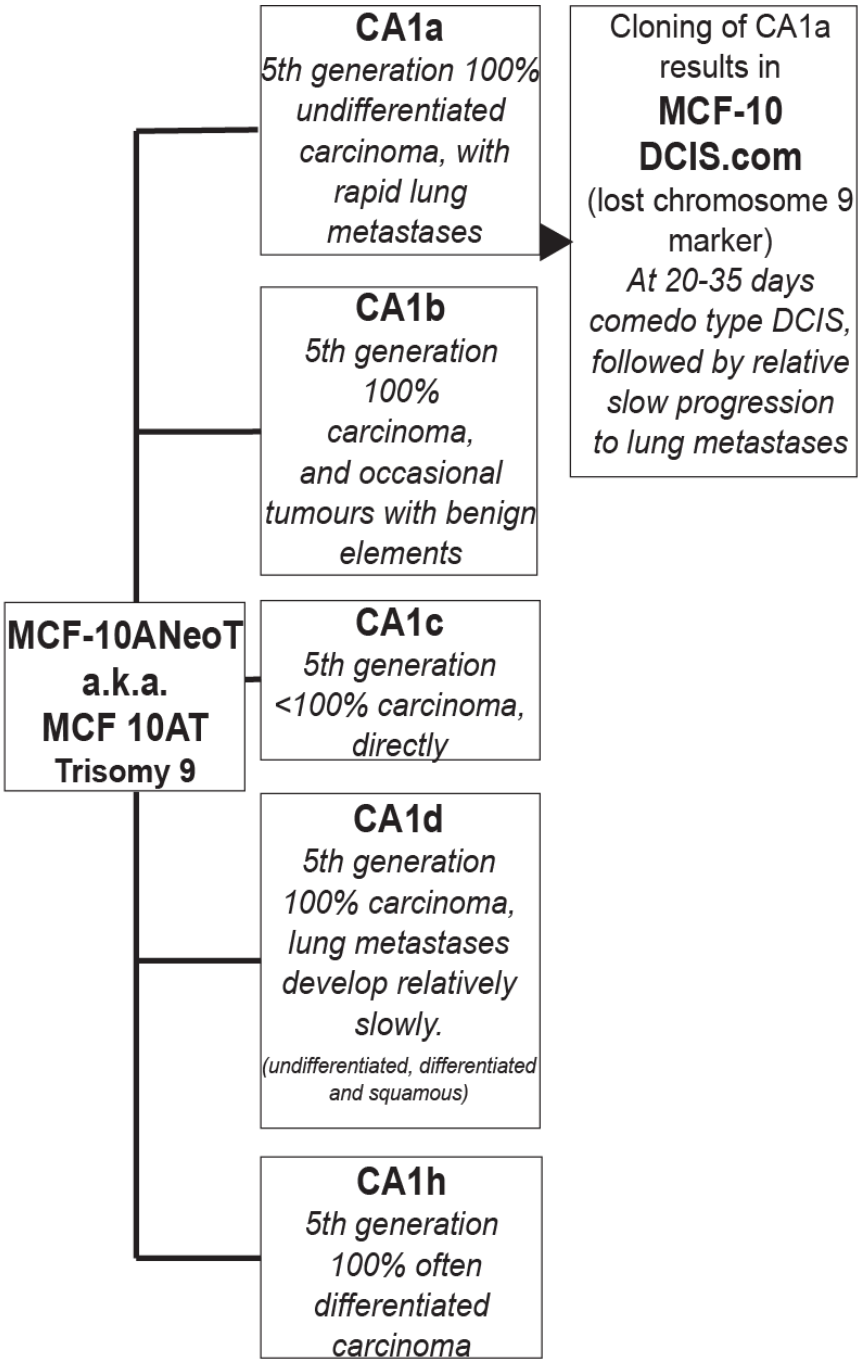

Figure 33 The MCF-10CA1 cell series [234].

3.5.3 Mouse Keratinocyte cell line

Immortalised *wild-type* mouse keratinocytes were prepared from the temperature-sensitive SV40 large T mouse (Immortomouse) as described previously [233]. Briefly, primary mouse keratinocytes were immortalised from mouse skin and grown in KGM, at 33^{o}C. KGM consisted of low Ca^{2+} FAD (Cancer Research UK, London, UK), 10% FCS (chelated), 10^{-10}M cholera toxin, 0.4 μg/ml hydrocortisone, 5 μg/ml insulin (all from Sigma Chemical), 10 ng/ml EGF (Life Technologies), but *omitting* the interferon-γ. The omission of interferon-γ switches off the temperature-sensitive mutant of the SV40 large T antigen (tsA58) immortalisation gene and therefore the keratinocytes have a primary cell phenotype. Immortalised keratinocytes were used for all experiments.

Prior to seeding the keratinocytes, tissue culture plastic was pre-incubated with 'coating media', at 37^{o}C for at least one hour. The coating media comprised BSA (0.09 mg/ml; PAA Laboratories GmBH, Pasching, Austria), HEPES (18.5 mM; Sigma Chemical), calcium chloride (0.9 mM; Fisher Scientific UK Ltd, Leicestershire, UK) and Type 1 collagen (PureCol; diluted 1:100; Nutacon, The Netherlands) diluted in DMEM. After this period, the coating medium was removed and replaced with keratinocytes resuspended in KGM.[236]

3.5.4 Maintenance of cell lines

The A375P derived cells were sub-cultured approximately twice weekly by incubation with 0.25% (w/v) trypsin, followed by centrifugation and neutralisation of the trypsin with growth medium, and distribution of the cell suspension to fresh tissue culture flasks together with fresh growth medium.

The MCF-10CA1 series of lines were sub-cultured approximately twice weekly by incubation with 0.25% (w/v) trypsin followed by centrifugation and neutralisation of the trypsin with growth medium, and distribution of the cell suspension to fresh tissue culture flasks with fresh growth medium.

The MCF-10A and MCF-10AneoT series of lines were sub-cultured, approximately three times a week, using the following regime: three 8-10 minute incubations with 0.02% (w/v) versene, followed by differential trypsinisation with 0.5% (w/v) stock trypsin solution. This procedure was followed by centrifugation and neutralisation of the trypsin with growth medium, and distribution of the cell suspension to fresh tissue culture flasks with fresh growth medium.

The mouse keratinocytes were sub-cultured, approximately twice weekly, using differential trypsinisation with 0.25% (w/v) trypsin, at 37^{o}C. The incubation was followed by centrifugation and neutralisation of the trypsin with growth medium, and distribution of the cell suspension to 'coated' tissue culture flasks with fresh growth medium.

3.5.5 Long-term Storage of Cell Lines in Liquid Nitrogen

A375P derived cells in logarithmic-phase growth were detached as described above, the trypsin centrifuged off and neutralised by addition of growth media, and a single-cell suspension of cells generated by pipetting. The cells were then re-pelleted by centrifugation, re-suspended in DMEM supplemented with 20% foetal calf serum and 10% dimethyl sulphoxide (DMSO; BDH, distributed by VWR UK), transferred to 2ml cryovials (Falcon) and stored overnight within insulated polystyrene boxes (Eprak, Scotlab, Scotland) at -80^{o}C. The vials were then relocated to liquid Nitrogen for long-term storage. Vials subsequently were defrosted at 37^{o}C and the cells washed once in warm growth media before plating.

The breast cell lines in logarithmic-phase growth were detached as described above, the trypsin centrifuged off and neutralised by addition of growth media, and a single-cell suspension of cells generated by pipetting. The cells were then re-pelleted by centrifugation and re-suspended in DMEM/F12 medium containing 20% calf serum supplemented with 10% dimethyl sulphoxide (DMSO; BDH, distributed by VWR UK). Aliquots of this cell suspension were transferred to 2ml cryovials (Falcon) and stored overnight within insulated polystyrene boxes (Eprak, Scotlab, Scotland) at -80^{o}C. The vials were then transferred to liquid Nitrogen for long-term storage. Vials subsequently were defrosted at 37^{o}C and the cells washed once in warm growth media before plating.

The mouse keratinocytes in logarithmic-phase were detached as described above, the trypsin centrifuged off and neutralised by addition of growth media, and a single-cell suspension of cells generated by pipetting. The cells were then re-pelleted by centrifugation and re-suspended in Calcium-depleted FBS containing 10% dimethyl

sulphoxide (DMSO; BDH, distributed by VWR UK). Aliquots of this cell suspension were transferred to 2ml cryovials (Falcon) and stored overnight within insulated polystyrene boxes (Eprak, Scotlab, Scotland) at -80^{o}C. The vials were then transferred to liquid Nitrogen for long-term storage. Vials subsequently were defrosted at 37^{o}C and the cells washed once in warm growth media before plating.

3.6 Peptides

All peptide sequences used in this report are given in **Appendix I**. Peptides B-DBD1 and B-Ran were supplied by Bachem (Merseyside, UK). All other peptides were synthesised by Cancer Research UK Peptide Synthesis Laboratory using the following solid-phase peptide synthesis protocol (provided by Ms Rebecca Black). Protected amino acids and pre-loaded Wang resins were obtained from Calbiochem-Novabiochem (Nottingham, UK). Solvents and HBTU [2-(1H-benzotriazol-lyl)-1, 1, 3, 3-tetramethylironium hexafluorophosphate] were obtained from Applied Biosystems (Warrington, UK). The peptides were synthesised on a Model 433A Applied Biosystems Solid Phase Synthesiser on preloaded Wang resin using basic feedback monitoring cycles and HBTU as a coupling reagent. 9-fluoroenylmethylcarbonyl was used for temporary α-amino group protection and removed using piperidine. Side-chain protecting groups were tert-butloxycarbonyl for Lys; trityl for His, Asn and Gln; 2, 2, 4, 6, 7-pentamethyldihydro-benzofuran-5-sulfonyl for Arg; tert-butylester for Glu and Asp and tert-butyl ether for Thr, Ser and Tyr.

Cleavage of the resin and deprotection of the peptides was achieved by treating the peptidyl-resin with 10 mls of a mixture containing 9.25mls trifluoroacetic acid, 0.25mls ethanedithiol, 0.25mls tri-isopropylsilane and 0.25mls water at 20^{o}c (room temperature) for 4 hours. The peptide was precipitated using ice-cold di-ethylether and then filtered on a fine sintered glass filter funnel under light vacuum. The peptide precipitate was dissolved in 10% acetic acid / water solution and freeze-dried.

The crude peptides were analysed by Agilent 1100 reverse phase HPLC and electrospray mass spectroscopy. Peptides were purified by reverse phase HPLC to greater than 90% pure, on an Aquapore ODS 20 micron 250 x 10 mm column. Peptides were supplied lyophilised and stock solutions prepared in 0.1% Trifluoroacetic acid (TFA; Sigma Chemical).

Standard concentrations were confirmed spectrophometrically using absorption at 215nm, as follows: A 10 μl 0.1% TFA reconstituted sample was diluted to 1000 μl with UHP water. A blank was created using similar ratios of 0.1% TFA and UHP water. The absorbancies of the samples were measured at 215 nm, on a Beckman DU 600 general purpose UV/Vis spectrophotometer, with a 1250 ml quartz micro-cuvette. The concentration of the sample is thus calculated using the Beer-Lambert Law.

To a selection of peptides, the chelating agents diethylenetriamene pentaacetate-tetra (DTPA t-Bu ester; Macrocylcics, Texas, USA) or 1,4,7,10-Tetraazacyclododecane-1,4,7-tris-*tert*-butyl acetate-10-acetic acid (DOTA-tris *t*-Bu ester; Macrocylcics) were added to the N-terminus, and a lysine residue biotinylated. These peptides essentially were synthesised using the method described above. However, the DTPA / DOTA addition was carried out between synthesis and cleavage, when the final Fmoc had been removed but all the other protecting groups were still present. Furthermore, during cleavage the peptides were centrifuged for 10mins at 3700rpm, instead of filtering them in a sinter funnel to avoid contact with glass.

3.7 Flow Cytometry Experiments

3.7.1 Analysis Of Integrin Expression Using Flow Cytometry

Single cell suspensions were generated as described above and collected by centrifugation at 4^{o}C. All of the following steps occurred at 4^{o}C. The supernatant was removed, and cells were re-suspended in a buffer consisting of 20mM Tris pH 7.5, 150mM NaCl, 20mM EDTA, 0.1% azide, 0.1% BSA and distilled water (EDTA 0.1/0.1). The cells were washed (by centrifugation and pellet resuspension) a further two times in the aforementioned cation chelating buffer. Finally, the cells were washed three times, pelleted and resuspended in MgCa 0.1/0.1 buffer consisting of 20mM Tris pH 7.5, 150mM NaCl, 0.5mM $MgCl_2$, 1mM $CaCl_2$, 0.1% sodium azide, 0.1% BSA and distilled water. Cells were counted, and 100,000 cells were placed into each well of a Falcon 353911 flexible plate. Cells were then incubated for 40 min with the desired integrin-specific antibody (10 μg/ml) antibody, isotype IgG1

(10 μg/ml) control (DAKOCytomation Ltd., Ely, UK), or diluent alone [141]. All dilutions were made using MgCa 0.1/0.1 buffer. After washing, cells were incubated for 20 min with a 1:200 dilution of Alexa-488 conjugated goat anti-mouse IgG (Molecular Probes). Samples were again washed in MgCa 0.1/0.1 wash buffer. Finally, the cells were resuspended in 400μL of wash buffer and transferred to a Falcon 2054 tube. Cells were analysed on a Becton Dickinson FACS LSR1. Analysis was performed using Cell Quest (v3.3), measuring 10,000 events per sample and gating performed to exclude cell debris and apoptotic cells.

3.7.2 Confirmation of Biotinylated Peptide binding to Cells by Flow Cytometric Analysis

The method was similar to that for integrin profiling, but the integrin-specific antibody was substituted with biotinylated peptide, diluted to the desired concentration in MgCa 0.1/0.1 wash buffer. Furthermore, after the peptide incubation, the cells were washed and incubated for 30 min with a 1:120 dilution of mouse anti-biotin IgG (Jackson ImmunoResearch, Stratech, Soham, Cambridgeshire, UK). Once this incubation had been completed, the cells were washed and incubated for 20 min with a 1:200 dilution of Alexa-488 conjugated goat anti-mouse IgG (Molecular Probes). The protocol then continued as described above for the Analysis Of Integrin Expression.

3.7.3 Anti- αvβ6 Competition Assay to Confirm Binding Specificity of Peptide

Murine keratinocytes in suspension were washed three times with EDTA 0.1/0.1 cation chelating buffer and then three times with the TBS-Mn 0.1/0.1 wash buffer. TBS is Tris-Buffered-Saline and was prepared by CR-UK Media Services, using 25mM Trizma base, 15mM NaCl, 3mM KCl, 0.7mM NaH_2PO_4, 5.6 mM D-glucose and 0.04mM phenol red. The addition of 1mM manganese chloride, 0.1% azide and 0.1% BSA to TBS produced TBS-Mn 0.1/0.1 wash buffer. All of the following steps occurred at 4^oC. Cells ($2x10^5$/50µl) were resuspended in TBS-Mn 0.1/0.1 supplemented with either 10µg/ml 68G6 (mouse anti-αvβ6, Biogen Idec) or non-immune control IgG1. After a 30 minute incubation, biotinylated peptide was added to the aforementioned cell-antibody suspensions (final peptide concentration 10 nM). After a further 40 minute incubation, cells were washed three times in TBS-Mn 0.1/0.1. Bound biotinylated peptide was detected by incubation for 30 minutes with 10 µg/ml polyclonal rabbit anti biotin (Abcam, Cambridge, UK). After two washes with TBS-Mn 0.1/0.1, wells were designated to be incubated with either a 1:250 dilution of Alexa-647 goat anti-rabbit IgG (Molecular Probes) or a 1:200 dilution of Alexa-488 conjugated goat anti-mouse IgG (Molecular Probes), or both were added to the cells. Dual colour allowed differential detection of bound anti-αvβ6 antibody from bound biotinylated peptide. Following this 20 minute incubation, cells were washed three times with TBS-Mn 0.1/0.1 wash buffer, resuspended in 400µL of wash buffer and transferred to a FACS Falcon 2054 tube. Cells were analysed on a Becton Dickinson FACS LSR, using FL-1H, FL-5H and FL-3H channels. Analysis

was achieved using Cell Quest (v3.3), measuring 10,000 events per sample and propidium iodide gating performed to exclude dead cells.

A similar method was employed to confirm peptide binding specificity on the A375P derived cells. However, the use of EDTA 0.1/0.1 cation chelating buffer was not required and the TBS-Mn 0.1/0.1 wash buffer was substituted for DMEM 0.1/0.1 wash buffer. DMEM 0.1/0.1 comprises DMEM, 0.1% azide and 0.1% BSA.

3.8 Transwell® Invasion Assays

Cell invasion assays utilised Transwell® plates (Costar®, Corning Incorporated, Life Sciences, Corning NY, USA) in which an upper and lower chamber are divided by a polycarbonate insert. The polycarbonate membrane, incorporated for these assays, was 6.5 mm in diameter and penetrated by 8µm pores. Furthermore, these inserts were coated with 70 µL of diluted Matrigel® (Becton Dickinson) and allowed to polymerise at 37^{o}C, for 1 hour. Single cell suspensions were generated as described above and collected by centrifugation at 4^{o}C. However, the cells were re-suspended in serum-free media. Following Matrigel® polymerisation, 5 x 10^{4} cancer cells were plated in the upper chamber and the appropriate 'complete' media dispensed in the lower chamber, acting as a chemoattractant. The Transwell® plate was incubated for 24-72 hours in 100% humidified atmosphere of 8% (v/v) carbon dioxide / air, at 37^{o}C.

After incubation, the cells which invaded the Matrigel® and passed through the membrane into the lower chamber were counted. This counting procedure involved

collection of the complete media from the lower chamber and dispensing the cell suspension into a prepared counting tube containing a known volume of CASY®ton solution (Schärfe System GmbH, Reutlingen, Germany). The transfer of cells from the lower chamber and lower surface of the membrane was facilitated by trypsin / versene incubation for 1 hour, at 37^{o}C. Subsequent careful washing of the insert and lower chamber ensured maximal transfer of harvested cells from chamber to the counting tube. The cell counts were quantified using a CASY automated cell counter (Schärfe System GmbH). Each condition was replicated at least in triplicate and individual experiments were repeated at least three times.

Blocking experiments additionally used one of the anti-αvβ6 antibodies (68G6 or 63G9) which were pre-mixed with the cancer cells, 30 minutes prior to plating, and these treatments were compared to pre-mixing with a control antibody (e.g. 7.2)

.

3.9 Radiolabelled Peptide Studies

3.9.1 Peptide Radiolabelling

Lyophilised peptide preparations were reconstituted in 0.1% TFA and further diluted to desired concentrations (0.1-20 μg/μl). $^{111}InCl_3$ was added to the peptide at the desired specific activity, within a cryogenic vial (Corning, New York, USA), and buffered with ammonium acetate, pH 5.5 (20% of indium volume added). Precise specific activities were determined using a CRC-15 Beta dose calibrator (Capintec, New Jersey, USA). Sealed cryovials were vortexed briefly and incubated for thirty minutes, either at room temperature (DTPA peptides) or 100^{o}C (DOTA peptides). Following incubation the reaction was quenched with 0.1M Sodium EDTA (5% of

reaction volume) and buffered with PBS to the desired injection volume. Radiopeptides prepared for saturation assays also had 1μL of 1mg/ml cold $InCl_3$ added to the reaction mixture, prior to EDTA quenching.

Radiolabelling efficiency and purity of the radiolabelled compound were analysed by reverse phase high-performance liquid chromatography (RP-HPLC). Analysis was performed using a Beckmam system Gold HPLC (166 NM detector; Beckman, High Wycombe, UK), its proprietary software and a Jupiter 300A column (5μm C18, 259 x 4.60 mm; Phenomenex, Macclesfield, UK) with a flow rate of 1 ml/minute. The mobile phase consisted of a linear gradient of increasing acetonitrile in 0.1% aqueous TFA, according to the following schedule: 0-5 minutes, 0% acetonitrile; 5-25 minutes, 0-60% acetonitrile; 35-37 minutes, 100-0% acetonitrile. Radioactivity was detected via a sodium-iodide detector (Raytest 'Gabi'; Raytest UK Ltd, Chesterfield UK) interfaced to a multichannel analyser.

3.9.2 Radioligand binding studies: Saturation Assays

A375Pβ6 cells were incubated at 37^{o}C for 24-48 hours and grown to 60-80% confluency within six-well plates (Falcon, Tissue Culture treated, Becton Dickinson). After the desired confluency was reached, wells were washed with DMEM media in order to remove unbound cells. To each well was added a volume of 150 μl of ^{111}In-DTPA-A20FMDV2 (varying from 200nM to 1nM concentrations, diluted in PBS/1%BSA) together with 1.2 μl of DMEM/1% BSA /0/1% azide. To determine background non-specific binding, selected wells also had 150 μl of non-radiolabelled

DTPA-A20FMDV2 (10μM) added. To those wells not selected for the addition of non-radiolabelled DTPA-A20FMDV2, 150 μl of PBS/1%BSA was added to keep reaction volumes and concentrations comparable. The plates were incubated at 37^{o}C for ninety minutes, after which the wells were washed twice with ice-cold DMEM/1% BSA /0/1% azide, and then cells were lysed with 1ml of 1M NaOH for 15 min. Transfer of lysates into labelled scintillation tubes was facilitated by twice washing with PBS. Three 150 μl aliquots of ^{111}In-DTPA-A20FMDV2, at each prepared molarity, were placed in three scintillation tubes to provide standards and a method to relate radioactivity counts to molarity, for the assay. The radioactivity associated with lysates and standards was measured on a Gamma Counter (LKB Compugamma, Victoria, Australia). Each radioligand molarity was analysed in triplicate and the respective mean amount of bound radioactivity determined. The specific binding of the radiopeptide was calculated by subtracting the non-specific binding from the total cell-radioligand binding. After counting the radioactivity, protein was measured in cell lysates using a commercial kit (BioRad DC Assay, Netherlands). Using non-linear regression analysis with GraphPad Prism version 4.00 for Windows (GraphPad Software, San Diego California USA), K_d and B_{MAX} were determined.

3.9.3 Radioligand binding studies: Cell Internalisation Assay

The extent and rate of internalisation of the ^{111}In-DTPA-A20FMDV2 was studied with A375P β6 cells. Cells were grown to 60-80% confluency in six-well plates and washed with DMEM. A volume of 150 μl of ^{111}In-DTPA-A20FMDV2 (20 ng/ml,

diluted in PBS/1%BSA) was added together with 1.2 μl of ice-cold DMEM/1% BSA to each well, either in the absence or presence of 150 μl of unlabelled DTPA-A20FMDV2 (10μM). To those wells not selected for the addition of non-radiolabelled DTPA-A20FMDV2, 150 μl of PBS/1%BSA was added to keep reaction volumes and concentrations comparable. The plates were incubated at 37^{o}C for various time points after which triplicate wells were analysed as follows:-

Internalisation was interrupted (at pre-selected time points) by removing the medium and washing twice with ice-cold DMEM/1% BSA. Surface-bound radioactivity was removed by a 25 minute treatment of intact cells with 1 ml DMEM-HCl acid buffer at pH 4, on ice. Please note, that the acid wash buffer and its duration was tested in separate optimisation experiments (see below). The transfer of the membrane-bound radioligand fraction into labelled scintillation tubes was facilitated by a further 30 second wash with the acid wash buffer. Following this, the internalised activity was collected after lysing the cells with 1 ml 1M NaOH and washing twice with PBS. Three 150 μl aliquots of ^{111}In-DTPA-A20FMDV2 were placed in three separate scintillation tubes to provide standards and a measure of the total radioactive counts for the assay. The radioactivity content of collected fractions and standards were measured on a gamma counter, and the specific internalised fraction expressed as a percentage of the initial radioactivity added per milligram of cell protein. In addition, the specific internalised fraction was expressed in relation to the total activity bound to cells i.e. the sum of the internalised and membrane bound fractions equates to the total cell-bound activity. After counting the radioactivity, protein was measured in cell lysates using a commercial kit (BioRad DC Assay, Netherlands).

3.9.3.1 Optimisation of Cell Internalisation Assay

In order to determine the most efficient acid wash buffer, to remove the membrane-bound radioligand fraction, optimisation experiments were carried out. A375P β6 cells were grown to 60-80% confluency in six-well plates and washed with DMEM. All of the following procedures were performed 'on-ice' (unless stated) to minimise internalisation. A volume of 150 μl of ^{111}In-DTPA-A20FMDV2 (20 ng/ml, in PBS/1%BSA) was added together with 1.2 μl of ice-cold DMEM/1% BSA to each well, either in the absence or presence of 150 μl of unlabelled DTPA-A20FMDV2 (10μM). To those wells not selected for the addition of non-radiolabelled DTPA-A20FMDV2, 150 μl of PBS/1%BSA was added to keep reaction volumes and concentrations comparable. The plates were incubated on ice for 30-60 minutes to permit radioligand and receptor interaction, but minimal internalisation. After this incubation, triplicate wells were analysed as follows:-

Radioligand and receptor interaction was interrupted (at pre-selected time points) by removing the medium and washing twice with ice-cold DMEM/1% BSA. Surface-bound radioactivity was removed by different acid wash buffers and at varying incubation times. The transfer of the membrane-bound radioligand fraction into labelled scintillation tubes was facilitated by a further 30 second wash with the acid wash buffer. Following this, the residual, undisplaced, membrane-bound radioligand activity was collected after lysing the cells with 1 ml 1M NaOH and washing twice with PBS. This assumes that minimal internalisation took place on ice. Three 150 μl aliquots of ^{111}In-DTPA-A20FMDV2 were placed in three separate scintillation tubes to provide standards and a measure of the total radioactive counts for the assay. The radioactivity content of collected fractions and standards were measured on a gamma

counter. The acid wash removed fraction was expressed as a percentage of the total membrane-bound radioligand.

3.9.3.2 Cell Viability Check

It is necessary to determine whether acid wash buffer exposure initiates membrane permeabilisation; thus potentially invalidating subsequent internalisation assay calculations. A375P β6 cells were grown to 60-80% confluency in six-well plates and washed with DMEM. Selected wells were subjected to the optimal duration of incubation of each acid wash buffer, on ice. Furthermore, selected wells were also subjected to the optimal durations with the addition of three minutes, on ice. After each incubation period, 0.25% trypsin was added to the well and incubated at 37^{o}C, followed by centrifugation and neutralisation of the trypsin with serum-free medium. A sample of the cell suspension was aspirated off and added to 0.08% trypan blue. After standing for 5 min at room temperature, a sample of the cell suspension and trypan blue was introduced into a haemocytometer and examined under a light microscope. The percentage of viable cells in each acid wash buffer condition was compared to control wells, which simply had DMEM incubation, followed by trypsinisation. Each condition was replicated at least in triplicate and individual experiments were repeated at least three times.

3.9.3.3 Correlation of Cell Protein with Cell Number

Single cell suspensions of A375P β6 were generated as described above using centrifugation, trypsinisation and re-suspension with serum-free growth medium.

The cells were washed (by centrifugation and pellet re-suspension) a further two times in PBS. The cell concentration was quantified on a Casy™ Counter (Schärfe System GmbH), using a sample of the suspension. Protein was measured in a further sample, after pellet formation, careful supernatant aspiration and cell lysis, using a commercial kit (BioRad DC Assay).

3.10 In vivo studies

Specific-pathogen-free mice were either purchased from Charles River or Harlan or bred at Clare Hall, South Mimms and housed in the Biological Services Unit, at Charterhouse Square, London. Food and water were available *ad libitum*. Animal care and treatment followed guidelines approved by the Home Office (United Kingdom).

Cells for injection were harvested by trypsin detachment (described above), then either washed three times in serum-free DMEM (A375P line), or in serum-free DMEM/F12 (MCF-10A descendants). Cells were then counted and the concentration adjusted to 2×10^7 cells/ml.

In one grouping of experiments, athymic mice were given subcutaneous injections of 2×10^6 A375Pβ6 cells (right shoulder) and 2×10^6 A375P puro cells (left shoulder).

In a separate category of experiments, 2×10^6 cells of the desired breast cancer line were injected subcutaneously into athymic mice (right shoulder only); either in serum-free media alone or mixed in 50% Matrigel. Depending on the experiment, CD1 nu/nu, Balb C nu/nu or ICRF nu/nu strains were used. Two to four weeks later,

once the tumours had reached at least 5-7 mm diameter, biodistribution and imaging experiments took place.

3.10.1 Plasma Stability Studies

To investigate stability in plasma, mouse plasma was collected from nu/nu mice and incubated with the radiolabelled peptide, at 37^{o}C. Simultaneously, a 'control' incubation in 0.1 M PBS (pH 7.2) also occurred, at 37^{o}C. At pre-selected time-points, samples of both incubation mixtures were mixed with an equal volume of acetonitrile, and solids were removed by centrifugation followed by RP-HPLC analysis of the supernatant.

3.10.2 Biodistribution

Tumour-bearing mice were given intravenous injections of between 1-10 MBq of Indium-labelled peptide, formulated as described above and in a volume of approximately 100μL. Exact injection quantities were determined for each mouse by recording the syringe mass before and after injection, on an electronic balance. At pre-selected timepoints, mice were killed and major organs removed by dissection. Organs were rinsed briefly in PBS and sealed in pre-weighed scintillation tubes. These tubes were then re-weighed to calculate the net tissue weight, and the associated radioactivity was quantified by analysis in a Gamma Counter (LKB Compugamma, Victoria, Australia).

‘Standards’ were created by adding a 10 ml mixture of PBS and BSA (concentration 1mg/ml) to a labelled 15 ml polypropylene centrifuge tube (Corning). To this mixture, a known volume of radiopeptide was injected using a syringe and needle, mimicking the method used for the intravenous murine injections. Once equilibrium within the mixture was attained, one millilitre samples were dispensed into separate scintillation tubes. Furthermore, a 1 mL sample was diluted 1 in 10 with PBS and mixed. Samples from the diluted mixture were taken and also dispensed into separate scintillation tubes. Simultaneous gamma measurement of the standards with tissue samples enabled calculations of the potential injected dose activities / counts. Thus, data could be recorded as the percentage injected dose per gram of tissue (%I.D./g). A375P β6 tumours to background ratios were calculated and a paired *t* test was used for statistical analysis between both xenografts.

3.10.2.1 Peptide Mass Studies

The ideal mass of DTPA-A20FMDV2 for injection was investigated by estimating the biodistribution of ^{111}In-DTPA-A20FMDV2 in tumour-bearing mice, at varying specific activities. A range of peptide masses (from 0.1µg to 20µg), each radiolabelled with the same amount of radioactivity (10 MBq), was injected into different cohorts of mice. Biodistribution was determined as described above, at 1-hr post-injection. The tumour-to-background ratios and %I.D./g were compared for each specific activity.

3.10.2.2 Co-injection Studies in vivo

The receptor(αvβ6)-mediated uptake of ^{111}In-DTPA-A20FMDV2 was investigated by estimating the biodistribution of ^{111}In-DTPA-A20FMDV2 (4μg / 1 MBq) injected into tumour-bearing mice, in the presence or absence of 100-fold excess (400μg) of non-radiolabelled DTPA-A20FMDV2. Biodistribution was determined as described above, at 1-hr post-injection.

To determine the effect of an excess of non-targeting peptide on the uptake of A20FMDV2, ^{111}In-DTPA-A20FMDV2 (4μg / 1 MBq) was co-injected into tumour-bearing mice with 400μg of non-radiolabelled DTPA-A20FMDVran. Biodistribution was determined as described above, at 1-hr post-injection.

3.10.2.3 NanoSPECT /CT

Mice bearing subcutaneous tumours were anaesthetised with isofluorane and each given intravenous injections of either ^{111}In-DTPA-A20FMDV2 (4μg/10-30 MBq), ^{111}In-DOTA-A20FMDV (4μg/10-30 MBq) or ^{111}In-DTPA-DBD2 (2μg/10-30 MBq); formulated as described above and in a volume of around 100μL. The animals were placed in a tail-first, prone position on the scanner bed, in an air-warmed animal chamber. Mice were imaged at half, one, two and four hour timepoints, using a CT-NanoSPECT small animal imager (Bioscan, Washington, D.C., USA). A typical SPECT study designed for 50,000 – 100,000 counts for 16 - 24 projections; resulting in a 20 – 60 minute scan time (dependent on injected activity). Images were analysed using *In Vivo Scope* software (Bioscan, Washington, D.C., USA).

3.11 Immunohistochemical staining and evaluation.

Murine tissues from three ICRF nu/nu mice were formalin-fixed and paraffin-embedded. Five-micron-thick, formalin-fixed and paraffin-embedded tissue histology sections were deparaffinised, hydrated, incubated at 37^{o}C with 3 Digest-All 3 Pepsin Solution (Invitrogen Corporation, Carlsbad, CA) for 5 minutes for antigen retrieval, and washed in phosphate buffer (PBS). Endogenous peroxidase was neutralised with 0.45% hydrogen peroxidase in methanol for 15 minutes. Avidin-biotin pre-treatment (Vector Laboratories, Burlingame, California, USA) was incorporated to block endogenous biotin. The slides were incubated, at room temperature, with mouse anti-αvβ6 (Biogen™ antibody - 6.2G2) at 2µg/ml for 30 min (n.b. later 62G2 batches required higher concentrations [6µg/ml] overnight incubations, at 4^{o}C). After washing, bound antibody was detected using a Mouse-on-Mouse kit (Vector BMK-2202 M.O.M Kit). The tissues were stained with 3, 3'-diaminobenzidine tetrahydrochloride (DAB) freshly prepared using the Dako K-3468 system, and then counterstained with Mayer's haematoxylin (1-2 minutes), dehydrated, and mounted in DPX. Formalin-fixed, paraffin-embedded, mouse keratinocyte specimens were used for antibody optimisation, and later as positive controls. Isotype-matched antibodies were used as negative controls.

Cell membrane staining was quantified by a pathologist, blinded to the sample identity. Staining in each sample was quantified from sections using an eight-value membrane Quick score (0 to 7+) based on algorithms developed and standardised for oestrogen receptor immunohistochemistry, in breast cancer [237]. The staining intensity was scored out of three (1, weak; 2, moderate; 3, strong), and the proportion of epithelial cells staining positively was scored out of four (1, <25%; 2, 25-50%; 3,

51-75%; 4, 76-100%). The score for intensity was added to the score for proportion to give a score in the range of 0 to 7 and grouped as - (score = 0), + (score = 1-3), ++ (score = 4-5), or +++ (score = 6-7) [238].

Chapter IV

Results: Characterisation and Optimisation of αvβ6 Targeting Agents

4.1 Melanoma Cell Model for Targeting αvβ6

The A375P puro and A375Pβ6 cell lines were tested for their surface integrin expression, using flow cytometry. The integrin subunit antibody was tested and compared with the appropriate isotype control (black line). **Figure 34** shows that A375P puro and A375Pβ6 both express four different *RGD-binding integrins*, but only A375P β6 expresses αvβ6 [235]. Therefore, this model is ideal for testing the sensitivity and specificity of RGD peptides against αvβ6.

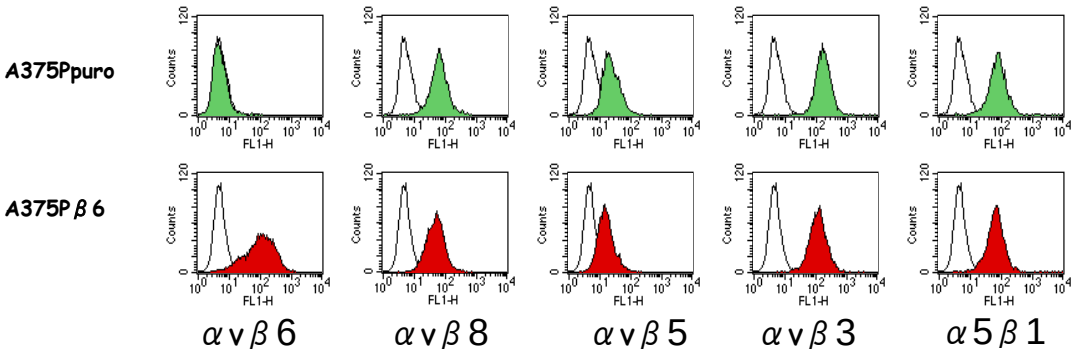

Figure 34 Integrin Expression Profiles of A375P puro and A375Pβ6, using flow cytometry

4.2 Assessment of Peptide Sensitivity and Specificity by Flow Cytometry

A20FMDV2 was tested at a range of concentrations (10µM-1nM; 30 mins incubation) on the melanoma cell model, described above. As A20FMDV2 was biotinylated, bound peptide was detected by antibody detection of the biotin. Results revealed a relationship between concentration of peptide and resultant binding to A375Pβ6 cells.

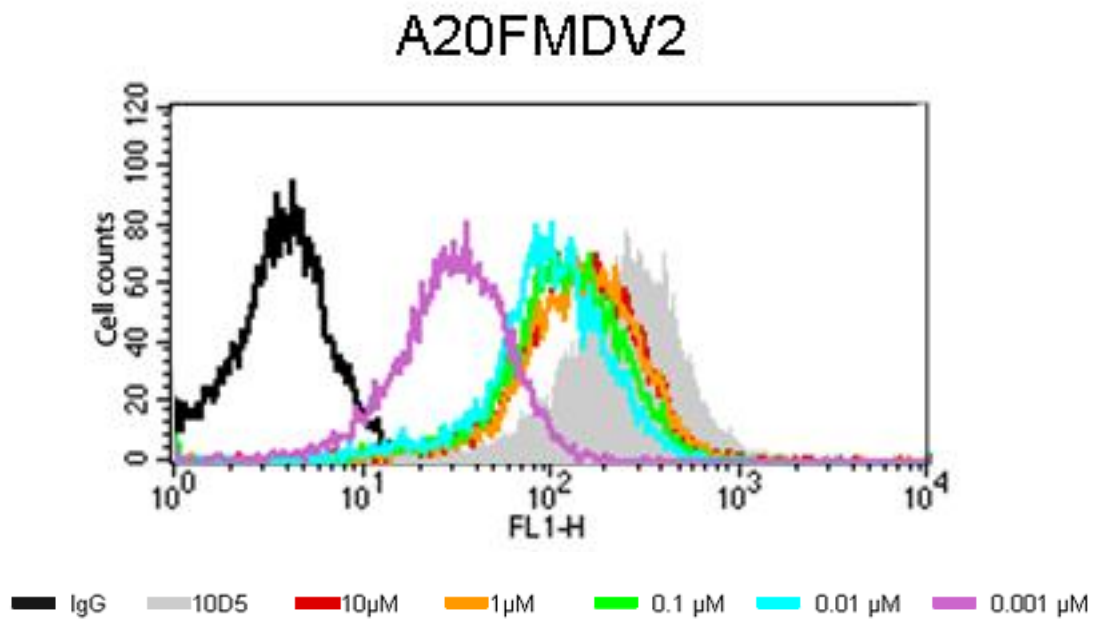

Figure 35 Peptide Affinity to the A375Pβ6 cell line, using flow cytometry.

The black lined histogram (see **Figure 35)** represents the negative control for the system, using mouse IgG. The grey shaded histogram represents clone 10D5 (commercial antibody to αvβ6) and serves as a positive control for the system, as well as a comparison for peptide binding. Clearly, the A375P β6 cell line expresses αvβ6 at its surface, as demonstrated by the approximate two log difference (median

fluorescence intensity) in binding compared with the negative control. Furthermore, an overlapping pattern of binding for the peptide was shown at a concentration of 10nM (red line). Although, the pattern is overlapping, this experiment cannot confirm whether the peptide is binding to the same molecule as the anti-αvβ6 clone - this will be tested in later competition assays. Nevertheless, there was a concentration-dependent relationship between varying amounts of peptide and constant levels of αvβ6; with even some binding occurring at 1nM (lowest concentration tested, violet line).

The specificity of A20FMDV2 was examined by analysing binding to the (non-β6 expressing) A375P puro cell line.

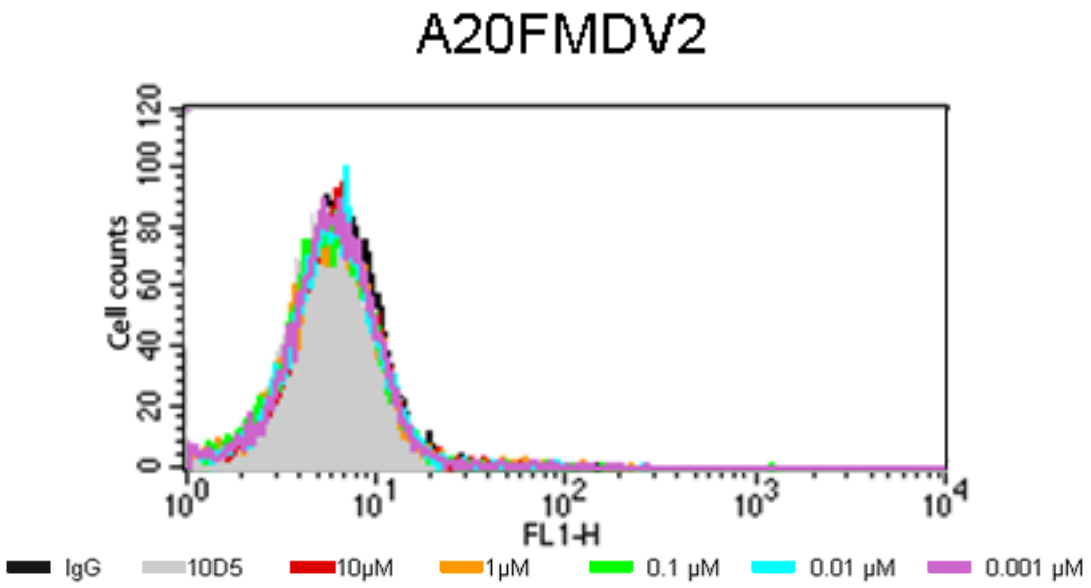

Figure 36 Peptide specificity using A375P puro (non-β6 expressing) cell line and flow cytometry.

The black lined and the grey shaded histograms (see **Figure 36)** again represent the mouse IgG negative and 10D5 positive controls for the system, respectively. The 10D5 overlap with the negative control confirms the absence of surface αvβ6 on the A375P puro cell line. With respect to the A20FMDV2, even at the highest concentration tested (10 μM), there was an absence of significant binding to the (non-β6 expressing) A375P puro cell line. That is, A20FMDV2 is at least 1000-fold (and maybe 10,000 fold) more specific for A375Pβ6 than for A375P puro. In summary, A20FMDV2 is specific and has good affinity for the β6 expressing cell line.

4.3 Peptide Derivatisation and Effects on Affinity and Specificity

Molecular modification techniques permit the synthesis of a variety of bioactive peptides with chelating groups, without necessarily compromising biological properties. A20FMDV2 was synthesised with the DTPA (diethylenetriamine penta-acetic acid) chelating agent on the N-terminus (DTPA-A20FMDV2). The DTPA chelating agent would facilitate future radiolabelling (see later). However, this modification had the potential to interfere with binding efficacy. Therefore studies comparing the affinity and specificity on the A375P cell lines were carried out.

Again, both peptides were biotinylated, and so bound peptide was detected by antibody detection of the biotin.

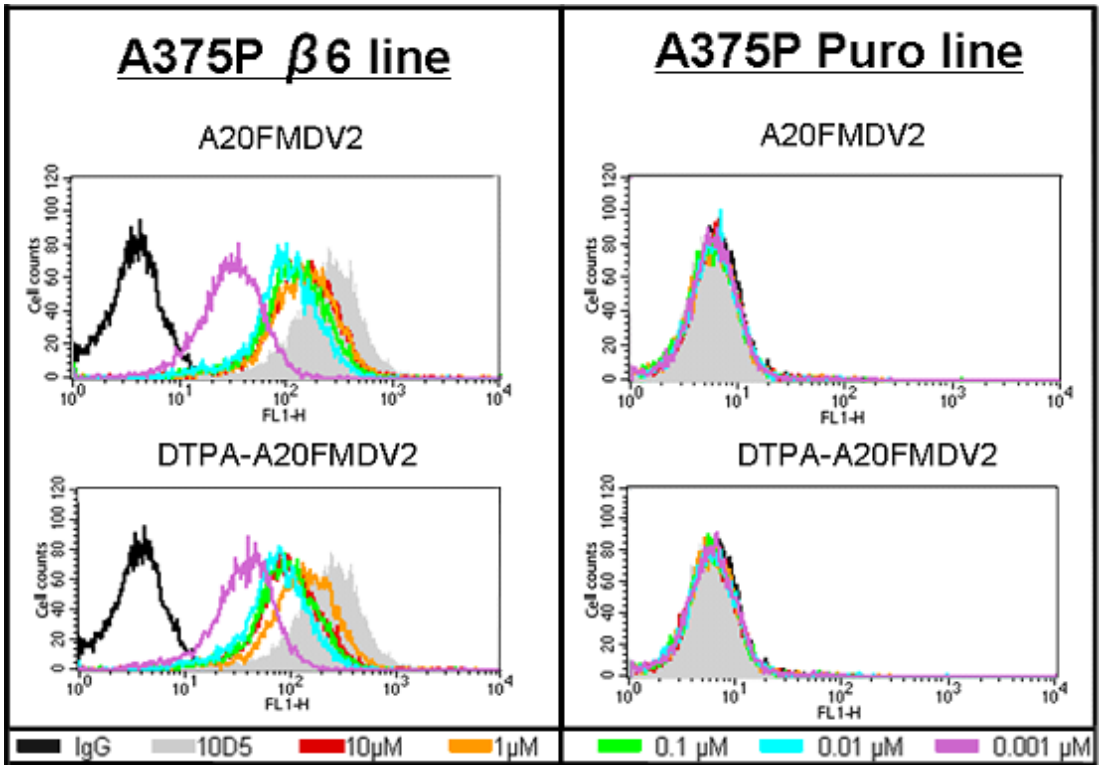

Figure 37 Comparing the affinity and specificity of A20FMDV2 with DTPA-A20FMDV2, using flow cytometry.

Figure 37 reveals a 'side-by-side' comparison of the original peptide and its derivative. Essentially, identical patterns of A375Pβ6 binding are seen with the peptide and the derivative. That is, at equal concentrations of peptide, both DTPA-A20FMDV2 and A20FMDV2 bound to almost identical levels to A375Pβ6 cells suggesting that both bind with similar affinity. Furthermore, identical absence of binding is seen with the peptide and its derivative, for the A375P puro line. That is, the addition of DTPA to A20FMDV2 did not result in any increased binding to other RGD integrins (α5β1, αvβ3, αvβ5, and αvβ8). Therefore, the comparison assays reveal that the DTPA modification did not alter the specificity and affinity significantly for the A375Pβ6 cell line. Additionally, the experiments were

performed in magnesium- and calcium-containing buffers and so it is highly likely that the derivative bound the cations; therefore chelate formation also did not seem to affect sensitivity or specificity.

We also tested the ability of our control, scrambled peptide (A20FMDV2ran), both as DTPA-modified and non-modified variants, to bind to A375Pβ6 and A375Ppuro cells. **Figure 38** shows that, even at the highest concentration (10µM), neither peptide bound to either cell line; confirming that scrambling the RGD motif in the peptide was sufficient to destroy any integrin-specific binding, but also did not generate any novel binding activity.

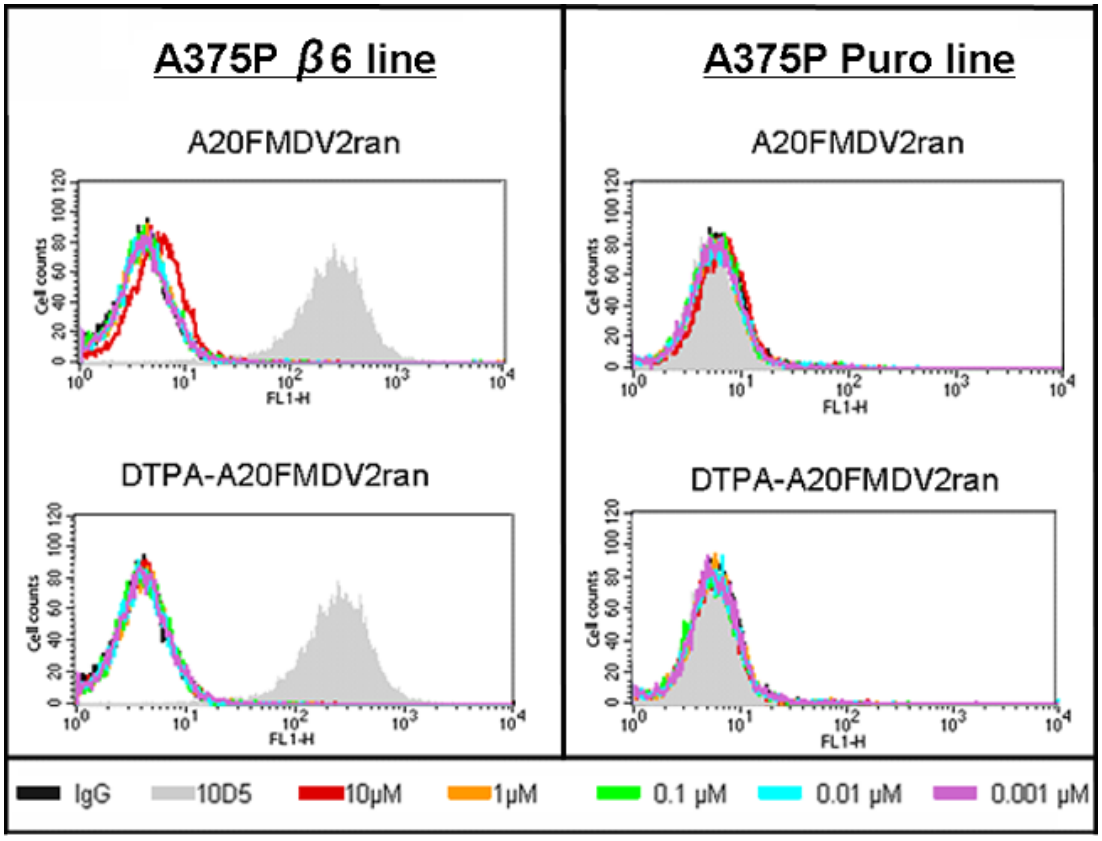

Figure 38 Comparing the affinity and specificity of A20FMDV2ran with DTPA-A20FMDV2ran, using flow cytometry.

4.4 Competition with αvβ6-Function Blocking Antibody in the A375P β6 cell line

The data in Section 5.3 suggested that DTPA-A20FMDV2 bound specifically to αvβ6 but, to prove this, A375Pβ6 cells were pre-incubated with the αvβ6-blocking antibody 68G6 (10μg/ml; Biogen Idec) [231] or control IgG1, for 30 minutes before adding 10nM DTPA-A20FMDV2 for an additional 40 minutes. After washing off unbound material and labelling cells with anti-biotin antibody, bound 68G6 was detected on the FL1-H channel, using Alexa-488 conjugated goat anti-mouse IgG (Molecular Probes). However, bound peptide (or absence of binding) was detected on the FL5-H channel, using Alexa-647 goat anti-rabbit IgG (Molecular Probes).

Results revealed that, whereas the presence of IgG1 (light-blue shaded histogram and dark-blue lined histogram of inset) had not changed the binding capacity of DTPA-A20FMDV2 (compared with nil antibody treatment), the presence of 68G6 (green shaded histogram and green-lined histogram of inset), however, had suppressed binding of the peptide completely. The complete abrogation of binding is signified by the essential overlap of the 68G6 green-shaded histogram with that of the negative control (black line). Thus DTPA-A20FMDV2 binds in an αvβ6-dependent manner to A375Pβ6 cells (**Figure 39**).

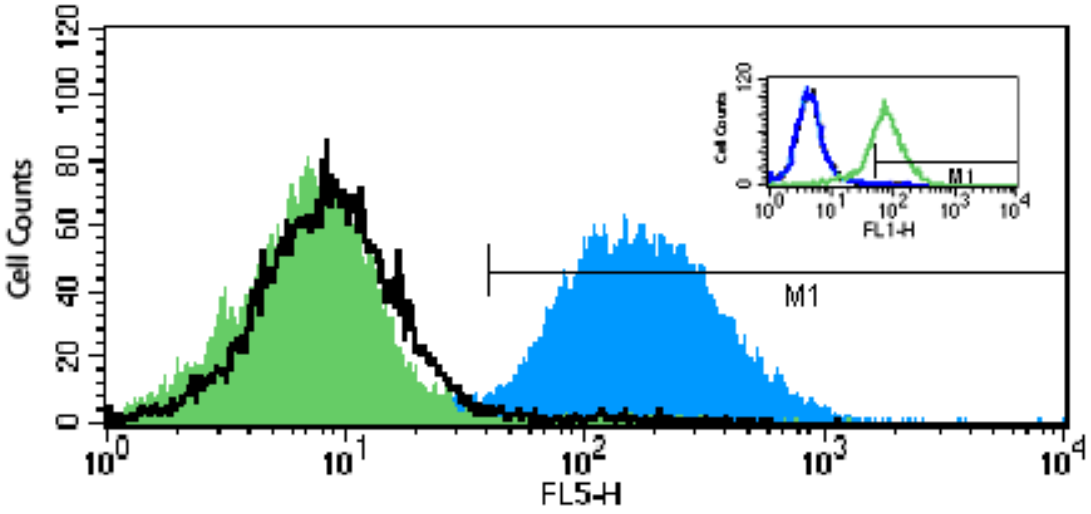

Figure 39 αvβ6-dependent adhesion of A20FMDV2 to A375P β6 cells, using flow cytometry (description within text).

4.5 Competition with αvβ6-Function Blocking Antibody in Mouse Keratinocytes

Since the DTPA-A20FMDV2 peptide was planned to be used for imaging αvβ6 in mice, the specificity for mouse αvβ6 integrin (as well as to human αvβ6 within the A375P line) had to be established. To prove that the binding of the peptide to mouse cells was αvβ6-dependent, a similar competition assay to that used in Section 5.4 was incorporated. In these assays, the αvβ6 ligand docking site was again inhibited by the ligand–mimetic 68G6, but now mouse keratinocytes were pre-incubated with either non-immune IgG or 68G6. This was followed by further incubation with 10nM of biotinylated A20FMDV2. Of note, all reagents and incubations were buffered with TBS-Mn^{2+}, to avoid terminal differentiation of the keratinocytes (see **Discussion**)

[239]. After a series of washes and incubations, bound 68G6 was detected on the FL1-H channel, using Alexa-488 conjugated goat anti-mouse IgG (Molecular Probes). However, bound peptide (or absence of binding) was detected on the FL5-H channel, using Alexa-647 goat anti-rabbit IgG (Molecular Probes).

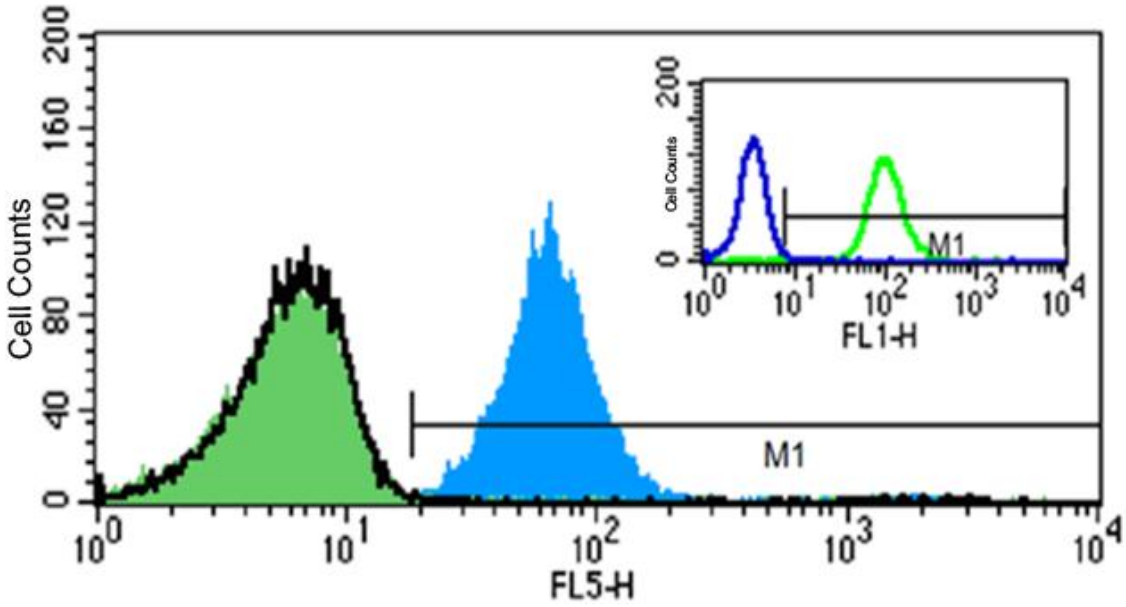

Figure 40 αvβ6-dependent adhesion of A20FMDV2 to mouse keratinocytes, using flow cytometry (description within text).

The competition assays (see **Figure 40**) revealed that 10nM of A20FMDV2 bound effectively to mouse keratinocytes (filled blue histogram, FL5-H), in the presence of non-immune IgG (dark blue line histogram, inset FL1-H). However, this binding was abolished totally (filled green histogram, FL5-H), when 68G6 was bound to mouse keratinocytes (light green line histogram, inset FL1-H). Of note, the black line histogram in FL5-H represents absence of peptide in the presence of non-immune IgG; that is, it represents the negative control. In summary, the binding of A20FMDV2 to mouse keratinocytes is αvβ6-dependent.

4.6 Immunohistochemical staining and Evaluation of Murine Tissues.

As stated above, the radiolabelled peptides were to be used for imaging αvβ6 in mice and although the expression of β6 mRNA had been documented in primates [134], the baseline levels of αvβ6 expression in mice had not been established. This expression profile is particularly important, given that A20FMDV2 recognises murine αvβ6, described in **Section 5.5**. Therefore, ICRF nude mice (n=3) bearing double subcutaneous xenografts of A375P β6 and A375P puro tumours were killed approximately two to three weeks after inoculation (see **Methods)**. Subsequently, organs were harvested, fixed and paraffin-embedded for histological examination. The following section describes staining patterns of the αvβ6-expressing organs and exhibits representative images. All the harvested organs were tested for αvβ6 expression (right-sided image) and compared with an isotype negative control antibody (left-sided image).

4.6.1 Skin

The majority of the skin essentially is negative. However, there is focal staining of the outer root sheath of a number of hair follicles. The intensity is moderate and is scored at 3+, using the eight-value membrane score.

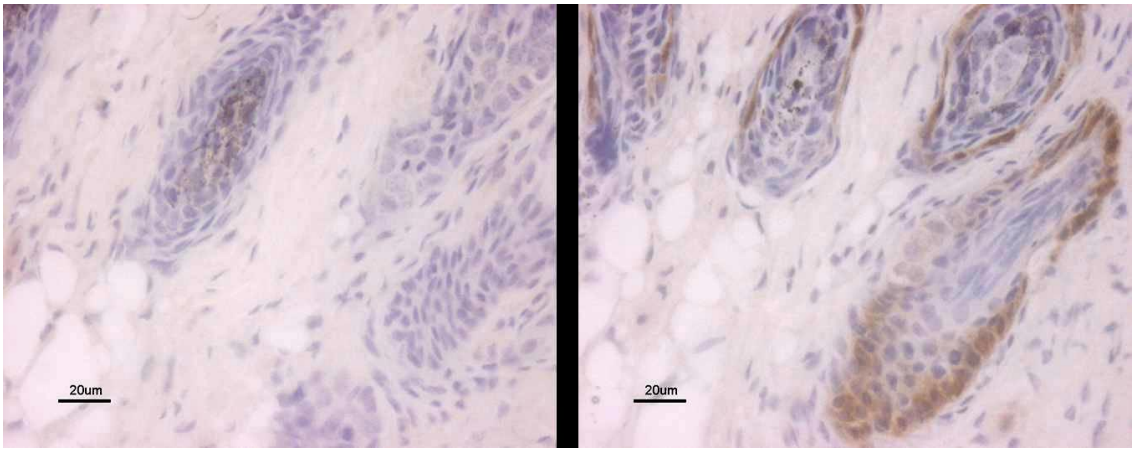

Figure 41 Murine skin staining for αvβ6. Left image is negative control and right is 62G2 staining.

4.6.2 Uterus

The uterus has occasional glands which stain for αvβ6. This positive staining is usually discovered in endometrium of a secretory phase uterus. Nevertheless, this staining is weak to moderate and scored only 2+, using the eight-value membrane scoring system.

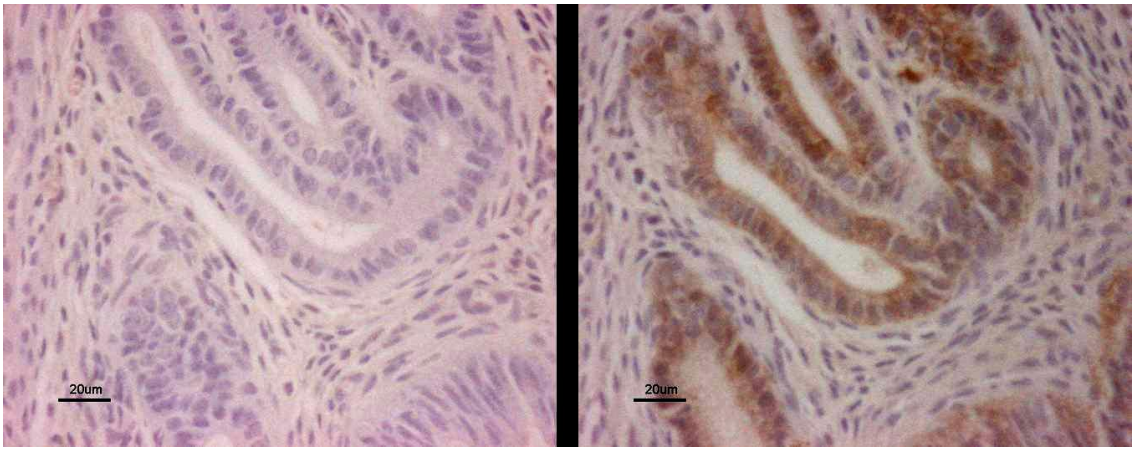

Figure 42 Murine uterine staining for αvβ6. Left image is negative control and right is 62G2 staining.

4.6.3 Gallbladder

The entire epithelilum of the gallbladder stained positively for αvβ6. The intensity was moderate-to-high and scored 6 to 7+, the highest levels of intensity.

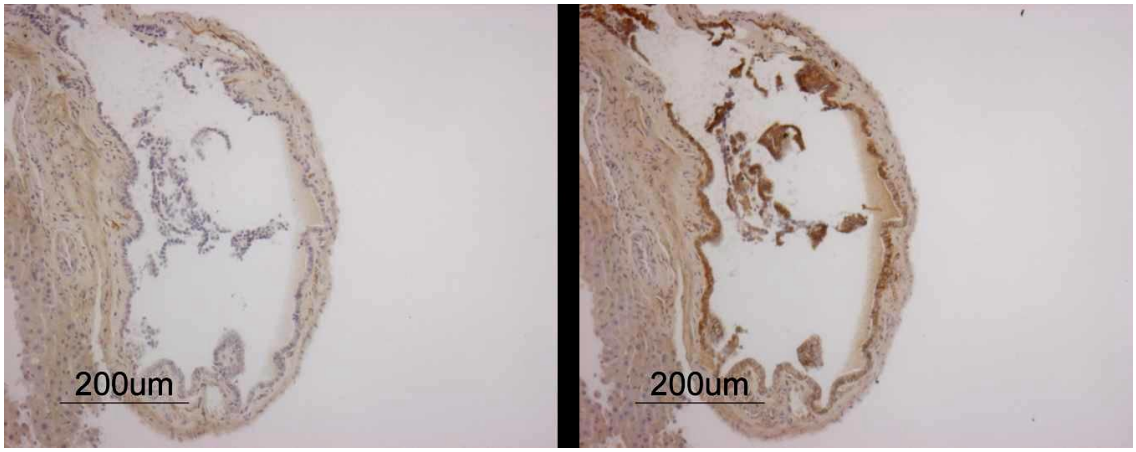

Figure 43 Murine gallbladder staining for αvβ6. Left image is negative control and right is 62G2 staining.

4.6.4 Urinary Bladder

There was moderate staining of the entire urinary bladder epithelium. It scored 6+, indicating a high level of αvβ6 expression.

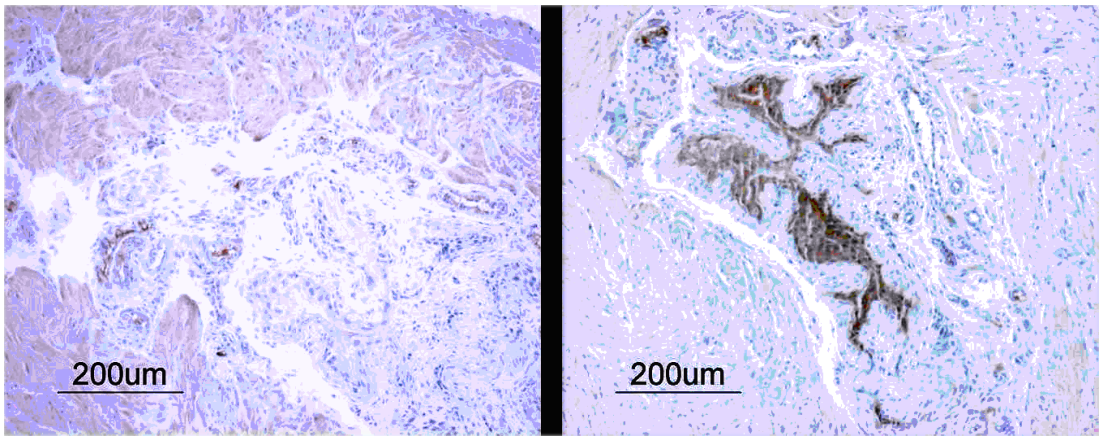

Figure 44 Murine urinary bladder staining for αvβ6. Left image is negative control and right is 62G2 staining.

4.6.5 Stomach

The entire epithelium of the stomach stained for αvβ6. All of the gastric glands were strongly positive and this tissue scored 7+, on our scoring system.

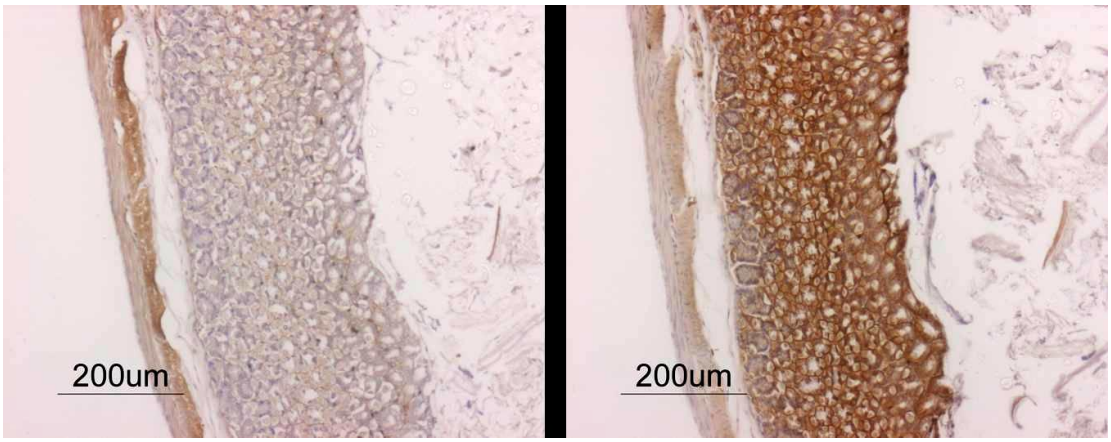

Figure 45 Murine gastric staining for αvβ6. Left image is negative control and right is 62G2 staining.

4.6.6 Duodenum

There was strong staining at the tips of the villi of the duodenum, with obvious membrane localisation between the individual enterocytes. However the intensity decreased as the villus was followed down to the crypts. As a result the overall score for the duodenum was assigned at 5+.

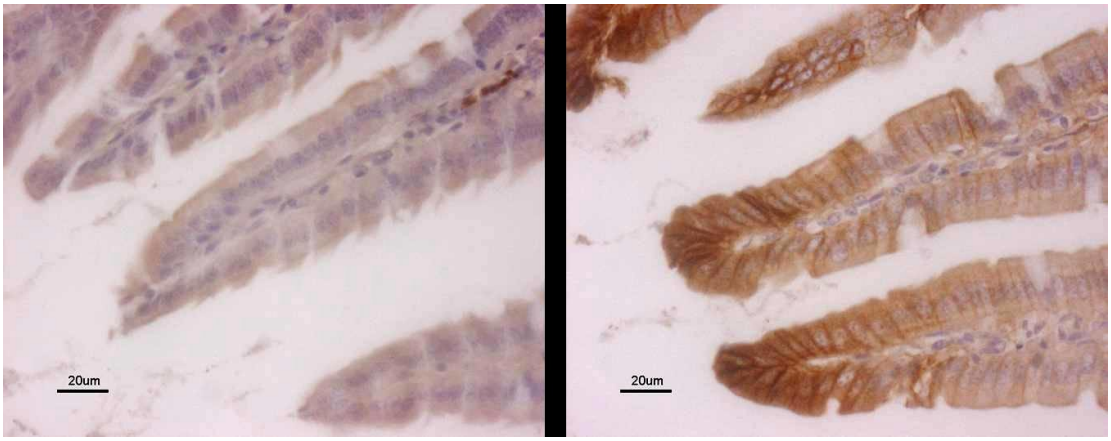

Figure 46 Murine duodenal staining for αvβ6. Left image is negative control and right is 62G2 staining.

4.6.7 Ileum

There was strong staining at the tips of the villi of the ileum, as can be seen in the 'honeycomb' type of appearance in the presented image. However the intensity decreased as the villus was followed down to the crypts. As a result the ileum scored 4+ overall.

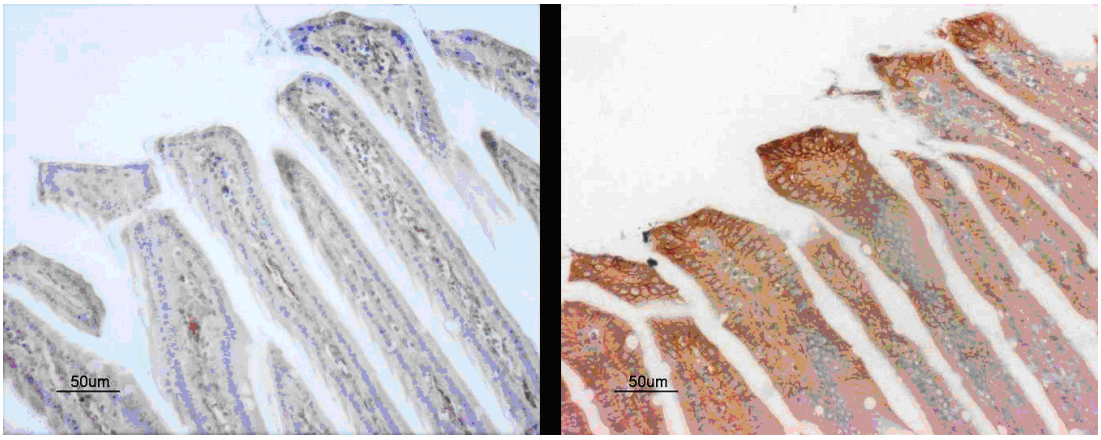

Figure 47 Murine ileal staining for αvβ6. Left image is negative control and right is 62G2 staining.

4.6.8 Colon

There is strong staining at the tips of the villi of the colon. However the intensity decreases as the villus is followed down to the crypts. As a result the colon scores 4+.

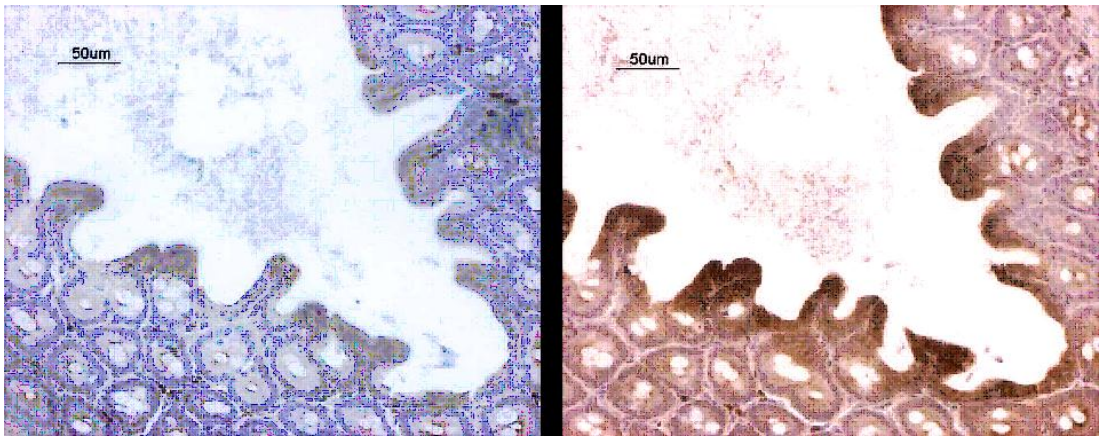

Figure 48 Murine colonic staining for αvβ6. Left image is negative control and right is 62G2 staining.

In summary, the entire GI tract stains for αvβ6. However, the strongest intensity was seen in the stomach, and in general this intensity was decreased as the GI tract was followed down its length, from proximal to distal portion.

4.6.9 Xenografts

The A375Pβ6 tumours revealed strong staining throughout the tumour and scored 7+.

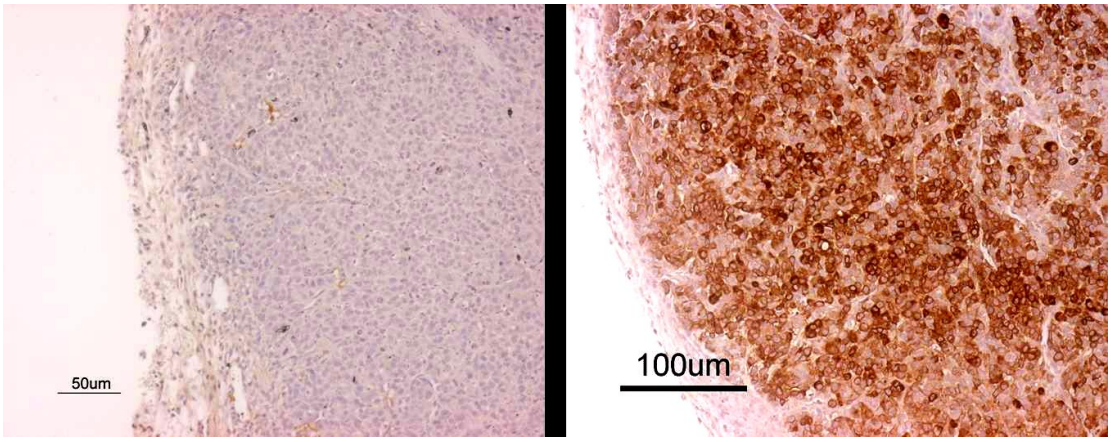

Figure 49 Murine A375P β6 xenograft staining for αvβ6. Left image is negative control and right is 62G2 staining.

As expected, the A375P puro tumours showed an absence of β6 expression, scoring 0. These results indicate that the A375P tumours maintained their β6 (or lack of) expression, *in vivo* and that growth within the animal did not result in *de novo* expression of this integrin subunit.

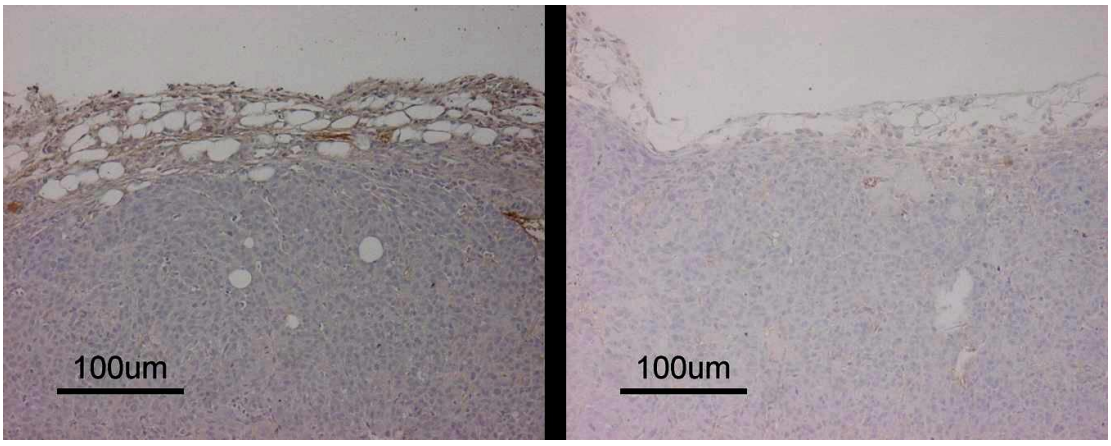

Figure 50 Murine A375P puro xenograft staining for αvβ6. Left image is negative control and right is 62G2 staining.

Therefore, these results demonstrate that murine keratinocytes, gallbladder, urinary bladder, secretory endometrium and GI tract normally express detectable levels of αvβ6 expression (see **Table 10**, page 174). This normal or baseline expression appears to be very different from that reported for primates [240] and this positivity of murine tissue has to be borne in mind, whilst using the mouse as a model for targeted imaging.

Immunohistochemistry using biotinylated A20FMDV2 was attempted on paraffin sections, but unfortunately did not yield any specific staining for αvβ6 and thus these results were not incorporated in this thesis.

Organ system and tissue	Score	Comment
Digestive System		
Salivary Glands	**0**	
Stomach	**7**	Entire epithelium stains strongly
Pancreas	**0**	
Liver	**0**	
Gallbladder	**6-7**	Moderate staining of entire epithelium
Duodenum	**5**	Strong staining at the tips of the villi. However the intensity decreases as the villus is followed down to the crypts.
Ileum	**4**	
Colon	**4**	
Urinary System		
Urinary Bladder	**6**	Moderate staining of entire epithelium
Kidney	**0**	
Female Reproductive System		
Uterus	**2**	Weak to moderate focal staining in glands, of secretory phase endometrium.
Mammary Glands	**0**	
Lymphatic system		
Residual Thymus	**0**	
Lymph Nodes	**0**	
Spleen	**0**	
Cardio-respiratory system		
Heart	**0**	
Lungs	**0**	
Nervous System		
Brain	**0**	
Eyes	**0**	
Endocrine System		
Thyroid	**0**	
Musculoskeletal System		
Bone	**0**	
Skeletal Muscle	**0**	
Skin	**3**	Focal staining of the outer root sheath of a number of hair follicles.
Xenografts		
A375P B6 tumour	**7**	Strong staining throughout the tumour
A375P Puro tumour	**0**	Complete absence of staining

Table 10 Pattern of αvβ6 expression in murine tissues, as detected by immunohistochemistry.

4.7 Peptide Radiolabelling and Quality Control

To create a γ-emitting probe, DTPA-A20FMDV2 was radiolabelled with indium to generate ^{111}In-DTPA-A20FMDV2. Reverse-phase HPLC was used to analyse the labelling efficiency and to evaluate the structural integrity of the radiolabelled targeting ligand. ^{111}In-DTPA-A20FMDV2 was eluted in a single peak, with a retention time of around 20 minutes (see **Figure 51**). The radiochemical purity of the radiolabelled ^{111}In-DTPA-A20FMDV2 was over 99%, according to this analysis. Furthermore, there was no evidence of fragmentation or aggregation during the labelling process, as indicated by the sharp single peak.

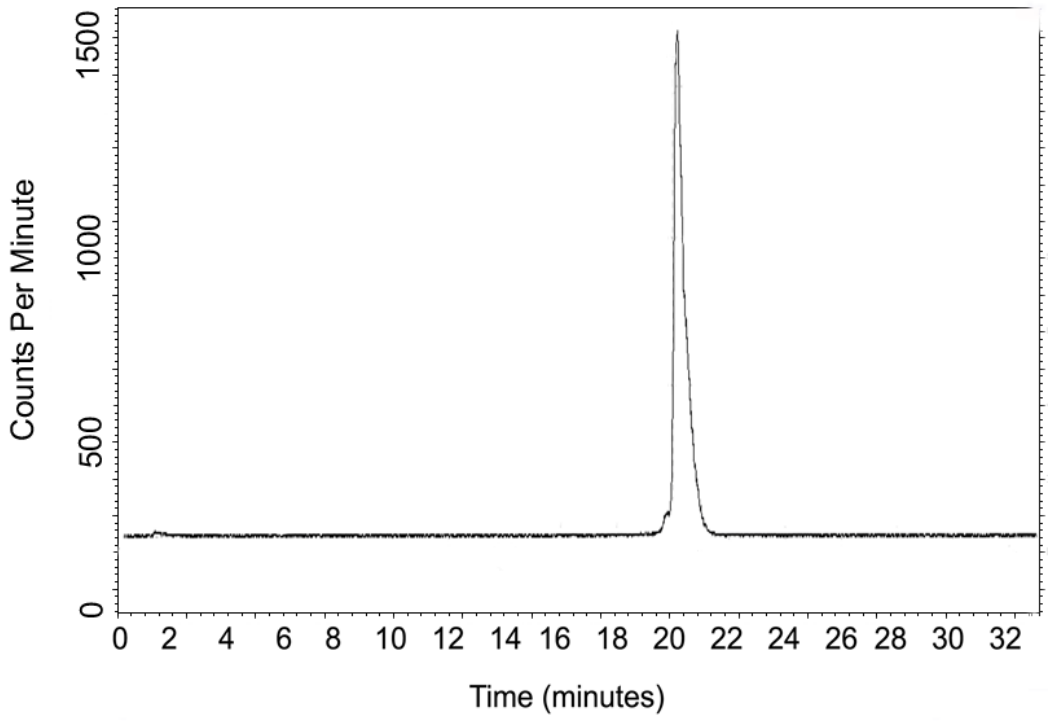

Figure 51 Reverse phase HPLC trace measuring ^{111}In-DTPA-A20FMDV2 radiolabelling efficiency.

Secondly, the scrambled peptide, DTPA-A20FMDV2ran also was radiolabelled with indium to generate ^{111}In-DTPA-A20FMDV2ran. It too was analysed by reverse-phase HPLC and found to elute in a single peak, with a retention time which also was around 20 minutes (see **Figure 52**). The radiochemical purity of the radiolabelled ^{111}In-DTPA-A20FMDV2ran approached 100%, with no evidence of fragmentation or aggregation of the compound.

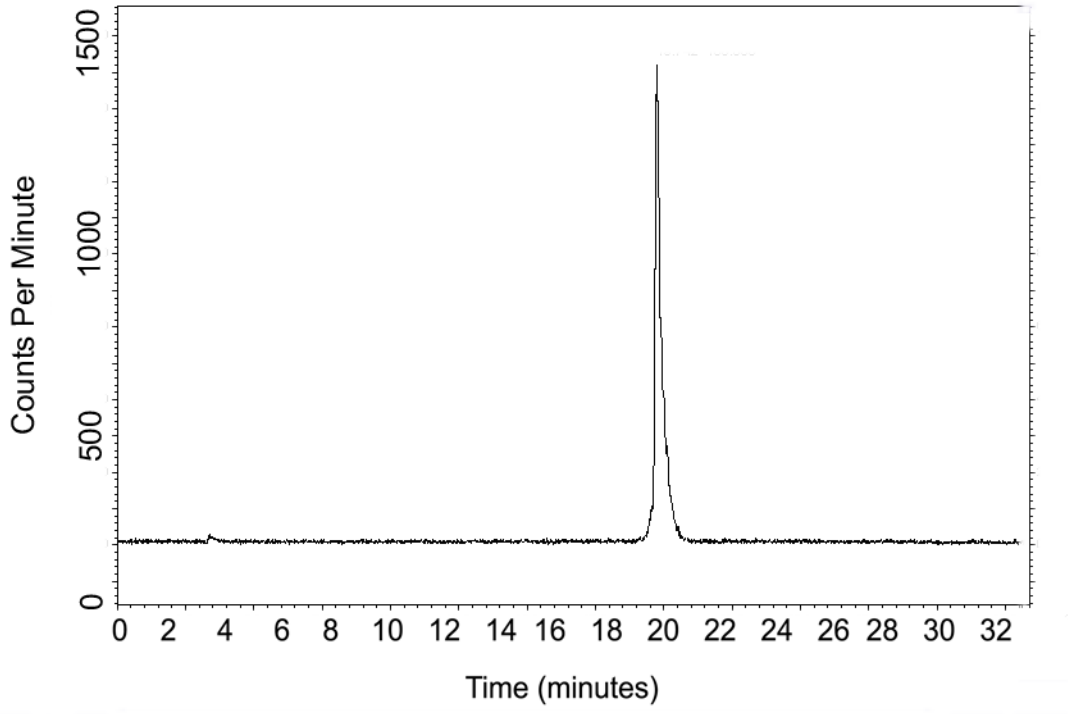

Figure 52 Reverse phase HPLC trace measuring ^{111}In-DTPA-A20FMDV2ran radiolabelling efficiency

4.8 Radioloigand binding studies

4.8.1 Saturation Binding Assays

Use of αvβ6-blocking antibodies revealed that the binding of DTPA-A20FMDV2 to the A375P β6 cell line is αvβ6-dependent i.e. single receptor binding (see **Section 4.4**). To determine the affinity of DTPA-A20FMDV2 binding to αvβ6 on A375P β6 cells, saturation binding assays were performed. These experiments involved incubating a range of concentrations of ^{111}In-DTPA-A20FMDV2 with adherent A375P β6 cells, in the presence and absence of 10,000-fold excess of non-radiolabelled peptide. Results of binding assays confirmed that, after labelling with Indium-111, DTPA-A20FMDV2 retained the ability to bind to its specific receptor and showed a dose-dependent binding to A375P β6 cells (**Figure 53**). After subtracting the non-specific background binding (that occurred in the presence of the excess cold peptide) the calculated mean affinity constant (K_d) was 1.73×10^{-9}M, ranging from 1.27×10^{-9} to 2.19×10^{-9} (95% confidence interval).

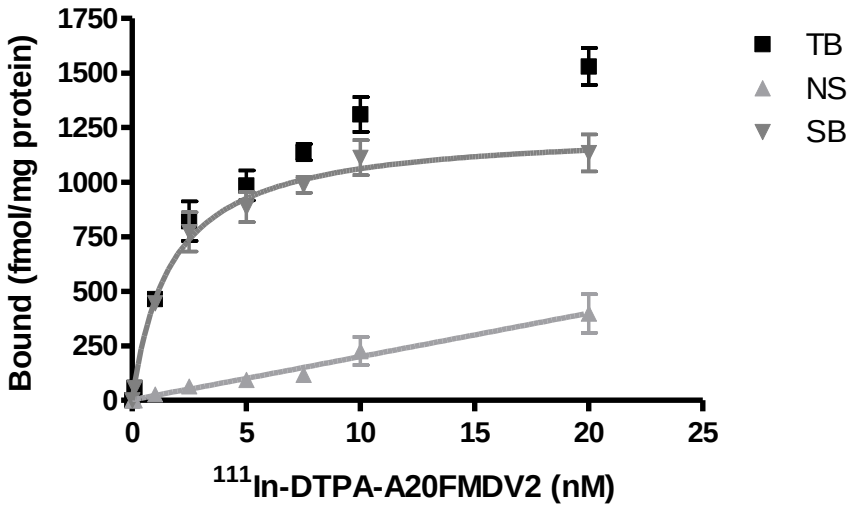

Figure 53 Saturation binding assay of ^{111}In-DTPA-A20FMDV2 to adherent A375P β6 cells. TB=Total Binding. Non-specific (NS) binding was determined by co-addition of excess non-radiolabelled DTPA-A20FMDV2. Specific-binding (SB) was calculated by the following formula: TB-NS = SB.

4.8.2 Internalisation Assays

αvβ6 mediates virus binding and internalisation, and thus infection of foot-and-mouth disease, via its RGD-containing capsid protein [108]. It was therefore hypothesised that ^{111}In-DTPA-A20FMDV2 also may be internalised. To confirm this hypothesis, internalisation assays of DTPA-A20FMDV2 on A375P β6 cells were performed.

4.8.2.1 Optimisation of Cell Internalisation Assay

However, in order to perform the calculations necessary for an accurate internalisation assay, an efficient acid wash buffer is required. An efficient acid wash buffer should remove the membrane-bound radioligand fraction, but without disrupting the cell's structural integrity and its internalised radioligand fraction. Therefore, optimisation experiments on a range of commonly used acid wash buffers were carried out. Firstly, Cell Viability experiments (see **Methods**) were performed to determine the maximum exposure time of A375P β6 cells to the different acid buffers, prior to membrane permeabilisation and significant percentage of cell death. Membrane permeabilisation was determined using the trypan blue reagent, with the percentages of viable cells counted and compared to control buffer incubations.

Secondly, using 'near-confluent' A375P β6 cells set 'on-ice' conditions (minimising internalisation); ^{111}In-DTPA-A20FMDV2 was added, either in the absence or presence of unlabelled DTPA-A20FMDV2. After a 30-60 minute 'ice-incubation' (permitting radioligand and receptor interaction, but minimal internalisation) the unbound radioligand was washed and decanted. Subsequently, the surface-bound radioactivity was removed by different acid wash buffers used at maximal exposure times. Finally, the residual, undisplaced, membrane-bound radioligand activity was collected after lysing the cells. The acid wash removed fraction was expressed as a percentage of the total membrane-bound radioligand (see **Table 11**, page 180). It should be noted that the exposure time for each buffer (documented in parentheses) is the maximum permitted, prior to significant numbers of A375P β6 cell permeabilisation / death, as determined in the Cell Viability experiments.

	Removed Surface Fraction	Residual Surface Fraction	% Surface Removal Efficiency
E4 / BSA 'Control' Media (30 minutes)	6186	9037	40.64%
Glycine pH 2.8 (5 minutes)	6752	12137	37.75
Acetate pH 5 (12 minutes)	16289	5980	73.15%
E4/HCl pH 4 (25 minutes)	26652	1637	94.21%

Table 11 Comparison of Different Acid Wash Buffer Efficiencies.

Table 11 (above) reveals that E4/HCl (pH 4), at an exposure time of 25 minutes, is the most efficient acid wash buffer, without causing significant cell permeabilisation.

4.8.2.2 Internalisation Assay with ^{111}In-DTPA-A20FMDV2 on A375P β6 cells, using E4/HCl (pH 4)

Having established the optimal conditions, internalisation assays of DTPA-A20FMDV2 on A375P β6 cells were performed. These assays involved variable incubation periods of a set concentration of ^{111}In-DTPA-A20FMDV2 with adherent A375P β6 cells, in the presence and absence of 10,000-fold excess of non-radiolabelled peptide. Experiments compared surface-bound radioactivity to internalised activity. Results revealed that the internalisation of ^{111}In-DTPA-

A20FMDV2 in A375P β6 cells was rapid, reaching a plateau after about 60 minutes (see **Figure 55**). A similar experiment was performed and analysed by confocal microscopy, detecting the internalising DTPA-A20FMDV2 by labelling the biotin tag. It can be seen that at time 0 minutes most of the peptide remained at the membrane of A375P β6 but by 45 minutes, most of the peptide was located in the cytoplasm (see **Figure 56**). In contrast, almost no peptide bound to, or was internalised by, A375P puro, suggesting that internalisation into A375P β6 is αvβ6-dependent (see **Figure 54**).

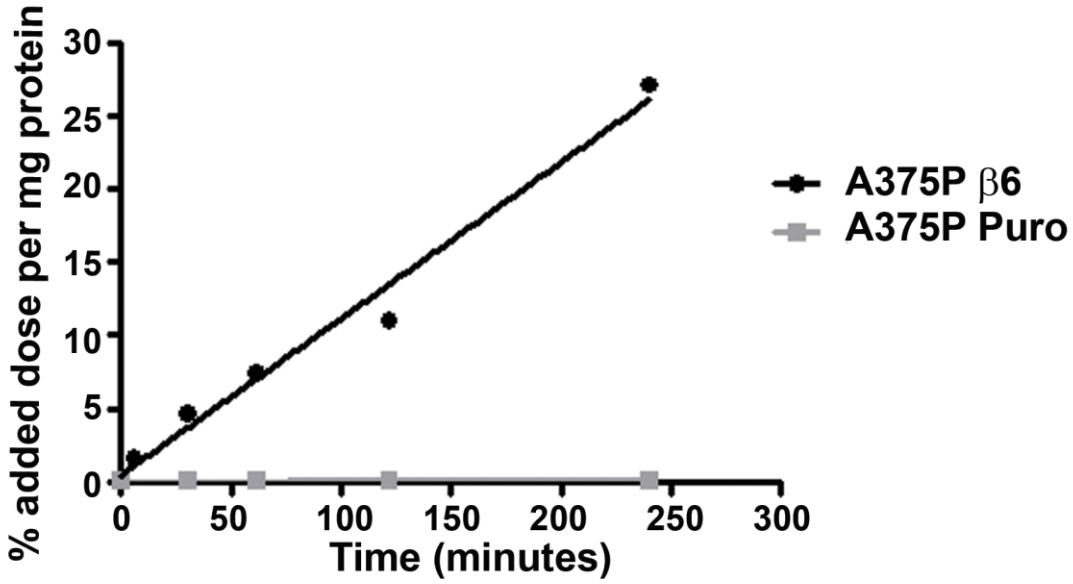

Figure 54 Internalisation Assay: ^{111}In-DTPA-A20FMDV2 (20 ng/ml) was added to adherent A375Pβ6 cells and incubated at 37^{o}C. Acid washes removed the surface-bound fraction. The residual radioactivity represented the internalised fraction. Internalisation is represented as a proportion of the added dose, per milligram of cellular protein for both A375P β6 and A375P Puro cell lines.

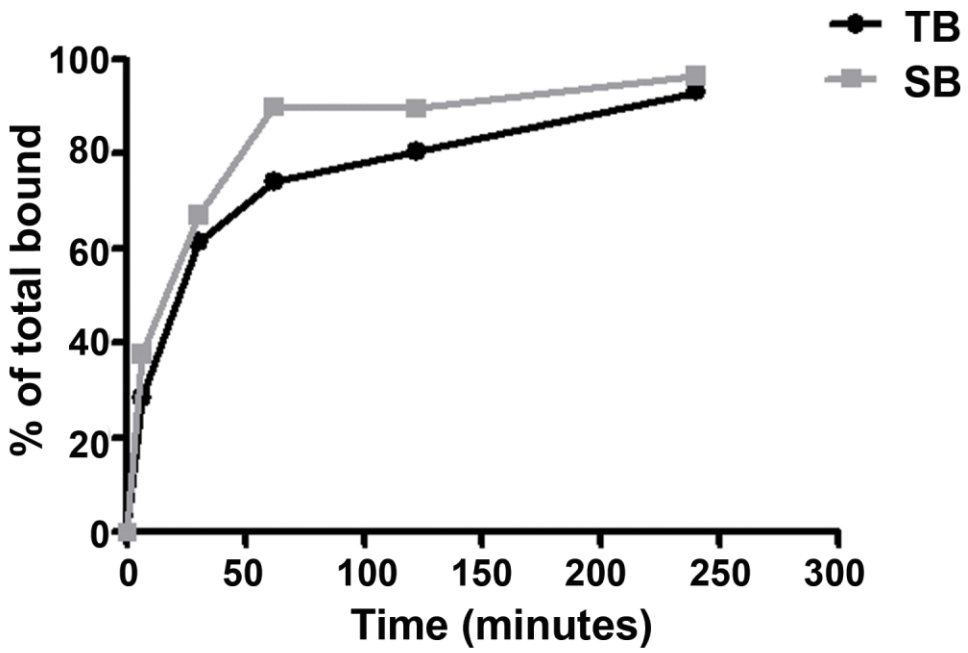

Figure 55 Internalisation Assay: Results for ^{111}In-DTPA-A20FMDV2 expressed as percentage of bound ligand, rather than added dose, for A375P β6 cells only.

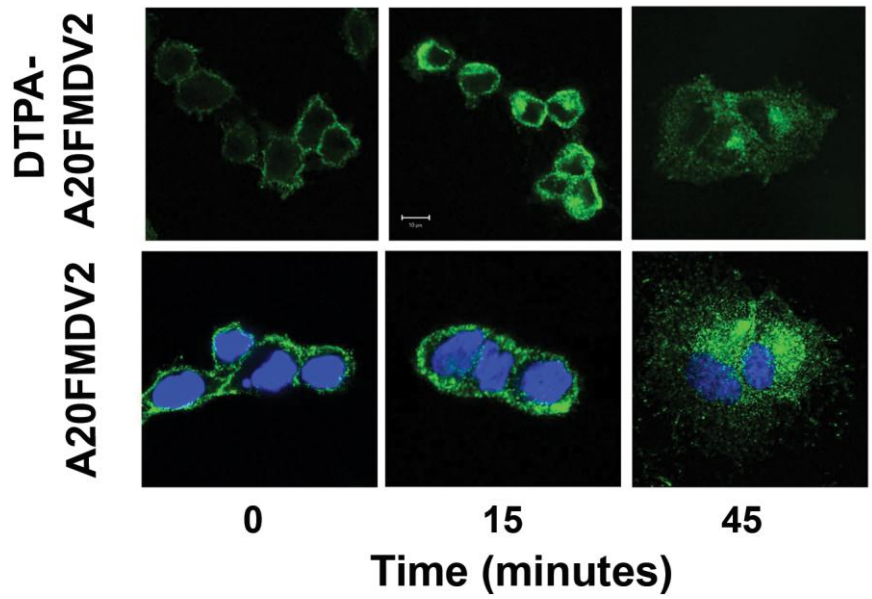

Figure 56 Internalisation Assay: Pictures are confocal images which reveal initial membrane localisation of the peptide, but this is followed by cytoplasm translocation at 45 minutes in A375Pβ6 cells. Note: DAPI nuclear staining was performed only with A20FMDV2 (lower panel).

4.9 In vivo studies

4.9.1 Plasma Stability Studies

Plasma stability is an important parameter to consider in drug discovery and development. Peptides are exposed in plasma to enzymatic processes (proteinases, esterases), which may result in intra-molecular rearrangement, aggregation or degradation. Therefore, the stability of a compound in plasma can strongly influence its *in vivo* efficacy. Plasma stability assays were thus performed on ^{111}In-DTPA-A20FMDV2, using RP-HPLC to measure structural integrity of the labelled peptide. ^{111}In-DTPA-A20FMDV2 was incubated at 37^{o}C in either PBS or murine plasma for various periods of time. Firstly, incubation in PBS showed high stability, with only around 10% loss of purity at 24 hours. This result was considered to be a favourable point with regard to chemical storage and transport. In contrast, and as expected for a linear peptide, there was degradation of the radioligand in plasma. **Figure 57** shows that at 2 hours, 63% of the radiopeptide remained intact whereas by 4 hours only 46% remained undegraded. The RP-HPLC trace, after 4 hours plasma incubation, displays obvious fragmentation and aggregation of the peptide (see **Figure 57**, inset).

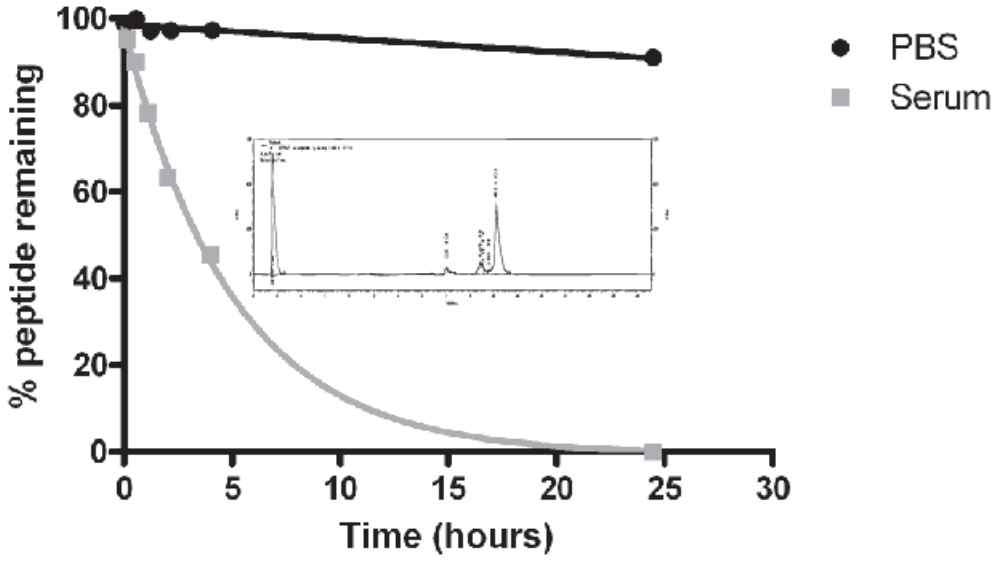

Figure 57 Plasma Stability Study: ^{111}In-DTPA-A20FMDV2 was incubated at 37^{o}C in either PBS or murine plasma for various periods of time. After the selected time periods, samples of the incubation mixture were analysed on an RP-HPLC. Stability was preserved in PBS up to 24 hours after initation of incubation; whereas plasma stability was affected considerably after only 4 hours incubation.

4.9.2 Biodistribution

Preclinical biodistribution studies are designed to investigate the dissemination of a test compound within an appropriate animal model. The resulting pattern of dissemination can inform on the likely efficacy of *in vivo* targeting and from such results, it may be possible to infer potential toxicity from the non-target tissue data. ^{111}In-DTPA-A20FMDV2 was injected intravenously into each 'bi-xenografted' mouse (described in **Methods**). Mice were killed at the pre-selected time-points, dissected and major organs were harvested. The associated radioactivity of each organ was quantified (expressed as percentage of injection dose per unit mass of tissue) and used as an indirect measure of peptide uptake and organ retention.

4.9.2.1 Post-Injection Interval Studies

Initially, 10 MBq of ^{111}Indium was radiolabelled onto 2μg of DTPA-A20FMDV2 and the peptide uptake in the xenografts was compared at various time points (see **Figure 58**). A combination of properties (maximal differential uptake between the A375P β6 and the A375P puro tumours and high %I.D./g in the A375P β6 tumour) occurred between 1 to 2 hours p.i. (post-injection). The ratio of A375P β6 tumour uptake and retention to that of A375P puro consistently was around 7:1. At 1 hour post-injection, the mean % injected dose per gram was around 2.1% ± 0.25 for the A375P β6 tumour, compared with 0.31% ± 0.07 for the A375P puro tumour. An interval of 1 hour post-injection was therefore chosen for further analyses.

4.9.2.2 Peptide Mass Studies

To determine the optimal peptide mass for biodistribution and imaging, ranges of peptide masses (from 0.1µg to 20µg) of DTPA-A20FMDV2, but labelled with similar amounts of radioactivity (^{111}In), were injected into different cohorts of mice; tumour retention at 1-hour post-injection was then measured. **Figure 59** reveals that the maximum %I.D./g tumour occurred with an injection mass of 2 µg peptide; attaining 1.72%+/-0.41 %I.D./g and a retention 5.6-fold more in the A375Pβ6 tumour than in the A375Ppuro tumour. Subsequent experiments showed that a 4 µg peptide injection could also deliver excellent, and sometimes superior, results. Thus subsequent experiments used peptide injection masses in the range of 2 to 4 µg.

4.9.2.3 Species Generalisation Experiments

To be certain that our findings could be generalised to other athymic mouse models, uptake of radiopeptide in xenografts grown in ICRF nu/nu mice were compared with xenografts grown in CD1 nu/nu and Balb/C nu/nu mouse strains. The results at 1h post-injection showed (see **Figure 60**) that uptake and retention ratios of A375Pβ6:A375P puro were maintained, regardless of the strain of athymic mouse studied. Ratio of uptake of A375Pβ6:A375P puro for CD1, Balb/C and ICRF athymic mice was 7:1, 8:1 and 9:1, respectively. Furthermore, for CD1 nudes, at one hour post-injection, the A375Pβ6 tumour-to-muscle ratio and tumour-to-blood ratio was 9:1 (n=3).

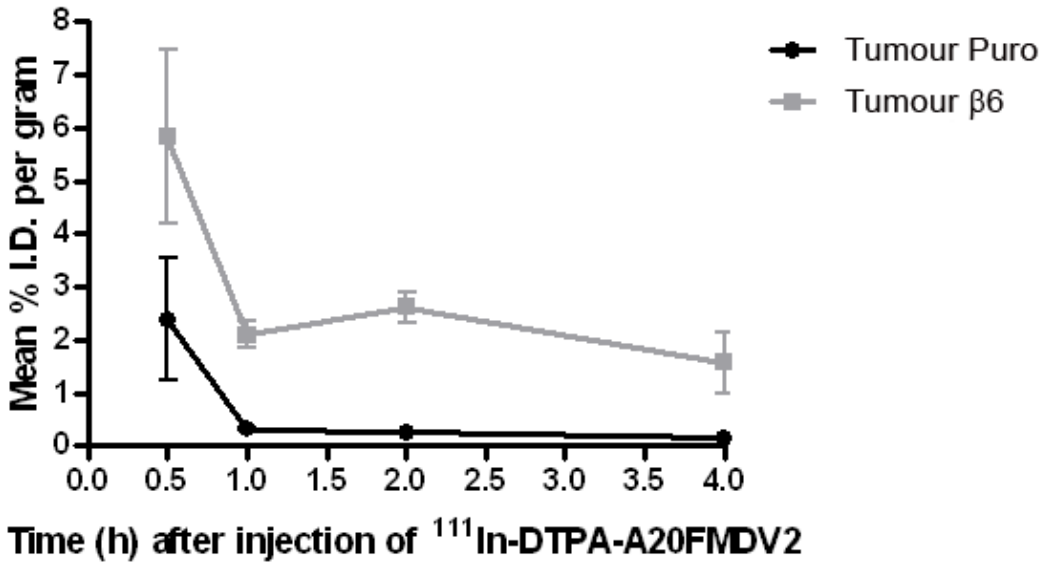

Figure 58 Determining the optimal parameters for pre-clinical imaging studies of αvβ6. ^{111}In-DTPA-A20FMDV2 (10 MBq) was injected into groups of tumour-bearing mice. At 0.5, 1, 2 and 4 hours post-injection three mice were killed and tumours removed and the % ID/g tissue determined. Data suggested that examining mice 1-2 hours after injection of ^{111}In-DTPA-A20FMDV2 would be the optimal time point for such assessments.

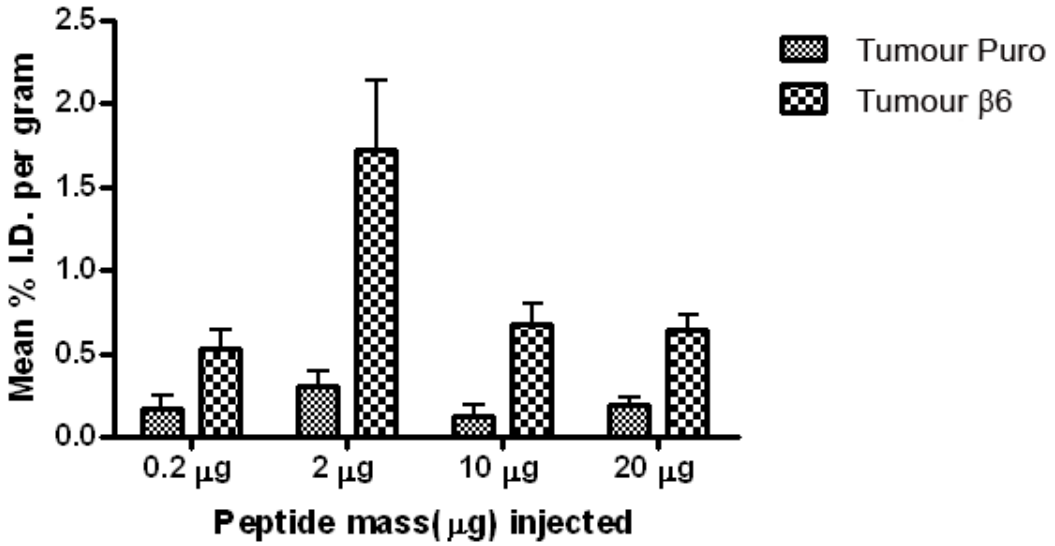

Figure 59 Determining the optimal parameters for pre-clinical imaging studies of αvβ6. To determine the optimal specific activity for studies various different masses of DTPA-A20FMDV2, each labelled with 10 MBq of indium-111, were injected into tumour-bearing mice. At 1 hour post-injection three mice were killed and tumours removed and the % ID/g tissue determined.

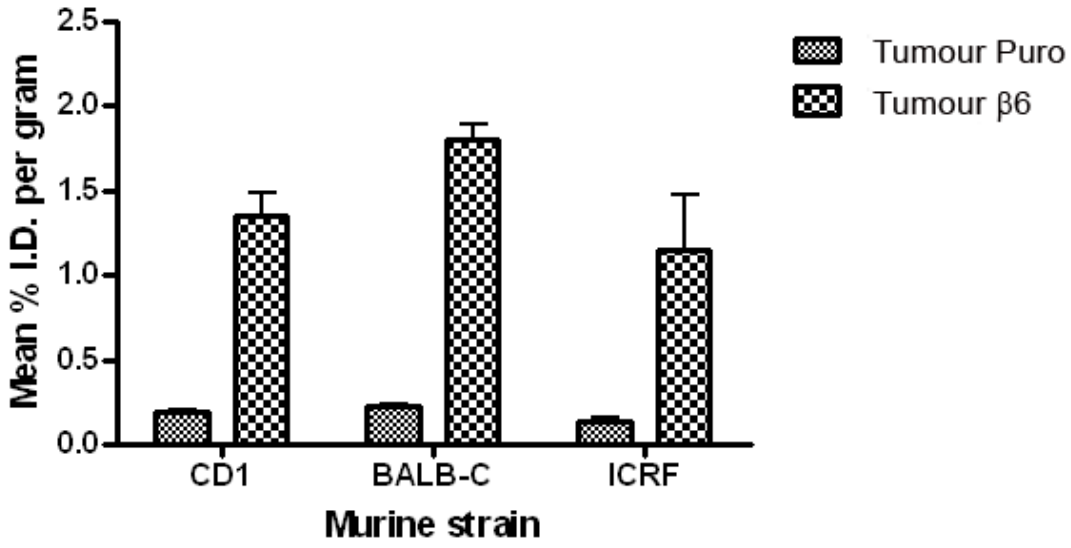

Figure 60 A375Pβ6 and A375Ppuro xenografts. CD1, Balb/C and ICRF nu/nu athymic mice bearing A375 β6 and A375 puro tumours were injected with 10 MBq of ^{111}In-DTPA-A20FMDV2 and after 1 hour the tumours removed and the %I.D./g tissue determined. Results suggested that the strain of mouse did not affect the ratio of uptake in A375Pβ6 versus A375Ppuro tumours.

4.9.2.4 Whole body biodistribution

Having optimised the time-frame for analysis, peptide mass for injection, and established that all mouse strains tested performed equally well, full tissue biodistribution on tumour-bearing mice was undertaken; harvesting organs at 1h post-injection of ^{111}In-DTPA-A20FMDV2 (1 MBq / 4 µg). **Figure 61** indicates that several organs retained significant amounts of radioactivity at 1 hour. In addition to the A375P β6 tumour, the lower gastrointestinal (GI) tract, lungs, stomach, skin and gall bladder all have retained significantly more radioactivity than either A375P puro tumour or skeletal muscle. With the exception of the kidneys and lungs, these positive tissues all express αvβ6 endogenously as described in **Section 4.6,** which suggests that ^{111}In-DTPA-A20FMDV2 recognises and binds to endogenous αvβ6-expressing tissues.

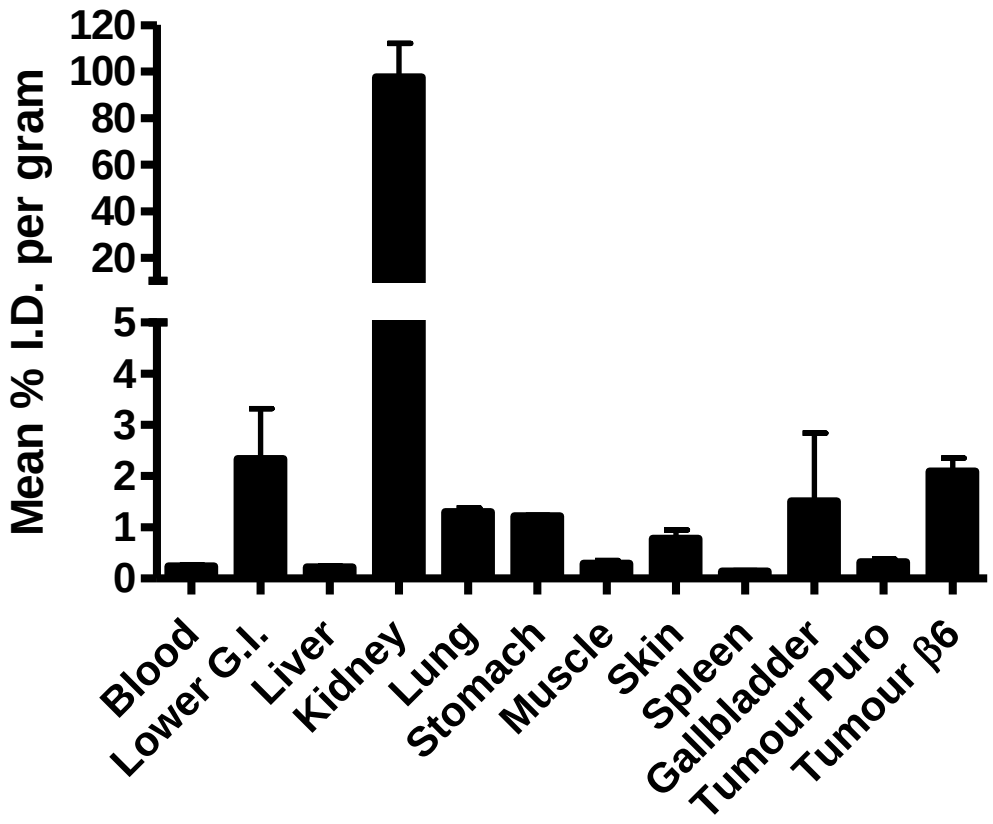

Figure 61 ^{111}In-DTPA-A20FMDV2 tissue biodistribution. ^{111}In-DTPA-A20FMDV2 was injected into tumour bearing mice. After 1 hour animals were killed and tumours and major organs were harvested and the % ID/g tissue determined. Data show that several organs retained significant amounts of radiopeptide.

4.9.2.5 Co-injection Studies in vivo

To establish that the measured ^{111}In-DTPA-A20FMDV2 retention within organs was through a receptor-dependent mechanism, rather than via a peptide-dependent increase in vasodilatation and vessel permeability (blood pooling), receptor specificity studies were performed. A 100-fold (400µg) excess of non-radioactive DTPA-A20FMDV2 peptide was co-injected with 4µg ^{111}In-DTPA-A20FMDV2 and a full tissue biodistribution performed at 1 hour post-injection. If peptide residence within the A375P β6 tumour was solely as a consequence of a vasodilatory mechanism then an excess of cold peptide, co-injected with the radiolabelled peptide, should *increase* subsequent hot peptide retention. However, if peptide residence within the A375P β6 tumour was as a consequence of a receptor-mediated mechanism, an excess of cold peptide co-injected with the radiolabelled peptide, would be expected to *decrease* the subsequent hot peptide retention. The results show that the excess cold peptide significantly decreased the uptake of ^{111}In-DTPA-A20FMDV2 in the stomach, lower GI tract, skin and in the A375P β6 tumour (see **Figure 62**). For example, A375Pβ6 tumour uptake of ^{111}In-DTPA-A20FMDV2 was reduced from 2.0% ID/g to 0.68% ID/g; whereas, in contrast, there was no significant change in uptake into the A375P puro tumour (0.81% to 0.88% ID/g). Therefore, these data suggest that the peptide retention in αvβ6-expressing tissues is a consequence of a receptor-ligand interaction and, therefore they also imply that this mechanism potentially is 'saturable'.

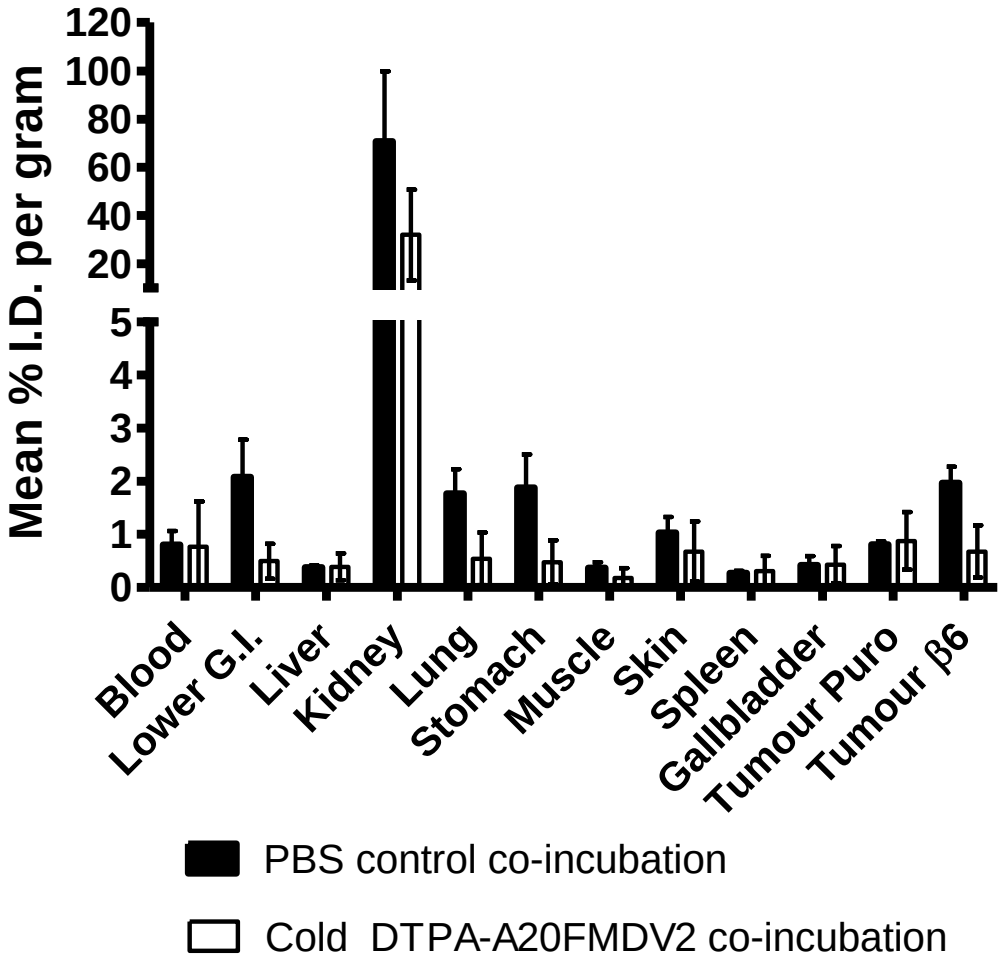

Figure 62 100-fold excess of non-radiolabelled DTPA-A20FMDV2 was co-injected with 4µg/1MBq of ^{111}In-DTPA-A20FMDV2. After 1 hour animals were killed and tumours and major organs were harvested and the %I.D./g tissue determined. Black shaded histograms represent 'control' comparison of 4µg/1MBq of ^{111}In-DTPA-A20FMDV2, whereas white histograms represent co-injections. The data show that 'cold' peptide suppressed uptake in all αvβ6-expressing tissues, but also within kidneys and lungs; endogenous αvβ6 expression was not detected in latter two organs.

It should be noted that co-injection of cold DTPA-A20FMDV2 caused a >50% reduction in the retention of ^{111}In-DTPA-A20FMDV2 within the kidneys (71%+/-29 to 32%+/-19 I.D./g) and within the lungs (1.8%+/-0.5 to 0.5%+/-1.5 I.D./g). However, since kidney and lung expression of αvβ6 were not detected by immunohistochemistry, radiopeptide retention in these organs may not be related to receptor (αvβ6)-specific binding, but instead may occur via a different saturable mechanism. Biodistribution of an indium-111-radiolabelled scrambled peptide (^{111}In-DTPA-A20FMDV2ran), which was composed of the identical amino-acids to A20FMDV2 and thus had identical charge and hydrophobicities, was undertaken to ensure that these physical properties were not responsible for distribution patterns. **Figure 38** showed that DTPA-A20FMDV2ran does not recognise β6 *in vitro* and **Figure 63** confirms the same activity *in vivo*. Thus there was no significant difference in uptake by the A375P β6 versus the A375P puro (0.16 +/-0.04% versus 0.18 +/-0.03% ID/g, respectively) tumour.

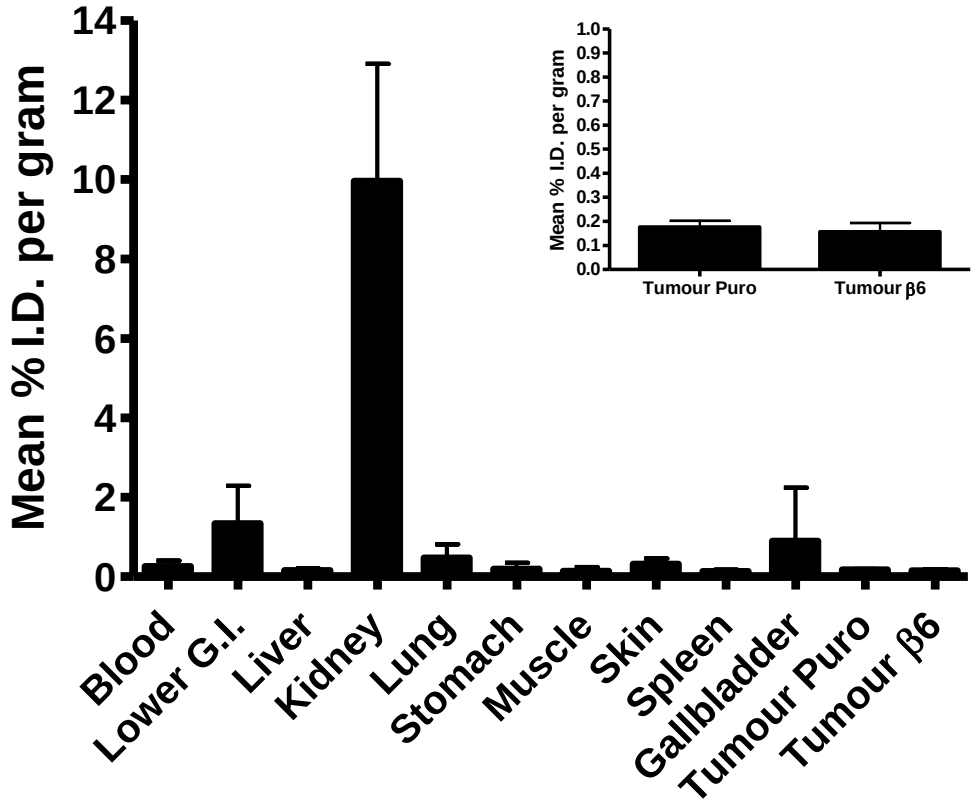

Figure 63 Biodistribution of ^{111}In-DTPA-A20FMDV2ran (scrambled peptide). ^{111}In-DTPA-A20FMDV2ran was injected into tumour bearing mice. After 1 hour animals were killed and tumours and major organs were harvested and the %I.D./g tissue determined. Data showed no significant radiopeptide uptake in A375P puro or A375P β6 tumours, nor in most other tissues (excluding kidney, the site of excretion). Inset displays data for xenografts only, with scale adjusted to show the minimal % I.D./g of ^{111}In-DTPA-A20FMDV2ran in these tumours. Some radiopeptide was associated with the lower GI tract.

Having established that the DTPA-A20FMDV2ran peptide behaved *in vivo* as it did *in vitro*, this peptide next was tested to see whether its renal retention was also via a saturable recycling mechanism. A 100-fold excess (400µg) of non-radiolabelled DTPA-A20FMDV2ran was co-injected with 4µg/1MBq of ^{111}In-DTPA-A20FMDV2, and biodistribution performed at 1 hour post-injection in the normal fashion.

Firstly, **Figure 64** shows that co-injection of 'cold' DTPA-A20FMDV2ran has had no significant effect on radiopeptide uptake and retention in the αvβ6-expressing tissues, including A375Pβ6 tumours, compared with the control group.

However there was a moderate, although not significant, reduction in the retention of ^{111}In-DTPA-A20FMDV2 in the kidney (70 +/-8% to 47 +/-16% I.D./g) following scrambled peptide co-injection; a reduction that was similar to that achieved with the wild-type peptide. Since the kidney retention of ^{111}In-DTPA-A20FMDV2 can be partially suppressed by saturating the retention mechanism with scrambled peptide, these results suggest that the mechanism of kidney retention may not be fully RGD-specific, and thus is not likely to be operating via an αvβ6-dependent system.

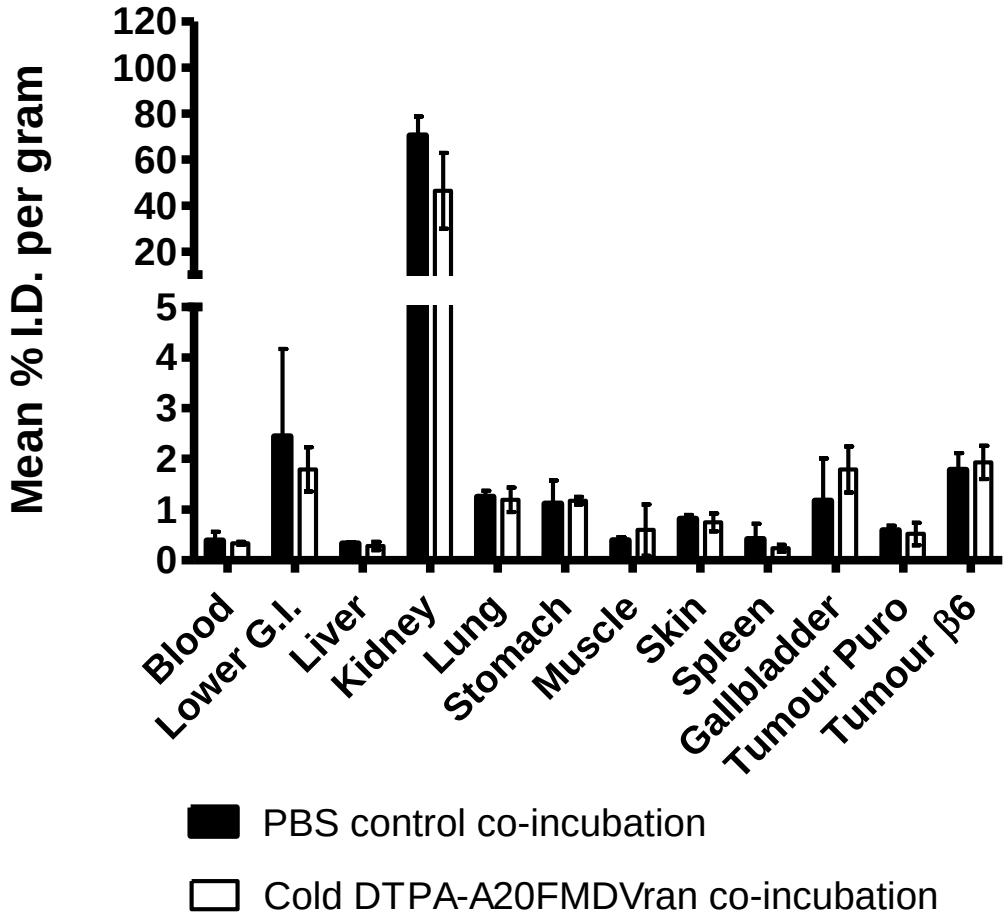

Figure 64 100-fold excess of non-radiolabelled scrambled peptide (DTPA-A20FMDV2ran) co-injected with 4µg/1MBq of ^{111}In-DTPA-A20FMDV2. Black shaded histograms represent 'control' comparison of 4µg/1MBq of ^{111}In-DTPA-A20FMDV2, whereas white histograms represent co-injections. After 1 hour tumours and major organs were harvested and the %I.D./g tissue determined. Results show that the scrambled peptide had no effect on uptake in αvβ6-expressing tissues but brought about a reduced uptake in the kidney.

4.9.2.6 Non-Biotinylated ^{111}In-DTPA-A20FMDV2

Although the renal retention of ^{111}In-DTPA-A20FMDV2 can be suppressed with scrambled peptide and the level of radioactivity retention is acceptable for imaging studies, it is desirable to limit the kidney's exposure further when considering potential therapeutic studies and repeated doses of radiopeptide. It was hypothesised that the biotinylated lysine may affect renal filtration, reabsorption and secretion of the ^{111}In-DTPA-A20FMDV2. Therefore, biodistribution experiments, at 1h post-injection, compared the dissemination of a non-biotinylated form of ^{111}In-DTPA-A20FMDV2 (2µg/1MBq) to the wild-type peptide (2µg/1MBq). **Figure 65** shows that the renal uptake and retention of the non-biotinylated radiopeptide was over double that of the wild-type peptide (160%+/-9 to 71%+/-8 I.D./g). Conversely, the lower GI tract and gallbladder had higher uptake and retention values for the wild-type peptide over the non-biotinylated form. However, the standard deviations were relatively large in these organs, making interpretation of these data difficult. Fortunately, there did not seem to be any significant differences in uptake and retention of the xenografts or remaining αvβ6-expressing tissues. Therefore, these results suggest that biotinylation of a lysine residue within ^{111}In-DTPA-A20FMDV2 can affect renal handling, but that such a procedure seems not to affect the affinity and specificity for αvβ6, *in vivo*.

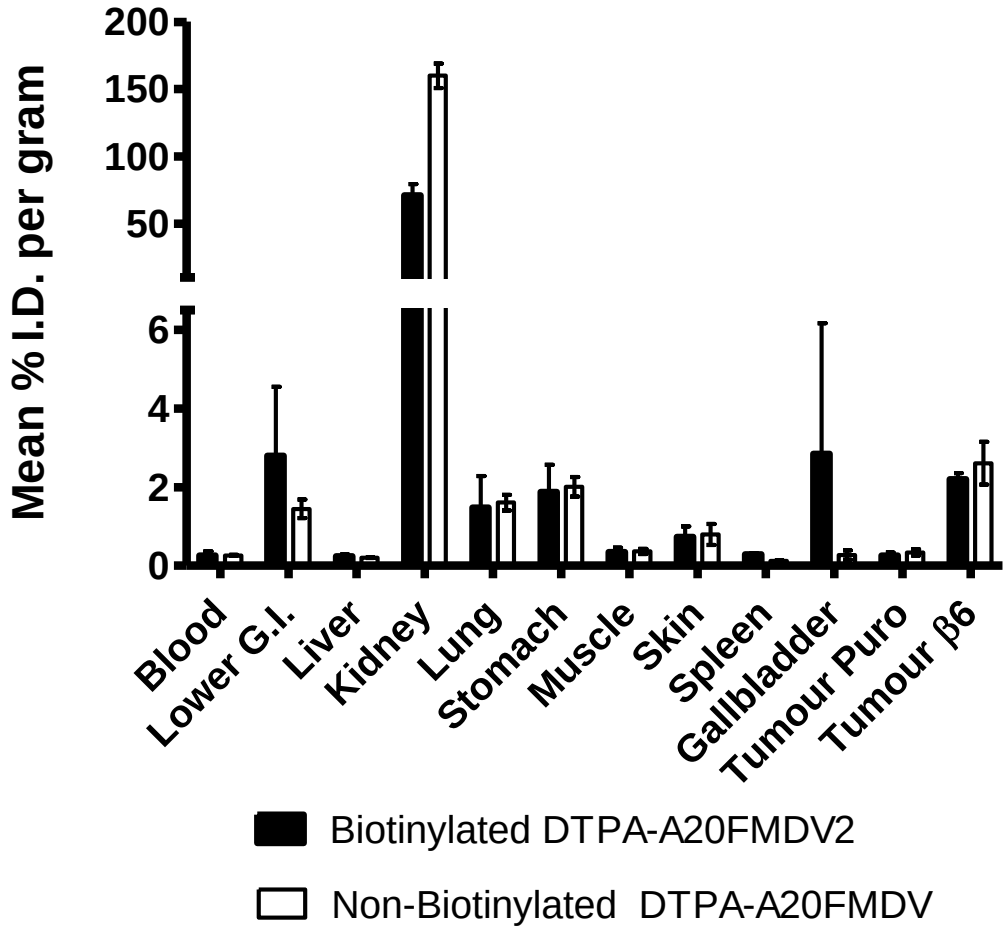

Figure 65 Biodistribution of biotinylated peptide vs. non-biotinylated peptide. Both versions of radiolabelled DTPA-A20FMDV2 (2µg/1MBq) were injected into separate cohorts of tumour bearing mice. After 1 hour animals were killed and tumours and major organs were harvested and the % ID/g tissue determined. Black shaded histograms represent biotinylated ^{111}In-DTPA-A20FMDV2, whereas white histograms represent non-biotinylated ^{111}In-DTPA-A20FMDV2. Data showed that biotinylation of a lysine residue within ^{111}In-DTPA-A20FMDV2 can affect renal handling, but that such a procedure seems not to affect the affinity and specificity for αvβ6, *in vivo*.

4.9.3 NanoSPECT/CT Small Animal Imaging

DTPA-A20FMDV2 has been shown, in the studies so far, to exhibit high sensitivity and specificity for αvβ6, both *in vitro* and *in vivo.* To determine whether ^{111}In-DTPA-A20FMDV2 (4μg/10-30 MBq per mouse) could be used as a molecular-specific imaging agent, it was injected intravenously into the aforementioned 'bi-xenografted' athymic mice. The mice were anaesthetised and imaged at pre-selected time-points, using a high-resolution single photon emission computed tomography small animal imager fitted with a separate, computed tomography scanner (NanoSPECT/CT).

The imaging findings generally were in harmony with the biodistribution results and a representative coronal image is shown (see **Figure 66**). The signals from the A375P β6 tumours consistently were found to be higher than those from the non-β6 expressing control tumours. Moreover, the resolution of the NanoSPECT/C.T permitted the observation that the radioligand was not distributed uniformly through the tumour but rather appeared to be located in high-activity nodules, which were spatially distinct. Images, with a clearly identifiable β6-positive tumour, routinely were obtained as early as 30 min, and as late as 4 hours, post-injection. The best images, delineating ideal differentiation between the A375P β6 and the A375P puro tumours and other background tissues, occurred at 1 hour post-injection; correlating with the biodistribution results already reported. This experiment was repeated (n=9) with similar results. High signals were observed from the kidneys and bladder, when injected without co-injection of 'cold' DTPA-A20FMDV2ran. **Figure 66** also shows a Maximal Intensity Projection (MIP) which displays uptake in the GI tract, corresponding with localisation of endogenous αvβ6 expression. Thus ^{111}In-DTPA-

A20FMDV2 specifically is retained by αvβ6-expressing tissues and this suggests strongly that this is a reagent which can be used to identify αvβ6-expressing cancers selectively.

In summary, the findings reported in this section have shown that ^{111}In-DTPA-A20FMDV2 selectively localises to β6 expressing tissues in a 'bi-xenograft' athymic mouse model. This selective localisation can be discerned, and visualised, on a NanoSPECT/CT and the distribution patterns indicate that there was not homogenous distribution throughout the entire tumour mass.

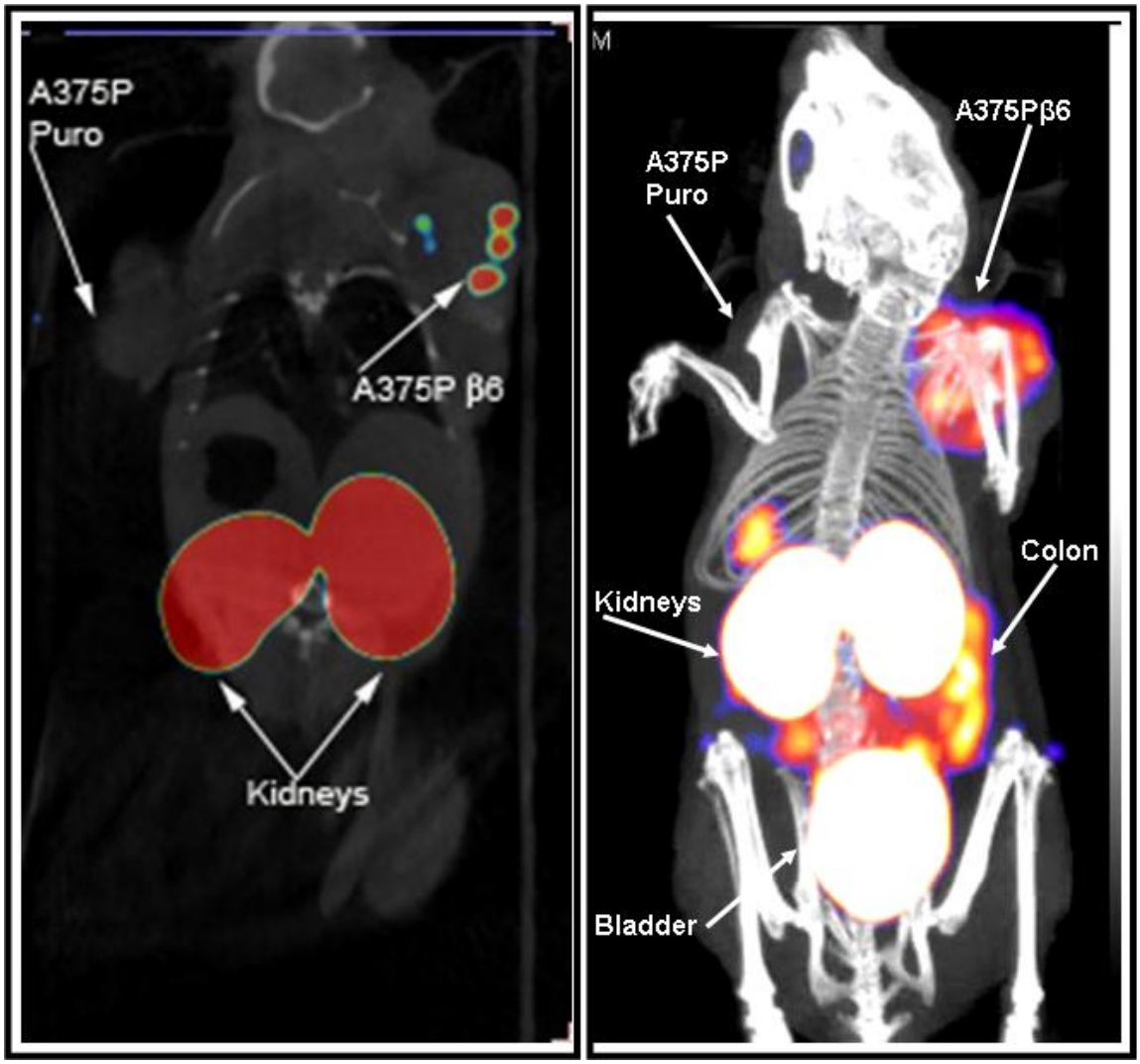

Figure 66 Non-invasive imaging of αvβ6-expressing tumour with ^{111}In-DTPA-A20FMDV2. 10-30MBq of ^{111}In-DTPA-A20FMDV2 was injected i.v. into mice bearing A375P puro (left-shoulder) and A375P β6 (right-shoulder) tumours. After 1 hour the mice were imaged on a NanoSPECT/CT. LEFT: Coronal slice showing that the radiopeptide has accumulated selectively in the A375P β6 tumour. In contrast the A375P puro tumour was negative. RIGHT: Maximum Intensity Projection (MIP) of images from a different mouse; confirming that the A375P β6 tumour, kidneys, bladder and lower GI tract all labelled strongly.

Chapter V

Results: Validation of αvβ6 Targeting on other Models and the Study of other Peptide Variants

5.1 Breast Cancer Model for Targeting αvβ6.

5.1.1 Integrin Expression Profile on Breast Cell Lines.

The panel of human breast cell lines (derived from the immortalised MCF-10A line [234]): MCF-10A, MCF-10AneoT, AT1K.c12, Ca1h, CA1a and MCF-10 DCIS.com were tested for their surface integrin expression, using flow cytometry. Each integrin antibody was tested and geometric mean values were compared with appropriate isotype controls. **Table 12** (page 204) shows that all of breast cancer cell lines endogenously express αvβ6, at varying levels, on their cell surface. Therefore, these lines are suitable for validating the targeting efficacy of the ^{111}In-DTPA-A20FMDV2 peptide. It also was noted that the RGD-binding integrin, αvβ3, is not expressed on MCF-10A, MCF-10AneoT, AT1K.c12 and CA1a cells.

Integrin / Cell Line	α1	α2	α3	α4	α5	α6	α9β1
MCF-10A	++	++++	++++	-	++		+
MCF-10AT1K.c12	+	++++	++++	-	++		+
MCF-10AneoT	++	++++	++++	-	++		+
MCF-10A.CA1a	+	++++	++++	-	++		+
MCF-10A.Ca1h	+	++++	++++	-	++		++
MCF-10.DCIS.com	+	++++	++++	-	+		+
A375P β6	++	++	++	+	++		++

Integrin / Cell Line	β4	αvβ3	αvβ5	αvβ6	αvβ8
MCF-10A	++++	-	+	++++	++
MCF-10AT1K.c12	++++	-	+	+++	++
MCF-10AneoT	++++	-	+	++	+
MCF-10A.CA1a	++++	-	++	++++	++
MCF-10A.Ca1h	++++	+	++	++++	++
MCF-10.DCIS.com	++++	++	++	++++	++
A375P β6	-	++	+	+++	+

Table 12 Surface integrin expression by breast cancer cell lines in comparison with the A375P β6 melanoma line. Measured by flow cytometry. Pluses designate the abundance of the integrin, according to a grading system [241] derived from geometric mean values relative to isotype negative control antibodies.

5.1.2 Invasive Activity of an αvβ6-expressing Breast Cancer Cancer Cell Line

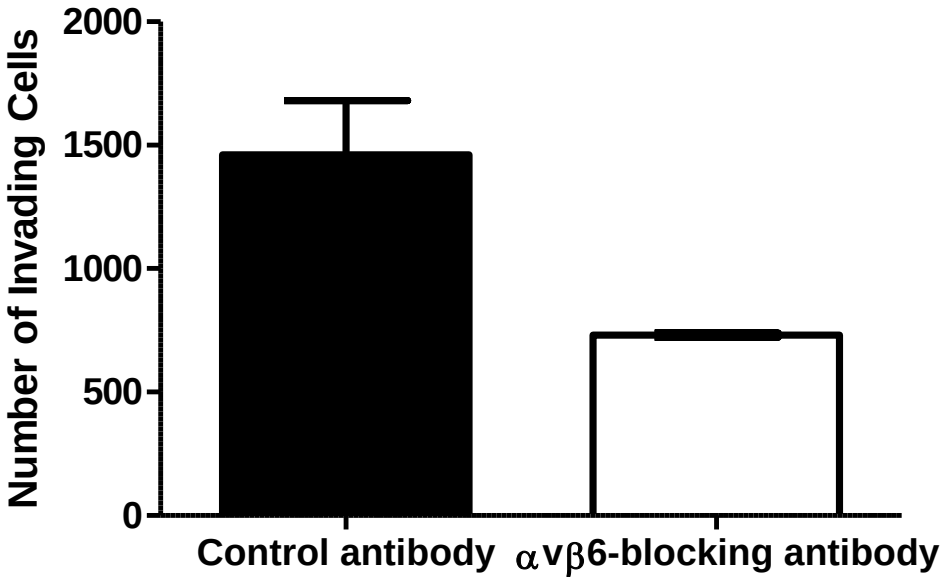

Figure 67 Transwell Invasion Assay with MCF-10A.CA1a cells, in the presence of αvβ6-blocking (63G9) and non-blocking antibodies (7.2).

Owing to Santner et al's description of MCF-10A.CA1a's ability to form fast growing tumours in all murine subjects [234], and MCF-10A.CA1a's high expression of αvβ6, but not αvβ3, this cell line was studied in further detail. Its ability to invade Matrigel-coated Transwell invasion chambers, in the presence of αvβ6-blocking (63G9) and non-blocking antibodies (7.2), was quantified. The numbers of invading cells were counted after 72 hours incubation and replicates were averaged. **Figure 67** shows that MCF-10A.CA1a's ability to invade was reduced significantly ($p<0.03$) in the presence of an αvβ6-blocking antibody; suggesting that, in this assay, this cell line exhibited significant αvβ6-dependent invasion.

5.1.3 Maintenance of αvβ6 expression within Tumour Xenografts

Hu et al also recently reported on Santner's MCF10.DCIS.com cell line [234, 242], as a subcutaneous xenograft, and commented on the importance of αvβ6 in affecting tumourigenic behaviour [243]. The MCF10.DCIS.com cell line was injected subcutaneously into female nude mice, alone or together with 50% Matrigel, in this report [243]. Therefore, it was decided to replicate this model and possibly attempt to validate the targeting of ^{111}In-DTPA-A20FMDV2, as an addition to the "engineered" cell lines that previously were used in this thesis. However, prior to targeting experiments, it was important to confirm that tumour xenografts maintained their αvβ6 expression, *in vivo*. Therefore, CD1 nude mice were either inoculated subcutaneously with MCF- MCF-10 DCIS.com alone or with MCF-10 DCIS.com / Matrigel to determine the effect on xenograft formation. Mice were killed after the development of 'palpable' tumours (see **Methods)** and subsequently tumours were dissected, fixed and paraffin-embedded for histological examination. Tumour sections were stained for αvβ6 expression and the results compared with those obtained using an isotype negative control antibody. **Figure 68** reveals staining patterns of the xenografts and is a representative image.

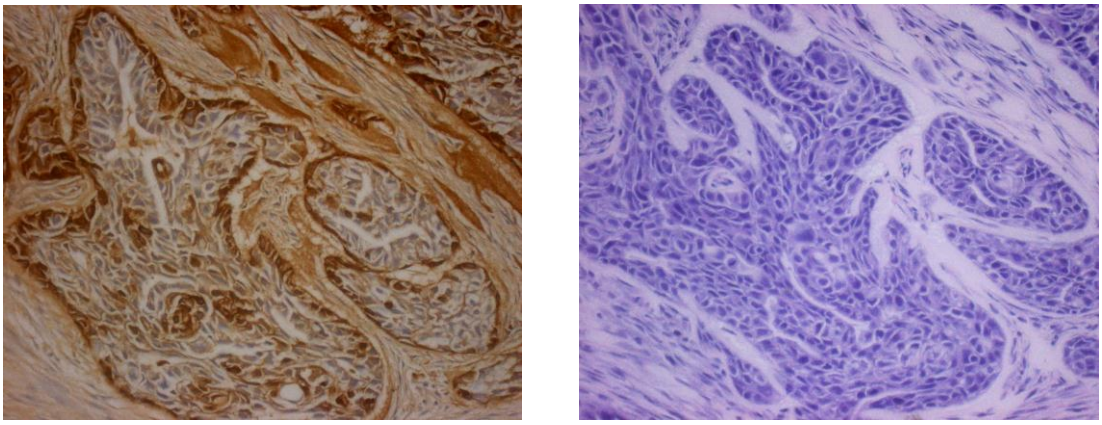

Figure 68 Murine MCF-10 DCIS.com / Matrigel xenograft staining for αvβ6.

Left image is 62G2 staining and right is Haematoxylin stain.

The MCF-10 DCIS.com / Matrigel xenograft (shown above) revealed strong staining, especially at the periphery of the tumour islands. Similar findings were discovered in the MCF-10 DCIS.com alone xenograft (data not shown), suggesting that the presence of Matrigel had little impact on the level or localisation of αvβ6

5.1.4 Biodistribution Experiments using CD1 mice bearing MCF-10 DCIS.com / Matrigel Xenografts

Having established breast cancer xenograft models, with a tumour line which endogenously (as opposed to genetically engineered) expressed αvβ6, validation of ^{111}In-DTPA-A20FMDV2's targeting was undertaken. Full tissue biodistribution on tumour-bearing mice was performed; harvesting organs / tumours at 1h post-injection of ^{111}In-DTPA-A20FMDV2 (1 MBq / 4 µg). Since the breast cell lines were injected with Matrigel, a cohort of animals, in which Matrigel alone was injected subcutaneously, was used as a negative control. Although, the constituents

of Matrigel were not expected to express αvβ6, and thus an αvβ6-targeting agent theoretically should not be retained in the Matrigel-alone plug, **Figure 69** indicates that the Matrigel alone plug retained significant amounts of radioactivity (1.15 ± 0.28 % ID/g) at 1 hour. Having proven *in vivo* specificity for targeting αvβ6 in the previous **Results** section, this unexpected experimental finding suggested that Matrigel alone was not a suitable negative control for any future peptide targeting experiments.

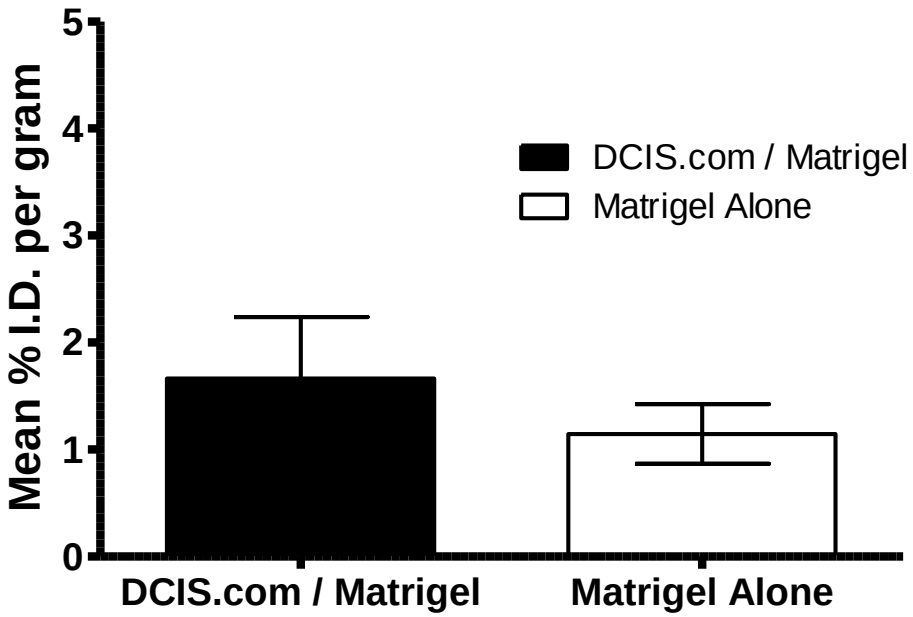

Figure 69 ^{111}In-DTPA-A20FMDV2 biodistribution in Matrigel xenografts, with or without MCF-10 DCIS.com cells. ^{111}In-DTPA-A20FMDV2 was injected into tumour bearing mice; tumours were harvested after 1 hour and % ID/g tissue determined.

5.1.5 Biodistribution Experiments using CD1 mice bearing either MCF-10 DCIS.com or MCF-10A.CA1a Xenografts (No Matrigel)

Owing to the apparent unsuitability of Matrigel for peptide targeting experiments (described section 5.1.4.), it was decided not to continue to use this preparation for xenograft models. That is, either MCF-10 DCIS.com or MCF-10A.CA1a tumour cells, suspended in serum-free media alone were injected subcutaneously into mice. Thereafter, full tissue biodistribution was performed on these tumour-bearing mice; harvesting organs / tumours at 1h post-injection of ^{111}In-DTPA-A20FMDV2 (1 MBq / 4 μg).). **Figure 70** reveals a similar biodistribution pattern for both cohorts of mice. That is, in addition to the tumour xenografts, the lower gastrointestinal (GI) tract, lung, stomach, skin, gall bladder, kidneys and lungs all have retained significantly more radioactivity than skeletal muscle. This biodistibution pattern is markedly similar to that found in the nude mice described in **Chapter 4** (see **Section 4.9**). Furthermore, both the tumour xenografts retained significant amounts of radioactivity, at 1 hour. The MCF-10 DCIS.com. xenograft attained 2.1 ± 0.63 % ID/g (19:1 tumour to muscle ratio); whereas the MCF-10A.CA1a xenograft achieved 2.34 ± 0.35 % ID/g (17:1 tumour to muscle ratio). The tumours to blood ratios for both cohorts of mice were 15:1 and 16:1, respectively.

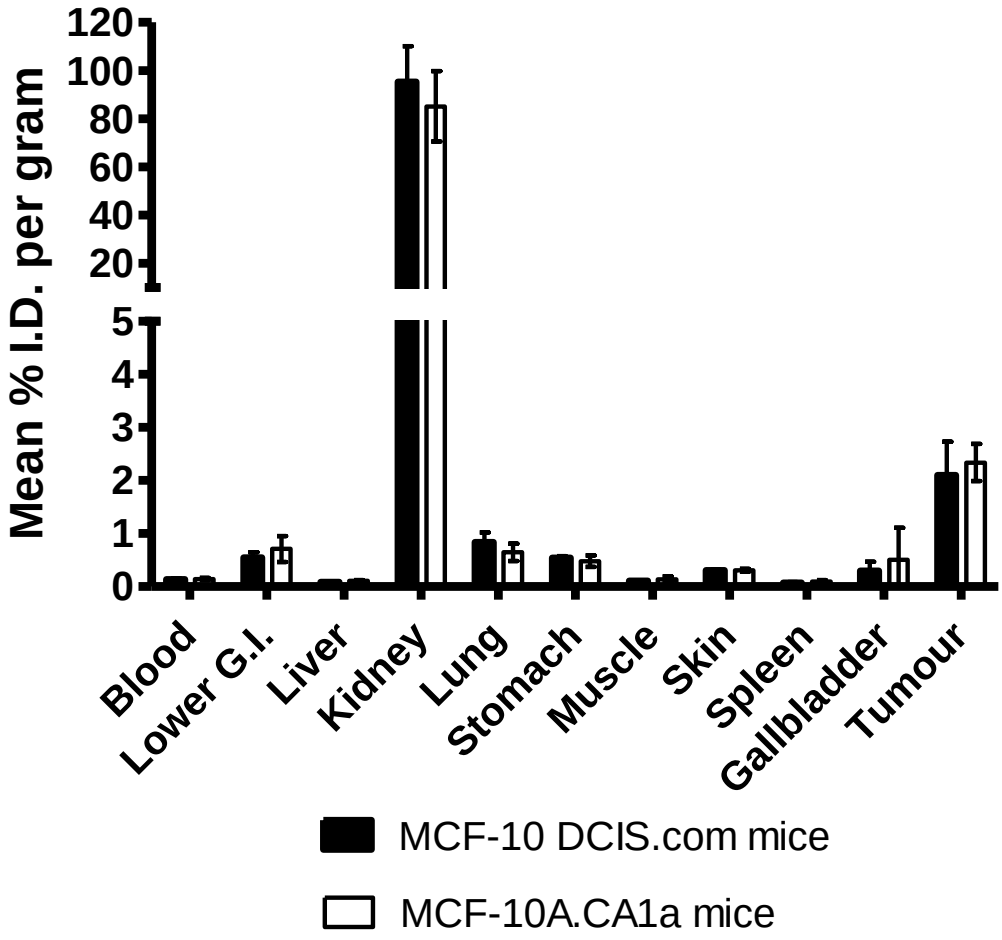

Figure 70 ^{111}In-DTPA-A20FMDV2 biodistribution in mice bearing either MCF-10 DCIS.com or MCF-10A.CA1a xenografts. ^{111}In-DTPA-A20FMDV2 was injected into tumour bearing mice; organs and tumours were harvested after 1 hour and the %I.D./g tissue determined.

5.1.6 NanoSPECT/ CT Small Animal Imaging of Breast Cancer Models

Results reported in **Section 5.1.5** revealed that ^{111}In-DTPA-A20FMDV2 was retained within tumour xenografts that express αvβ6 endogenously. To determine whether ^{111}In-DTPA-A20FMDV2 (4μg / 10-30 MBq per mouse) could be used as a molecular-specific imaging agent for these breast cancer models, radiolabelled peptide was injected intravenously into cohorts of athymic mice bearing either MCF-10 DCIS.com or MCF-10A.CA1a xenografts. The mice were anaesthetised and imaged at pre-selected time-points, using a high-resolution single photon emission computed tomography small animal imager fitted with a separate, computed tomography scanner (NanoSPECT/CT).

Once more the imaging findings were in harmony with the biodistribution results and representative coronal images are shown in **Figure 71**. The signals from the MCF-10 DCIS.com or or MCF-10A.CA1a tumours consistently were found to be higher than non-β6 expressing 'background' tissues e.g. skeletal muscle. The resolution of the NanoSPECT/CT again revealed that the radioligand was not distributed uniformly throughout the tumour mass, but appeared rather to be located in nodular regions which manifested high-activity. Images with a clearly identifiable β6-positive tumour routinely were obtained as early as 30 min, and as late as 4 hours, post-injection. However, the best images, delineating optimal differentiation between the tumours and other background tissues, occurred at 1 hour post-injection, correlating with the biodistribution results. High signals were observed from the kidneys and bladder, when injected without co-injection of 'cold' DTPA-A20FMDV2ran. Additionally, **Figure 71** confirms uptake within the GI tract, which corresponds with the endogenous αvβ6 expression observed in this organ. Therefore ^{111}In-DTPA-

A20FMDV2 is retained specifically by αvβ6-expressing tissues and its targeting capacity has been validated on these αvβ6-expressing breast tumour models.

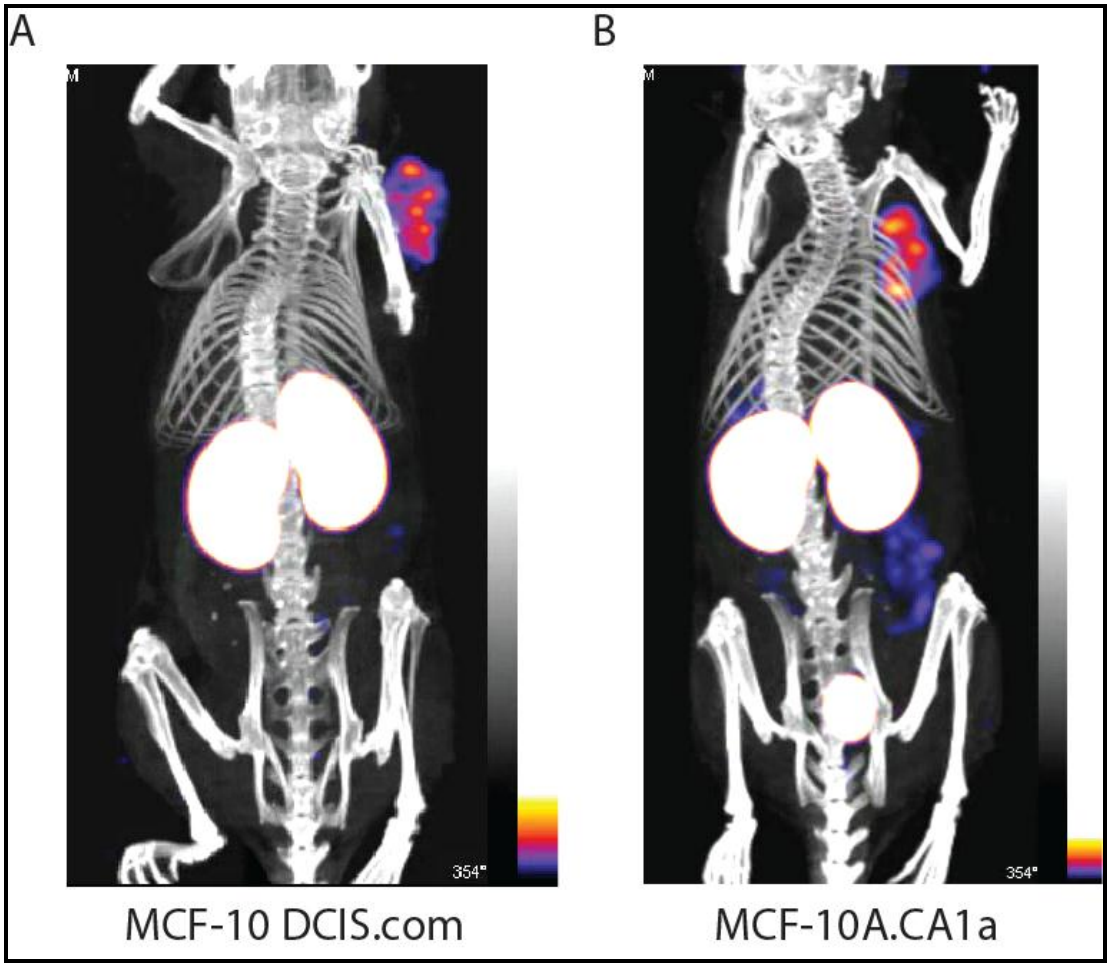

Figure 71 ^{111}In-DTPA-A20FMDV2 injected i.v. into mice bearing either MCF-10 DCIS.com or MCF-10A.CA1a breast tumours. After 1 hour the mice were imaged on a NanoSPECT/CT. A: Maximum Intensity Projection (MIP) of images from a mouse bearing MCF-10 DCIS.com xenograft on right shoulder. The MCF-10 DCIS.com tumour labelled strongly with radiopeptide, again showing that peptide does not distribute uniformly. B: MIP of images from a mouse bearing MCF-10A.CA1a xenograft on right shoulder. The MCF-10A.CA1a tumour again labelled strongly with radiopeptide, together with the kidneys, bladder and the lower GI tract.

5.2 Colon Cancer Model for Targeting αvβ6.

A range of mouse models of colorectal cancer have been developed to study this multistage disease:-

Moser et al described the production of a mouse model where, after ethylnitrosurea treatment, a single germline mutation in a gene which was dominantly expressed and fully penetrant, resulted in susceptibility to tumour formation [244]. The mutant gene was inherited in an autosomal dominant manner and charcterised as ‘multiple intestinal neoplasia’ (‘Min’); owing to the development of multiple adenomas throughout the entire intestinal tract with progression to adenocarcinomas in the intestine in older mice [244]. Consequently, the mice passed bloody faeces and became anaemic, eventually these manifestations were so severe that they resulted in death of the affected animals [244].

Some time later, Marsh et al described a transgenic model involving the combined deletion of both PTEN and Apc genes [245]. Inactivation of Apc is the most frequent genetic event in colorectal cancer; where it appears to be important for differentiation control and cellular migration [246]. On the other hand, mutations of phosphatidylinositol 3-kinase (PI3K/Akt) pathway components have been reported in almost 40% of all human colorectal cancers [247]. The PI3K/Akt pathway normally promotes proliferation and cell survival, and stimulates progression of the cell cycle. Conversely, PTEN acts as a tumour suppressor through its antagonism of the PI3K/Akt pathway [245]. Marsh et al showed that loss of PTEN, in the context of Apc deficiency, accelerates tumourigenesis through increased activation of Akt; leading to rapid development of adenocarcinomas [245].

Tumour sections from both these murine models were kindly donated by Professor A.R. Clarke's and Professor Sir N. Wright's groups. If these tumours also expressed αvβ6, then these models, potentially could, be used to validate ^{111}In-DTPA-A20FMDV2 targeting. Therefore, both sets of sections were derived from mice which were killed at time points expected to result in different stages of tumour formation. Subsequently, intestines and tumours were harvested, fixed and paraffin-embedded for histological examination. Representative images taken from several mice at different stages of tumour progression,are shown below.

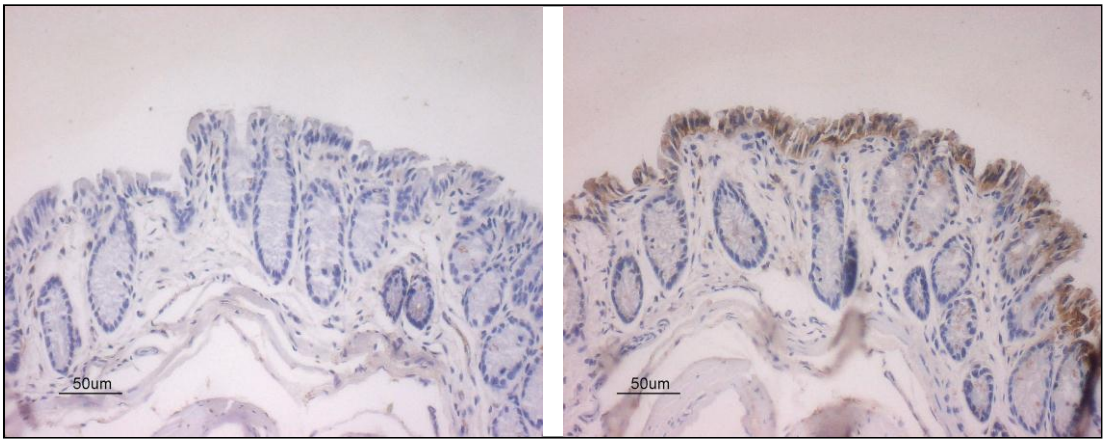

Figure 72 Min mouse: normal colon staining for αvβ6 (x100). Left image is negative control and right is 62G2 staining.

Figure 72 reveals strong αvβ6 staining at the surface of enterocytes, forming the mucosa of the colon, similar to that previously described in the immunodeficient mice used in earlier experiments (see **Section 4.6**). Again, the intensity decreases as the epithelial layer is followed down to the crypts.

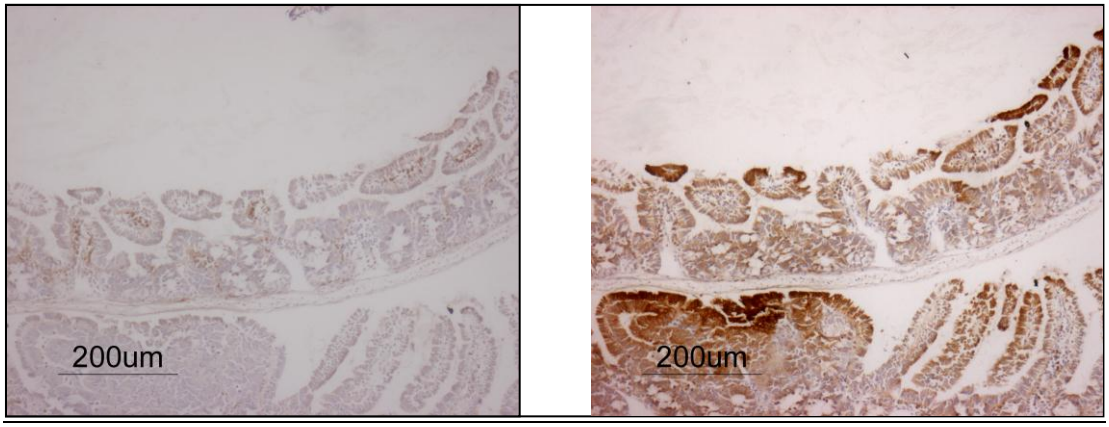

Figure 73 Min mouse: adenoma staining for αvβ6 (x100). Left image is negative control and right is 62G2 staining.

Marked epithelial dysplasia of the large intestine with glandular growth into the muscularis layer is shown in **Figure 73**. The periphery of the polyp stains strongly for αvβ6.

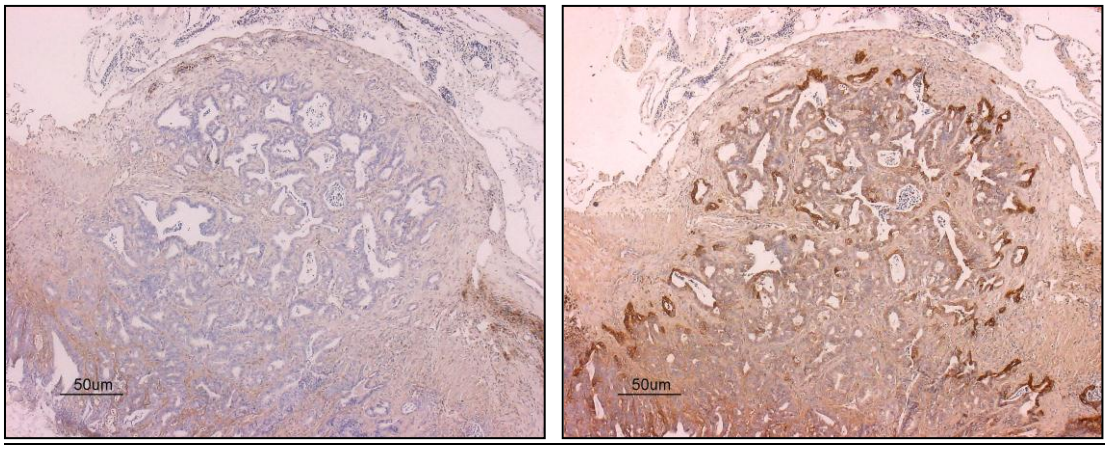

Figure 74 Apc $^{f/+}$; Pten $^{f/f}$ mouse: adenocarcinoma staining for αvβ6 (x100). Left image is negative control and right is 62G2 staining.

Figure 74 reveals an advanced, ulcerating, invasive adenocarcinoma that has penetrated the full thickness of the small intestinal wall, destroying the muscularis propria. The dysplastic glandular area, within the main tumour mass, stains strongly for αvβ6 expression. Moreover, **Figure 75** shows that 'escaping' tumour islands (x200 magnification), leaving the main tumour mass and invading underlying tissue, also stain strongly for αvβ6.

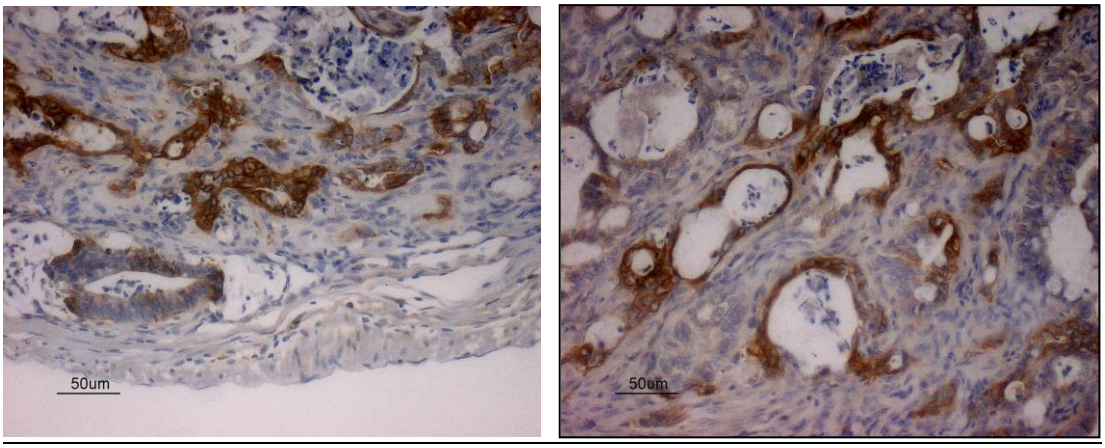

Figure 75 Apc $^{f/+}$; Pten $^{f/f}$ mouse: adenocarcinoma staining for αvβ6 (x200).

Although there is background expression of αvβ6 on normal intestinal surface epithelium, the strong tumour cell expression of αvβ6 suggests that both mouse models would be suitable models for validating the suitability of ^{111}In-DTPA-A20FMDV2 for targeting intestinal tumours. Accordingly, collaborative experiments are being planned between the involved groups. Unfortunately, the projected schedule for these collaborative experiments is beyond the time limits of my training degree and such studies will be undertaken by my successors.

5.3Peptide Variants and Probe Stabilisation Methods

5.3.1 Cyclisation: A Method of Inhibiting Proteolysis of Peptides

Cyclisation already has been mentioned (see **Table 6**, page 105) as a technique to improve peptide stability, whilst maintaining (and sometimes improving) their biological activity [190]. Therefore, several peptide variants were designed, using disulphide cyclisation and based on A20FMDV's structure.

5.3.1.1 Assessment of Cyclic Peptides' Sensitivity and Specificity by Flow Cytometry

Two variants, DBD1 and DBD2, were tested at a range of concentrations (10μM-1nM; 30 mins incubation) on the A375P melanoma cell model and compared to A20FMDV2. Both variants were biotinylated and so bound peptide was detected by antibody detection of the biotin. Results revealed a relationship between concentration of peptide and resultant binding to A375Pβ6 cells. **Figure 76** reveals a 'side-by-side' comparison of the original peptide and its cyclic derivatives. The black lined histogram represents the negative control for the system, using mouse IgG. The grey shaded histogram represents clone 10D5 (commercial antibody to αvβ6) and serves as a positive control for the system, as well as a comparison for peptide binding. There were concentration-dependent relationships between varying amounts of each peptide and constant levels of αvβ6. Essentially, identical patterns of A375Pβ6 binding are seen with the native peptide and its cyclic derivatives. That is, at similar concentrations of A20FMDV2, both DBD1 and DBD2 bind at almost identical levels to A375Pβ6 cells; suggesting that A20FMDV2 and its cyclic

derivatives bind with similar affinity to αvβ6. However, there appears to be some binding of the cyclic derivatives (especially DBD1), at higher peptide concentrations, to the A375P puro line. That is, cyclisation seems to have reduced the specificity of the peptide derivatives to αvβ6**.**

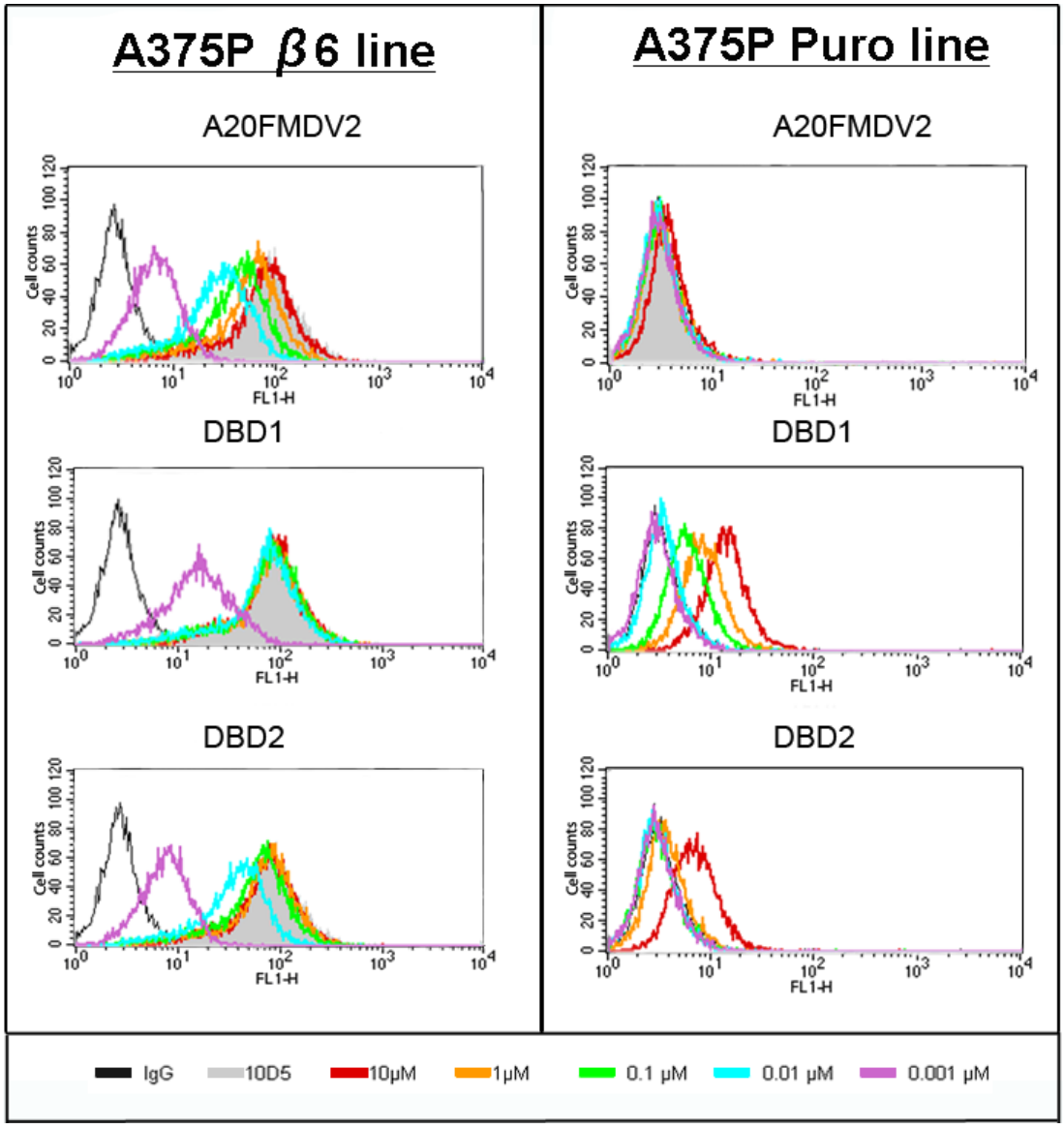

Figure 76 Comparing the affinity and specificity of A20FMDV2 with DTPA-A20FMDV2, using flow cytometry.

Nonetheless, the reduction of specificity mainly was a characteristic of DBD1; DBD2 still had relatively good affinity and specificity for αvβ6, and so was selected for further evaluation.

5.3.1.2 DTPA-DBD2 Radiolabelling and Quality Control

DTPA-DBD2 was radiolabelled with indium to generate ^{111}In-DTPA-DBD2. Reverse-phase HPLC was used to analyse the labelling efficiency and to evaluate the structural integrity of the radiolabelled targeting ligand. ^{111}In-DTPA-DBD2 was eluted in a single peak, with a retention time of around 21 minutes (see **Figure 77**). The radiochemical purity of the radiolabelled ^{111}In-DTPA-DBD2 was over 99%, according to this analysis. Furthermore, there was no evidence of fragmentation or aggregation during the labelling process, as indicated by the sharp single peak.

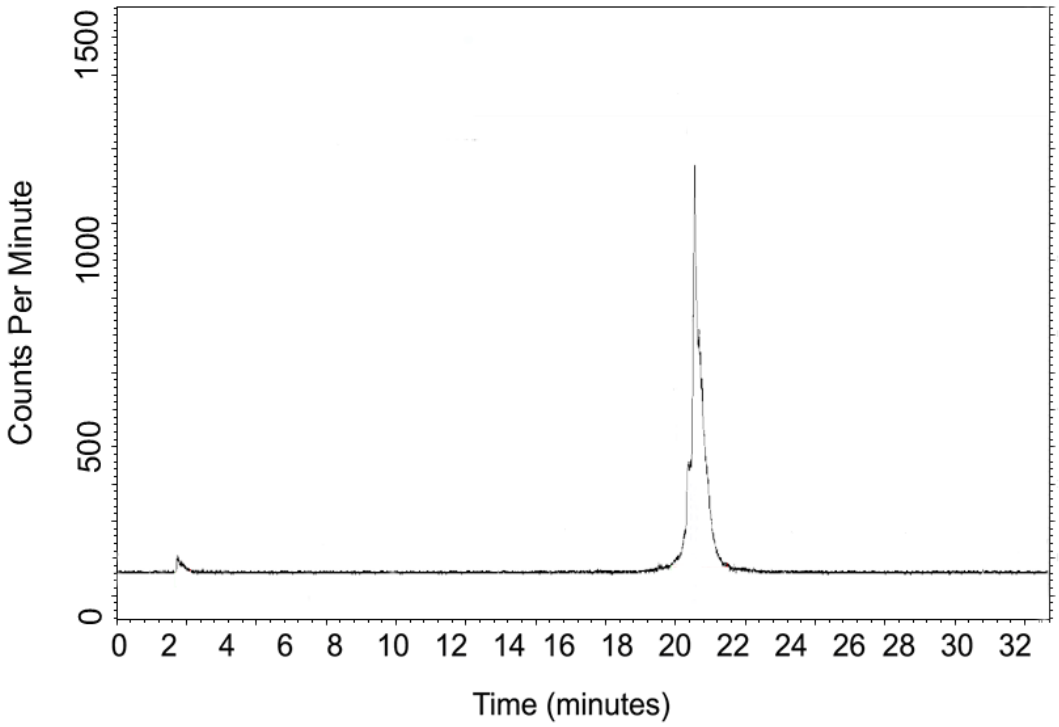

Figure 77 RP- HPLC trace measuring ^{111}In-DTPA-DBD2 radiolabelling efficiency.

5.3.1.3 Plasma Stability Studies of ^{111}In-DTPA-DBD2

The aim of cyclisation was to improve peptide stability from the relatively harsh enzymatic environment, contained within the plasma. An improvement in probe stability of a compound in plasma can strongly influence its *in vivo* efficacy. Plasma stability assays were thus performed on ^{111}In-DTPA-DBD2, using RP-HPLC to measure structural integrity of the labelled peptide.

^{111}In-DTPA-DBD2 was incubated at 37^{o}C in either PBS or murine plasma for various periods of time. Firstly, incubation in PBS showed high stability, with only around 10-15% loss of purity at 24 hours. This result was considered to be a favourable point with regard to chemical storage and transport. In contrast, and as expected for a linear peptide, there was degradation of the radioligand in plasma. **Figure 78** shows that at 2 hours, 81% of the radiopeptide remained intact whereas by 4 hours only 64% remained undegraded.

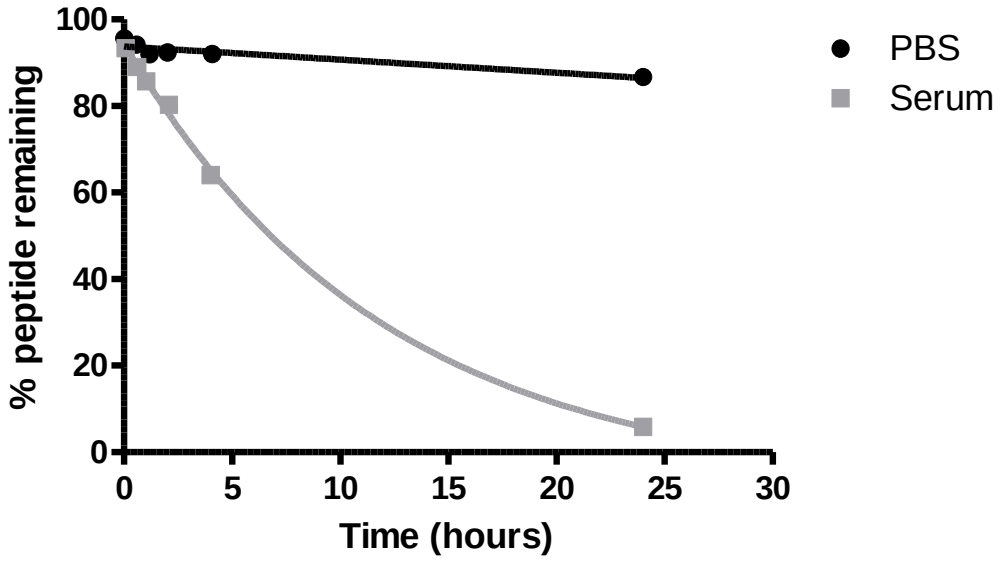

Figure 78 Plasma Stability Study: ^{111}In-DTPA-DBD2 was incubated at 37^{o}C in either PBS or murine plasma for various periods of time. After the selected time periods, samples of the incubation mixture were analysed on an RP-HPLC. Stability was preserved in PBS up to 24 hours after initation of incubation; whereas plasma stability was affected considerably after only 4 hours incubation.

5.3.1.4 Biodistribution of ^{111}In-DTPA-DBD2

The previous experience with A20FMDV2 suggested that the addition of a DTPA chlelating agent and ^{111}In radiolabelling would not adversely affect DBD2's affinity to αvβ6 (see **Sections 4.3 & 4.8**). Therefore, ^{111}In-DTPA-DBD2 was injected intravenously into each 'bi-xenografted' mouse (described in **Methods**). Mice were killed at the pre-selected time-points, dissected and major organs were harvested. The associated radioactivity of each organ was quantified (expressed as percentage of injection dose per unit mass of tissue) and used as an indirect measure of peptide uptake and organ retention. Initially, 1 MBq of ^{111}Indium was radiolabelled onto 2μg of DTPA-DBD2 and peptide uptakes in the xenografts were compared, at various time points (see **Figure 79**). Of note, this 2μg mass for injection was derived from the previous peptide mass experiments with DTPA-A20FMDV2 (see **Section 4.9.2.2)**.

Maximal differential uptake between the A375P β6 and the A375P puro (non-αvβ6 expressing) tumours occurred at 1 hour (post-injection). However, good differential uptake, although at relatively lower % ID/g, was seen up to 4 hours, p.i.. The ratio of A375P β6 tumour uptake and retention to that of A375P puro consistently was around 3:1; thus reduced in comparison to linear DTPA-A20FMDV2. At 1 hour post-injection, the mean % injected dose per gram was around 1.36% ± 0.5 for the A375P β6 tumour, compared with 0.47% ± 0.1 for the A375P puro tumour.

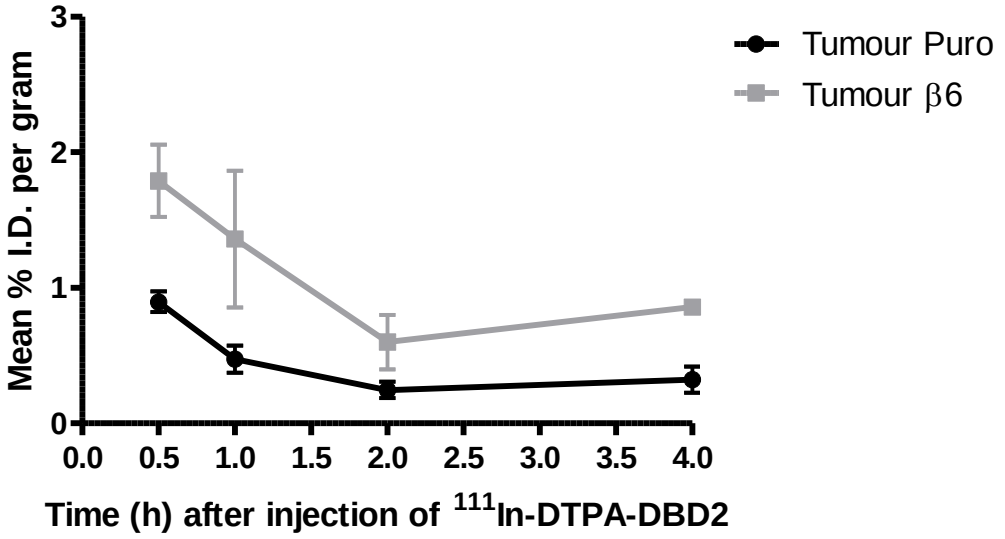

Figure 79 ^{111}In-DTPA-DBD2 (1 MBq / 2µg) injected into groups of tumour-bearing mice. At 0.5, 1, 2 and 4 hours post-injection three mice were killed and tumours removed and the % ID/g tissue determined.

The 30 minute mean %I.D./g within the A375P β6 tumour was 1.79% ± 0.27, for ^{111}In-DTPA-DBD2; contrasting with 5.83% ± 1.63 for ^{111}In-DTPA-A20FMDV2. Furthermore, the 30 minute mean %I.D./g within the A375P puro tumour was 0.9% ± 0.08 for ^{111}In-DTPA-DBD2, and 2.39% ± 1.16 for ^{111}In-DTPA-A20FMDV2. Nonetheless, the later timepoints for the cyclic DBD2 peptide reveal a higher and more persistent mean %I.D./g, in the A375P puro tumour, compared to the linear ^{111}In-DTPA-A20FMDV2 (0.32 vs. 0.15 at 4h p.i., respectively). Since DBD2 and A20FMDV2 have conserved RGD-integrin-binding motifs (see **Section 4.9.2.5**), it appears that the process of cyclisation indirectly has affected the affinity and specificity for αvβ6, *in vivo*.

In addition**, Figure 80** indicates that several organs retained significant amounts of radioactivity at 1 hour. The lower gastrointestinal (GI) tract, lungs, stomach, skin and gall bladder (as well as the A375P β6 tumour) all have retained significantly more radioactivity than either A375P puro tumour or spleen. Therefore, this pattern of biodistribution is consistent with that of ^{111}In-DTPA-A20FMDV2 (see **Section 4.9.2.4**). That is, ^{111}In-DTPA-DBD2 is also able to recognise and bind to endogenous αvβ6-expressing tissues.

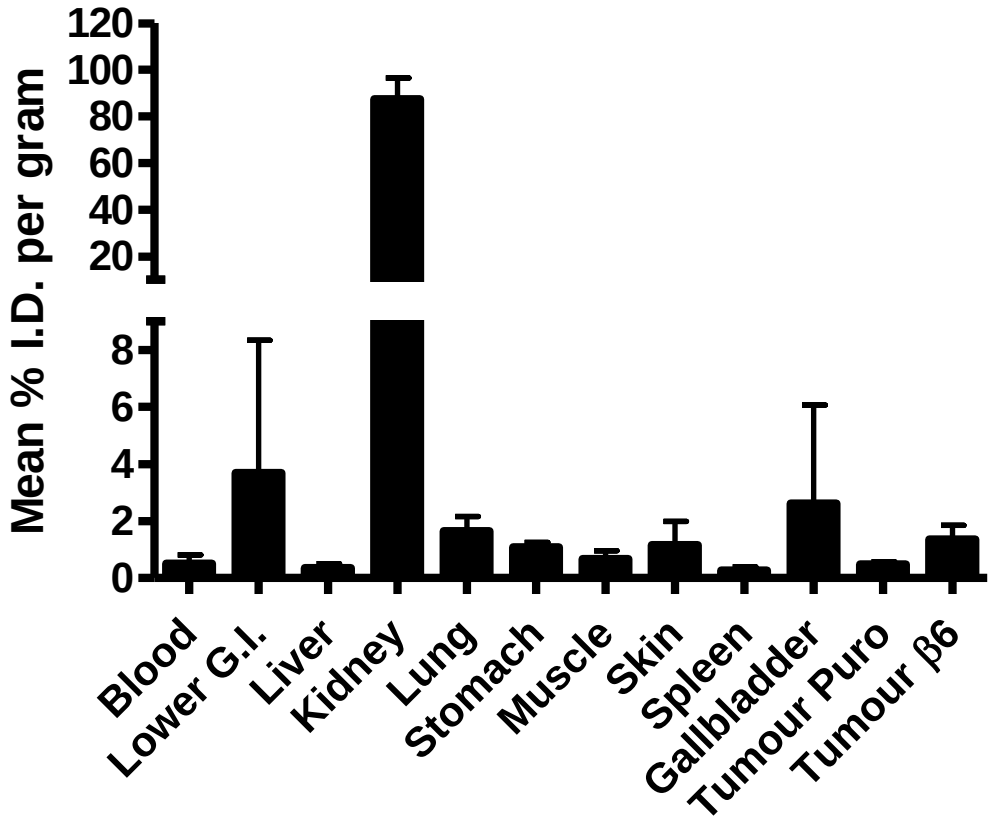

Figure 80 ^{111}In-DTPA-DBD2 tissue biodistribution. ^{111}In-DTPA-DBD2 was injected into tumour bearing mice. After 1 hour animals were killed and tumours and major organs were harvested and the % ID/g tissue determined. Data show that several organs retained significant amounts of radiopeptide.

5.3.2 The DOTA Chelator Variant of A20FMDV2

The DOTA chelator has some advantages over its DTPA counterpart (see **Section 2.2.3**). DOTA is able to chelate a range of radioisotopes, which include those necessary for PET imaging or peptide radiotherapy. Furthermore, DOTA complexes tend to be more thermodynamically and kinetically stable than the DTPA complexes [219]. These properties could explain the significantly higher specific uptake of the DOTA-bound somatostatin analogue, compared to the DTPA variant, in octreotide receptor-expressing tissues [191]. Therefore, DOTA-A20FMDV2 was designed, purified and studied.

5.3.2.1 DOTA-A20FMDV2 Radiolabelling and Quality Control

DOTA-A20FMDV2 was radiolabelled with indium to generate ^{111}In-DOTA-A20FMDV2. Reverse-phase HPLC was used to analyse the labelling efficiency and to evaluate the structural integrity of the radiolabelled targeting ligand. ^{111}In- DOTA-A20FMDV2 was eluted in a single peak, with a retention time of around 21 minutes (see **Figure 81**). The radiochemical purity of the radiolabelled ^{111}In-DOTA-A20FMDV2 was over 99%, according to this analysis. Furthermore, there was no evidence of fragmentation or aggregation during the labelling process, as indicated by the sharp single peak.

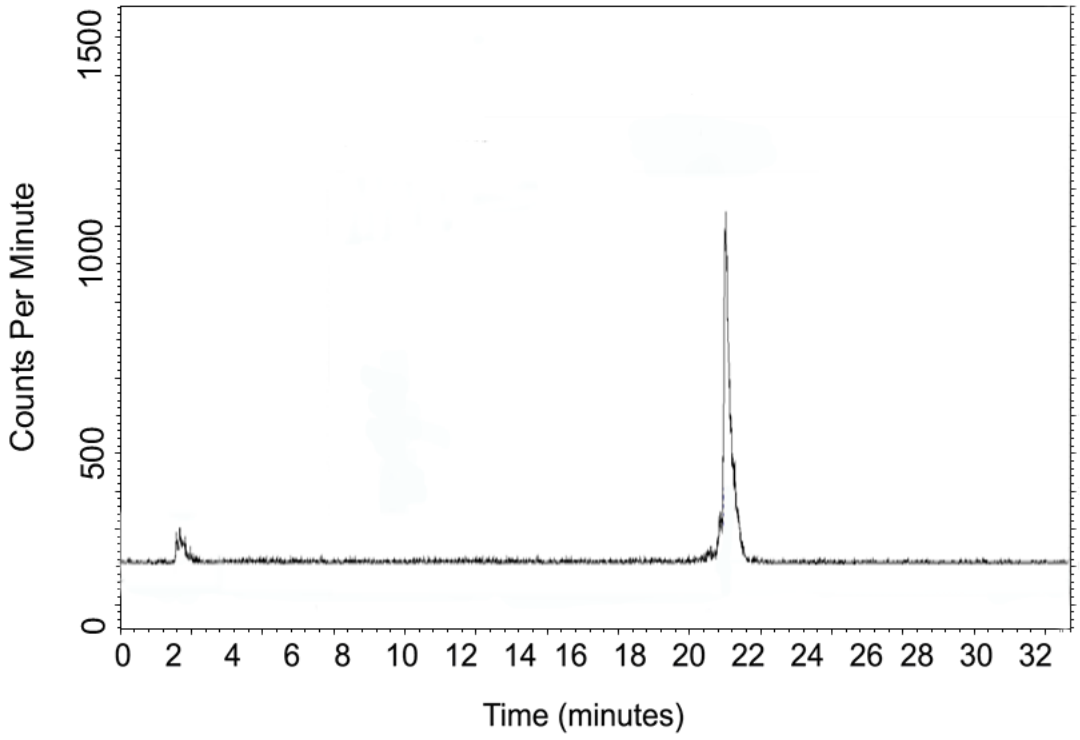

Figure 81 Reverse phase HPLC trace measuring ^{111}In-DOTA-A20FMDV2 radiolabelling efficiency.

5.3.2.2 Biodistribution of ^{111}In- DOTA-A20FMDV2

The previous experience with DTPA-A20FMDV2 suggested that the addition of a chlelating agent and ^{111}In radiolabelling would not adversely affect A20FMDV2's affinity to αvβ6 (see **Sections 4.3 & 4.8**). Therefore, ^{111}In-DOTA-A20FMDV2 was injected intravenously into each 'bi-xenografted' mouse and biodistibution experiments performed, at selected timepoints (described in **Methods**). The associated radioactivity of each organ was quantified and expressed as a percentage of injection dose per unit mass of tissue.

Initially, 1 MBq of ^{111}Indium was radiolabelled onto 4μg of DOTA-A20FMDV2 and peptide uptakes in the xenografts were compared, at pre-selected time points (see

Figure 82). It should be noted that the 4μg mass for injection was derived from the previous peptide mass experiments with DTPA-A20FMDV2 (see **Section 4.9.2.2)**.

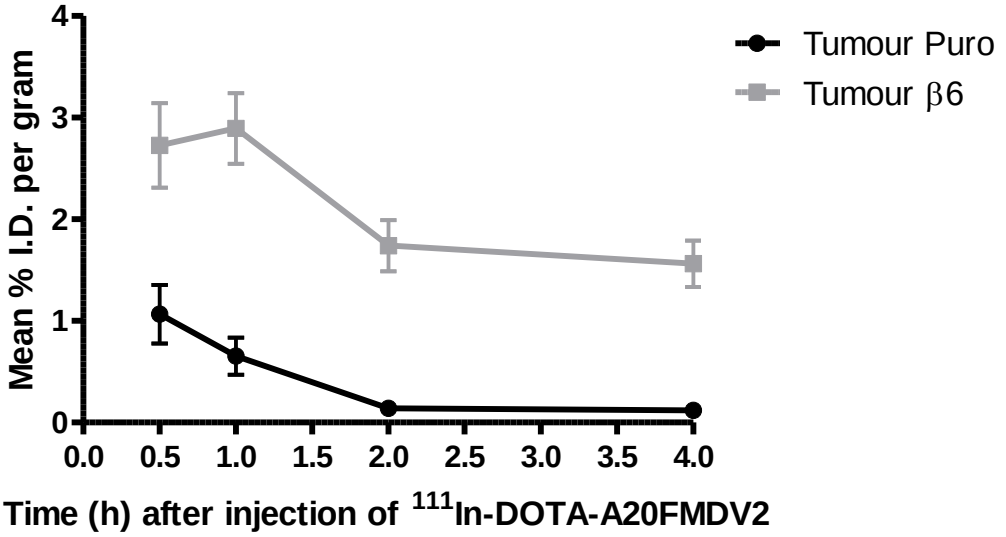

Figure 82 ^{111}In-DOTA-A20FMDV2 (1 MBq / 4μg) injected into groups of tumour-bearing mice. At 0.5, 1, 2 and 4 hours post-injection three mice were killed and tumours removed and the % ID/g tissue determined.

Maximal differential uptake between the A375P β6 and the A375P puro tumours occurred at 2 and 4 hours (post-injection). Unfortunately, the 4h p.i. timepoint was the latest timepoint planned in this experiment, and so it is not known whether a later timepoint would have resulted in a greater differential. However, the combination of properties (maximal differential uptake between the A375P β6 and the A375P puro tumours and high %I.D./g in the A375P β6 tumour) seemed to occur between 1 to 2 hours p.i. (post-injection) timepoints. The ratio of A375P β6 tumour uptake and retention to that of A375P puro was around 4:1 at the 1 h p.i. timepoint; but around 12:1 at the 2 h p.i. timepoint. At 1 hour post-injection, the mean % injected dose per

gram was around 2.89% ± 0.35 for the A375P β6 tumour, compared with 0.65% ± 0.18 for the A375P puro tumour. Therefore, these values were at least on a par with those of ^{111}In-DTPA-A20FMDV2. Although, the 30 minute mean %I.D./g within the A375P β6 tumour was 2.73% ± 0.41 for ^{111}In-DOTA-A20FMDV2 (cf. 5.83% ± 1.63 for ^{111}In-DTPA-A20FMDV2), the pattern of uptake and retention within both xenografts was otherwise not significantly different.

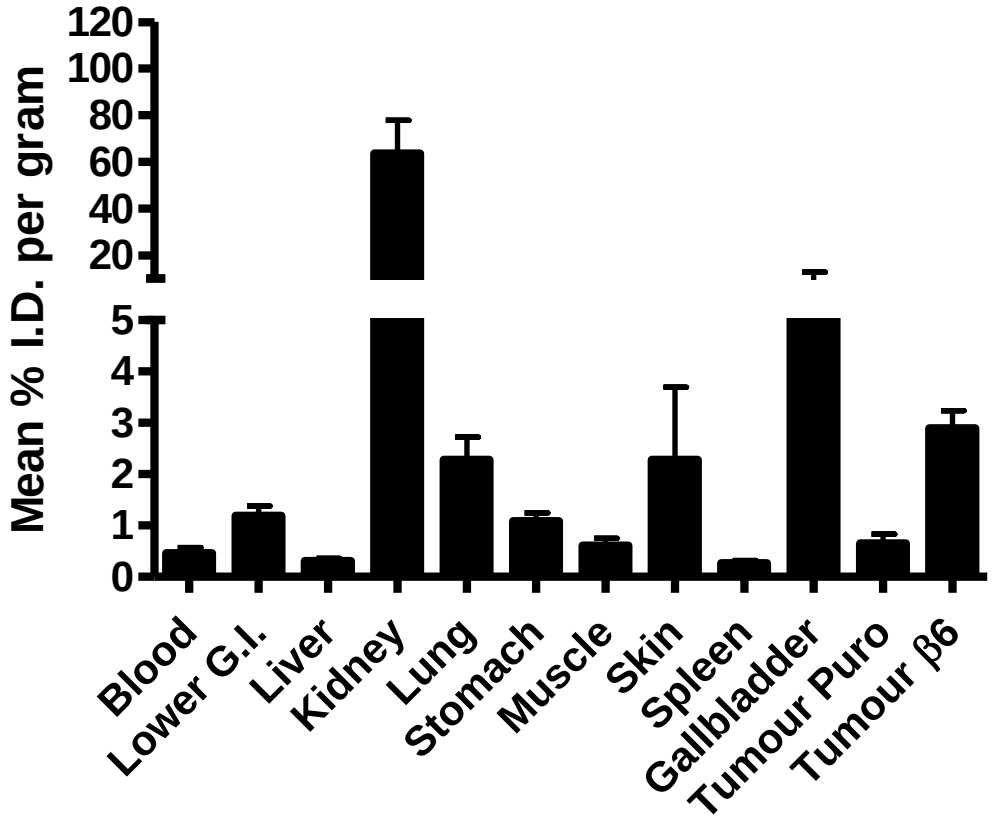

Figure 83 ^{111}In-DOTA-A20FMDV2 tissue biodistribution. ^{111}In-DOTA-A20FMDV2 was injected into tumour bearing mice. After 1 hour animals were killed and tumours and major organs were harvested and the % ID/g tissue determined. Data show that several organs retained significant amounts of radiopeptide.

The biodistribution of ^{111}In-DOTA-A20FMDV2 (see **Figure 83)** reveals that several organs retained significant amounts of radioactivity at 1 hour. The lower GI tract, lungs, stomach, skin and gall bladder, in addition to the A375P β6 tumour, all have retained significantly more radioactivity than either A375P puro tumour or spleen. Therefore, this pattern of biodistribution again is consistent with that of ^{111}In-DTPA-A20FMDV2 (see **Section 4.9.2.4**). That is, ^{111}In-DOTA-A20FMDV2 is also able to recognise and bind to endogenous αvβ6-expressing tissues.

5.3.2.3 DOTA-A20FMDV2ran Radiolabelling and Quality Control

In addition, the scrambled A20FMDV2 DOTA variant, DOTA-A20FMDVran, was radiolabelled with ^{111}In to generate ^{111}In-DOTA-A20FMDVran. Reverse-phase HPLC analysed the labelling efficiency and evaluated the structural integrity of the radiolabelled targeting ligand. ^{111}In- DOTA-A20FMDV2ran was eluted in a single peak, with a retention time of around 20 minutes (see **Figure 84**). The radiochemical purity of the radiolabelled ^{111}In-DOTA-A20FMDV2 was over 99%, according to this analysis. Furthermore, there was no evidence of fragmentation or aggregation during the labelling process, as indicaed by the sharp single peak.

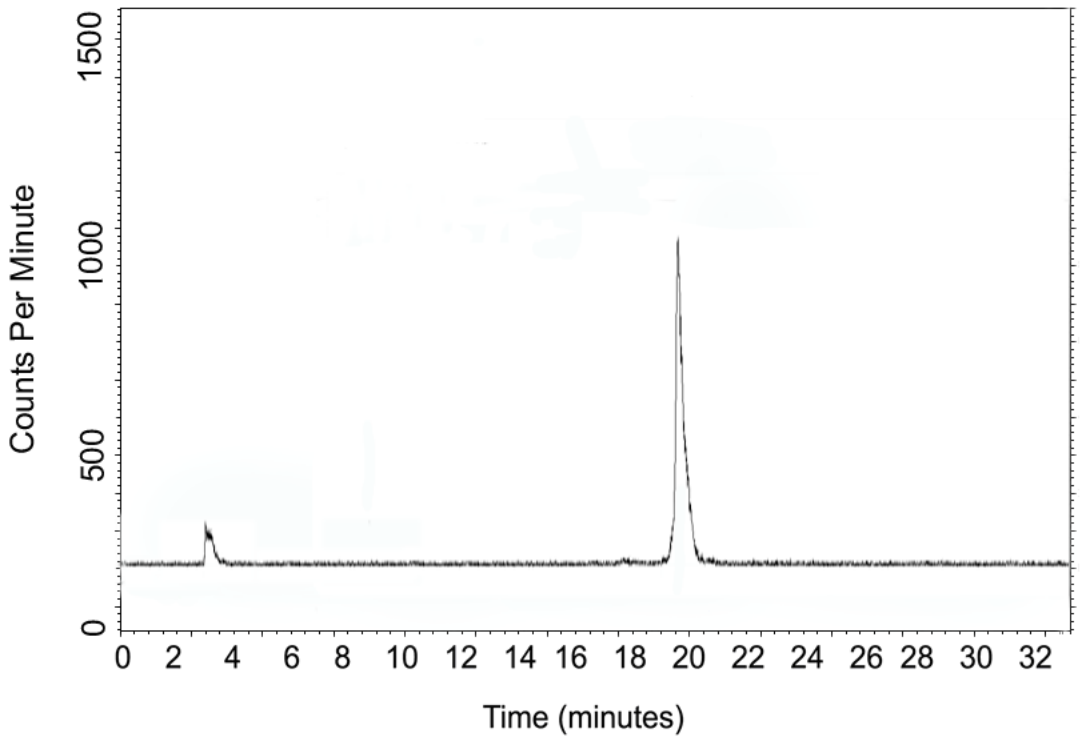

Figure 84 Reverse phase HPLC trace measuring ^{111}In-DOTA-A20FMDV2 radiolabelling efficiency.

5.3.2.4 Biodistribution of ^{111}In- DOTA-A20FMDV2ran

^{111}In-DOTA-A20FMDV2ran (1MBq / 4μg / mouse) was injected into a cohort of bi-xenografted mice. After 1 hour the animals were killed, tumours and major organs were harvested, and the %I.D./g tissue determined. **Figure 85** reveals that there was no significant difference in uptake by the A375P β6 versus the A375P puro (0.10 +/- 0.02% versus 0.2 +/-0.08% ID/g, respectively) tumours. Furthermore, no significant uptake occurred in most of the other tissues (excluding kidney, the site of excretion). Inset displays data for xenografts only, with scale adjusted, confirming the minimal % I.D./g of ^{111}In-DOTA-A20FMDV2ran in these tumours. These data corroborate

that for ^{111}In-DTPA-A20FMDV2ran and reinforces the necessity of the RGD motif for αvβ6 recognition and binding, *in vivo*.

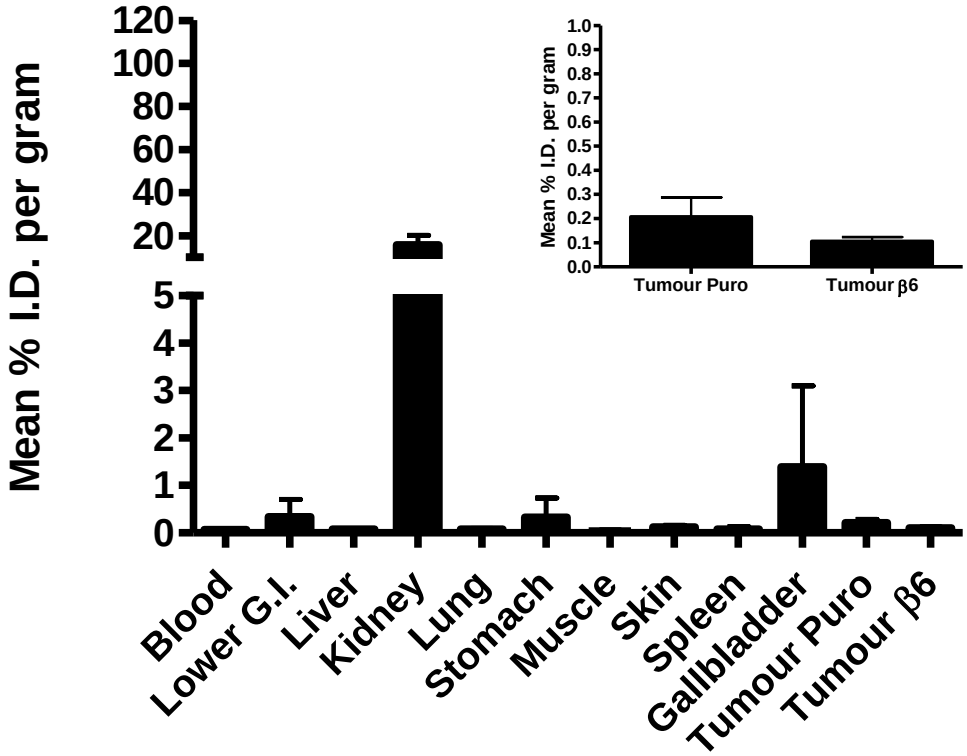

Figure 85 Biodistribution of ^{111}In-DOTA-A20FMDV2ran (scrambled peptide).

5.3.2.5 NanoSPECT/CT Small Animal Imaging

In summary, ^{111}In-DOTA-A20FMDV2 also now has been confirmed to exhibit high affinity and specificity for αvβ6, *in vivo.* However, to determine whether ^{111}In-DOTA-A20FMDV2 (4µg/10-35 MBq per mouse) could be used as a molecular-specific imaging agent, it again was injected intravenously into the 'bi-xenografted' athymic mice. The mice were anaesthetised and imaged at pre-selected time-points, using a high-resolution single photon emission computed tomography small animal imager fitted with a separate, computed tomography scanner (NanoSPECT/CT).

The imaging findings generally were consistent with the biodistribution results and a representative coronal image is shown (see **Figure 86A**). Signals from the A375P β6 tumours consistently were found to be higher than those from the non-β6 expressing control tumours. Images, with a clearly identifiable β6-positive tumour, routinely were obtained as early as 30 min, and as late as 4 hours, post-injection. However, the best images, delineating ideal differentiation between the A375P β6 and the A375P puro tumours and other background tissues, occurred at 1 hour post-injection; correlating with the biodistribution results (see **Section 5.3.2.2**). High signals were observed from the kidneys and bladder, reflecting the primary exretion route. **Figure 86B** also shows a Maximal Intensity Projection (MIP), which displays uptake in the GI tract, corresponding with localisation of endogenous αvβ6 expression. Thus ^{111}In-DOTA-A20FMDV2 now also has been shown to be retained specifically within αvβ6-expressing tissues, using a non-invasive NanoSPECT/CT small animal imager. These findings suggest that the DOTA chelator has not adversely affected A20FMDV2's ability to recognise and bind to αvβ6, *in vivo*.

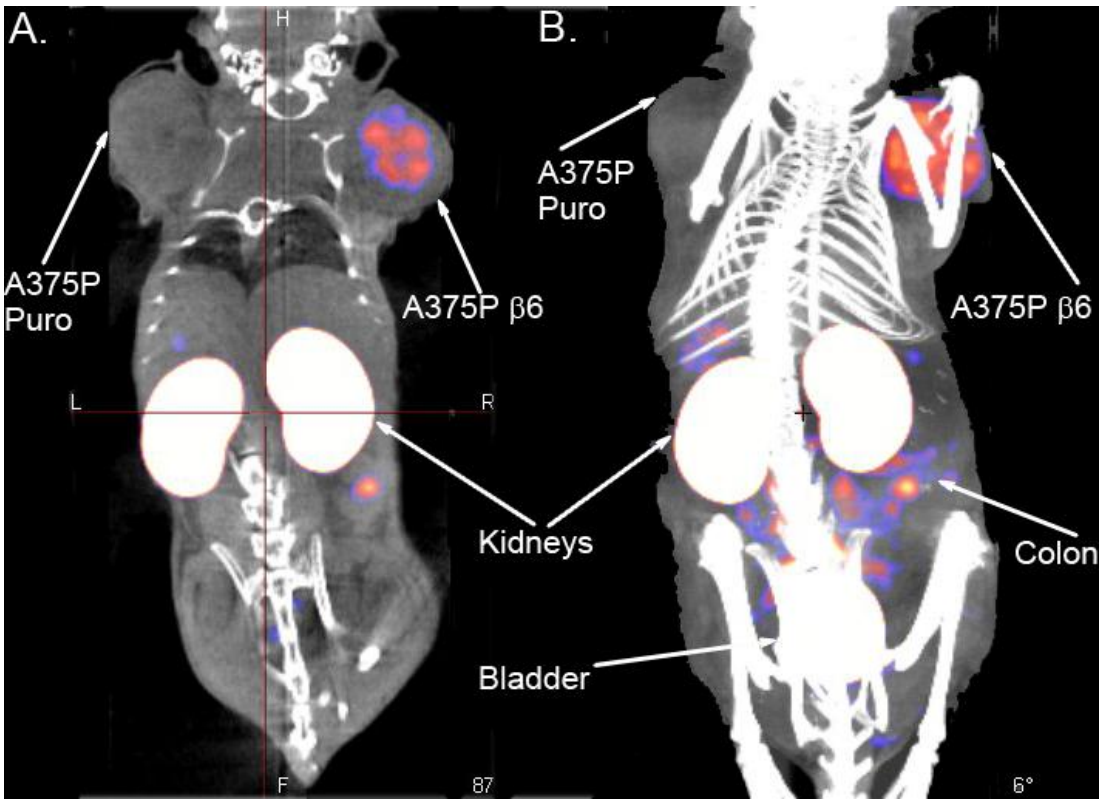

Figure 86 NanoSPECT/CT imaging of αvβ6-expressing tumour with ^{111}In-DOTA-A20FMDV2:

A. Coronal slice showing that the radiopeptide has accumulated selectively in the A375P β6 tumour in discrete areas or 'nodules'. In contrast the A375P puro tumour was negative. The kidneys also are clearly labelled.

B. Maximum Intensity Projection (MIP) of images from same mouse. The A375P β6 tumour labelled strongly with radiopeptide again showing clearly that peptide does not distribute uniformly. In contrast the A375P puro tumour again was negative. The kidneys and bladder were labelled strongly, as is the lower GI tract, in accord with the biodistribution of ^{111}In-DOTA-A20FMDV2 and the results of ^{111}In-DTPA-A20FMDV2.

Chapter VI: Discussion

Integrins are the principal cell surface receptors that enable both normal and transformed cells to attach, and respond, to their extra-cellular environment. Integrins have been shown to mediate cell-to-cell or cell-to-ECM adhesion, traction during cell movement and the promotion of many signalling pathways that regulate diverse processes including proliferation, migration, cell survival, differentiation, tumour invasion and metastasis [12]. Increased expression of αvβ6 has been shown to be important in cell migration, cell proliferation, activation of TGF-β, suppression of anoikis, modulation of protease activity and invasion of carcinoma cells [33, 104, 140-142, 152]. Additionally αvβ6 has been proposed as a marker of malignant transformation in oral epithelial tumours [104] and more recently it has been identified as a prognostic marker for the behaviour of a range of carcinomas. Epidemiological studies of colon, cervical and non-small cell lung cancer all have noted that high expression of αvβ6 correlates with poor prognosis; increasing the hazard of dying by greater than 60% in colon cancer for example [101, 248, 249]. Therefore, identification of this marker *in vivo* could be a valuable aid in the management of cancer patients. Additionally, the integrin αvβ6 appears to fulfil all the criteria necessary to be an ideal targeted imaging agent, in cancer patients. It is expressed on the cell surface, is weak or absent on normal tissues and is associated with cancer progression. The aforementioned associations and attributes led to development of αvβ6-specific targeting agents that function effectively *in vivo*. The primary objective of this project was to develop and characterise radiolabelled agents for targeting αvβ6 and to show that such reagents could localise specifically to

cancer. This would permit selective visualisation of αvβ6 regions within tumours, using gamma cameras combined with conventional imaging techniques. My data describe the development of αvβ6-directed peptide probes *in vitro*; and demonstrates the selective localisation of such probes to αvβ6-positive tumours *in vivo*, for SPECT and PET imaging. Furthermore, I show that αvβ6 receptor localisation by peptide targeting correlates closely with αvβ6 receptor detection by immunohistochemistry.

6.1 The αvβ6 Receptor and Peptide Pharmacology

DiCara et al originally described the characterisation of A20FMDV2, a peptide derived from the VP1 coat-protein of foot-and-mouth-disease virus [229]. DiCara and colleagues reported that αvβ6 is capable of forming high affinity, long-lived complexes with short RGD peptides [229]. The paper described the importance of the RGDLXX(L/I) motif and post-RGD helix in promoting anti-αvβ6 activity. This stable integrin-peptide binding may be a multi-step process and certainly it features cation-dependence. Furthermore, since αvβ3 and αvβ6 share a high degree of homology [250], it has been proposed that, as for αvβ3, the aspartate from the RGD sequence (Asp^9 in A20FMDV2) will bind to the beta subunit of the integrin, via its MIDAS while arginine binds to the alpha subunit's β propeller domain [251].

In order to take advantage of the high resolution and sensitivity of the NanoSPECT/CT small animal imager, it was decided to develop A20FMDV2 into a SPECT targeting agent for αvβ6. Therefore, synthesised biotinylated-A20FMDV2 was conjugated to the chelating agents, DTPA and DOTA, via the N-terminal residue. Flow cytometry, described in **Sections 4.3 & 4.4**, with and without αvβ6-

blocking antibodies, revealed that the addition of DTPA (and chelate formation) had no effect on the specificity or affinity of the peptide compared with A20FMDV2; both exhibiting >1000-fold selectivity for αvβ6 over the other RGD-directed integrins present (α5β1, αvβ3, αvβ5, αvβ8).

Radiolabelling with Indium was not expected to further change the spatial structure of the peptide. However, HPLC analysis allowed formal evaluation of this expectation and the assessment of labelling efficiency. Optimal radiolabelling conditions are required to ensure maximal labelling efficiency. That is, unbound radionuclide (Indium) should be kept to a minimum, with maximal radionuclide attached to the peptide complex. Free radionuclide, when injected into test subjects, has the potential to disseminate throughout the body without necessarily targeting the desired tumour; lowering the target-to-backround ratio and increasing the radiation dose to non-target tissues [252]. Fortunately, the radiolabelling efficiency was greater than 95% for ^{111}In-DTPA-DBD2, ^{111}In-DTPA-A20FMDV2 and ^{111}In-DOTA-A20FMDV2, using HPLC analysis. Furthermore, the HPLC traces for all the probes did not reveal any evidence of fragmentation or aggregation. Therefore, HPLC analyses seemed to indicate that indium radiolabelling did not affect the structural integrity of the probes adversely.

Nevertheless, cell binding assays were required to confirm that the radiolabelling procedure did not affect the targeting-ligand's functional capacity for recognition of αvβ6. Saturation binding assays measure specific radioligand binding, at equilibrium, for various concentrations of the radioligand. The subsequent data

analysis is able to determine receptor number (maximum specific binding, B_{max}) and affinity (equilibrium dissociation constant, K_d). It clearly is desirable for the probe to have a high affinity for the target receptor, since this forms the basis of tumour sensitivity and specificity. The calculated equilibrium dissociation constant (K_d) for ^{111}In-DTPA-A20FMDV2 on A375P β6 cells was 1.73×10^{-9}M. Furthermore, since the difference between 10% and 90% of the specific binding spans a 100-fold concentration range (i.e. two logs), it can be assumed that only one-binding site is involved [253]. This assumption is consistent with the previous competition flow cytometry experiments, which demonstrated that the binding of DTPA-A20FMDV2 to A375P β6 cells was totally αvβ6-dependent. Typical K_d values of useful radioligands range between 10 pM and 10 nM; and thus ^{111}In-DTPA-A20FMDV2 is within this range and has a high affinity for the αvβ6 receptor [253]. In summary, it appears that conjugation of the DTPA chelator and indium radiolabelling of the A20FMDV2 have not significantly influenced its affinity for αvβ6.

The previous experiments on A20FMDV2 studied IC50, rather than K_d, to confirm that the radiolabelling did not affect peptide specificity or efficacy [228]. Hausner and colleagues, using competitive binding ELISA experiments, tested the ability of either A20FMDV2 or ^{19}F-FBA-A20FMDV2, to inhibit binding of biotinylated fibronectin to immobilised, recombinant soluble αvβ6. With this model, the authors reported that both A20FMDV2 and ^{19}F-FBA-A20FMDV2 had IC50 values of 3 ± 1 nmol/L; confirming that the addition of ^{19}F-FBA to A20FMDV2 did not affect its potency [228, 229]. Of note, cyclo-(RGDy(Me)K), an αv-binding peptide, was shown to have an IC50 value of 35 ± 15 nmol/L, using the same system [228]. During the course of this PhD project, other groups also have sought to explore

αvβ6-specific targeting agents, *in vivo*. Hausner and colleagues recently have described the 'PEGylated' A20FMDV2 variants: ^{18}F-FBA-PEG-A20FMDV2, ^{18}F-FBA-PEG$_{28}$-A20FMDV2, ^{18}F-FBA-(PEG$_{28}$)$_2$-A20FMDV2, ^{64}Cu-DOTA-PEG-A20FMDV2 and ^{64}Cu-CB-TE2A-PEG-A20FMDV2 [254, 255]. Using the same competitive ELISA system described above, the PEGylated variants were shown to possess equivalent IC50 values with the parent A20FMDV2 peptide (3 to 6 nmol/L) [254, 255]. Furthemore, a group from Germany described the development of another linear RGD peptide, HBP-1, and its ^{125}I radiolabelling (^{125}I-HBP-1) [256]. An IC50 value for ^{125}I-HBP-1 of 38.9 nM was calculated, using an αvβ6-expressing head and neck squamous cell carcinoma line (HNO97) and increasing concentrations of unlabelled HBP-1 (competitor) [256]. However, since different systems were used for IC50 calculations, of ^{125}I-HBP-1 and ^{19}F-FBA-A20FMDV2, it is not possible to compare these values directly. Ideally, the different peptides (and their variants) should all be tested on the same experimental system to compare the affinity of each compound to αvβ6 fairly.

In addition to high receptor affinity, probe internalisation is a valuable property; allowing the radioligand to accumulate within the tumour cell before it can dissociate and increasing the tumour-to-background ratio. The internalisation experiments measured the net amount of probe specifically 'trafficked' to the interior of the cell, at various incubation times and at body temperature (37^{o}C). These experiments revealed relatively rapid internalisation of ^{111}In-DTPA-A20FMDV2 into A375P β6 cells, reaching a plateau after about one hour. This quantification was consistent with the peptide's spatial distribution, detecting DTPA-A20FMDV2 via its biotin tag and

using confocal microscopy. The absence of significant radioligand internalisation, by A375P puro cells, suggested that the cellular internalisation of ^{111}In-DTPA-A20FMDV2 was αvβ6-dependent.

Elayadi et al recently described another 20-mer RGD peptide, TP H2009.1, which targets αvβ6 [248]. This peptide subsequently was synthesised on a trilysine core and conjugated to a streptavidin-coated, fluorescent quantum dot (SAQdot605). Elayadi demonstrated, with the aid of fluorescence microscopy, that SAQdot605 association with αvβ6-expressing (H2009) cells was mediated via the RGD peptide [248]. Furthermore, the authors also suggested that the mechanism of peptide-Qdot internalisation was via αvβ6-mediated endocytosis [248]. However, these experiments suggesting internalisation were analysed with 2-D microscopy only, without quantification and at one peptide incubation timepoint (10 minutes) [248]. Nonetheless, this timeframe for TP H2009.1 internalisation into H2009 cells appears to be quicker in comparison to that for A20FMDV2 into A375P β6 cells (see **Figure 56**). The same group later published on a tetrameric, but truncated, H2009.1 peptide [257]. This tetramer was conjugated with fluorochrome (Alexa Fluor 488 or SAQdot605), incubated for 10 minutes with H2009 cells and analysed with confocal microscopy using a Z-stacking protocol [257]. The Z-stacked series confirmed the cellular internalisation of the tetramer, co-localisation of the tetramer with αvβ6, but still lacked quantification and later timepoints [257].

Nothelfer and colleagues also performed internalisation experiments with ^{125}I-HBP-1 and HNO97 cells [256]. This group's internalisation assays were more similar to those described with A20FMDV2. Quantitative studies were undertaken at several timepoints, and internalisation expressed as a percentage of the applied dose per 10^6

cells. However, glycine buffer acid washes (50 mM glycine, 100 mM NaCl, pH 2.8) were chosen to remove the membrane-bound radioligand fraction. No mention of acid wash exposure time to the HNO97 cells was reported, nor is any reference made to any optimisation procedures performed prior to the cell internalisation assay. The absence of these optimisation procedures casts doubt on the effectiveness of glycine to remove the membrane-bound radioligand fraction, in their cell model. **Table 11** (page 180) revealed that the glycine acid wash buffer was the least effective reagent, at removing membrane-bound ^{111}In-DTPA-A20FMDV2, from the A375P β6 cell model. Indeed, the A375P β6 could not be exposed to longer than 5 minutes of glycine acid wash; longer exposure resulted in significant numbers of cells which underwent permeabilisation and death, with consequent release of the internalised radioligand. These factors have an enormous bearing on the accuracy of internalisation calulations. Taking this into account, Nothelfer reported fast internalisation into HNO97 cells, with values of 78.6%, 60.5%, and 46.3% of total bound peptide after 10, 60 and 120 min, respectively [256]. This compares to values of approximately 38%, 90% and 90% after 5, 60 and 120 min, respectively (^{111}In-DTPA-A20FMDV2 into A375P β6 cells). Although different cell lines were used, it seems that the rate and pattern of internalisation are different. Nothelfer and colleagues suggested that the decrease in intracellular radioactivity was as a consequence of cytosolic peptide degradation [256]. This phenomenon did not seem to happen with ^{111}In-DTPA-A20FMDV2, which had a slower initial internalisation rate, but achieved higher internalisation levels at later timepoints. However, the aforementioned lack of optimisation procedures with the ^{125}I-HBP-1 system may make direct comparisons impossible.

Hausner et al also studied internalisation in the PEGylated A20FMDV2 variants, within the DX3 puro β6 and BxPC-3 cell lines [255]. This DX3 melanoma cell model has similarities to the A375P model, but Hausner chose an acetate acid buffer (0.2 mol/L sodium acetate, 0.5 mol/L sodium chloride, pH 2.5) to release surface-bound activity [255]. Again, no optimisation procedures seemed to be carried out to determine the appropriateness of the acetate acid buffer wash; the referenced paper justifying this choice of acid buffer wash actually examined a different cell and receptor model [258]. Furthermore, only the 1 hour incubation time point was studied. Hausner reported that approximately two-thirds of the bound radioactivity was internalised, in αvβ6-expressing cell lines, for the two PEGylated A20FMDV2 variants; whereas less than half of the bound ^{18}F-FBA-A20FMDV2 was internalised [255]. The value for the 1 hour internalisation of ^{18}F-FBA-A20FMDV2 is lower than that found for ^{111}In-DTPA-A20FMDV2. However, the absence of other timepoints, the differing cell systems and the lack of optimisation procedures all inhibit direct comparisons. However, Hausner's findings suggest that internalisation experiments with PEGylated ^{111}In-DTPA-A20FMDV2 variants are warranted.

To sum up, the current evidence indicates that the aforementioned RGD peptides are being internalised, through association with αvβ6, and by a variety of cancer cells. As yet, the precise mechanism of internalisation is not clear. However, since FMDV infects cultured cells via its highly conserved RGD motif (located on GH loop of the viral surface protein VP1) [259], mechanisms of internalisation may be similar. It is known that FMDV, utilising the αv integrins as receptors, enters the cell via a clathrin-mediated endocytic pathway, trafficking throughout the acidified endocytic vesicles, where its capsid rapidly dissociates with resultant release of the RNA

genome [124, 260]. In addition, Ramsay et al have shown that αvβ6 endocytosis is clathrin-mediated and this process is important for carcinoma cell motility and invasion [261]. Therefore, it is highly plausible that the RGD peptides are internalised, by cancer cells, through a clathrin-dependent pathway. However, formal experiments, which may use specific inhibitors of clathrin-mediated endocytosis, would need to be performed to prove this hypothesis.

Plasma stability assays simulate *in vivo* protease exposure and thus are necessary to provide an indication of probable probe degradation in recipient animals. It is clearly undesirable for the probe to degrade prior to reaching its target tumour. Furthermore, if degradation results in release of free radionuclide or even radionuclide attached to peptide fragment, the radionuclide complex may be directed away from its original target. These factors may contribute to decreased target-to-background signal and increased radiation exposure to non-target organs. A PBS (at physiological pH 7.2) control incubation was performed simulataneously with the plasma incubation. Although the PBS incubation occurred at 37^{o}C, ^{111}In-DTPA-A20FMDV2 showed high stability with minimal loss of purity after 24 hours; indicating an adequate level of radiolytic resistance. In addition, since the storage and transport of radiopharmaceuticals at 4^{o}C is possible, this lower energy state may further reduce the kinetics of degradation. Therefore, it seems that ^{111}In-DTPA-A20FMDV2 does not demand extreme storage and transport conditions in order to maintain probe stability. Nevertheless, as expected for a linear peptide, there was decreased ^{111}In-DTPA-A20FMDV2 stability in plasma. This clearly has an impact on optimal imaging times and non-target radiation exposure. Nonetheless, the *in vitro* stability

of ^{111}In-DTPA-A20FMDV2 compares favourably to the ^{125}I-HBP-1 peptide. Nothelfer and colleagues reported that the half-life of ^{125}I-HBP-1 was 55 minutes (human plasma) [262], and this contrasts with the calculated half-life of ^{111}In-DTPA-A20FMDV2 at 210 minutes (athymic mouse plasma). Therefore the improved plasma stability of ^{111}In-DTPA-A20FMDV2 enables a larger timeframe in which to acquire images of the putative target confidently. However, it should be noted that Nothelfer et al have stated that the TP H2009.1 and A20FMDV2 peptides have human plasma half-lives of 14.5 and 42 minutes, respectively [256]. It seems that Nothelfer and colleagues synthesised TP H2009.1 and A20FMDV2, as well as their ^{125}I-HBP-1 peptide. Although Nothelfer used human plasma and the experiments performed in this thesis used athymic mouse plasma, the exact details of Nothelfer's comparative plasma stability studies were not documented [256], casting doubt on the reported half-lives and perhaps explaining the discrepancy (210 vs. 42 minutes) in the stability results.

Cyclisation also has been mentioned previously as a technique to improve peptide stability (see **Table 6**, page 105). However, cyclisation unexpectedly resulted in a reduction of specificity to αvβ6. Flow cytometric experiments revealed binding of both DBD1 and DBD2, at higher peptide concentrations, to the A375P puro line. Currently, it is not known whether the higher concentrations imparted greater non-specific binding, or whether cyclisation even led to increased binding of the other RGD integrins (α5β1, αvβ3, αvβ5, and αvβ8). However, once the appropriate materials are available, my successor intends to test the binding affinity to the aforementioned individual integrins. Nonetheless, the reduced specificity phenomenon mainly was a characteristic of the DBD1 peptide. DBD2 still had

relatively good affinity and specificity for αvβ6, and so *in vivo* experiments proceeded with this compound. The DTPA chelating agent was conjugated to DBD2 and this facilitated indium radiolabelling (^{111}In-DTPA-DBD2). The plasma half-life of ^{111}In-DTPA-DBD2 was calculated to be 495 minutes (*in vitro*, athymic mouse plasma); thus it was superior to that of ^{111}In-DTPA-A20FMDV2. However, the %I.D./g of ^{111}In-DTPA-DBD2 in the A375P β6 tumour did not seem as high as for the linear peptide. There are many potential reasons for this reduced tumour uptake and retention. However, it should be noted that the net charge is the same (positive and so basic) for A20FMDV2 and DBD2. Therefore, since the plasma stability is superior for DBD2, it might be peptide delivery, internalisation or retention which could be affected adversely by its cyclic structure. It is possible that cyclic conformation might hinder penetration of tumour vasculature, limiting delivery of the radioligand to the tumour. Alternatively, the cyclic structure may inhibit ^{111}In-DTPA-DBD2's internalisation by tumour cells; thereby affecting the retention of the radioligand within the cancer mass. Furthermore, ^{111}In-DTPA-DBD2 seemed to have greater and more persistent retention in background tissues (including non-αvβ6 expressing tumours), when compared with the linear peptides. This finding, ultimately, led to lower target-to-background ratios and thus this was considered to limit its efficiency as an imaging agent. It already has been mentioned that linear peptides tend to be degraded / metabolised *in vivo*, allowing their rapid clearance from blood and other non-target tissues. Peptide cyclisation potentially would delay degradation and thus the chances of non-specific localisation could increase. This clearly is not desirable in terms of non-target (normal) tissue radiation exposure, as well as for imaging efficiency. Therefore, a fine balance seems to exist between too

little stability (decreased target delivery) and too much stability (increased background exposure). Similar problems with high background tissue exposure have been described with the larger multimers of H2009.1 [257]:

Probe multimerisation has the potential to improve target-to-background ratios. Multivalent Foot-and-Mouth-Disease-Virus capsids have been shown to stimulate endocytosis of the integrin and that the integrin serves to deliver the virus into the early and recycling endosomes [124]. This virus-induced uptake of αvβ6 seems to have resulted from cross-linking of the integrin by the multivalent ligand and not merely from integrin ligation alone [124]. Therefore, multimerisation may trigger neoplastic cell internalisation as well as permitting a greater chance of receptor-ligand interaction. That is, the possibility of multiple αvβ6 receptors binding to a probe (avidity) may alter integrin-peptide interactions to prolong 'receptor-on' kinetics favourably or even trigger cell internalisation. Consequently, Li and colleagues analysed the plasma stability (*in vitro* and rat plasma) of ^{111}In-DOTA labelled, tetrameric H2009.1 peptide variants, but only at two timepoints [257]. The tetrameric H2009.1 peptide variants were approximately 75% and 65% intact, after 1h and 4h plasma incubation, respectively [257]. The same group also examined the stability of a monomeric, PEGylated H2009.1 peptide, finding 60% and 46% intactness at 1h and 4h timepoints, respectively [257]. The corresponding 1h and 4h values for: ^{111}In-DTPA-A20FMDV2 were 78% and 45%, respectively; ^{111}In-DTPA-DBD2 were 89% and 64%, respectively. Firstly, it is noted that the plasma stability of ^{111}In-DTPA-A20FMDV2 seems initially superior to its ^{111}In-DOTA labelled, PEGylated H2009.1 counterpart. Furthermore, cyclic DBD2 also seems, initially, to have superior plasma stability in comparison to the tetrameric H2009.1 peptide

variants. However, the different species used to donate plasma does hinder direct comparison. The tetrameric H2009.1 peptide variants subsequently were tested using biodistribution experiments, in αvβ6-expressing, tumour-bearing, severe-combined-immunodeficiency mice [257]. At 1 hour p.i., the %I.D./g in the tumour was 3.15 ± 0.47, but tumour-to-blood ratio was only 1.37 ± 0.14; at 4 hours p.i., the tumour demonstrated 2.25 ± 0.47 %I.D./g, with a tumor-to-blood ratio which was 2.43 ± 0.14 [257]. Although the %I.D./g within the tumour was good, it was at the expense of very high uptake and retention within background tissues; limiting the value of this agent to discern cancers from other tissues in imaging experiments. Therefore, for *in vivo* target delivery and imaging, there does seem to be a fine balance between affinity, stability, non-specific uptake and clearance [257]. However, Li and colleagues only published the biodistribution results of the tetrameric H2009.1 peptide variants [257]. A comparision with the monomeric, PEGylated H2009.1 peptide was not documented; thus, without this study, the increased uptake and retention within background tissues cannot totally be ascribed to tetramerisation. Therefore, the reduced specificity phenomenon of DBD2 (found in the flow cytometry experiments) and the potential binding to other RGD integrins predominantly may explain the retention in non-αvβ6 expressing tissues.

6.1.1 Limitations of Peptide Pharmacology Experiments

In contrast to the other flow cytometry studies, the competition assays in mouse keratinocytes utilised a buffer system in which Mn^{2+} was the only bivalent metal present. Mouse keratinocytes terminally differentiate in the presence of high calcium

concentrations [239]. Therefore, for practical reasons, calcium-containing buffers had to be substituted with Mn^{2+}-TBS buffer, in flow cytometry experiments. This buffer system is less physiological than the Mg^{2+}/Ca^{2+}-containing buffers, but still promotes an 'activated' integrin conformation with high ligand affinity [17].

The HPLC setup is important for the recognition of radiolabelled products. An acetonitrile and 0.1% aqueous TFA system was used as the standard approach for radiopeptide analysis. This system eluted radiolabelled products at approximately 20 minutes. Previously, an ethanol and 0.1% aqueous TFA system was tested for ^{111}In-DTPA-A20FMDV2 analysis (data not shown). Unfortunately, this alternative resulted in the elution of the probe at 40 minutes; thus the extra 20 minute analysis time would delay the commencement of *in vivo* experiments, performed later in the day. In certain situtations, Ion Pair Chromatography can be employed for greater separation of ionic or polar compounds. This technique uses an 'ion pair reagent' (e.g. alkylsulphonate), which modulates the retention of ionic species [263]. However, since ^{111}In-DTPA-DBD2, ^{111}In-DTPA-A20FMDV2 and ^{111}In-DOTA-A20FMDV2 were eluted as single peaks on the RP-HPLC, no further development of the RP-HPLC system was necessary.

Although, the RP-HPLC demonstrated structural integrity of ^{111}In-DTPA-A20FMDV2 and the cell binding assays demonstrated good affinity of ^{111}In-DTPA-A20FMDV2 for A375P β6 cells, indium radiolabelling still may have had an effect on the targeting ligand's selectivity for αvβ6. Ideally, competition and internalisation experiments, using αvβ6-blocking antibodies (similar to flow cytomery), would be performed with ^{111}In-DTPA-A20FMDV2. However, the availability of the αvβ6-blocking antibodies was limited and thus prohibited this experimental design.

Nevertheless, the internalisation experiments were performed on A375P puro cells, which demonstrated negliglible internalisation of the ^{111}In-DTPA-A20FMDV2 in cells without αvβ6 expression; suggesting maintenance of specificity for αvβ6.

Pre-collected plasma and a 37^{o}C incubation attempted to simulate the blood environment, with regards to protease exposure, likely to be encountered *in vivo.* However, an alternative method may be to inject the radiolabelled peptide into a murine subject and collect plasma samples, at various timepoints. This alternative method would be more representative of the probe's exposure to *in vivo* conditions, and would additionally factor in the clearance rate of the peptide within an animal. However, repeated blood sampling from a mouse is not always practical, and this difficulty may cause problems in subsequent calculations, while the situation with regard to ethics and Home Office regulations tend to militate against such a study. In addition, the resultant peptide fragments after exposure to plasma were not fully characterised. For example, mass spectrometry could help elucidate the sequence of the resultant peptide fragments and thereby determine the sites of enzymatic vulnerability. This information would not only confirm the intactness of the RGD binding site (validating the proposed mechanism of peptide attachement), but would also help with subsequent peptide re-designs to strengthen against plasma degradation. However, practical considerations, such as timing and the introduction of radioactive and biological material into a controlled equipment resource, prevented this experiment.

6.2 Tumour Xenograft Model in Mice

Biodistribution experiments quantify the amount of radioactivity within tissues, after the administration of a radioligand to an animal; it is the standard technique for the study of a probe's organ dissemination and its pharmacokinetics. The initial biodistribution results demonstrated that ^{111}In-DTPA-A20FMDV2 selectively localises to αvβ6-expressing tumours, *in vivo*. In order to maximise the tumour to background ratios, the optimal time for imaging, the optimal peptide mass for injection and the optimal strain of mouse all were investigated. These experiments suggested that imaging / biodistribution optimally should occur 1 hour after injection of 2-4 μg of ^{111}In-DTPA-A20FMDV2. Using these parameters, it was established that A375P β6 tumours retained up to 9-fold more ^{111}In-DTPA-A20FMDV2 than the αvβ6-negative control tumour on the opposite shoulder. Over multiple experiments, these optimal conditions resulted in the retention of ^{111}In-DTPA-A20FMDV2 by A375P β6 xenografts consistently at around 2 – 4 %I.D./g; significantly higher (**$p < 0.0001$**, n=15, using Wilcoxon matched-pairs signed rank test) than the uptake and retention seen in the A375P puro xenografts. Tumour-to-background ratios were also favourable, with αvβ6-expressing tumours showing a tumour-to-muscle ratio of around 7:1, for the same parameters. Low levels of ^{111}In-DTPA-A20FMDV2 retention were found in the blood, such that these were negligible at 4 hours p.i.; suggesting minimal plasma protein association with either free radionuclide, probe or probe fragment. These promising results do not seem to be mouse strain-specific, since similar ratios were obtained using Balb-C and CD1 nude mice. In addition, ^{111}In-DTPA-A20FMDV2 was retained in tissues at 4 hours p.i., and so it is likely that some of this retention was due to αvβ6's ability to internalise ^{111}In-DTPA-

A20FMDV2; protecting the probe from plasma degradation and dissociation from the membrane. Hausner et al showed that radiolabelling A20FMDV2 with fluorine-18 permitted non-invasive imaging of αvβ6-positive versus –negative paired tumours [228]. Although these initial studies promisingly showed that injected ^{18}F-A20FMDV2 could discriminate between the two tumours, tumour retention of radioactivity was relatively low (0.66% ID/g at 1 hour post-injection). Furthermore, the αvβ6-positive tumour-to blood and tumour-to-muscle ratios, at 1 hour p.i., were just 2.4:1 and 1.2:1, respectively [228]. Translation of imaging into humans ideally requires improved tumour to background ratios. In this thesis, the systematic enhancement of the specific uptake and retention of ^{111}In-DTPA-A20FMDV2 has been described; routinely showing a threefold increase in the original target to background ratio, reported with ^{18}F-A20FMDV2 [228].

Hausner and colleagues later performed biodistribution experiments, using αvβ6-positive versus –negative paired DX3 tumours and PEGylated A20FMDV2 variants [255]. Unfortunately, the uptake of the PEGylated radiotracers in the target tissue (at 1 hour p.i.) was slightly below the level previously seen for the non-PEGylated ^{18}F-FBA-A20FMDV [255]. However, the introduction of the PEG unit(s) seemed to permit higher tumour retention of radioactivity, at the 2 and 4 hour time points, enabling greater target-to-background ratios at these later post-injection times [255]. These findings have proposed the synthesis of PEGylated ^{111}In-DTPA-A20FMDV2 variants and biodistribution experiments currently are being explored. Nevertheless, the higher renal retention seen with PEGylated ^{18}F-FBA-A20FMDV variants [255] is of concern and may limit the utility of the PEGylated ^{111}In-DTPA-A20FMDV2 model.

The optimal peptide mass established for ^{111}In-DTPA-A20FMDV2 was extrapolated to ^{111}In-DOTA-A20FMDV2 and ^{111}In-DTPA-DBD2 biodistribution experiments, resulting in similar retention within the αvβ6-expressing tumour.

However, it should be noted that there are other possible explanations for the selective uptake in αvβ6-expressing tissues and these include:-

1. αvβ6-specific and dependent binding
2. Specific binding to a different (unknown) receptor to αvβ6
3. Differences in vascularity, or vascular permeability, of the two tumours implanted in recipient animals.

Clearly the first option is the desired scenario, fulfilling the objective of this project and thus providing evidence for the development of a selective, targeted, imaging probe.

However, the second explanation also remains a possible alternative, though it is less likely given the correlation of the murine αvβ6 expression pattern found using immunohistochemistry with results of the biodistribution analysis (**see below**). Furthermore, the A375P cell lines seem to differ only in αvβ6 expression, and not in any other RGD binding integrin. Nevertheless, at this time, the presence of a different co-existent receptor cannot be ruled out formally – see limitations, below.

The immunohistochemistry pattern, and its consistency, also makes the third explanation for enhanced delivery less likely. Nevertheless, to demonstrate whether the two xenografts have no significant differences in vascular supply, endothelial staining in representative tumour sections could be performed and the results compared. Comparable numbers of blood vessels in tumours originating from both

lines would provide formal evidence that there was no difference in evoked angiogenesis, between αvβ6 non-expressing and αvβ6-expressing growths (as inferred by the comparable growth rates of the two lines). Additionally, real-time tracking of the radiolabelled peptide by the SPECT/CT could demonstrate that there is an equal chance of the peptide reaching both tumour destinations. However, the co-injection method was chosen to elucidate the mechanism of tissue peptide retention. The intravenous injection of 'excessive' *unlabelled* (cold) DTPA-A20FMDV2 a few minutes prior to radiolabelled peptide was fundamental to answering this question. In a targeted event, the cold peptide would be expected to bind to the integrin receptor and to inhibit the radiolabelled peptide competitively, thereby reducing tumour uptake and, therefore, subsequent levels of gamma ray signals. However, if there were no decrease in tumour uptake, peptide retention would be less likely to be due to a saturable receptor-ligand phenomenon; implying that simple pooling or non-specific peptide excretion may be alternative explanations for peptide residency within tissue. The results of the co-injection of a 100-fold excess of 'cold' DTPA-A20FMDV2 revealed suppression of uptake in A375P β6 tumours, and other αvβ6-positive tissues (see **Figure 62**); thus confirming that the uptake of ^{111}In-DTPA-A20FMDV2 was receptor-mediated, rather than via a peptide-dependent increase in vasodilatation and vessel permeability. This type of *in vivo* mechanistic result has not been shown previously for any αvβ6-specific agent, or indeed for many other integrin-targeting peptides.

6.2.1 Limitations of the Tumour Xenograft Model in Mice

It should be noted that Hausner's study used ^{18}F-A20FMDV2 and the human melanoma cell line, DX3, expressing puromycin-resistance alone (DX3puro) or, αvβ6 as well as puromycin resistance (DX3β6) [228, 264]; whereas in this project a similar model, based on the A375P human melanoma cell line, for optimisation of ^{111}In-DTPA-A20FMDV2 was used: the two, related lines being A375P β6 and A375P puro. Characterised recently for their patterns of integrin expression [235], the A375P cell lines have identical levels of four RGD-directed integrins, α5β1, αvβ3, αvβ5 and αvβ8, and differ only in that αvβ6 is expressed exclusively by A375P β6. Nevertheless, there may be other subtle differences between DX3 and A375P melanoma cell lines (e.g. differing levels of pathological angiogenesis; unequal expression levels of the target receptor; or incongruent levels of necrosis within each tumour model), which may hinder direct comparisons. Furthermore, it is for these reasons that the biodistribution results of ^{111}In-DTPA-A20FMDV2 cannot be directly compared to those for ^{125}I-HBP-1 and indium-labelled H2009.1 peptide variants. The differing tumour and mouse models, used for each RGD peptide, introduce too many variables. Ideally, the different peptides (and their variants) should all be tested on the same experimental model to compare fairly the uptake and retention of each compound in an αvβ6-expressing tumour, *in vivo*.

The presence of a different (unknown) receptor being responsible for targeted tissue retention of ^{111}In-DTPA-A20FMDV2 also cannot be ruled out at this time (see **Section 6.2**). Ideally, to prove the tissue retention mechanism is an αvβ6-dependent

system, co-injection with ^{111}In-DTPA-A20FMDV2 should occur with a different known αvβ6-specific agent. Previously, 68G6 [231] antibody was used for *in vitro* blocking experiments in order to test for potential αvβ6-dependent mechanisms (see **Sections 4.4 & 4.5**). However, it is not known whether this antibody effectively blocks αvβ6 *in vivo.* Indeed, at present, there is no universally accepted reagent which is known to block αvβ6 *in vivo*; thus creating a barrier to the proposed experiment.

Ideally, separate optimisation experiments should have been performed with ^{111}In-DOTA-A20FMDV2 and ^{111}In-DTPA-DBD2, rather than a simple extrapolation from the results of ^{111}In-DTPA-A20FMDV2. However, owing to the constraints of resources and the similar single RGD binding site of each peptide variant, it was decided only to study tissue dissemination and their variation over time (i.e. not to vary peptide mass or strain for the DOTA or cyclic variants).

The targeting of αvβ6, by ^{111}In-DTPA-A20FMDV2, was validated in the endogenously αvβ6-expressing breast cancer lines, CA1a and DCIS.com (cf. A375P - genetically-engineered) and described in **Section 5.1**. However, the subcutaneous xenograft model may not always be representative of the genetics and histology of the corresponding cancer found within humans [265-267]. Firstly, xenografts have to grow in an immunodeficient mouse and metastasis is not always evident [267]. Furthermore, although human cancer cells lines tend to be used for xenografting, these cells have been passaged and maintained on a plastic plate for many years. Selection pressures, under these artifical culture conditions, mean that the passaged lines often are not representative of the original tumour and its native state. For example, cells in culture lack the complex cellular networks found *in vivo*. Growth

and communication with inflammatory cells, vasculature, and other stromal components all are absent within culture conditions [266]. On the other hand, transgenic mouse models usually arise in immunocompetent animals, and the tumours develop spontaneously *in situ*, within the appropriate tissue compartment. Furthermore, the stages of tumour progression can be studied over time with the opportunity to investigate a cancer, at early timepoints. Nonetheless, there are several disadvantages with the transgenic model [267]. These include the relatively long length of time required to develop neoplasia and the unpredictable nature of tumour development, with regards to frequency and latency of tumour formation [266]. This heterogeneity can lead to the requirement of greater mouse numbers and study costs. Therefore, both human tumour xenograft and transgenic mouse models have advantages and disadvantages in the study of cancer development and treatment [265]. Ideally, transgenic mouse models, such as those described for colon cancer (see **Section 5.2**), also would be used to validate the targeting of αvβ6, by ^{111}In-DTPA-A20FMDV2. Unfortunately, the projected schedule for proposed collaborative experiments was beyond the time limits of my training degree and such studies will be undertaken by my successors

6.3 Immunohistochemical Correlation with Flow Cytometry and Biodistribution

A systematic analysis of murine tissues was performed, which has not been reported previously in the literature. Xenografts of the two A375P cell lines were examined for expression of αvβ6 and it was confirmed that A375P puro tumours lacked any αvβ6, whilst A375Pβ6 expressed αvβ6 at high levels (+7 score) uniformly throughout tumours (**Figures 49 & 50**). Furthermore, **Table 10** (page 174) documents that while most tissues examined do not express αvβ6, several murine tissues express significant amounts of αvβ6, particularly the stomach and the lower gastrointestinal tract. Such data suggest that the reagent-attracting capacity of these αvβ6-positive organs should be taken into consideration whilst using mouse models for developing αvβ6-specific targeting. This possibility was supported further by the previous flow cytometry experiments, which showed that A20FMDV2 specifically binds to mouse keratinocytes through murine αvβ6 (**Figure 40**). Confirmation of this hypothesis was achieved when it was shown that ^{111}In-DTPA-A20FMDV2 was retained significantly in the lower gastrointestinal (GI) tract, lung, stomach, skin and gall bladder, as well as the A375Pβ6 tumours; which all have more radioactivity than either A375P puro tumour or skeletal muscle. Subsequent co-injection studies using a 100-fold excess of 'cold' DTPA-A20FMDV2 (**Figure 62**), indicated that the uptake of ^{111}In-DTPA-A20FMDV2 was receptor-mediated in the peptide-retaining tissues, rather than via a peptide-dependent increase in vasodilatation and vessel permeability. As a result, with the exception of the kidneys and lungs, since these tissues all endogenously express αvβ6**,** it suggests that ^{111}In-DTPA-A20FMDV2

recognises and binds to endogenous αvβ6 receptors on these tissues. Furthermore, the inability of a random peptide, ^{111}In-DTPA-A20FMDV2ran, to be retained differentially further supported the premise that ^{111}In-DTPA-A20FMDV2 localises specifically to αvβ6-integrin-positive tissues via its RGDLXXL/I motif (**Figure 63**). Finally, the biodistributions patterns of ^{111}In-DOTA-A20FMDV2, ^{111}In-DTPA-DBD2 and their relevant scrambled variants, were all consistent with the results obtained for ^{111}In-DTPA-A20FMDV2 and ^{111}In-DTPA-A20FMDV2ran, respectively; suggesting a 'RGD class effect'.

Nothelfer et al studied squamous cell carcinoma of the head and neck (HNSCC) and selected cell lines [256], and initially reported that their HNSCC cell lines were all positive, via fluorescence-activated cell sorter analysis, for the αvβ6 integrin [256]. These αvβ6-expressing cell lines were later injected subcutaneously into nude mice, which subsequently formed into tumours. Frozen sections from these xenografts were obtained and immunhistochemistry performed using fluorescence-labelled HBP-1 and Bright field microscopy. The authors illustrated moderate to strong staining in most tumour cells, and the absence of staining in the surrounding stromal cells [256]. Although, Nothelfer did not directly show the maintenance of αvβ6 expression within the HNSCC tumours, the HBP-1 immunhistochemistry is in keeping with the results discussed earlier in this section.

The expression of αvβ6, in adult tissues, has been studied in other species [106, 123, 134, 240, 260, 268]. Brown et al screened normal ovine and bovine tissues for the β6 integrin, by RT-PCR and immunocytochemistry [268]. Of note, Brown and colleagues performed immunohistochemistry using the mouse monoclonal antibody, 10D5 (described in **Section 3.2**), and frozen sections. αvβ6 expression was detected

in epithelia of the airways, oral cavity, gastrointestinal tract, kidney, sweat glands, hair follicle sheaths, and the epidermis of pedal coronary band, but not of normal skin [268]. There was no evidence of β6 transcription in ovine liver, spleen, or mesenteric and bronchial lymph nodes. These histochemical and RT-PCR results generally are consistent with the murine αvβ6 expression pattern (detected with immunohistochemistry) in this thesis. However, Brown reported that the integrin αvβ6 appeared to be constitutively expressed in the normal airways of both cattle and sheep; proposing an inhalatory route of infection by FMDV [268]. Although the murine respiratory epithelium was not positive for αvβ6 expression in the immunohistochemistry experiments (**Table 10**, page 174), biodistribution experiments, consistently within this thesis and by other groups, suggest significant uptake and retention of radiolabelled RGD radioligands in the lungs (see **Sections 4.9.2, 5.1.5, 5.3.1.4, 5.3.2.2** and [262]). Macroscopically, there was no evidence of overt pulmonary haemorrhage during the biodistribution experiments and so these results simply are not explained by blood pooling. Notably, Brown and co-workers and colleagues stated that there was minimal evidence for specific staining when labelling was performed in standard PBS containing 0.5% Tween 80. However, well-defined labelling of the membranes of airway epithelial cells was observed when the staining buffer was supplemented with 4 mM $MgCl_2$ [268]. In addition, even though Brown did not show the data, it was suggested that the epitope targeted by 10D5 was readily denatured by methanol [268]. The immunohistochemistry technique (employed in this thesis) used the 62G2 monoclonal antibody [231], paraffin-embedded sections, and specifically used methanol / hydrogen peroxide (destruction of endogenous peroxidase), but did not supplement cations. However, the 62G2

antibody has been classified as ‘nonligand-mimetic’ and not cation-dependent; thus binding to a different epitope when compared to 10D5 [231]. Nevertheless, these variances may explain the absence of αvβ6 staining seen in murine pulmonary tissues within this report. Future experiments could adjust for these factors and if subsequent testing does detect αvβ6 within airway epithelium, it could explain the relatively high uptake and retention of ^{111}In-DTPA-A20FMDV2, of ^{111}In-DOTA-A20FMDV2 ^{111}In-DTPA-DBD2 and ^{131}I-HBP-1 seen in murine lungs (see **Sections 4.9.2, 5.1.5, 5.3.1.4, 5.3.2.2** and [262]). Furthermore, differences in experimental technique and model may also explain why Munger and colleagues could only detect diffuse and low-level expression of αvβ6, in airway and alveolar epithelial cells of wild-type $\beta6^{+/+}$ (129/terSVEMS strain) mice; contrasting with focal areas of markedly increased expression of αvβ6 within lungs of bleomycin-treated animals [106]. The immunohistochemistry performed by Munger’s group was on frozen section and using the rabbit anti-β6 monoclonal, B1 [106]. It is possible, that bleomycin exposure up-regulated and / or focally concentrated αvβ6 expression into a ‘threshold’ level, previously not adequately detected by the B1 antibody system. Alternatively, bleomycin may further expose the epitope for B1, which initially was hidden / cryptic in normal lungs. Repeat immunohistochemistry using a range of monoclonal antobodies, which recognise a variety of epitopes, could help address this issue and determine whether there indeed is a difference in pulmonary αvβ6 expression within species.

6.3.1 Limitations of Immunohistochemistry

Variations in immunohistochemical conditions, as suggested in **Section 6.3**, could be trialled in order to detect αvβ6 expression within the lungs. However, prior to these tests, RT-PCR could be attempted on appropriately prepared murine tissues. Evidence of β6 transcription would help justify subsequent immunohistochemical optimisation procedures. Indeed, appropriate primers have been designed and RNA from various murine organs is stored. Unfortunately, these experiments could not be completed during the time set for this training degree and are now being attempted by my successor.

The murine antibody, 62G2, was used to immunostain mouse tissues for αvβ6, with the aid of a mouse-on-mouse kit (Vector BMK-2202). Although this created certain technical issues, a number of controls within the procedure ensured a valid system of αvβ6 detection. Furthermore, a novel human Fc / mouse chimeric monoclonal antibody, 2A1, is now available to detect αvβ6 within murine tissues [269]. Although the data on murine tissues have yet to be formally published, the manufacturers of 2A1 have confirmed that the immunohistochemical results are qualitatively similar to those obtained using 62G2 (see **Section 4.6**).

6.4 Peptide Excretory Experiments

The highest levels of radioactivity per unit mass were found in the bladder and kidney. Owing to the absence of αvβ6-immunostaining in the murine kidney (see above) and high levels of radioligand in the urine (data not shown), these data probably are representative of the high and rapid peptide excretion through the urinary tract. The next highest levels of radioactivity per unit mass were found in the A375Pβ6 (β6 expressing) tumour and the stomach; which does correlate closely with histochemical results (see above).

Furthermore, since there is a relatively low %I.D./g within the liver, renal excretion is most likely the *major route* of clearance for the peptide; and the associated radiation exposure could be dose-limiting. However, it should be noted that co-injection of cold DTPA-A20FMDV2 caused the renal retention of ^{111}In-DTPA-A20FMDV2 to decrease by >50% and, since expression of αvβ6 was not detected by immunohistochemistry in the kidney, renal radiopeptide retention may not be related to receptor (αvβ6)-specific binding. That is, a different saturable mechanism may be responsible. This non-αvβ6-specific renal retention hypothesis is supported by the fact that co-injection of a 100-fold excess of a scrambled peptide (DTPA-A20FMDV2ran) together with ^{111}In-DTPA-A20FMDV2 had no effect on αvβ6-specific uptake, but suppressed the kidney uptake by nearly 50% (**Figure 64**). DTPA-A20FMDV2ran does not recognise β6 *in vitro* and *in vivo* and, since the kidney retention of ^{111}In-DTPA-A20FMDV2 can be suppressed by saturating the retention mechanism with this scrambled peptide, it confirms that the mechanism of

retention is not RGD-specific; possibly via a generalised peptide uptake mechanism, rather than an αvβ6-dependent system.

Previous studies have reported that peptides can be reabsorbed by the renal system [270, 271]. The transmembrane scavenger-receptor, megalin, is one important mechanism of peptide re-absorption [272]; although many other mechanisms have been proposed and they are not fully understood [270]. Once reabsorbed, the renal tubular cells have the potential to further metabolise (e.g. lysosomal degradation) the radiopeptide and could, in theory, uncouple the ^{111}In from the DTPA-A20FMDV2 [271]. It is known that metals (e.g. ^{111}In) are retained in certain tissues to a greater degree than other ions (e.g. ^{18}F) [254, 271] and this may be a possible explanation for the different renal handling after 1 hour, of ^{111}In-DTPA-A20FMDV2 (97.56 ± 14.67 %I.D./g) compared to [^{18}F]FBA-A20FMDV2 (3.56 ± 1.38 %I.D./g) [228]. Saturation of the renal uptake mechanisms by DTPA-A20FMDV2ran may minimise the amount of ^{111}In-DTPA-A20FMDV2 exposed to uncoupling agents and thus reduce retention. Furthermore, different labelling moieties may alter peptide properties, such as hydrophobicity and lipophilicity. The DTPA chelating agent may also affect the peptide's properties. Attachment of a hydrophilic ^{111}In-DTPA chelating moiety to a peptide has been reported to enhance renal excretion and minimise hepatobiliary clearance, thus reducing abdominal radioactivity levels [273]. Hydrophobicity transformation may alter peptide quaternary structure and so alter its binding affinity. Moreover the lipophilic profile of the peptide may affect organ uptake and excretion and thus other blocking strategies could be explored, such as infusion with gelofusine [270]

Other mechanisms for renal uptake and retention were explored in the comparison of the biodistibution of non-biotinylated ^{111}In-DTPA-A20FMDV2 and the wild-type peptide. There was a significant difference in renal handling of the non-biotinylated and biotinylated forms of the peptide. The biotinylated form had 50% less renal retention and it was thought that this may be due to its larger size. The larger molecule may have reduced filterable, or reabsorbable, capacity in comparison with the non–biotinylated peptide. Alternatively, the biotinylation may have had substantial effects on steric hinderance or lipid solubility [254, 271]. Whatever the precise mechanism, these results suggest that re-designing the peptide has the potential to reduce renal uptake and retention. That is, if the peptide could be redesigned so that uncoupling of the ^{111}In from DTPA-A20FMDV2 could be resisted, then this strategy might also reduce renal radioactivity exposure. However, the detailed exploration of potential renal blocking mechanisms and peptide manipulation was beyond the scope of this project. Furthermore, the single doses of radiopeptide required for human imaging studies minimise any potential renal hazards. Nevertheless, it is possible that a similar peptide renal retention mechanism may occur in humans and this potential radiation accrual could have an impact on future therapeutic studies (**see Chapter VII**). Therefore, the important discovery that renal retention can be suppressed by pre-saturating appropriate receptors suggests that a similar strategy could be employed in humans, to limit dose-limiting toxicity during peptide receptor radiotherapy trials. If the targeted agent could be labelled with a β-emitting isotope, it could home in on the tumour, cause local cell death and, potentially, provide a useful therapeutic tool. However, β-emitter metals, such as Yttrium, when coupled to DTPA-A20FMDV2 would possibly require multiple doses

to be an effective therapeutic agent and thus would require strategies to minimise renal radioactivity exposure. However, peptide receptor radiotherapy is one possible therapeutic approach; coupling of the peptide to a non-metallic chemotherapeutic agent is another potential manoeuvre [274]. The uncoupling mechanism in the renal tubular cells may not be as effective for a non-metallic substance and thus the potential renal toxicity could be minimised through rapid excretion.

6.4.1 Limitations of Peptide Excretory Experiments

Brown et al reported that the integrin αvβ6 appeared to be expressed in the normal distal convoluted tubular epithelium, in the kidneys from sheep [268]. Although the murine kidneys were not positive for αvβ6 expression in the immunohistochemistry experiments (see **Table 10**, page 174), the biodistribution experiments reported in this thesis consistently have suggested significant retention of radiolabelled RGD radioligands within the kidneys (see **Sections 4.9.2, 5.1.5, 5.3.1.4 and 5.3.2.2**). Although peptide excretory mechanisms are assumed to be the primary reasons for this retention, the questions regarding probable immunohistochemical variables (described in **Section 6.3**) suggest that constitutive αvβ6 expression within murine kidneys cannot totally be ruled out. RT-PCR and evidence of β6 transcription would help clarify this dilemma. However, post-translational modifications, the presence of co-activators and receptor turnover will not be necessarily addressed by RT-PCR techniques, and so proof of the presence of a functional αvβ6 cell-surface receptor in the kidney may still require further investigation.

Ideally, to prove that the peptide renal retention mechanism is not an αvβ6-dependent system, co-injection with ^{111}In-DTPA-A20FMDV2 should occur with a different known αvβ6-specific agent. *In vitro* blocking experiments utilised the 68G6 monoclonal antibody [231] and tested for potential αvβ6-dependent mechanisms. However, it is not known whether this antibody effectively blocks αvβ6 *in vivo.* Indeed, at present, there is no universally accepted reagent known to block αvβ6 *in vivo*; thus creating a barrier to the proposed experiment.

The theory of metal radiolabel being uncoupled from ^{111}In-DTPA-A20FMDV2 (or the DOTA variant) being responsible for the differences in renal retention (as compared to [^{18}F]FBA-A20FMDV2) is difficult to prove. Future experiments could use different labelling methods and non-metals, as well as re-designing the peptide. However, this investigation is beyond the scope of this project.

It also is possible that this peptide renal retention mechanism is only pertinent to the mouse model. Therefore, other animal models could be tested prior to human trials. However, this is time-consuming, expensive and there is no guarantee that data from other species are more representative of humans, compared to murine models.

6.5 In vivo Imaging

In order to take advantage of the high resolution and sensitivity of the multi-pinhole NanoSPECT/CT small animal imager, A20FMDV2 was modulated into a SPECT targeting agent for αvβ6. The biodistribution results were reflected in the imaging experiments; revealing selective localisation of labelled peptide in αvβ6-expressing tissues. **Figure 66** shows a coronal slice, taken by a NanoSPECT/CT, 1 hour after injecting 10MBq ^{111}In-DTPA-A20FMDV2 into a mouse bearing paired A375P β6/A375P puro tumours. It clearly is apparent that there is little or no activity in the A375P puro tumour whereas the A375P β6 tumour has distinct 'hot-spots' within the growing tumour mass. The kidneys also show significant radioactivity but no other organs are revealed in this analysis. Maximum Intensity Projections (MIPs) were also generated in separate studies from several mice. Although represented in 2-dimensions, **Figure 66** shows that, again, the A375P β6 tumour retained significant amounts of radioactivity whereas the A375P puro tumour effectively is negative. The MIP (especially when rotated through 360 degrees) confirms that the distribution of the radioactivity in the A375P β6 tumour was not uniform, but rather appears as a series of higher activity nodules, approximately 1mm diameter, interconnected by lower activity areas. The reasons for this localised distribution are not known, but may relate to local blood supply or regions of hypoxia. The MIP image also reveals the significant retention of ^{111}In-DTPA-A20FMDV2 by the lower GI tract as well as by the kidneys and bladder. Therefore ^{111}In-DTPA-A20FMDV2 is retained selectively by αvβ6-expressing tissue and is the first specific radioligand for the non-invasive imaging of αvβ6-positive cancers by SPECT.

Hausner et al's [228] imaging of DX3-paired tumours using PET did not reveal discrete areas within the growing mass of the αvβ6-positive tumour. Instead, the [^{18}F]FBA-A20FMDV2 tumour uptake images were less well-defined and more dispersed; possibly as a result of the inferior resolution of their microPET system (see **Section 2.1.4.2**). This resolution difference may also explain the absence of images revealing uptake of [^{18}F]FBA-A20FMDV2 in the stomach and gallbladder, despite the high %I.D./g shown in their biodistribution experiments [228]. Hence the superior resolution of a multi-pinhole NanoSPECT/CT has provided interesting data as well as opening up future research questions.

6.5.1 Limitations of NanoSPECT/CT Experiments

Hausner et al imaged DX3-paired tumours on a microPET system using [^{18}F]FBA-A20FMDV2 [228], PEGylated and ^{64}Cu variants [254]; whereas the imaging experiments performed in this thesis studied A375P-paired tumours on a NanoSPECT/CT system using ^{111}In-DTPA-A20FMDV2 and the DOTA variant, thus making direct comparisons between the two studies somewhat difficult. It may be that the differential distribution seen within the A375P β6 tumour is not really present in the DX3puro β6 tumour; and so not related to resolution differences within the imaging systems. The Department (at Queen Mary's, University of London) recently has purchased a PET scanner, which currently is being optimised. Sequential imaging using the different imaging systems on the same mice may help provide an answer to this question.

It has been hypothesised that potential reasons for the localised distribution of radioligand within the A375P β6 tumour might relate to local blood supply or regions of hypoxia. However to prove these theories, markers of hypoxia or of tumour vasculature would need to be imaged simultaneously with ^{111}In-DTPA-A20FMDV2. It should then be possible to compare corresponding areas within the tumours. However, although there have been numerous agents which have been published and claimed to image tissue hypoxia [275] and tumour angiogenesis [276], *in vivo*, none have yet been accepted as a universal standard for use in murine models. Furthermore, some of these published agents have been optimised on different imaging modalities (e.g. MRI, rather than PET or SPECT). Therefore, issues of standardisation and image registration (from multiple imaging modalities) will create further problems when testing the proposed hypotheses.

Ideally, one would like to correlate tissue %I.D./g found in biodistribution experiments with NanoSPECT/CT estimates. SPECT quantification of radioligand dissemination has been shown to be very accurate in rat kidney models [277]. However, at present, the sensitivity of our machine is not sufficient to do this type of quantification in *all* organs, especially with relatively moderate amounts of radioactivity (data not shown). Once the sensitivity can be optimised, the reduction of time-consuming and laborious biodistribution experiments could be a useful objective. Consequently, imaging would have the additional advantage in that small tissues (which usually may not be sampled in biodistribution experiments) could be examined for radioactivity *in situ* and at a time distant from the original experiment. However, some organs may be hard to fully delineate using imaging techniques e.g. intestines; thus quantification of these organs may not be as accurate. Recently a

number of investigators have used Standardised Uptake Values (SUVs), to measure and compare tumour uptake, within microPET systems and mice; instead of the standard %I.D./g measures [255, 278]. However, SUVs can be influenced by a number of different factors and so it is not known how accurate these values are (as compared to data from the gold standard biodistribution experiments), so that one should be cautious about over-emphasising the value of such approaches [278].

6.6 Summary

The integrin αvβ6 is *not* expressed by most normal tissues but is upregulated strongly on many carcinomas [134].

It has been shown that αvβ6 promotes carcinoma cell migration as well as invasion [140], matrix-metalloproteinase production [141], and tumour cell survival [152], both *in vitro* and *in vivo*.

85-95% of oral squamous carcinomas and 40% of breast cancers express αvβ6, whereas corresponding normal tissues are negative. Recently a study of nearly 500 colon cancers showed that the hazard of dying was 60% higher in patients with strong expression of αvβ6 [101]. Together these data suggest that αvβ6 actively promotes cancer progression; possibly explaining the poor prognosis associated with its expression by tumour cells.

High affinity αvβ6-binding peptides have been generated, whose activity is dependent on an RGD motif.

The work presented in this thesis has shown that these peptides are selective and specific for αvβ6–positive tumour cell lines, in *in vitro* assays.

Furthermore, it has been demonstrated that these peptides selectively locate to αvβ6-expressing tumours *in vivo.* ^{111}In-DTPA-A20FMDV2 is internalised by αvβ6-expressing cells and this may be important for *in vivo* tumour retention, given that peptides are degraded by plasma proteases.

A systematic improvement in the uptake and retention of ^{111}In-DTPA-A20FMDV2 has been described and this forms the basis of the first documented, αvβ6-specific SPECT imaging agent (see **Appenidix** for publication).

In addition, a method to reduce renal toxicity during peptide receptor radiotherapy has been developed, which may have widespread applicability.

Finally it has been discovered that, unlike the situation reported for human tissues, several murine tissues express αvβ6 and this characteristic must be accounted for when screening for αvβ6-specific targeting agents.

In conclusion, this project provides valuable information on the best type of αvβ6-targeting agents to translate from bench to the clinic and can serve as a paradigm for pre-clinical evaluation of targeting agents in general. Future experiments could exploit these findings to target human cancer.

Chapter VII: Potential Human Trials

7.1 Proposed Phase I trial schema: ^{68}Ga-DOTA-A20FMDV2

The pre-clinical experiments were performed in order to form the basis of a rationale, for the translation of the αvβ6-targeting agents into a useful imaging tool for the clinical investigation of human cancers. Currently, imaging in oncology helps with diagnosis, staging, prognostication, the monitoring of treatment response and screening (see **Chapter II**). However, prior to widespread use of a proposed imaging agent, its potential toxicity / safety profile must be established. A Phase I trial is the generally accepted method to evaluate tolerability and identify a safe dosage range.

.

Background

DOTA-A20FMDV2 has been shown to detect αvβ6-expressing tumours in pre-clinical models; and serve as a diagnostic imaging agent. αvβ6 is over-expressed in many human epithelial cancers, such as pancreas, oral and breast. Therefore, this new agent permits the opportunity to examine these cancers through their biomarker. Future studies could correlate the plasticity of αvβ6 expression with ^{68}Ga-DOTA-A20FMDV2 imaging and survival, following targeted therapy.

Objective To determine ^{68}Ga-DOTA-A20FMDV2 safety

To determine its plasma stability

To study the distribution and kinetics of the tracer

To accrue preliminary data on potential diagnostic value

Requirements:

MHRA approval – Investigational Medicinal Product

ARSAC (Administration of Radioactive Substance Advisory Committee) approval

GCP Radiopharmacy and Gallium generator

PET and CT scanners

Ethics approval

Nuclear Medicine Physician

Informed consent

Methods

Inclusion Criteria:

- Biopsy proven stage IV breast cancer
- Aged over 18 years old
- ECOG performance status 0-2
- Post-menopausal, surgically sterile, post-hysterectomy, or having a negative pregnancy test on day of scan.
- At least one lesion of greater than 1cm diameter, that has not been irradiated previously.

Exclusion Criteria:

- Receiving chemotherapy within four weeks of scan
- Received a trial drug within four weeks of scan.
- If in lactating period
- Impaired renal function (serum creatinine > 106 μmol/L)

Records: Patient demographics

Number of previous treatments

Hormonal and c-erbB_2 status

Whether primary has been removed

Other disease sites found on recent CT, MRI, ^{18}F-FDG-PET or Clinical Examination.

Procedure:

Physical Examination pre PET scan

Slow bolus (over 1 minute) intravenous injection of radioligand

Dynamic scan of selected lesions from t=0 and acquire ten second frames for 5 minutes. After this period 1 minute frames for next ten minutes; followed by 5 minute frames for next fifteen minutes. The final sequence involves 10 minute frames for thirty minutes.

Static scan at 60 minutes post-injection for whole body and thus all lesions.

Define region of interest / lesions from scout and low-dose CT scans and previous ^{18}F-FDG-PET emissions.

Pharmacokinetic Measures:

Blood sampling at 5, 10, 30 and 60 minutes post-injection to determine plasma : blood activity; and HPLC analysis examining stability and metabolite formation.

PET measures of tissue activity over time (decay corrected and normalised for injection dose; SUV m^2/ml)

Patlak graphical method: Rate constant (K_i) measure of net irreversible retention of radioligand, within imaging time (assuming that the metabolites do not bind to the receptor).

Assessment of the fractional retention of the radioligand and the mean residence time (MRT)

Toxicity Measures:

Before, during and up to 24 hours post injection:-

Vital signs

Physical Examination

ECG and continuous lead II during and up to 15 minutes post administration of radioligand

Blood tests (FBC, clotting and full biochemistry profile) at 30 minutes, 150 minutes and 24 hours post-injection.

Urinalysis

Two weeks post scan:-

Telephone interview with subject; with clinic review, if symptoms warrant further investigation.

Biomarker Correlation:

Immunohistochemistry of biopsy sample for αvβ6 expression.

Data analysis and Statistics:

Two-tailed Wilcoxon matched-pairs test to compare the uptake and kinetic parameters in tumour lesions with corresponding normal tissues.

7.1.1 Limitations of Proposed Phase I trial schema

Traditional phase I studies can be a slow and costly process [279], especially if the other peptide variants are to be examined within human subjects. Furthermore, the dose of investigational agent producing a 'dose-limiting toxicity' (a limit of tolerability) may not be relevant to the dose required to detect its related biomarker [279, 280]. Therefore, a relatively recent development is the phase 0 study. In this type of study, 'microdoses' (sub-therapeutic) of the investigational agents are administered to gather initial pharmacokinetic and pharmacodynamic data [281]. A microdose is defined as less than 1/100th of the dose calculated to yield a pharmacological effect of the test substance based on primary pharmacodynamic data obtained *in vitro* and *in vivo* (typically doses in, or below, the low microgram range) and at a maximum dose of ≤ 100 microgram [282]. In addition, owing to differences in molecular weights, as compared to synthetic drugs, the maximum dose for protein products is ≤30 nanomoles [279]. That is, the exact microdose (selected for study) is based on pre-clinical safety studies. These studies should demonstrate that a large multiple (e.g. 100x) of the proposed human dose does not induce adverse

effects in the experimental animals; establishing a margin of safety and limiting the risk to future human subjects [279]. However, controlled allometric scaling from animals to humans (based on body surface area or pharmacokinetic / pharmacodynamic modelling) may be possible to select the dose for use in the subsequent clinical trial [279]. It should be noted that Phase 0 studies do not give detailed data on safety and efficacy and so later phase studies still will need to be performed [283]. Furthermore, phase 0 trials are limited to investigational agents with a wide therapeutic index, a known target, and a validated biomarker [281]. Notwithstanding these conditions, phase 0 studies potentially are able rank similar candidate investigational compounds with respect to pharmacokinetic / pharmacodynamic parameters; narrowing down the the number of agents to take forward into further development.

Clinical trials of radioactive substances must follow the Ionising Radiations Regulations [284] and should be approved by the Administration of Radioactive Substances Advisory Committee (ARSAC). ARSAC guidelines state that the radiation dose to a trial subject should be as low as reasonably practical and must not exceed 10 milliSievert per annum [285]. ARSAC expects trial investigators to estimate the radiation to a trial subject by referencing the best information available at the time of their applications. Where such estimates are not possible (from similar existing human studies) data from animal dosimetry studies, or where practicable from human studies involving extremely low radiation doses, should be utilised [285]. Therefore, this data will be taken together with other experiments (e.g. labelling efficiency) to determine the initial activity to be used within early phase trials.

7.2 Proposed Phase II / III trial schema: A20FMDV2

Once initial safety data have been accrued, a further evaluation of toxicity is made, in a larger group of subjects (phase II). However, an initial evaluation of the diagnostic performance (efficiency) of the imaging agent can also be performed (phase II/III). This involves the assessment of whether the imaging agent can detect the presence of absence of disease (sensitivity, specificity and accuracy). It may be that the threshold criteria, for deciding whether a test is positve or not, is a fine balance between acceptable sensitivity and specificity rates. Ideally, these rates would be compared against a standard imaging agent, currently in clinical use (phase III).

Objective Extension of toxicity data

Compare A20FMDV2 to FDG in primary lesions, as well as metastatic lesions.

To determine sensitivity of A20FMDV for lesion identification.

Requirements:

MHRA approval – Investigational Medicinal Product

ARSAC (Administration of Radioactive Substance Advisory Committee) approval

GCP Radiopharmacy

PET and CT scanners

Ethics approval

Experienced Radiologist to interpret scans

Informed consent

Methods

Inclusion Criteria:

- Biopsy proven stage IV breast cancer
- Aged over 18 years old
- ECOG performance status 0-2
- Post-menopausal, surgically sterile, post-hysterectomy, or having a negative pregnancy test on day of scan.
- At least one lesion of greater than 1cm diameter, that has not been previously irradiated

Exclusion Criteria:

- Receiving chemotherapy within three weeks of scan
- Received a trial drug within thirty days of scan, or due to receive a investigational medicine up to 24 hours after scan.
- If undergoing occupational monitoring for radiation exposure
- If in lactating period
- Impaired renal function (>106 μmol/L)
- Diabetic patients or fasting glucose >7.

Record: Patient demographics

Number of previous treatments

Hormonal and c-erbB_2 status

Whether primary has been removed

Other disease sites found on recent CT or Clinical Examination.

Procedure:

Patient to be fasted 6 hours before FDG PET scan

Physical Examination pre PET scan

CT scan is required to be within four weeks of PET scan for formal comparison.

Calibrate PET with suitable source

Bolus intravenous injection of radiolabelled A20FMDV2

Scan at 60 minutes post-injection

Define up to 5 target lesions for each patient (choose lesion with highest tracer uptake if afflicted organ has multiple lesion). Outline a volume of interest for calculations of SUV.

Pharmacokinetic Measures:

Blood sampling at 5, 10, 30 and 60 minutes post-injection to determine plasma : blood activity; and HPLC analysis examining stability and metabolite formation.

PET measures of tissue / lesion activity over time (decay corrected and normalised for injection dose and body surface area; SUV m^2/ml)

Rate constant (K_i) measure of net irreversible retention of radioligand, within imaging time (assuming that the metabolites do not bind to the receptor).

Toxicity Measures:

Before, during and up to 24 hours post injection:-

Vital signs

Physical Examination

ECG and continuous lead II during and up to 15 minutes post administration of radioligand

Blood tests (FBC, clotting and full biochemistry profile) at 30 minutes, 150 minutes and 24 hours post-injection.

Urinalysis

Biomarker Correlation:

Immunohistochemistry of biopsy sample for αvβ6 expression.

Statistics:

Sensitivity comparisons between FDG and A20FMDV2 are based on lesion identification, number of lesions in each scan and comparison to Clinical and CT staging.

Correlations of parameters using linear regression and Pearson's coefficient

Comparisons of qualitative parameter using ANOVA

Wilcoxon test.

Outcomes:

To compare and correlate SUV for primary lesions against metastatic lesions (organ by organ) for both A20FMDV2 and FDG.

Any missed lesions for either radiotracer.

7.3 Diagnostic, Therapeutic and Health Impact

One of the measures of the effectiveness of an imaging agent is its diagnostic impact. Ultimately, if the results of an imaging agent do not influence a clinican's diagnostic confidence, then it has no diagnostic impact. Alternatively, if the diagnostic impact of the investigational imaging agent is superior to the standard technique, it may diplace older technologies. The calculation of diagnostic impact will be aided by the biomarker correlation studies included in the proposed trial schemes for A20FMDV2 (see **Section 7.1 & 7.2**).

Future studies may also look at the therapeutic impact of an A20FMDV2-based imaging agent. Since αvβ6 expression is associated with poor prognosis in several cancers, the use of ^{111}In-DTPA-A20FMDV2 could enable non-invasive identification of higher risk cancers and, thus, might be a prognostic marker. Consequently, these higher risk cancers could be stratified into different treatment arms. If a certain treatment is benefical to 'poor-prognosis' cancers, identified by the A20FMDV2-based imaging agent, then this imaging agent has therapeutic, and thus health, impact.

7.4 Possible Barriers to the Translation of A20FMDV2 into a Successful Clinical Imaging Agent

Although clinical trials ultimately will decide the future of A20FMDV2, a few problems may be predicted from human trials of other RGD peptides and pre-clinical experience:

7.4.1 Adverse Effects

A technetium-99m labelled RGD-containing synthetic peptide already has been used in human imaging studies to localise αvβ3 tumour expression [286]. Fourteen patients, previously diagnosed with metastatic melanoma, underwent gamma camera imaging 20–180 min after intravenous administration of the radiolabelled, synthetic, linear, decapeptide αP2 [286]. However it needs documenting that neither *in vitro* nor pre-clinical *in vivo* studies have been published to demonstrate the sensitivity and specificity of the binding of this peptide to αvβ3. Nevertheless, encouraging results were obtained regarding sensitivity in humans and the peptide even detected a metastatic site within the brain [286]. Furthermore, no toxicity or adverse events were recorded during administration and in the 12-month follow-up period. Platelet function, as well as prothrombin time, remained within baseline values. It should be noted that the linear peptide showed high persistent background activity in certain organs and therefore was limited in its imaging efficacy; as a consequence, none of the mediastinal metastases were detected [286].

7.4.2 Potential Immunogenicity of A20FMDV2

Peptides have been proposed to have low immunogenicity *in vivo* owing to their rapid degradation [190]. RGD peptides, and their potential to induce neutralising antibodies, have been studied in their role as a potential vaccine for FMDV [287]. FMDV C-SC1 has a conserved RGDL sequence at its antigenic site. As a consequence, one study generated FMDV C-S8C1-based peptide immunogens (coupled to keyhole limpet haemocyanin in complete Freund's adjuvant) and explored their ability to evoke neutralising antibodies in rabbits and guinea pigs [287]. Although, anti-peptide antibody titres generally were high, the sera bound with heterologous RGDL-containing antigens to a much lesser extent than with the homologous peptide; this finding suggesting that there was a low proportion of antibodies directed to RGDL, as the sole target [287]. Of note, although the first booster improved anti-peptide antibody levels, later inoculations had no effect. Furthermore, the neutralising activity by the anti-peptide sera on C-S8cl FMDV itself was investigated. Neutralising activity of the sera generally was low, confined to the IgM isotype, and significant decreases in neutralising titres were observed with boosting (two to three times every three weeks). The confinement of neutralising activity to the IgM subtype strongly suggests that auto-antibodies are produced at an early stage of the immune response and later suppressed, thus preventing the switch to IgGs from lymphocyte clones recognising both self antigens, FMDV virions and peptides [288]. This is not surprising, since the RGD sequence is found in a variety of widely distributed proteins involved in cell adhesion / signalling (mentioned in the **Introduction**), and the immune system could limit the anti-RGD antibody production for self tolerance. Therefore, the rapid degradation, and relatively low

potential for neutralisation, permits the repeat administration of peptides for imaging, without the concern for reduced targeting and detection. The low potential for neutralisation is also important when using peptides as therapeutic agents (see **Section 7.4.4**). A therapeutic agent which triggers the immune system of the host may cause neutralisation of the agent before it can even achieve its intended therapeutic benefit. Furthermore, the relatively low immunogenicity of RGD peptides also suggests that the potential for troublesome allergic or anaphylactic reactions is low.

7.4.3 The Gastrointestinal Tract and the αvβ6 Integrin

Hsiung *et al* recently have demonstrated successsful delivery of topically administered peptide into the colonic lumen, via an endoscope [289]. Detection of the fluorescently labelled peptide occurred using the aforementioned fluorescence confocal microendoscope. The authors stated over 80% sensitivity and specificity for dysplastic colonocytes over normal cells [289]. This different route of peptide administration and novel method of dysplasia detection could be examined with the A20FMDV2 peptide; particularly in view of the encouraging results obtained with the murine colon cancer models (see **Section 5.2**).

The radioimaging and fluorescent peptide applications of A20FMDV2 (and other RGD peptides) have been proposed, owing to the perceived minimal αvβ6 expression within normal human tissue [134, 240]. However the expression data which have given rise to this premise are based on, immunohistochemistry and *in situ* hybridisation, results performed on Rhesus monkey tissues [134, 240]. Breuss

and colleagues did report luminal αvβ6 expression on the surface epithelium of colon, but described it as 'low-level' [134]. However, this relatively 'low-level' expression may still be clinically significant. Furthermore, Brown and colleagues have demonstrated αvβ6 expression in the gastrointestinal tract, of normal ovine and bovine subjects [268]. This species variation questions any extrapolation, albeit within the primate family, from monkeys to humans. For these reasons, samples of normal human colon were obtained and examined for αvβ6 expression, using immunohistochemistry.

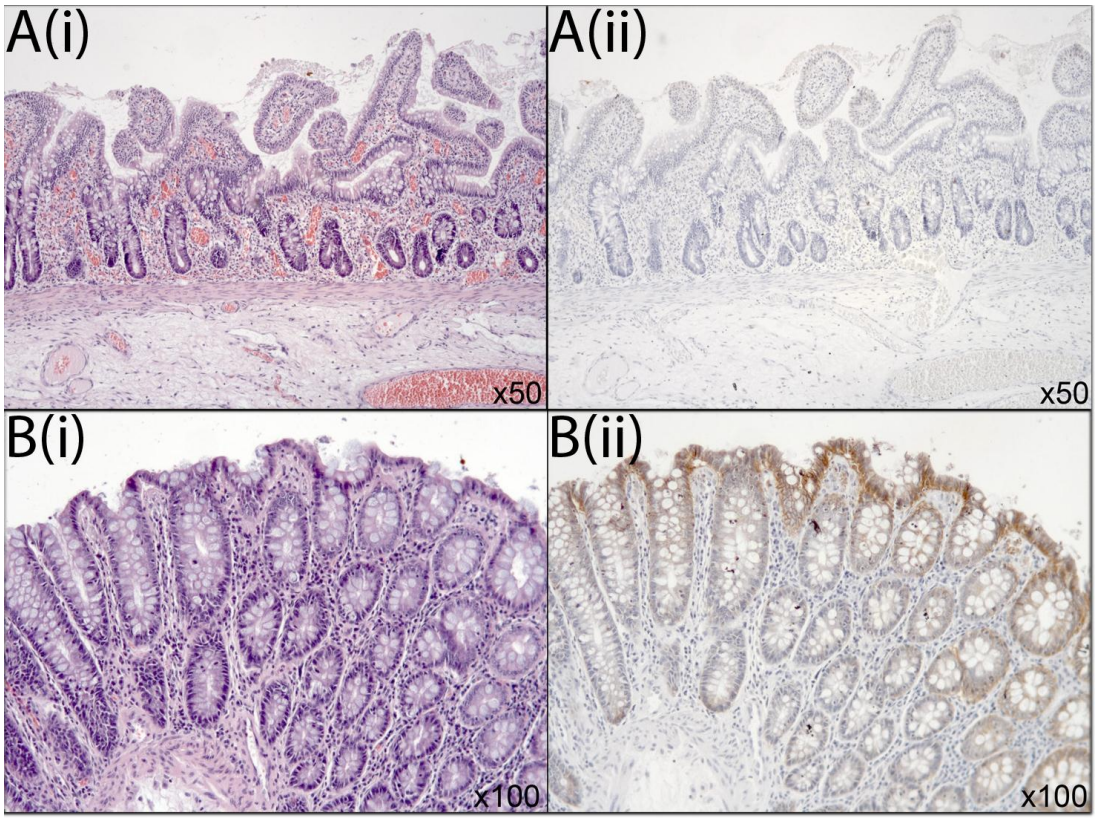

Figure 87 Colonic Tissue samples from two 'normal' human donors (A & B). Left image (i) is Haematoxylin stain and right (ii) is corresponding 62G2 staining.

Human colon tissues were obtained from a total of six different, 'normal', human donors. Firstly, **figure 87** reveals colonic specimens, from two different donors (A & B), with normal morphological appearances, using a Haematoxylin stain. However, case B (right side) displays strong αvβ6 staining at the surface of enterocytes, forming the mucosa of the colon, similar to that previously described in the immunodeficient mice (see **Section 4.6**). Again, the intensity decreases as the epithelial layer is followed down to the crypts. Notably, case A (right side) does not show any evidence of αvβ6 staining; thus there is absence of αvβ6 expression. This lack of αvβ6 staining was seen in the majority of normal human donors (four of the six). Nevertheless, from this small sample, it seems that a third of normal donors stain positively with respect to 62G2; thereby constitutively expressing αvβ6 on their colonic mucosa. This analysis would have to be replicated on a larger sample, to validate the exact proportion of 'constitutive expressers'. Furthermore, although these donors were labelled 'normal', their full clinical details are not known, owing to anonymised data requirements. Nonetheless, if these αvβ6-expressers are assumed to be normal, it follows that there is a proportion of normal humans who will constitutively express αvβ6. This constitutive expression will have implications, regarding the sensitivity and specificity of detection for αvβ6-expressing cancers, within the lower gastrointestinal tract. Furthermore, gastrointestinal toxicity also must be factored in for a radionuclide imaging study or in potential therapeutic roles (see **Section 7.4.4**).

7.4.4 Peptide Therapeutics

My PhD project was concerned primarily with targeting αvβ6 for imaging. However, if the primary tumour and metastases can be tracked specifically using such selective agents then the potential for targeted therapy exists. This therapy simply could comprise the peptide itself or the peptide attached to a chemotherapeutic agent [290] or a β-emitting agent [291]. In theory, the latter two options would permit local tumour cell death and overcome the non-specific toxicity of chemotherapy and external beam radiotherapy towards normal tissues. The former option (peptide alone) may result in a variety of consequences depending on which cell pathways are stimulated. Therefore, future projects could investigate the cell signalling mechanisms activated upon peptide binding. Furthermore, dose-finding and toxicity studies would need to be carried out. Imaging experiments in humans are not expected to cause significant toxicity, since plasma peptide concentrations are expected to be in the nanomolar range. However, therapeutic studies may require higher doses, as well as repeated administrations. Peptides containing the RGD motif can inhibit platelet aggregation [292], and therefore careful haematological studies should be included in any such toxicological assessments.

Furthermore, the high renal excretion seen with ^{111}In-DTPA-A20FMDV2 could be a major issue in therapeutic development. During imaging the 'once-off' dose, rapid peptide destruction and excretion are parameters which are protective to renal toxicity. However, if a β-emitter is coupled to the peptide and repeated courses of peptide administration are planned, kidney damage and loss of function potentially are of major concern [270]. Therefore the mechanisms already described to limit renal retention may need to be further explored.

7.4.5 Cancer Cell Plasticity

Cell plasticity refers to the ability of one lineage of cells to take on the characteristics of a different cell lineage [293]. This plasticity may arise from the exposure of a cancer cell to a different micro-environment and is entwined in the cancer stem cell hypothesis [294]. A discussion on the cancer stem hypothesis is beyond the scope of this PhD thesis. Nonetheless, it is accepted that the molecular progression of αvβ6-expressing cancers, within humans, still is unknown. That is, it is currently not known whether αvβ6-expressing cancers lose their αvβ6 expression, in response to various treatments (e.g. chemotherapy or radiotherapy). Furthermore, if an αvβ6-expressing cancer is exposed to an RGD-radiopeptide, during imaging, it is not certain whether the αvβ6 expression is maintained for subsequent imaging / therapeutic studies. In other words, if the integrin expression profile of a tumour changes in response to ^{111}In-DTPA-A20FMDV2 imaging, an initial 'positive' result indicating αvβ6 expression may not be truly informative for subsequent αvβ6-directed therapy.

However, all of the aforementioned potential barriers to A20FMDV2, becoming a successful clinical agent, can only be ascertained once it has been tested in properly designed and controlled human trials.

Chapter VIII: References

1. Hanahan, D. and R.A. Weinberg, *The hallmarks of cancer.* Cell, 2000. **100**(1): p. 57-70.

2. Hahn, W.C. and R.A. Weinberg, *Rules for making human tumor cells.* N Engl J Med, 2002. **347**(20): p. 1593-603.

3. de Vries Reilingh, T.S., et al., *"Components separation technique" for the repair of large abdominal wall hernias.* J Am Coll Surg, 2003. **196**(1): p. 32-7.

4. Great Britain. Office for National, S., *Cancer statistics registrations : registrations of cancer diagnosed in 2004, England*. 2006.

5. Forman, D., et al., *Cancer prevalence in the UK: results from the EUROPREVAL study.* Ann Oncol, 2003. **14**(4): p. 648-54.

6. Great Britain. Office for National, S., *Mortality statistics : cause: review of the Registrar General on deaths by cause, sex and age, in England and Wales, 2005*. 2006.

7. Dollinger, M., G. Cable, and E.H. Rosenbaum, *Everyone's guide to cancer therapy*. 3rd ed. 1997, Kansas City, Mo.: Andrews McMeel Pub. xxiii, 824.

8. Therasse, P., et al., *New guidelines to evaluate the response to treatment in solid tumors. European Organization for Research and Treatment of Cancer, National Cancer Institute of the United States, National Cancer Institute of Canada.* J Natl Cancer Inst, 2000. **92**(3): p. 205-16.

9. Stroobants, S., et al., *18FDG-Positron emission tomography for the early prediction of response in advanced soft tissue sarcoma treated with imatinib mesylate (Glivec).* Eur J Cancer, 2003. **39**(14): p. 2012-20.

10. Evilevitch, V., et al., *Reduction of glucose metabolic activity is more accurate than change in size at predicting histopathologic response to neoadjuvant therapy in high-grade soft-tissue sarcomas.* Clin Cancer Res, 2008. **14**(3): p. 715-20.

11. Hynes, R.O., *Integrins: a family of cell surface receptors.* Cell, 1987. **48**(4): p. 549-54.

12. Hynes, R.O., *Integrins: versatility, modulation, and signaling in cell adhesion.* Cell, 1992. **69**(1): p. 11-25.

13. Hynes, R.O., *Integrins: bidirectional, allosteric signaling machines.* Cell, 2002. **110**(6): p. 673-87.

14. de Melker, A.A. and A. Sonnenberg, *Integrins: alternative splicing as a mechanism to regulate ligand binding and integrin signaling events.* Bioessays, 1999. **21**(6): p. 499-509.

15. Ruoslahti, E., *RGD and other recognition sequences for integrins.* Annu Rev Cell Dev Biol, 1996. **12**: p. 697-715.

16. Guo, W. and F.G. Giancotti, *Integrin signalling during tumour progression.* Nat Rev Mol Cell Biol, 2004. **5**(10): p. 816-26.

17. Plow, E.F., et al., *Ligand binding to integrins.* J Biol Chem, 2000. **275**(29): p. 21785-8.

18. Alberts, B. and I. National Center for Biotechnology, *Molecular biology of the cell [electronic resource]*. 4th , Electronic version. ed, Bethesda, MD ; Abingdon: Garland Science/National Center for Biotechnology Information (NCBI).

19. Weisel, J.W., et al., *Examination of the platelet membrane glycoprotein IIb-IIIa complex and its interaction with fibrinogen and other ligands by electron microscopy.* J Biol Chem, 1992. **267**(23): p. 16637-43.

20. Humphries, M.J., *Integrin structure.* Biochem Soc Trans, 2000. **28**(4): p. 311-39.

21. Xiong, J.P., et al., *Crystal structure of the extracellular segment of integrin alpha Vbeta3.* Science, 2001. **294**(5541): p. 339-45.

22. Bork, P., et al., *Domains in plexins: links to integrins and transcription factors.* Trends Biochem Sci, 1999. **24**(7): p. 261-3.

23. Mizejewski, G.J., *Role of integrins in cancer: survey of expression patterns.* Proc Soc Exp Biol Med, 1999. **222**(2): p. 124-38.

24. Humphries, M.J., et al., *Integrin structure: heady advances in ligand binding, but activation still makes the knees wobble.* Trends Biochem Sci, 2003. **28**(6): p. 313-20.

25. Otey, C.A., F.M. Pavalko, and K. Burridge, *An interaction between alpha-actinin and the beta 1 integrin subunit in vitro.* J Cell Biol, 1990. **111**(2): p. 721-9.

26. Hood, J.D. and D.A. Cheresh, *Role of integrins in cell invasion and migration.* Nat Rev Cancer, 2002. **2**(2): p. 91-100.

27. Coppolino, M., et al., *Inducible interaction of integrin alpha 2 beta 1 with calreticulin. Dependence on the activation state of the integrin.* J Biol Chem, 1995. **270**(39): p. 23132-8.

28. Michalak, M., et al., *Calreticulin.* Biochem J, 1992. **285 (Pt 3)**: p. 681-92.

29. Sastry, S.K. and K. Burridge, *Focal adhesions: a nexus for intracellular signaling and cytoskeletal dynamics.* Exp Cell Res, 2000. **261**(1): p. 25-36.

30. Miranti, C.K. and J.S. Brugge, *Sensing the environment: a historical perspective on integrin signal transduction.* Nat Cell Biol, 2002. **4**(4): p. E83-90.

31. Ruoslahti, E. and J.C. Reed, *Anchorage dependence, integrins, and apoptosis.* Cell, 1994. **77**(4): p. 477-8.

32. Frisch, S.M. and H. Francis, *Disruption of epithelial cell-matrix interactions induces apoptosis.* J Cell Biol, 1994. **124**(4): p. 619-26.

33. Frisch, S.M. and E. Ruoslahti, *Integrins and anoikis.* Curr Opin Cell Biol, 1997. **9**(5): p. 701-6.

34. Giancotti, F.G. and E. Ruoslahti, *Integrin signaling.* Science, 1999. **285**(5430): p. 1028-32.

35. Howe, A., et al., *Integrin signaling and cell growth control.* Curr Opin Cell Biol, 1998. **10**(2): p. 220-31.

36. Falcioni, R., et al., *Alpha 6 beta 4 and alpha 6 beta 1 integrins associate with ErbB-2 in human carcinoma cell lines.* Exp Cell Res, 1997. **236**(1): p. 76-85.

37. Liddington, R.C. and L.A. Bankston, *The structural basis of dynamic cell adhesion: heads, tails, and allostery.* Exp Cell Res, 2000. **261**(1): p. 37-43.

38. Stewart, M. and N. Hogg, *Regulation of leukocyte integrin function: affinity vs. avidity.* J Cell Biochem, 1996. **61**(4): p. 554-61.

39. Lub, M., Y. van Kooyk, and C.G. Figdor, *Ins and outs of LFA-1.* Immunol Today, 1995. **16**(10): p. 479-83.

40. Shimaoka, M., J. Takagi, and T.A. Springer, *Conformational regulation of integrin structure and function.* Annu Rev Biophys Biomol Struct, 2002. **31**: p. 485-516.

41. Hughes, P.E. and M. Pfaff, *Integrin affinity modulation.* Trends Cell Biol, 1998. **8**(9): p. 359-64.

42. Zhang, Z., et al., *Integrin activation by R-ras.* Cell, 1996. **85**(1): p. 61-9.

43. Hughes, P.E., et al., *Suppression of integrin activation: a novel function of a Ras/Raf-initiated MAP kinase pathway.* Cell, 1997. **88**(4): p. 521-30.

44. Keely, P.J., et al., *Cdc42 and Rac1 induce integrin-mediated cell motility and invasiveness through PI(3)K.* Nature, 1997. **390**(6660): p. 632-6.

45. Kuijpers, T.W., et al., *Freezing adhesion molecules in a state of high-avidity binding blocks eosinophil migration.* J Exp Med, 1993. **178**(1): p. 279-84.

46. Takagi, J., et al., *Global conformational rearrangements in integrin extracellular domains in outside-in and inside-out signaling.* Cell, 2002. **110**(5): p. 599-11.

47. Frelinger, A.L., 3rd, et al., *Occupancy of an adhesive glycoprotein receptor modulates expression of an antigenic site involved in cell adhesion.* J Biol Chem, 1988. **263**(25): p. 12397-402.

48. Lu, C., et al., *Epitope mapping of antibodies to the C-terminal region of the integrin beta 2 subunit reveals regions that become exposed upon receptor activation.* J Immunol, 2001. **166**(9): p. 5629-37.

49. Beglova, N., et al., *Cysteine-rich module structure reveals a fulcrum for integrin rearrangement upon activation.* Nat Struct Biol, 2002. **9**(4): p. 282-7.

50. Dransfield, I., et al., *Divalent cation regulation of the function of the leukocyte integrin LFA-1.* J Cell Biol, 1992. **116**(1): p. 219-26.

51. Lee, J.O., et al., *Crystal structure of the A domain from the alpha subunit of integrin CR3 (CD11b/CD18).* Cell, 1995. **80**(4): p. 631-8.

52. Aplin, A.E., A.K. Howe, and R.L. Juliano, *Cell adhesion molecules, signal transduction and cell growth.* Curr Opin Cell Biol, 1999. **11**(6): p. 737-44.

53. Fidler, I.J., *The pathogenesis of cancer metastasis: the 'seed and soil' hypothesis revisited.* Nat Rev Cancer, 2003. **3**(6): p. 453-8.

54. Mainiero, F., et al., *The coupling of alpha6beta4 integrin to Ras-MAP kinase pathways mediated by Shc controls keratinocyte proliferation.* Embo J, 1997. **16**(9): p. 2365-75.

55. Xia, Y., S.G. Gil, and W.G. Carter, *Anchorage mediated by integrin alpha6beta4 to laminin 5 (epiligrin) regulates tyrosine phosphorylation of a membrane-associated 80-kD protein.* J Cell Biol, 1996. **132**(4): p. 727-40.

56. Gale, N.W., et al., *Grb2 mediates the EGF-dependent activation of guanine nucleotide exchange on Ras.* Nature, 1993. **363**(6424): p. 88-92.

57. Treisman, R., *Journey to the surface of the cell: Fos regulation and the SRE.* Embo J, 1995. **14**(20): p. 4905-13.

58. Felding-Habermann, B., et al., *Involvement of integrin alpha V gene expression in human melanoma tumorigenicity.* J Clin Invest, 1992. **89**(6): p. 2018-22.

59. Shaw, L.M., et al., *Activation of phosphoinositide 3-OH kinase by the alpha6beta4 integrin promotes carcinoma invasion.* Cell, 1997. **91**(7): p. 949-60.

60. Takeichi, M., *Cadherins in cancer: implications for invasion and metastasis.* Curr Opin Cell Biol, 1993. **5**(5): p. 806-11.

61. Perl, A.K., et al., *A causal role for E-cadherin in the transition from adenoma to carcinoma.* Nature, 1998. **392**(6672): p. 190-3.

62. Fujita, Y., et al., *Hakai, a c-Cbl-like protein, ubiquitinates and induces endocytosis of the E-cadherin complex.* Nat Cell Biol, 2002. **4**(3): p. 222-31.

63. Gimond, C., et al., *Induction of cell scattering by expression of beta1 integrins in beta1-deficient epithelial cells requires activation of members of the rho family of GTPases and downregulation of cadherin and catenin function.* J Cell Biol, 1999. **147**(6): p. 1325-40.

64. Takayama, T., et al., *Beta-catenin expression in human cancers.* Am J Pathol, 1996. **148**(1): p. 39-46.

65. Nieto, M.A., *The snail superfamily of zinc-finger transcription factors.* Nat Rev Mol Cell Biol, 2002. **3**(3): p. 155-66.

66. Sternlicht, M.D. and Z. Werb, *How matrix metalloproteinases regulate cell behavior.* Annu Rev Cell Dev Biol, 2001. **17**: p. 463-516.

67. Monteagudo, C., et al., *Immunohistochemical distribution of type IV collagenase in normal, benign, and malignant breast tissue.* Am J Pathol, 1990. **136**(3): p. 585-92.

68. Brooks, P.C., et al., *Localization of matrix metalloproteinase MMP-2 to the surface of invasive cells by interaction with integrin alpha v beta 3.* Cell, 1996. **85**(5): p. 683-93.

69. Deryugina, E.I., et al., *Matrix metalloproteinase-2 activation modulates glioma cell migration.* J Cell Sci, 1997. **110 (Pt 19)**: p. 2473-82.

70. Stetler-Stevenson, W.G., L.A. Liotta, and D.E. Kleiner, Jr., *Extracellular matrix 6: role of matrix metalloproteinases in tumor invasion and metastasis.* Faseb J, 1993. **7**(15): p. 1434-41.

71. Stetler-Stevenson, W.G., *Dynamics of matrix turnover during pathologic remodeling of the extracellular matrix.* Am J Pathol, 1996. **148**(5): p. 1345-50.

72. Brooks, P.C., et al., *Disruption of angiogenesis by PEX, a noncatalytic metalloproteinase fragment with integrin binding activity.* Cell, 1998. **92**(3): p. 391-400.

73. Vempati, P., F. Mac Gabhann, and A.S. Popel, *Quantifying the proteolytic release of extracellular matrix-sequestered VEGF with a computational model.* PLoS One. **5**(7): p. e11860.

74. Hsu, M.Y., et al., *Adenoviral gene transfer of beta3 integrin subunit induces conversion from radial to vertical growth phase in primary human melanoma.* Am J Pathol, 1998. **153**(5): p. 1435-42.

75. Chapman, H.A. and Y. Wei, *Protease crosstalk with integrins: the urokinase receptor paradigm.* Thromb Haemost, 2001. **86**(1): p. 124-9.

76. Hauck, C.R., et al., *FRNK blocks v-Src-stimulated invasion and experimental metastases without effects on cell motility or growth.* Embo J, 2002. **21**(23): p. 6289-302.

77. Webb, D.J., J.T. Parsons, and A.F. Horwitz, *Adhesion assembly, disassembly and turnover in migrating cells -- over and over and over again.* Nat Cell Biol, 2002. **4**(4): p. E97-100.

78. Raftopoulou, M. and A. Hall, *Cell migration: Rho GTPases lead the way.* Dev Biol, 2004. **265**(1): p. 23-32.

79. Raucher, D. and M.P. Sheetz, *Cell spreading and lamellipodial extension rate is regulated by membrane tension.* J Cell Biol, 2000. **148**(1): p. 127-36.

80. Gu, J., et al., *Shc and FAK differentially regulate cell motility and directionality modulated by PTEN.* J Cell Biol, 1999. **146**(2): p. 389-403.

81. Palecek, S.P., A.F. Horwitz, and D.A. Lauffenburger, *Kinetic model for integrin-mediated adhesion release during cell migration.* Ann Biomed Eng, 1999. **27**(2): p. 219-35.

82. Palecek, S.P., et al., *Physical and biochemical regulation of integrin release during rear detachment of migrating cells.* J Cell Sci, 1998. **111 (Pt 7)**: p. 929-40.

83. Mariotti, A., et al., *EGF-R signaling through Fyn kinase disrupts the function of integrin alpha6beta4 at hemidesmosomes: role in epithelial cell migration and carcinoma invasion.* J Cell Biol, 2001. **155**(3): p. 447-58.

84. Trusolino, L., A. Bertotti, and P.M. Comoglio, *A signaling adapter function for alpha6beta4 integrin in the control of HGF-dependent invasive growth.* Cell, 2001. **107**(5): p. 643-54.

85. Kiosses, W.B., et al., *Rac recruits high-affinity integrin alphavbeta3 to lamellipodia in endothelial cell migration.* Nat Cell Biol, 2001. **3**(3): p. 316-20.

86. Hanahan, D. and J. Folkman, *Patterns and emerging mechanisms of the angiogenic switch during tumorigenesis.* Cell, 1996. **86**(3): p. 353-64.

87. Hynes, R.O., *A reevaluation of integrins as regulators of angiogenesis.* Nat Med, 2002. **8**(9): p. 918-21.

88. Ramjaun, A.R. and K. Hodivala-Dilke, *The role of cell adhesion pathways in angiogenesis.* Int J Biochem Cell Biol, 2009. **41**(3): p. 521-30.

89. Felding-Habermann, B., et al., *Integrin activation controls metastasis in human breast cancer.* Proc Natl Acad Sci U S A, 2001. **98**(4): p. 1853-8.

90. del Regato, J.A., *Pathways of metastatic spread of malignant tumors.* Semin Oncol, 1977. **4**(1): p. 33-8.

91. Paget, S., *The distribution of secondary growths in cancer of the breast.* The Lancet, 1889. **133**(3421): p. 571-573.

92. *Neoplastic Diseases: A Treatise on Tumours. By James Ewing, A.M., M.D., Sc.D., Professor of Pathology at Cornell University Medical College, N.Y.; Pathologist to the Memorial Hospital. Third edition. Royal 8vo. Pp. 1127, with 546 illustrations. 1928. Philadelphia and London: W. B. Saunders Co. Ltd. 63s. net.* British Journal of Surgery, 1928. **16**(61): p. 174-175.

93. Hart, I.R. and I.J. Fidler, *Role of organ selectivity in the determination of metastatic patterns of B16 melanoma.* Cancer Res, 1980. **40**(7): p. 2281-7.

94. Fidler, I.J., *Metastasis: guantitative analysis of distribution and fate of tumor embolilabeled with 125 I-5-iodo-2'-deoxyuridine.* J Natl Cancer Inst, 1970. **45**(4): p. 773-82.

95. Pignatelli, M. and G. Stamp, *Integrins in tumour development and spread.* Cancer Surv, 1995. **24**: p. 113-27.

96. Xu, L.H., et al., *The focal adhesion kinase suppresses transformation-associated, anchorage-independent apoptosis in human breast cancer cells. Involvement of death receptor-related signaling pathways.* J Biol Chem, 2000. **275**(39): p. 30597-604.

97. Zhang, Z., et al., *The alpha 5 beta 1 integrin supports survival of cells on fibronectin and up-regulates Bcl-2 expression.* Proc Natl Acad Sci U S A, 1995. **92**(13): p. 6161-5.

98. Weaver, V.M., et al., *beta4 integrin-dependent formation of polarized three-dimensional architecture confers resistance to apoptosis in normal and malignant mammary epithelium.* Cancer Cell, 2002. **2**(3): p. 205-16.

99. Busk, M., R. Pytela, and D. Sheppard, *Characterization of the integrin alpha v beta 6 as a fibronectin-binding protein.* J Biol Chem, 1992. **267**(9): p. 5790-6.

100. Sheppard, D., et al., *Complete amino acid sequence of a novel integrin beta subunit (beta 6) identified in epithelial cells using the polymerase chain reaction.* J Biol Chem, 1990. **265**(20): p. 11502-7.

101. Bates, R.C., et al., *Transcriptional activation of integrin beta6 during the epithelial-mesenchymal transition defines a novel prognostic indicator of aggressive colon carcinoma.* J Clin Invest, 2005. **115**(2): p. 339-47.

102. Scott, K.A., et al., *TNF-alpha regulates epithelial expression of MMP-9 and integrin alphavbeta6 during tumour promotion. A role for TNF-alpha in keratinocyte migration?* Oncogene, 2004. **23**(41): p. 6954-66.

103. Bates, R.C. and A.M. Mercurio, *Tumor necrosis factor-alpha stimulates the epithelial-to-mesenchymal transition of human colonic organoids.* Mol Biol Cell, 2003. **14**(5): p. 1790-800.

104. Thomas, G.J., M.L. Nystrom, and J.F. Marshall, *Alphavbeta6 integrin in wound healing and cancer of the oral cavity.* J Oral Pathol Med, 2006. **35**(1): p. 1-10.

105. Azare, J., et al., *Constitutively activated Stat3 induces tumorigenesis and enhances cell motility of prostate epithelial cells through integrin beta 6.* Mol Cell Biol, 2007. **27**(12): p. 4444-53.

106. Munger, J.S., et al., *The integrin alpha v beta 6 binds and activates latent TGF beta 1: a mechanism for regulating pulmonary inflammation and fibrosis.* Cell, 1999. **96**(3): p. 319-28.

107. Annes, J.P., D.B. Rifkin, and J.S. Munger, *The integrin alphaVbeta6 binds and activates latent TGFbeta3.* FEBS Lett, 2002. **511**(1-3): p. 65-8.

108. Jackson, T., et al., *The epithelial integrin alphavbeta6 is a receptor for foot-and-mouth disease virus.* J Virol, 2000. **74**(11): p. 4949-56.

109. Heldin, C.H., K. Miyazono, and P. ten Dijke, *TGF-beta signalling from cell membrane to nucleus through SMAD proteins.* Nature, 1997. **390**(6659): p. 465-71.

110. Roberts, A.B., et al., *Transforming growth factor type beta: rapid induction of fibrosis and angiogenesis in vivo and stimulation of collagen formation in vitro.* Proc Natl Acad Sci U S A, 1986. **83**(12): p. 4167-71.

111. Munger, J.S., et al., *Latent transforming growth factor-beta: structural features and mechanisms of activation.* Kidney Int, 1997. **51**(5): p. 1376-82.

112. Gray, A.M. and A.J. Mason, *Requirement for activin A and transforming growth factor--beta 1 pro-regions in homodimer assembly.* Science, 1990. **247**(4948): p. 1328-30.

113. Crawford, S.E., et al., *Thrombospondin-1 is a major activator of TGF-beta1 in vivo.* Cell, 1998. **93**(7): p. 1159-70.

114. Ludlow, A., et al., *Characterization of integrin beta6 and thrombospondin-1 double-null mice.* J Cell Mol Med, 2005. **9**(2): p. 421-37.

115. Sheppard, D., *Transforming growth factor beta: a central modulator of pulmonary and airway inflammation and fibrosis.* Proc Am Thorac Soc, 2006. **3**(5): p. 413-7.

116. Wrana, J.L., et al., *Mechanism of activation of the TGF-beta receptor.* Nature, 1994. **370**(6488): p. 341-7.

117. Nakao, A., et al., *TGF-beta receptor-mediated signalling through Smad2, Smad3 and Smad4.* Embo J, 1997. **16**(17): p. 5353-62.

118. Liu, F., et al., *A human Mad protein acting as a BMP-regulated transcriptional activator.* Nature, 1996. **381**(6583): p. 620-3.

119. Alexandersen, S., et al., *The pathogenesis and diagnosis of foot-and-mouth disease.* J Comp Pathol, 2003. **129**(1): p. 1-36.

120. Jackson, T., et al., *Integrin alphavbeta1 is a receptor for foot-and-mouth disease virus.* J Virol, 2002. **76**(3): p. 935-41.

121. Neff, S., et al., *Foot-and-mouth disease virus virulent for cattle utilizes the integrin alpha(v)beta3 as its receptor.* J Virol, 1998. **72**(5): p. 3587-94.

122. Jackson, T., et al., *Integrin alphavbeta8 functions as a receptor for foot-and-mouth disease virus: role of the beta-chain cytodomain in integrin-mediated infection.* J Virol, 2004. **78**(9): p. 4533-40.

123. Monaghan, P., et al., *The alpha(v)beta6 integrin receptor for Foot-and-mouth disease virus is expressed constitutively on the epithelial cells targeted in cattle.* J Gen Virol, 2005. **86**(Pt 10): p. 2769-80.

124. Berryman, S., et al., *Early events in integrin alphavbeta6-mediated cell entry of foot-and-mouth disease virus.* J Virol, 2005. **79**(13): p. 8519-34.

125. Lyon, M., et al., *Elucidation of the structural features of heparan sulfate important for interaction with the Hep-2 domain of fibronectin.* J Biol Chem, 2000. **275**(7): p. 4599-606.

126. Felding-Habermann, B. and D.A. Cheresh, *Vitronectin and its receptors.* Curr Opin Cell Biol, 1993. **5**(5): p. 864-8.

127. Huang, X., et al., *The integrin alphavbeta6 is critical for keratinocyte migration on both its known ligand, fibronectin, and on vitronectin.* J Cell Sci, 1998. **111 (Pt 15)**: p. 2189-95.

128. Hsia, H.C. and J.E. Schwarzbauer, *Meet the tenascins: multifunctional and mysterious.* J Biol Chem, 2005. **280**(29): p. 26641-4.

129. Roth-Kleiner, M., E. Hirsch, and J.C. Schittny, *Fetal lungs of tenascin-C-deficient mice grow well, but branch poorly in organ culture.* Am J Respir Cell Mol Biol, 2004. **30**(3): p. 360-6.

130. Phillips, G.R., L.A. Krushel, and K.L. Crossin, *Domains of tenascin involved in glioma migration.* J Cell Sci, 1998. **111 (Pt 8)**: p. 1095-104.

131. Prieto, A.L., G.M. Edelman, and K.L. Crossin, *Multiple integrins mediate cell attachment to cytotactin/tenascin.* Proc Natl Acad Sci U S A, 1993. **90**(21): p. 10154-8.

132. Van Aarsen, L.A., et al., *Antibody-mediated blockade of integrin alpha v beta 6 inhibits tumor progression in vivo by a transforming growth factor-beta-regulated mechanism.* Cancer Res, 2008. **68**(2): p. 561-70.

133. Jones, J., F.M. Watt, and P.M. Speight, *Changes in the expression of alpha v integrins in oral squamous cell carcinomas.* J Oral Pathol Med, 1997. **26**(2): p. 63-8.

134. Breuss, J.M., et al., *Expression of the beta 6 integrin subunit in development, neoplasia and tissue repair suggests a role in epithelial remodeling.* J Cell Sci, 1995. **108 (Pt 6)**: p. 2241-51.

135. Hamidi, S., et al., *Expression of alpha(v)beta6 integrin in oral leukoplakia.* Br J Cancer, 2000. **82**(8): p. 1433-40.

136. Sipos, B., et al., *Immunohistochemical screening for beta6-integrin subunit expression in adenocarcinomas using a novel monoclonal antibody reveals strong up-regulation in pancreatic ductal adenocarcinomas in vivo and in vitro.* Histopathology, 2004. **45**(3): p. 226-36.

137. Kawashima, A., et al., *Expression of alphav integrin family in gastric carcinomas: increased alphavbeta6 is associated with lymph node metastasis.* Pathol Res Pract, 2003. **199**(2): p. 57-64.

138. Smythe, W.R., et al., *Integrin expression in non-small cell carcinoma of the lung.* Cancer Metastasis Rev, 1995. **14**(3): p. 229-39.

139. Agrez, M., et al., *The alpha v beta 6 integrin promotes proliferation of colon carcinoma cells through a unique region of the beta 6 cytoplasmic domain.* J Cell Biol, 1994. **127**(2): p. 547-56.

140. Thomas, G.J., et al., *Expression of the alphavbeta6 integrin promotes migration and invasion in squamous carcinoma cells.* J Invest Dermatol, 2001. **117**(1): p. 67-73.

141. Thomas, G.J., et al., *AlphaVbeta6 integrin promotes invasion of squamous carcinoma cells through up-regulation of matrix metalloproteinase-9.* Int J Cancer, 2001. **92**(5): p. 641-50.

142. Niu, J., et al., *Integrin-mediated signalling of gelatinase B secretion in colon cancer cells.* Biochem Biophys Res Commun, 1998. **249**(1): p. 287-91.

143. Li, X., et al., *Alphavbeta6-Fyn signaling promotes oral cancer progression.* J Biol Chem, 2003. **278**(43): p. 41646-53.

144. Siegel, P.M. and J. Massague, *Cytostatic and apoptotic actions of TGF-beta in homeostasis and cancer.* Nat Rev Cancer, 2003. **3**(11): p. 807-21.

145. Thiery, J.P., *Epithelial-mesenchymal transitions in development and pathologies.* Curr Opin Cell Biol, 2003. **15**(6): p. 740-6.

146. Thiery, J.P., *Epithelial-mesenchymal transitions in tumour progression.* Nat Rev Cancer, 2002. **2**(6): p. 442-54.

147. Oft, M., K.H. Heider, and H. Beug, *TGFbeta signaling is necessary for carcinoma cell invasiveness and metastasis.* Curr Biol, 1998. **8**(23): p. 1243-52.

148. Bhowmick, N.A., et al., *Transforming growth factor-beta1 mediates epithelial to mesenchymal transdifferentiation through a RhoA-dependent mechanism.* Mol Biol Cell, 2001. **12**(1): p. 27-36.

149. Moody, S.E., et al., *The transcriptional repressor Snail promotes mammary tumor recurrence.* 2005. **8**(3): p. 197-209.

150. Xue, C., et al., *The gatekeeper effect of epithelial-mesenchymal transition regulates the frequency of breast cancer metastasis.* Cancer Res, 2003. **63**(12): p. 3386-94.

151. Tarin, D., E.W. Thompson, and D.F. Newgreen, *The fallacy of epithelial mesenchymal transition in neoplasia.* Cancer Res, 2005. **65**(14): p. 5996-6000; discussion 6000-1.

152. Janes, S.M. and F.M. Watt, *Switch from alphavbeta5 to alphavbeta6 integrin expression protects squamous cell carcinomas from anoikis.* J Cell Biol, 2004. **166**(3): p. 419-31.

153. Ahmed, N., et al., *Direct integrin alphavbeta6-ERK binding: implications for tumour growth.* Oncogene, 2002. **21**(9): p. 1370-80.

154. Novelline, R.A. and L.F. Squire, *Squire's fundamentals of radiology*. 5th ed / Robert A. Novelline ed. 1997, Cambridge, Mass. ; London: Harvard University Press. xiv,621p.

155. Rontgen, W.C., *On a New Kind of Rays.* Science, 1896. **3**(59): p. 227-31.

156. Hendee, W.R. and E.R. Ritenour, *Medical imaging physics*. 4th ed. 2002, New York: Wiley-Liss. xix, 512 p.

157. Suetens, P., *Fundamentals of medical imaging*. 2002, Cambridge ; New York, NY: Cambridge University Press. xiv, 280 p.

158. Hounsfield, G.N., *Computerized transverse axial scanning (tomography). 1. Description of system.* Br J Radiol, 1973. **46**(552): p. 1016-22.

159. Filler, A.G. *The History, Development and Impact of Computed Imaging in Neurological Diagnosis and Neurosurgery: CT, MRI, and DTI.* Nature Precedings 2009; Available from: http://dx.doi.org/10.1038/npre.2009.3267.5.

160. Kalender, W.A., et al., *Spiral volumetric CT with single-breath-hold technique, continuous transport, and continuous scanner rotation.* Radiology, 1990. **176**(1): p. 181-3.

161. Tole, N.M., et al., *Basic physics of ultrasonographic imaging*. 2005, Geneva: World Health Organization. 95 p.

162. Holmes, J.H., et al., *The ultrasonic visualization of soft tissue structures in the human body.* Trans Am Clin Climatol Assoc, 1954. **66**: p. 208-25.

163. Lauterbur, P.C., *Image formation by induced local reactions : examples employing nuclear magnetic resonance*. 190-191.

164. Damadian, R., *Tumor detection by nuclear magnetic resonance.* Science, 1971. **171**(976): p. 1151-3.

165. Carr, D.H., et al., *Intravenous chelated gadolinium as a contrast agent in NMR imaging of cerebral tumours.* Lancet, 1984. **1**(8375): p. 484-6.

166. Schillaci, O., et al., *Single-photon emission computed tomography/computed tomography in abdominal diseases.* Semin Nucl Med, 2007. **37**(1): p. 48-61.

167. Ohtaki, Y., et al., *Differential effects comparing exercise and pharmacologic stress on left ventricular function using gated Tc-99m sestamibi SPECT.* Ann Nucl Med, 2008. **22**(3): p. 185-90.

168. Taylor, Harry L., P. Whitley, and A. Heaton, *A historical perspective on platelet radiolabeling techniques.* Transfusion, 2006. **46**(s3): p. 53S-58S.

169. Gottschalk, A., *Radioisotope scintiphotography with technetium 99m and the gamma scintillation camera.* Am J Roentgenol Radium Ther Nucl Med, 1966. **97**(4): p. 860-8.

170. Hudson, F.R., H.I. Glass, and S.L. Waters, *The assay of iodine-123.* J Nucl Med, 1976. **17**(3): p. 220-2.

171. Liburdy, R.P., et al., *Indium-114m in dual-nuclide studies with Cr-51: comparison with indium-111.* J Nucl Med, 1980. **21**(10): p. 992-4.

172. Shokeen, M. and C.J. Anderson, *Molecular imaging of cancer with copper-64 radiopharmaceuticals and positron emission tomography (PET).* Acc Chem Res, 2009. **42**(7): p. 832-41.

173. Ter-Pogossian, M., et al., *Radioactive oxygen 15 in study of kinetics of oxygen of respiration.* Am J Physiol, 1961. **201**: p. 582-6.

174. Walsh, W.F., H.R. Fill, and P.V. Harper, *Nitrogen-13-labeled ammonia for myocardial imaging.* Semin Nucl Med, 1977. **7**(1): p. 59-66.

175. Camici, P.G., *Positron emission tomography and myocardial imaging.* Heart, 2000. **83**(4): p. 475-80.

176. Fani, M., J.P. Andre, and H.R. Maecke, *68Ga-PET: a powerful generator-based alternative to cyclotron-based PET radiopharmaceuticals.* Contrast Media Mol Imaging, 2008. **3**(2): p. 67-77.

177. Le Bars, D., *Fluorine-18 and medical imaging: Radiopharmaceuticals for positron emission tomography.* Journal of Fluorine Chemistry, 2006. **127**(11): p. 1488-1493.

178. Hulka, B.S., T.C. Wilcosky, and J.D. Griffith, *Biological markers in epidemiology*. 1990, New York: Oxford University Press. xi, 236 p.

179. Mayeux, R., *Biomarkers: potential uses and limitations.* NeuroRx, 2004. **1**(2): p. 182-8.

180. Geering, G., L.J. Old, and E.A. Boyse, *Antigens of leukemias induced by naturally occurring murine leukemia virus: their relation to the antigens of gross virus and other murine leukemia viruses.* J Exp Med, 1966. **124**(4): p. 753-72.

181. Sklar, J., et al., *Biclonal B-cell lymphoma.* N Engl J Med, 1984. **311**(1): p. 20-7.

182. Nakao, M., et al., *Rapid and reliable quantification of minimal residual disease in acute lymphoblastic leukemia using rearranged immunoglobulin and T-cell receptor loci by LightCycler technology.* Cancer Res, 2000. **60**(12): p. 3281-9.

183. de Jong, M., et al., *Radiolabelled peptides for tumour therapy: current status and future directions. Plenary lecture at the EANM 2002.* Eur J Nucl Med Mol Imaging, 2003. **30**(3): p. 463-9.

184. Sawyers, C.L., *The cancer biomarker problem.* Nature, 2008. **452**(7187): p. 548-52.

185. Shah, N.P., et al., *Sequential ABL kinase inhibitor therapy selects for compound drug-resistant BCR-ABL mutations with altered oncogenic potency.* J Clin Invest, 2007. **117**(9): p. 2562-9.

186. Rossi, H.H. and M. Zaider, *Radiogenic lung cancer: the effects of low doses of low linear energy transfer (LET) radiation.* Radiat Environ Biophys, 1997. **36**(2): p. 85-8.

187. Levine, G., et al., *Localization of I-131-labeled tumor-specific monoclonal antibody in the tumor-bearing BALB/c mouse.* J Nucl Med, 1980. **21**(6): p. 570-3.

188. Weissleder, R. and M.J. Pittet, *Imaging in the era of molecular oncology.* Nature, 2008. **452**(7187): p. 580-9.

189. Van Den Bossche, B. and C. Van de Wiele, *Receptor imaging in oncology by means of nuclear medicine: current status.* J Clin Oncol, 2004. **22**(17): p. 3593-607.

190. Okarvi, S.M., *Peptide-based radiopharmaceuticals: future tools for diagnostic imaging of cancers and other diseases.* Med Res Rev, 2004. **24**(3): p. 357-97.

191. de Jong, M., et al., *Yttrium-90 and indium-111 labelling, receptor binding and biodistribution of [DOTA0,d-Phe1,Tyr3]octreotide, a promising somatostatin analogue for radionuclide therapy.* Eur J Nucl Med, 1997. **24**(4): p. 368-71.

192. Kishore, R., et al., *Autoradiolysis of iodinated monoclonal antibody preparations.* Int J Rad Appl Instrum B, 1986. **13**(4): p. 457-9.

193. Chakrabarti, M.C., et al., *Prevention of radiolysis of monoclonal antibody during labeling.* J Nucl Med, 1996. **37**(8): p. 1384-8.

194. van Hagen, P.M., et al., *Evaluation of a radiolabelled cyclic DTPA-RGD analogue for tumour imaging and radionuclide therapy.* Int J Cancer, 2000. **90**(4): p. 186-98.

195. Som, P., et al., *A fluorinated glucose analog, 2-fluoro-2-deoxy-D-glucose (F-18): nontoxic tracer for rapid tumor detection.* J Nucl Med, 1980. **21**(7): p. 670-5.

196. Monakhov, N.K., et al., *Physicochemical properties and isoenzyme composition of hexokinase from normal and malignant human tissues.* J Natl Cancer Inst, 1978. **61**(1): p. 27-34.

197. Gallagher, B.M., et al., *Radiopharmaceuticals XXVII. 18F-labeled 2-deoxy-2-fluoro-d-glucose as a radiopharmaceutical for measuring regional*

myocardial glucose metabolism in vivo: tissue distribution and imaging studies in animals. J Nucl Med, 1977. **18**(10): p. 990-6.

198. Bomanji, J.B., D.C. Costa, and P.J. Ell, *Clinical role of positron emission tomography in oncology.* Lancet Oncol, 2001. **2**(3): p. 157-64.

199. Munker, R., et al., *Contribution of PET imaging to the initial staging and prognosis of patients with Hodgkin's disease.* Ann Oncol, 2004. **15**(11): p. 1699-704.

200. Weiner, R.E. and M.L. Thakur, *Radiolabeled peptides in diagnosis and therapy.* Semin Nucl Med, 2001. **31**(4): p. 296-311.

201. Colcher, D., et al., *Pharmacokinetics and biodistribution of genetically-engineered antibodies.* Q J Nucl Med, 1998. **42**(4): p. 225-41.

202. Orlando, R.A. and D.A. Cheresh, *Arginine-glycine-aspartic acid binding leading to molecular stabilization between integrin alpha v beta 3 and its ligand.* J Biol Chem, 1991. **266**(29): p. 19543-50.

203. Klee, G.G., *Human anti-mouse antibodies.* Arch Pathol Lab Med, 2000. **124**(6): p. 921-3.

204. Winter, G. and C. Milstein, *Man-made antibodies.* Nature, 1991. **349**(6307): p. 293-9.

205. Ledermann, J.A., et al., *Repeated antitumour antibody therapy in man with suppression of the host response by cyclosporin A.* Br J Cancer, 1988. **58**(5): p. 654-7.

206. Ritter, G., et al., *Serological analysis of human anti-human antibody responses in colon cancer patients treated with repeated doses of humanized monoclonal antibody A33.* Cancer Res, 2001. **61**(18): p. 6851-9.

207. Buchsbaum, D.J., *Experimental approaches to increase radiolabeled antibody localization in tumors.* Cancer Res, 1995. **55**(23 Suppl): p. 5729s-5732s.

208. Ellis, R.J., et al., *Four-year biochemical outcome after radioimmunoguided transperineal brachytherapy for patients with prostate adenocarcinoma.* Int J Radiat Oncol Biol Phys, 2003. **57**(2): p. 362-70.

209. Ellis, R.J., et al., *Radioimmunoguided imaging of prostate cancer foci with histopathological correlation.* Int J Radiat Oncol Biol Phys, 2001. **49**(5): p. 1281-6.

210. Perik, P.J., et al., *Indium-111-labeled trastuzumab scintigraphy in patients with human epidermal growth factor receptor 2-positive metastatic breast cancer.* J Clin Oncol, 2006. **24**(15): p. 2276-82.

211. Srikant, C.B., *Somatostatin*. Endocrine updates. 2004, Boston, Mass. ; London: Kluwer Academic. xvi, 311.

212. Krenning, E.P., et al., *Somatostatin receptor scintigraphy with [111In-DTPA-D-Phe1]- and [123I-Tyr3]-octreotide: the Rotterdam experience with more than 1000 patients.* Eur J Nucl Med, 1993. **20**(8): p. 716-31.

213. Froidevaux, S., et al., *Neuroendocrine tumor targeting: study of novel gallium-labeled somatostatin radiopeptides in a rat pancreatic tumor model.* Int J Cancer, 2002. **98**(6): p. 930-7.

214. Coenen, H.H., et al., *Radioionidation reactions for pharmaceuticals : compendium for effective synthesis strategies*. 2006, Dordrecht: Springer. xi, 101.

215. Salacinski, P.R., et al., *Iodination of proteins, glycoproteins, and peptides using a solid-phase oxidizing agent, 1,3,4,6-tetrachloro-3 alpha,6 alpha-diphenyl glycoluril (Iodogen).* Anal Biochem, 1981. **117**(1): p. 136-46.

216. Bolton, A.E. and W.M. Hunter, *The labelling of proteins to high specific radioactivities by conjugation to a 125I-containing acylating agent.* Biochem J, 1973. **133**(3): p. 529-39.

217. Liu, S., D.S. Edwards, and J.A. Barrett, *99mTc labeling of highly potent small peptides.* Bioconjug Chem, 1997. **8**(5): p. 621-36.

218. Rhodes, B.A., *Direct labeling of proteins with 99mTc.* Int J Rad Appl Instrum B, 1991. **18**(7): p. 667-76.

219. Sosabowski, J.K. and S.J. Mather, *Conjugation of DOTA-like chelating agents to peptides and radiolabeling with trivalent metallic isotopes.* Nat Protoc, 2006. **1**(2): p. 972-6.

220. Wester, H.J., K. Hamacher, and G. Stocklin, *A comparative study of N.C.A. fluorine-18 labeling of proteins via acylation and photochemical conjugation.* Nucl Med Biol, 1996. **23**(3): p. 365-72.

221. Schubiger, P.A., R. Alberto, and A. Smith, *Vehicles, chelators, and radionuclides: choosing the "building blocks" of an effective therapeutic radioimmunoconjugate.* Bioconjug Chem, 1996. **7**(2): p. 165-79.

222. Arano, Y., et al., *Conventional and high-yield synthesis of DTPA-conjugated peptides: application of a monoreactive DTPA to DTPA-D-Phe1-octreotide synthesis.* Bioconjug Chem, 1997. **8**(3): p. 442-6.

223. Deshpande, S.V., et al., *Yttrium-90-labeled monoclonal antibody for therapy: labeling by a new macrocyclic bifunctional chelating agent.* J Nucl Med, 1990. **31**(4): p. 473-9.

224. Forrer, F., et al., *A comparison of (111)In-DOTATOC and (111)In-DOTATATE: biodistribution and dosimetry in the same patients with metastatic neuroendocrine tumours.* Eur J Nucl Med Mol Imaging, 2004. **31**(9): p. 1257-62.

225. Stromblad, S. and D.A. Cheresh, *Integrins, angiogenesis and vascular cell survival.* Chem Biol, 1996. **3**(11): p. 881-5.

226. Haubner, R., et al., *Noninvasive imaging of alpha(v)beta3 integrin expression using 18F-labeled RGD-containing glycopeptide and positron emission tomography.* Cancer Res, 2001. **61**(5): p. 1781-5.

227. Haubner, R., et al., *Noninvasive visualization of the activated alphavbeta3 integrin in cancer patients by positron emission tomography and [18F]Galacto-RGD.* PLoS Med, 2005. **2**(3): p. e70.

228. Hausner, S.H., et al., *Use of a peptide derived from foot-and-mouth disease virus for the noninvasive imaging of human cancer: generation and evaluation of 4-[18F]fluorobenzoyl A20FMDV2 for in vivo imaging of integrin alphavbeta6 expression with positron emission tomography.* Cancer Res, 2007. **67**(16): p. 7833-40.

229. DiCara, D., et al., *Structure-function analysis of Arg-Gly-Asp helix motifs in alpha v beta 6 integrin ligands.* J Biol Chem, 2007. **282**(13): p. 9657-65.

230. Logan, D., et al., *Structure of a major immunogenic site on foot-and-mouth disease virus.* Nature, 1993. **362**(6420): p. 566-8.

231. Weinreb, P.H., et al., *Function-blocking integrin alphavbeta6 monoclonal antibodies: distinct ligand-mimetic and nonligand-mimetic classes.* J Biol Chem, 2004. **279**(17): p. 17875-87.

232. Giard, D.J., et al., *In vitro cultivation of human tumors: establishment of cell lines derived from a series of solid tumors.* J Natl Cancer Inst, 1973. **51**(5): p. 1417-23.

233. DiPersio, C.M., et al., *Mouse keratinocytes immortalized with large T antigen acquire alpha3beta1 integrin-dependent secretion of MMP-9/gelatinase B.* J Cell Sci, 2000. **113 (Pt 16)**: p. 2909-21.

234. Santner, S.J., et al., *Malignant MCF10CA1 cell lines derived from premalignant human breast epithelial MCF10AT cells.* Breast Cancer Res Treat, 2001. **65**(2): p. 101-10.

235. Kogelberg, H., et al., *Engineering a single-chain Fv antibody to alpha v beta 6 integrin using the specificity-determining loop of a foot-and-mouth disease virus.* J Mol Biol, 2008. **382**(2): p. 385-401.

236. Dlugosz, A.A., et al., *Isolation and utilization of epidermal keratinocytes for oncogene research.* Methods Enzymol, 1995. **254**: p. 3-20.

237. Lee, H., et al., *The effect of fixation and processing on the sensitivity of oestrogen receptor assay by immunohistochemistry in breast carcinoma.* J Clin Pathol, 2002. **55**(3): p. 236-8.

238. Nystrom, M.L., et al., *Cyclooxygenase-2 inhibition suppresses alphavbeta6 integrin-dependent oral squamous carcinoma invasion.* Cancer Res, 2006. **66**(22): p. 10833-42.

239. Hennings, H., et al., *Calcium regulation of growth and differentiation of mouse epidermal cells in culture.* Cell, 1980. **19**(1): p. 245-54.

240. Breuss, J.M., et al., *Restricted distribution of integrin beta 6 mRNA in primate epithelial tissues.* J Histochem Cytochem, 1993. **41**(10): p. 1521-7.

241. Marshall, J.F., et al., *Integrin expression in human melanoma cell lines: heterogeneity of vitronectin receptor composition and function.* Int J Cancer, 1991. **49**(6): p. 924-31.

242. Miller, F.R., et al., *MCF10DCIS.com xenograft model of human comedo ductal carcinoma in situ.* J Natl Cancer Inst, 2000. **92**(14): p. 1185-6.

243. Hu, M., et al., *Regulation of in situ to invasive breast carcinoma transition.* Cancer Cell, 2008. **13**(5): p. 394-406.

244. Moser, A.R., H.C. Pitot, and W.F. Dove, *A dominant mutation that predisposes to multiple intestinal neoplasia in the mouse.* Science, 1990. **247**(4940): p. 322-4.

245. Marsh, V., et al., *Epithelial Pten is dispensable for intestinal homeostasis but suppresses adenoma development and progression after Apc mutation.* Nat Genet, 2008. **40**(12): p. 1436-44.

246. Sansom, O.J., et al., *Loss of Apc allows phenotypic manifestation of the transforming properties of an endogenous K-ras oncogene in vivo.* Proc Natl Acad Sci U S A, 2006. **103**(38): p. 14122-7.

247. Parsons, D.W., et al., *Colorectal cancer: mutations in a signalling pathway.* Nature, 2005. **436**(7052): p. 792.

248. Elayadi, A.N., et al., *A peptide selected by biopanning identifies the integrin alphavbeta6 as a prognostic biomarker for nonsmall cell lung cancer.* Cancer Res, 2007. **67**(12): p. 5889-95.

249. Hazelbag, S., et al., *Overexpression of the alpha v beta 6 integrin in cervical squamous cell carcinoma is a prognostic factor for decreased survival.* J Pathol, 2007. **212**(3): p. 316-24.

250. Michishita, M., V. Videm, and M.A. Arnaout, *A novel divalent cation-binding site in the A domain of the beta 2 integrin CR3 (CD11b/CD18) is essential for ligand binding.* Cell, 1993. **72**(6): p. 857-67.

251. Xiong, J.P., et al., *Crystal structure of the extracellular segment of integrin alpha Vbeta3 in complex with an Arg-Gly-Asp ligand.* Science, 2002. **296**(5565): p. 151-5.

252. Biersack, H.J. and L.M. Freeman, *Clinical nuclear medicine*. 2007, Berlin ; New York: Springer. xxvii, 548 p.

253. Tomlinson, G. and M.R. Hnatowich, *Apparent competitive inhibition of radioligand binding to receptors: experimental and theoretical considerations in the analysis of equilibrium binding data.* J Recept Res, 1988. **8**(6): p. 809-30.

254. Hausner, S.H., et al., *Evaluation of [(64)Cu]Cu-DOTA and [(64)Cu]Cu-CB-TE2A Chelates for Targeted Positron Emission Tomography with an alpha(v)beta(6)-Specific Peptide.* Mol Imaging, 2009. **8**(2): p. 111-21.

255. Hausner, S.H., et al., *Targeted in vivo imaging of integrin alphavbeta6 with an improved radiotracer and its relevance in a pancreatic tumor model.* Cancer Res, 2009. **69**(14): p. 5843-50.

256. Nothelfer, E.M., et al., *Identification and Characterization of a Peptide with Affinity to Head and Neck Cancer.* J Nucl Med, 2009.

257. Li, S., et al., *Synthesis and characterization of a high-affinity {alpha}v{beta}6-specific ligand for in vitro and in vivo applications.* Mol Cancer Ther, 2009.

258. Reilly, R.M., et al., *111In-labeled EGF is selectively radiotoxic to human breast cancer cells overexpressing EGFR.* J Nucl Med, 2000. **41**(3): p. 429-38.

259. Leippert, M., et al., *Point mutations within the betaG-betaH loop of foot-and-mouth disease virus O1K affect virus attachment to target cells.* J Virol, 1997. **71**(2): p. 1046-51.

260. O'Donnell, V., et al., *Analysis of foot-and-mouth disease virus integrin receptor expression in tissues from naive and infected cattle.* J Comp Pathol, 2009. **141**(2-3): p. 98-112.

261. Ramsay, A.G., et al., *HS1-associated protein X-1 regulates carcinoma cell migration and invasion via clathrin-mediated endocytosis of integrin alphavbeta6.* Cancer Res, 2007. **67**(11): p. 5275-84.

262. Nothelfer, E.M., et al., *Identification and characterization of a peptide with affinity to head and neck cancer.* J Nucl Med, 2009. **50**(3): p. 426-34.

263. Cecchi, T., *Ion-pair chromatography and related techniques*. Analytical chemistry series, Boca Raton, Fla.: Crc. xiii, 201.

264. Saha, A., et al., *High-resolution in vivo imaging of breast cancer by targeting the pro-invasive integrin alphavbeta6.* J Pathol. **222**(1): p. 52-63.

265. Richmond, A. and Y. Su, *Mouse xenograft models vs GEM models for human cancer therapeutics.* Dis Model Mech, 2008. **1**(2-3): p. 78-82.

266. Becher, O.J. and E.C. Holland, *Genetically engineered models have advantages over xenografts for preclinical studies.* Cancer Res, 2006. **66**(7): p. 3355-8, discussion 3358-9.

267. Talmadge, J.E., et al., *Murine models to evaluate novel and conventional therapeutic strategies for cancer.* Am J Pathol, 2007. **170**(3): p. 793-804.

268. Brown, J.K., et al., *Integrin-alphavbeta6, a putative receptor for foot-and-mouth disease virus, is constitutively expressed in ruminant airways.* J Histochem Cytochem, 2006. **54**(7): p. 807-16.

269. Hahm, K., et al., *Alphav beta6 integrin regulates renal fibrosis and inflammation in Alport mouse.* Am J Pathol, 2007. **170**(1): p. 110-25.

270. Gotthardt, M., et al., *Indication for different mechanisms of kidney uptake of radiolabeled peptides.* J Nucl Med, 2007. **48**(4): p. 596-601.

271. Akizawa, H., T. Uehara, and Y. Arano, *Renal uptake and metabolism of radiopharmaceuticals derived from peptides and proteins.* Adv Drug Deliv Rev, 2008. **60**(12): p. 1319-28.

272. de Jong, M., et al., *Megalin is essential for renal proximal tubule reabsorption of (111)In-DTPA-octreotide.* J Nucl Med, 2005. **46**(10): p. 1696-700.

273. Akizawa, H., et al., *Significance of (111)In-DTPA chelate in renal radioactivity levels of (111)In-DTPA-conjugated peptides.* Nucl Med Biol, 2001. **28**(4): p. 459-68.

274. Guan, H., et al., *Peptide-targeted polyglutamic acid doxorubicin conjugates for the treatment of alpha(v)beta(6)-positive cancers.* Bioconjug Chem, 2008. **19**(9): p. 1813-21.

275. Padhani, A.R., et al., *Imaging oxygenation of human tumours.* Eur Radiol, 2007. **17**(4): p. 861-72.

276. Cai, W. and X. Chen, *Multimodality molecular imaging of tumor angiogenesis.* J Nucl Med, 2008. **49 Suppl 2**: p. 113S-28S.

277. Forrer, F., et al., *In vivo radionuclide uptake quantification using a multi-pinhole SPECT system to predict renal function in small animals.* Eur J Nucl Med Mol Imaging, 2006. **33**(10): p. 1214-7.

278. Thie, J.A., *Understanding the standardized uptake value, its methods, and implications for usage.* J Nucl Med, 2004. **45**(9): p. 1431-4.

279. *Guidance for Industry, Investigators, and Reviewers Exploratory IND Studies*. U.S. Department of Health and Human Services Food and Drug Administration 2006; Available from: http://www.fda.gov/downloads/Drugs/GuidanceComplianceRegulatoryInformation/Guidances/ucm078933.pdf.

280. Kummar, S., et al., *Compressing drug development timelines in oncology using phase '0' trials.* Nat Rev Cancer, 2007. **7**(2): p. 131-9.

281. *Phase 0 trials: a platform for drug development?* Lancet, 2009. **374**(9685): p. 176.

282. EMEA, *Position Paper on Non-Clinical Safety Studies to Support Clinical Trials with a Single Microdose.* 2004. **CPMP/SWP/2599**/(02/Rev1): p. 1 - 4.

283. Murgo, A.J., et al., *Designing phase 0 cancer clinical trials.* Clin Cancer Res, 2008. **14**(12): p. 3675-82.

284. *The Ionising Radiations Regulations 1999*. Statutory Insturments. 2000, London: Stationery Office. 67 p.

285. Health Protection Agency . Administration of Radioactive Substances Advisory, C., *Notes for guidance on the clinical administration of radiopharmaceuticals and the use of sealed radioactive sources*. 2006, Chilton Didcot: Health Protection Agency.

286. Sivolapenko, G.B., et al., *Imaging of metastatic melanoma utilising a technetium-99m labelled RGD-containing synthetic peptide.* Eur J Nucl Med, 1998. **25**(10): p. 1383-9.

287. Taboga, O., et al., *A large-scale evaluation of peptide vaccines against foot-and-mouth disease: lack of solid protection in cattle and isolation of escape mutants.* J Virol, 1997. **71**(4): p. 2606-14.

288. Novella, I.S., et al., *Use of substituted and tandem-repeated peptides to probe the relevance of the highly conserved RGD tripeptide in the immune response against foot-and-mouth disease virus.* FEBS Lett, 1993. **330**(3): p. 253-9.

289. Hsiung, P.L., et al., *Detection of colonic dysplasia in vivo using a targeted heptapeptide and confocal microendoscopy.* Nat Med, 2008. **14**(4): p. 454-8.

290. Zhou, X., et al., *Cell-specific delivery of a chemotherapeutic to lung cancer cells.* J Am Chem Soc, 2004. **126**(48): p. 15656-7.

291. Spies, S.M., *Imaging and dosing in radioimmunotherapy with yttrium 90 ibritumomab tiuxetan (Zevalin).* Semin Nucl Med, 2004. **34**(1 Suppl 1): p. 10-3.

292. Haverstick, D.M., et al., *Inhibition of platelet adhesion to fibronectin, fibrinogen, and von Willebrand factor substrates by a synthetic tetrapeptide derived from the cell-binding domain of fibronectin.* Blood, 1985. **66**(4): p. 946-52.

293. Lipkin, G., *Plasticity of the cancer cell: implications for epigenetic control of melanoma and other malignancies.* J Invest Dermatol, 2008. **128**(9): p. 2152-5.

294. Alison, M.R., et al., *Stem cell plasticity and tumour formation.* Eur J Cancer, 2006. **42**(9): p. 1247-56.

Appendix A

GROUP	NAME	SEQUENCE	COMMENTS
Biotinylated linear peptides	A20FMDV2	Bio-eahx-NAVPNLRGDLQVLAQKVART	N- terminal biotinylation with EAHX spacer
	A20FMDV2ran	Bio-eahx-RQLNVDALNVAGVRALKPTQ	
Biotinylated cyclic peptides	DBD1	Bio-eahx-EY*KCPNLRGDLQVLAQKVCRTK	
	DBD2	Bio-eahx-CKVPNLRGDLQVLAQKVAKC	
Non-biotinylated linear peptides	DTPA-A20FMDV2[§]	DTPA-NKVPNLRGDLQVLAQKVART	N-terminal addition of DTPA. [§]indicates non-biotinylated form
DTPA / linear biotinylated peptides	DTPA-A20FMDV2	DTPA-N*KVPNLRGDLQVLAQKVART	N-terminal addition of DTPA. Asterisk indicates biotinylated lysine
	DTPA-A20FMDV2ran	DTPA-N*KLRDQTGLKNPVQLARVAV	
DTPA / cyclic biotinylated peptides	DTPA-DBD2	DTPA-C*KVPNLRGDLQVLAQKVAKC	
	DTPA-DBD2ran	DTPA-C*KLRDQVGPKNLAQKVLAVC	
DOTA / biotinylated peptides	DOTA-A20FMDV2	DOTA–N*KVPNLRGDLQVLAQKVART	N-terminal addition of DOTA Asterisk indicates biotinylated lysine
	DOTA-A20FMDV2ran	DOTA–N*KLRDQTGLKNPVQLARVAV	

Journal of Pathology
J Pathol 2010; **222:** 52–63
Published online in Wiley InterScience
(www.interscience.wiley.com) DOI: 10.1002/path.2745

ORIGINAL PAPER

High-resolution *in vivo* imaging of breast cancer by targeting the pro-invasive integrin αvβ6

Antonio Saha,[1] David Ellison,[2] Gareth J Thomas,[1] Sabarinath Vallath,[1] Stephen J Mather,[2] Ian R Hart[1] and John F Marshall[1]*

[1] *Centre for Tumour Biology, Queen Mary University of London, Barts and London School of Medicine & Dentistry, Institute of Cancer and CR-UK Clinical Centre, John Vane Science Centre, Charterhouse Square, London EC1M 6BQ, UK*
[2] *Centre for Molecular Oncology and Imaging, Queen Mary University of London, Barts and London School of Medicine & Dentistry, Institute of Cancer and CR-UK Clinical Centre, John Vane Science Centre, Charterhouse Square, London EC1M 6BQ, UK*

Correspondence to: John F Marshall, Centre for Tumour Biology, Institute of Cancer and CR-UK Clinical Research Centre, John Vane Science Centre, Barts and London School of Medicine & Dentistry, Charterhouse Square, London EC1M 6BQ, UK. e-mail: j.f.marshall@qmul.ac.uk

Abstract

The integrin αvβ6 is expressed only on epithelia and then usually only during processes of tissue remodelling including cancer, where its high expression correlates with reduced survival. Thus, αvβ6 represents an important target for imaging and therapy of cancer and new molecular-specific targeting agents are required. We have developed A20FMDV2, a peptide derived from the VP1 coat protein of foot-and-mouth-disease virus that binds specifically and stably to αvβ6. Using a newly generated pair of isogenic human cell lines that differ only in αvβ6 expression, it was shown, using biodistribution and SPECT imaging, that indium-111-labelled A20FMDV2 locates specifically to αvβ6-expressing tissues *in vivo*, achieving at least seven-times higher retention in αvβ6-positive than in αvβ6-negative tumours. In further studies with MCF10.DCIS.COM and MCF10A.CA1a breast carcinoma cell lines, which express αvβ6 endogenously, the radiopeptide achieved similar levels of tumour retention and permitted excellent discriminatory imaging of tumours. Thus, A20FMDV2 can be used for molecular-specific targeting of αvβ6 for imaging *in vivo* the often more aggressive, αvβ6-positive cancers. In the future, A20FMDV2 could serve also to deliver therapy to these same cancers.

Keywords: integrin; αvβ6; imaging; SPECT; PET

Received 24 March 2010; Revised 20 May 2010; Accepted 29 May 2010

No conflicts of interest were declared.

Introduction

Integrins are heterodimeric glycoproteins composed of non-covalently linked α and β subunits [1]. Integrins dynamically translate extracellular matrix cues into intracellular responses, including mechanical, biochemical, and genetic signals, thereby modulating cell proliferation, survival, migration, and invasion [2]; thus, they are key determinants of the survival and spread of cancer. One of these integrins, αvβ6, is expressed only on epithelia and then usually only during processes of tissue remodelling; these include wound healing, chronic inflammation, and cancer [3,4]. We, and others, have shown clearly in experimental studies that αvβ6 imparts a pro-invasive and thus more aggressive phenotype when overexpressed on cancer cells [5–10]. This behaviour appears to reflect the clinical situation in humans, since survival from cancer of the colon, cervix or from non-small cell lung cancer is reduced significantly if the cancers express high levels of αvβ6 [11–13]. Thus, since αvβ6 is weak or absent in normal tissue but its presence can drive tumour invasion and shorten survival, this integrin represents a major new target for molecular-specific targeting for many cancers. To this end, we are developing peptides for αvβ6-specific imaging and therapy.

Integrins bind to their extracellular ligands partly through the recognition of specific amino acid sequences; eight different integrins, including αvβ6, recognize the RGD (Arg-Gly-Asp) motif [14]. We identified a 20-mer peptide, A20FMDV2 (NAVPNLRGDLQVLAQKVART), derived from the VP1 coat-protein of foot-and-mouth-disease virus, that exhibited exquisite specificity for αvβ6 over other RGD-directed integrins [15]. This specificity was dependent on the formation of a specific secondary structure when it bound to αvβ6, comprising a hairpin shape with RGD at the apex followed c-terminally by an α-helix [15]. Importantly, upon binding, A20FMDV2 formed a highly stable association with αvβ6 [16]. As a prelude to determining whether our peptide could be used as a therapeutic targeting agent, we first wished to establish that it could be used as a molecular-specific imaging agent. In this study, we have used

a combination of high-resolution single-photon emission computed tomography (SPECT), biodistribution *in vivo*, and immunochemsitry to show the absolute *in vivo* specificity of A20FMDV2 for αvβ6. Furthermore, we have shown that the A20FMDV2 peptide can, effectively and specifically, target two different αvβ6-expressing human breast cancer tumour models. We suggest that in addition to using A20FMDV2 for imaging αvβ6-expressing cancers, this same peptide can be used for delivering cytotoxic therapies to these often more aggressive forms of carcinoma.

Materials and methods

Cell lines

Creation and maintenance of the human A375Pβ6 and A375Ppuro cell lines have been described recently [17]. The human breast carcinoma cell lines MCF10A.DCIS.COM and MCF10A.CA1a were supplied by Steve Santner of the Karmanos Institute, Detroit, Michigan, USA. Development and maintenance of these lines were as described elsewhere [18].

Flow cytometric analysis

Flow cytometry was performed essentially as described previously [5]. Briefly, αvβ6 was detected with mouse antibody 10D5 (Chemicon, Millipore, Billerica, MA, USA) versus isotype controls (10 μg/ml). Biotinylated peptides were added to cells on ice at indicated concentrations (40 min), washed in chilled DMEM supplemented with 0.1% BSA and 0.1% NaN_3 (WaB) and then mouse anti-biotin antibody (Jackson ImmunoResearch, Stratech, Soham, Cambridgeshire, UK; 1 : 120 dilution) was added (30 min). Bound antibody was detected with Alexafluor-488 or -647-conjugated secondary antibody (Molecular Probes Inc., Invitrogen Ltd, Paisley, UK; 1 : 200 dilution). Cells were analysed on a Becton Dickinson LSR1 using Cell Quest (v3.3).

Serum stability studies

A20FMDV2 was synthesized with diethylenetriamene pentaacetate-tetra (DTPA t-Bu ester; Macrocyclics, Texas, USA) at the N-terminus to permit radiolabelling. The second residue was replaced with biotinyl-lysine; thus, the final peptide was DTPA-NK(biotinyl)VPNLRGDLQVLAQKVART (DTPA-A20FMDV2). ^{111}In-DTPA-A20FMDV2 (preparation details are given in the Supporting information, Supplementary Methods) was incubated in mouse sera or PBS at 37 °C. At various times, samples were removed and mixed with an equal volume of acetonitrile. After removal of precipitates by centrifugation, the supernatant was analysed by reverse phase (RP)-HPLC.

Biodistribution studies

Mice were purchased (Charles River or Harlan) or bred at Cancer Research UK facilities. Animal care and studies followed UK Home Office regulations. Athymic mice were given subcutaneous injections of 2×10^6 A375Pβ6 cells (100 μl; right shoulder) and 2×10^6 A375Ppuro cells (left shoulder). In some experiments, CD1 nu/nu, Balb C nu/nu or ICRF nu/nu strains were used. Once the tumours had reached at least 5–7 mm in diameter (14–21 days), ^{111}In-DTPA-A20FMDV2 was injected (100 μl) into the tail vein. Specific activity injected was determined by recording the syringe mass before and after injection and comparing with standards prepared from the injection mixture. Mice were killed at several time points post-injection and tissues were harvested, placed in pre-weighed scintillation tubes, and associated radioactivity was measured on a gamma counter (LKB Compugamma, Victoria, Australia). Cpm readings were converted to MBq and uptake was expressed as a percentage of the injected dose per gram of tissue (% ID/g).

Competitive inhibition studies *in vivo*

To confirm that the radiolabelled peptide was taken up specifically by αvβ6, the biodistribution of ^{111}In-DTPA-A20FMDV2 (4 μg/1 MBq) was repeated with or without co-injection of a 100-fold excess (400 μg) of non-radiolabelled (cold) DTPA-A20FMDV2. In separate experiments, to establish the effect of an excess of a non-targeting peptide on the uptake of A20FMDV2, ^{111}In-DTPA-A20FMDV2 (4 μg/1 MBq) was co-injected into tumour-bearing mice together with 400 μg of non-radiolabelled (cold) DTPA-A20FMDVran (DTPA-NK(biotinyl)LRDQTGL KNPVQLARAV), the randomized version of the targeting peptide. In both experiments, biodistribution was determined at 1 h post-injection as described above.

NanoSPECT/CT imaging

Mice bearing both A375Pβ6 and A375Ppuro tumours were anaesthetized (with isofluorane) and given intravenous injections ranging from 10 to 20 MBq of ^{111}In-DTPA-A20FMDV2 in a volume of 100 μl. The animals were placed, in a tail-first prone position, on the scanner bed in an air-warmed animal chamber and imaged at 1 h post-injection, using a NanoSPECT/CT small animal imager (Bioscan, Washington, DC, USA). Images were analysed using *In vivo Scope* software (Bioscan).

Internalization assays

For radiometric internalization assays, confluent monolayers of A375Pβ6 and A375Ppuro cells in six-well plates were washed (DMEM) and then incubated in 1.2 ml of DMEM/1% BSA supplemented with 150 μl of PBS or a molar excess (10 μM) of non-radiolabelled DTPA-A20FMDV2 (15 min at 37 °C), the latter to assess non-specific binding. At ambient temperature, 150 μl of ^{111}In-DTPA-A20FMDV2 (20 ng/ml) was added and the plates were incubated at 37 °C. At set time points, cells were washed in ice-cold DMEM/1%

BSA. Surface-bound radioactivity was removed with DMEM/HCl, pH4 (concentrated HCl added to DMEM until pH 4 was achieved) for 25 min and collected. Next the internalized fraction was collected by lysing the cells with 1 ml of 1 M NaOH. Total radioactivity bound (the sum of the surface-bound and the internalized radioactivity) was calculated at each time point. The 'total' radioactivity internalized (Figure 8A) was calculated as the internalized radioactivity expressed as a percentage of the total radioactivity bound. The 'specific' radioactivity internalized (Figure 8A) was similarly calculated after the non-specific bound radioactivity was subtracted.

For internalization by microscopy, A375Pβ6 cells were plated onto 13 mm diameter coverslips placed in a 24-well plate (2×10^4 cells per well) overnight. The cells were washed with DMEM, chilled on ice, and medium was replaced with ice-cold peptide (100 nM/200 µl serum-free DMEM). After 15 min on ice, unbound peptide was washed off with DMEM and 1 : 100 dilution (in DMEM) of mouse anti-biotin was added to cells on ice. After 15 min, the unbound antibody was washed off and cells were incubated at 37 °C. At various time points, coverslips were removed, fixed in formaldehyde (4% in PBS; 10 min) and then treated with 0.1% Triton X-100 (5 min). Rabbit Alexafluor-488-conjugated anti-mouse (Molecular Probes; 1 : 200 dilution) was added for 30 min to detect the bound antibody. Samples were analysed on a Zeiss LSM510 confocal microscope (Zeiss, Welwyn Garden City, UK).

Immunohistochemical staining and evaluation

Paraffin-embedded murine tissues were stained with 6.2G2 (anti-β6; a kind gift from Stromedix, Cambridge, MA, USA) using a mouse-on-mouse kit (M.O.M. Kit BMK-2202, Vector Labs Inc, Burlingame, CA, USA) after pepsin antigen retrieval. Cell membrane staining intensity was scored out of three (1, weak; 2, moderate; 3, strong), and the proportion of epithelial cells staining positively was scored out of four (1, <25%; 2, 25–50%; 3, 51–75%; 4, 76–100%). The score for intensity was added to the score for proportion to give a score in the range of 0–7 and grouped as — (score = 0), + (score = 1–3), ++ (score = 4–5), or +++ (score = 6–7).

Results

DTPA-A20FMDV2 peptide affinity and specificity

A375Pβ6 and A375Ppuro, which express equal amounts of four RGD-binding integrins (α5β1, αvβ3, αvβ5, αvβ8) but where only A375Pβ6 expresses αvβ6 [17], were used to assess peptide activity and specificity. Flow cytometry results showed that the addition of DTPA had no significant effect on either the specificity or the affinity of A20FMDV2. Thus, at 10 µM, DTPA-A20FMDV2 bound only to A375Pβ6 and at even 1 nM, good binding of DTPA-A20FMDV2 to A375β6 cells was observed, confirming the high affinity of these peptides (Figure 1). In contrast, the control biotinylated scrambled peptide (A20FMDV2ran) did not bind, even at 10 µM, to either cell line, whether or not DTPA was present. In separate experiments, αvβ6-blocking antibody completely inhibited the binding of DTPA-A20FMDV2 (data not shown), confirming the specificity of the peptide for αvβ6. Thus, DTPA-A20FMDV2 retains more than 1000-fold selectivity for αvβ6 versus α5β1, αvβ3, αvβ5, or αvβ8 and was therefore used for radio-binding studies.

Radio-peptide serum stability

^{111}In-DTPA-A20FMDV2 was added to mouse serum or PBS and samples were removed for RP-HPLC at various time points. Figure 2A shows that ^{111}In-DTPA-A20FMDV2 was very stable in PBS, more than 95% remaining intact after 24 h. In contrast, mouse serum caused ^{111}In-DTPA-A20FMDV2 to degrade such that only 50% remained intact after 4 h incubation. These data are in agreement with our previous report that fluorine-18-labelled A20FMDV2 was degraded in serum and appeared in urine as three discrete fragments [19]; the identity of the peptidases responsible for the degradation in this and our previous study remains unknown. Thus, we conducted *in vivo* assays up to a maximum of 4 h post-injection of the tracers. Using saturation binding assays, we also confirmed that the radiolabelled peptide retained its high affinity [15], since it bound to A375Pβ6 cells (but not A375Ppuro cells; data not shown) with a mean affinity constant (K_d) of 1.73 ± 0.46 nM (Supporting information, Supplementary Methods and Supplementary Figure 2).

Kinetics of tumour uptake of radiolabelled DTPA-A20FMDV2

In initial experiments, ^{111}In-DTPA-A20FMDV2 was injected intravenously and mice were killed at 0.5, 1, 2, and 4 h post-injection. Maximal differential uptake between the A375Pβ6 and the A375Ppuro (non-αvβ6-expressing) tumours occurred between 1 and 2 h (post-injection), and consistently was approximately 7 : 1 (Figure 2B). At 1 h post-injection, the mean % ID/g was $2.1\% \pm 0.25$ for the A375Pβ6 tumours, compared with $0.31\% \pm 0.07$ for the A375Ppuro tumours (Figure 2B). In subsequent experiments, we chose to examine mice at 1 h post-injection of tracer.

In separate experiments, we established that to maximize differential uptake in A375Pβ6 versus A375Ppuro tumours, 2–4 µg of peptide per mouse was the optimal mass for injection (Supporting information, Supplementary Methods and Supplementary Figure 1A) and that the genetic background of the athymic mice made no difference to selective targeting (Supporting information, Supplementary Figure 1B).

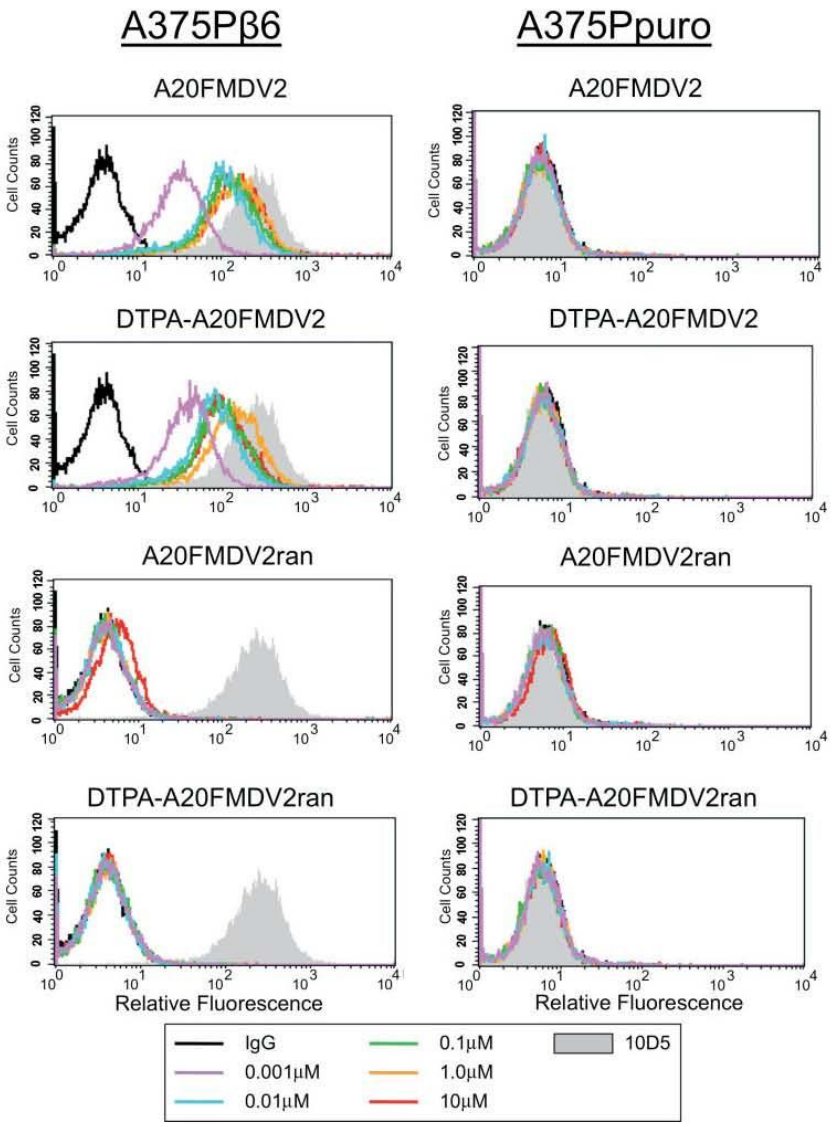

Figure 1. Flow cytometric analysis of biotinylated DTPA-A20FMDV2 versus biotinylated A20FMDV2. A375Pβ6 or A375Ppuro cells were exposed to several different concentrations (0.001–10 μM) of each peptide. After washing, bound peptide was detected by the addition of mouse anti-biotin antibody followed by Alexafluor488-conjugated goat anti-mouse IgG. Endogenous αvβ6 was detected with mouse mAb 10D5. Graphs show that conjugating DTPA does not affect the behaviour of A20FMDV2 and A20FMDV2ran.

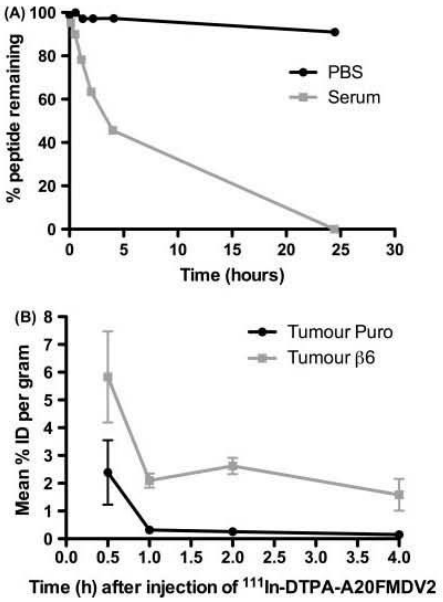

Figure 2. (A) Serum stability study. ^{111}In-DTPA-A20FMDV2 was incubated at 37°C in either PBS (black circles) or murine serum (grey squares) for various periods of time. At selected points, samples of the incubation mixture were analysed by RP-HPLC. (B) Determining the optimal time for pre-clinical imaging studies of αvβ6. ^{111}In-DTPA-A20FMDV2 (10 MBq) was injected into groups of tumour-bearing mice. At 0.5, 1, 2, and 4 h post-injection, three mice were killed and tumours were removed and the %ID/g tissue was determined. The data suggested that examining mice 1–2 h after injection of ^{111}In-DTPA-A20FMDV2 was optimal.

Biodistribution of radiolabelled DTPA-A20FMDV2

For biodistribution studies, 1 MBq of ^{111}In-DTPA-A20FMDV2 was injected. Figure 3 indicates good selective uptake in the A375Pβ6 tumours (2% ID/g) compared with the A375Ppuro tumours (7:1), to skeletal muscle (7:1) and to blood (9:1). Several organs also retained significant amounts of radioactivity at 1 h: specifically, the kidney, lower gastrointestinal (GI) tract, lung, stomach, skin, and gall bladder. Knowing that αvβ6 expression in adult tissues might vary according to species [20–22], it was investigated whether radioactivity retention correlated with levels of endogenously expressed murine αvβ6 using immunochemistry of paraffin-embedded murine tissues. Figure 4 and Table 1 show that in addition to the A375Pβ6 tumour, the gall bladder, stomach, and descending GI tract express significant amounts of endogenous αvβ6. Thus, in general, the biodistribution accurately reflected expression of αvβ6, both human in the xenograft and endogenously in the host tissues. (In separate studies, we confirmed

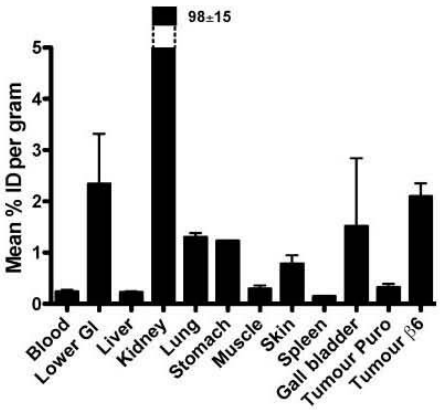

Figure 3. ^{111}In-DTPA-A20FMDV2 tissue biodistribution studies. ^{111}In-DTPA-A20FMDV2 was injected intravenously into tumour-bearing mice. After 1 h, animals were killed, tumours and major organs were harvested, and the %ID/g tissue was determined. The data show that in addition to tumours, several organs retained significant amounts of radio-peptide. (Note that the %ID/g for kidney was 98 ± 15%).

that A20FMDV2 binds specifically to murine αvβ6; data not shown.) Interestingly, we did not detect αvβ6 expression in the kidney, suggesting that the high activity seen by biodistribution was not αvβ6 receptor-mediated.

Retention of radiolabelled DTPA-A20FMDV2 *in vivo* is αvβ6-specific

To confirm that ^{111}In-DTPA-A20FMDV2 retention is receptor-mediated rather than the consequence of localized vascular leakage, we co-injected a 100-fold excess of non-radiolabelled DTPA-A20FMDV2 with ^{111}In-DTPA-A20FMDV2. Figure 5A shows that the 'cold' DTPA-A20FMDV2 markedly inhibited uptake of ^{111}In-DTPA-A20FMDV2 in αvβ6-positive tissues, including A375Pβ6 tumours, suggesting that localization of ^{111}In-DTPA-A20FMDV2 was due to specific binding. The 'cold' peptide also reduced uptake in the kidneys by more than 50%. Since we failed to detect αvβ6 expression in the kidneys, we assessed the effect of co-administration of a scrambled peptide (A20FMDV2ran) on kidney uptake. Co-injecting a 100-fold excess of non-radiolabelled DTPA-A20FMDV2ran together with ^{111}In-DTPA-A20FMDV2 had no effect on uptake by αvβ6-positive tissues, but did suppress uptake and retention by the kidney from 70 ± 8% to 47 ± 16% ID/g, confirming that uptake by the kidney is not RGD sequence-specific. (It should be noted that in separate studies, ^{111}In-DTPA-A20FMDV2ran was not retained by any major tissues; data not shown.)

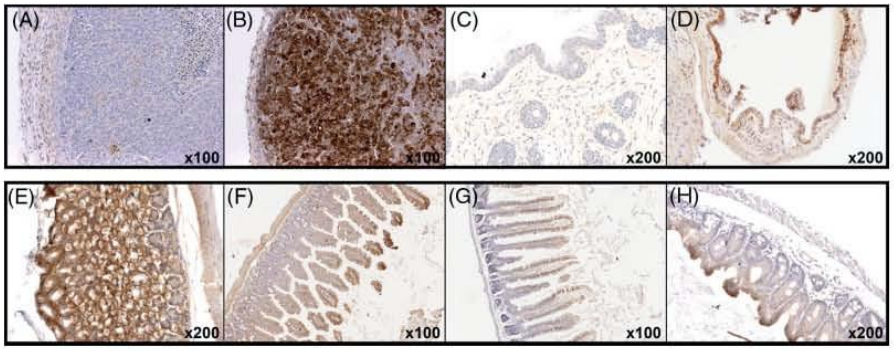

Figure 4. Immunochemical analysis of murine tissues and tumour xenografts for αvβ6 expression. Three mice bearing both A375Ppuro and A375Pβ6 tumours were killed and their organs and tumours harvested, processed to paraffin, and sectioned. Immunolabelling for αvβ6 shows that in contrast to A375Ppuro tumours (A), which lack expression, A375Pβ6 tumours (B) retain strong expression of this integrin. Strong endogenous αvβ6 expression was also detected in a number of murine organs including the gall bladder (D) and stomach (E). Moderate expression was found in the duodenum (F), ileum (G), and colon (H). Focal, but weak, staining was found within the skin (C).

High-resolution SPECT imaging of αvβ6-expressing tumours

Injection of ^{111}In-DTPA-A20FMDV2 permitted excellent non-invasive imaging of αvβ6-positive versus αvβ6-negative human xenografts. Figure 6 shows clear discrimination of the two tumours when imaged on a NanoSPECT/CT small animal imager. Interestingly, both in the coronal section (Figure 6A) and in the maximum intensity projection (Figure 6B), it is clear that the radiotracer locates to discrete areas of the tumours, concentrating in regions 1–2 mm in diameter. By contrast, the αvβ6-negative tumours retain, relatively, such little radioactivity that they appear almost completely negative. Figure 6 also highlights the retention in the excretory organs (kidneys and bladder) and the lower intestines, the latter correlating with endogenous αvβ6 expression. Thus, whole body imaging corresponds closely to the biodistribution analysis. A clearer impression of biodistribution can be seen in the Supporting information, Movie 1.

Targeting αvβ6 with DTPA-A20FMDV2 permits high-resolution imaging of human breast cancer xenografts

To avoid the possibility that retention of radiolabelled DTPA-A20FMDV2 by A375Pβ6 was largely due to the 'engineered' retroviral expression of β6, we applied our imaging approach to carcinoma cell lines that express αvβ6 endogenously. The breast carcinoma cell lines MCF10A.DCIS.COM and MCF10A.CA1a [18] are highly tumourigenic cell lines that express endogenous αvβ6, at levels comparable to their parental line, MCF10A, and retain αvβ6 expression *in vivo* [23] (and data not shown). Figure 7A shows that 1 h after injection of ^{111}In-DTPA-A20FMDV2 into mice bearing subcutaneous MCF10A.DCIS.COM or MCF10A.CA1a tumours, the selective uptake of radiotracer in these tumours versus skeletal muscle was more than 15 : 1. This specific localization permitted excellent high-resolution SPECT imaging of MCF10A.DCIS.COM or MCF10A.CA1a tumours (Figures 7B and 7C and Supporting information, Movies 2 and 3, respectively). Retention of radiotracer was similar to that of A375Pβ6, achieving over 2% ID/g for both tumour types. Thus, ^{111}In-DTPA-A20FMDV2 can be used for SPECT imaging of breast cancers that express αvβ6 endogenously, while our experimental A375Pβ6 model appears to represent an appropriate system for developing molecular-specific targeting agents for αvβ6 as it reflects endogenous expression of this integrin, at least for these breast carcinoma cell lines.

DTPA-A20FMDV2 internalization by αvβ6-expressing cells

Since αvβ6 mediates internalization of FMDV [24], we hypothesized that A20FMDV2 might also be internalized, perhaps giving it the potential to transport a therapeutic cargo intracellularly. Thus, we added ^{111}In-DTPA-A20FMDV2 to A375Pβ6 versus A375Ppuro cells and measured internalization. Reflecting the inability to bind to these cells, there was no binding or internalization of ^{111}In-DTPA-A20FMDV2 by A375Ppuro cells (data not shown). In contrast, Figure 8A shows that ^{111}In-DTPA-A20FMDV2 was internalized by A375Pβ6 cells. Internalization was expressed as a fraction of total-bound radioligand, showing that 50% of total bound ^{111}In-DTPA-A20FMDV2 internalized into A375Pβ6 cells within 20 min, reaching a plateau (89–96% internalization) at approximately 60 min (Figure 8A). Similar experiments were performed and analysed by confocal microscopy. At 0 min, the peptide was at the membrane of A375Pβ6 cells but by 30 min, most of the

Table 1. Immunohistochemical analysis of αvβ6 expression by murine tissues

Organ system and tissue	Score	Comment
Digestive system		
Salivary glands	0	
Stomach	+7	Entire epithelium stains strongly
Pancreas	0	
Liver	0	
Gall bladder	6–7	Moderate staining of entire epithelium
Duodenum	+5	Strong staining at the tips of the villi. However, the intensity decreases as the villus is followed down to the crypts
Ileum	+4	
Colon	+4	
Urinary system		
Urinary bladder	+6	Moderate staining of entire epithelium
Kidney	0	
Female reproductive system		
Uterus	+2	Weak to moderate staining in glands, of secretory phase endometrium
Mammary glands	0	
Lymphatic system		
Residual thymus	0	
Lymph nodes	0	
Spleen	0	
Cardio-respiratory system		
Heart	0	
Lungs	0	
Nervous system		
Brain	0	
Eyes	0	
Endocrine system		
Thyroid	0	
Musculoskeletal system		
Bone	0	
Skeletal muscle	0	
Skin	+3	Focal staining of the outer root sheath of a number of hair follicles
Xenografts		
A375Pβ6 tumour	+7	Strong staining throughout the tumour
A375Ppuro tumour	0	Complete absence of staining

peptide was in the cytoplasm (Figure 8B). The rate of internalization was not affected by DTPA as similar data were obtained with biotinylated A20FMDV2 (Figure 8B). Neither peptide showed significant internalization by A375Ppuro cells (data not shown). In these experiments, the chelating agent, DTPA, as it is attached to A20FMDV2, could be considered as internalized cargo, thus establishing that these peptides could be used to deliver conjugated therapeutic compounds intracellularly.

Discussion

The integrin αvβ6 represents a very good candidate as a tumour-selective target since its expression is weak or absent in normal tissues but up-regulated by many cancers [11–13]. Using cancer incidence data from both NIH (for the USA) and Cancer Research UK (for the UK) together with the αvβ6 expression data published recently [25], we calculate that in the USA and UK combined, approximately 250 000 new cancers arise each year that express significant levels of αvβ6; if non-melanoma skin cancers are included, then this figure rises to almost 1.2 million αvβ6-positive cancers annually. The importance of these data is underlined by studies of colon, cervical, and non-small cell lung cancers that reported significant correlations between high expression of αvβ6 and poor prognosis [11–13]. Such clinical observations were not unexpected since, experimentally, αvβ6 has been shown to promote and mediate the invasive phenotype of carcinomas while generating survival signals that protect cancer cells from anoikis [5,7–9,26]. Thus, αvβ6 is biologically active in promoting cancer progression and represents a promising novel target for the imaging and therapy

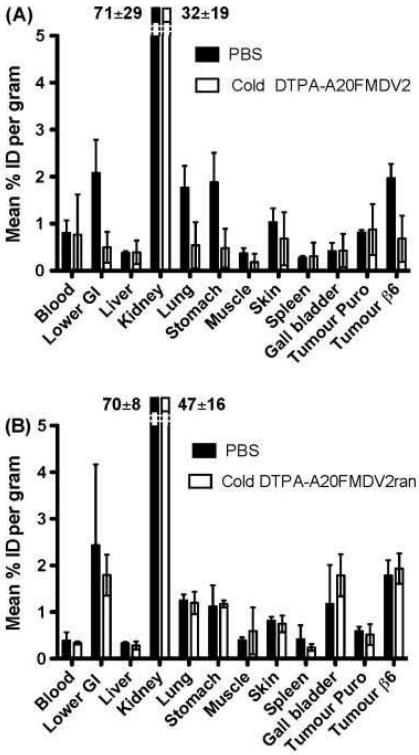

Figure 5. Competitive inhibition of ^{111}In-DTPA-A20FMDV2 tissue biodistribution. (A) A 100-fold excess of non-radiolabelled DTPA-A20FMDV2 was co-injected with 4 μg/1 MBq of ^{111}In-DTPA-A20FMDV2. After 1 h, tumours and major organs were harvested and the %ID/g tissue was determined. Black-shaded histograms represent 'control' comparison of 4 μg/1 MBq of ^{111}In-DTPA-A20FMDV2, whereas white histograms represent co-injections. The data show that 'cold' peptide suppressed uptake in all αvβ6-expressing tissues and also the kidneys. (B) A 100-fold excess of non-radiolabelled scrambled peptide (DTPA-A20FMDV2ran) was co-injected with 4 μg/1 MBq of ^{111}In-DTPA-A20FMDV2. Black-shaded histograms represent 'control' comparison of 4 μg/1 MBq of ^{111}In-DTPA-A20FMDV2, whereas white histograms represent co-injections. After 1 h, tumours and major organs were harvested and the %ID/g tissue was determined. Results show that the scrambled peptide had no effect on uptake in αvβ6-expressing tissues but reduced uptake in the kidney to a similar degree to that of wild-type peptide. (Note that actual kidney retention for each experiment is noted on the histograms).

of cancer. To that end, we have developed peptides that bind specifically to αvβ6.

Recently, we described the characterization of A20FMDV2, a peptide derived from the VP1 coat-protein of foot-and-mouth-disease virus [15]. We showed that radiolabelling A20FMDV2 with fluorine-18 permitted non-invasive PET imaging that discriminated between β6-non-expressing and β6-expressing human xenografts [19]. While these initial studies were promising, tumour retention of radioactivity was relatively low (0.66% ID/g at 1 h post-injection). In this study, we have introduced, and fully characterized, a new tumour model for the development of αvβ6 targeting agents. Our new model is based on the A375P human melanoma cell line, from which we have derived A375Pβ6 and A375Ppuro variants. These cell lines have identical levels of four RGD-directed integrins, α5β1, αvβ3, αvβ5, and αvβ8, whereas αvβ6 is expressed only by A375Pβ6 [17] and this differential αvβ6 expression is maintained *in vivo* (Figures 4A and 4B). We also developed a novel radiotracer for use in single-photon emission computed tomography (SPECT) studies. Compared with modern positron-emission tomography (PET) clinical scanners that can provide higher resolution and sensitivity, the advantages of SPECT imaging are that costs generally are lower than those for PET, the radiochemistry for tracer development is simpler, and owing to the longer half-life of most single-photon radionuclides and the wider availability of gamma cameras, SPECT imaging is more universally available. When we injected indium-111 labelled DTPA-A20FMDV2 into mice bearing both A375Ppuro and A375Pβ6 tumour xenografts, the radioligand was retained selectively in the αvβ6-positive tumour (Figure 3). Relative uptake in the A375Pβ6 versus A375Ppuro tumours routinely was approximately 7 : 1, with 2–4% ID/g in the A375Pβ6 tumour, a significant improvement over our original model [19]. Since these tumours are genetically identical except for expression of αvβ6, these data strongly suggest that DTPA-A20FMDV2 locates *in vivo* to αvβ6. This conclusion was supported by the capacity of an excess of 'cold' DTPA-A20FMDV2, but not DTPA-A20FMDV2ran, to inhibit retention of ^{111}In-DTPA-A20FMDV2 in A375Pβ6 tumours (Figure 5). Biodistribution studies showed retention of radioactivity in non-tumour tissues but immunochemical analysis (Figure 4 and Table 1) showed that most of these tissues expressed endogenous αvβ6. These data should be considered when developing αvβ6-specific targeting in murine models.

Retention of radio-peptide was highest in the kidney (Figures 3, 5, and 6) but our immunochemistry studies failed to detect significant amounts of αvβ6, in general agreement with recent studies that reported only 'occasional' staining of αvβ6 in histologically normal mouse and human kidney samples [27]. Since others have noted that kidneys can non-specifically retain radiolabelled peptides [28], we considered that the high retention of ^{111}In-DTPA-A20FMDV2 was non-specific. The ability of co-injection of 'cold' DTPA-A20FMDV2ran to suppress kidney retention of ^{111}In-DTPA-A20FMDV2 to the same degree as 'cold' DTPA-A20FMDV2 supports this conclusion (Figure 5). These data also suggest that it is possible to protect kidneys from toxicity by pretreating with excess non-specific peptide. However, such considerations may not always be necessary since in

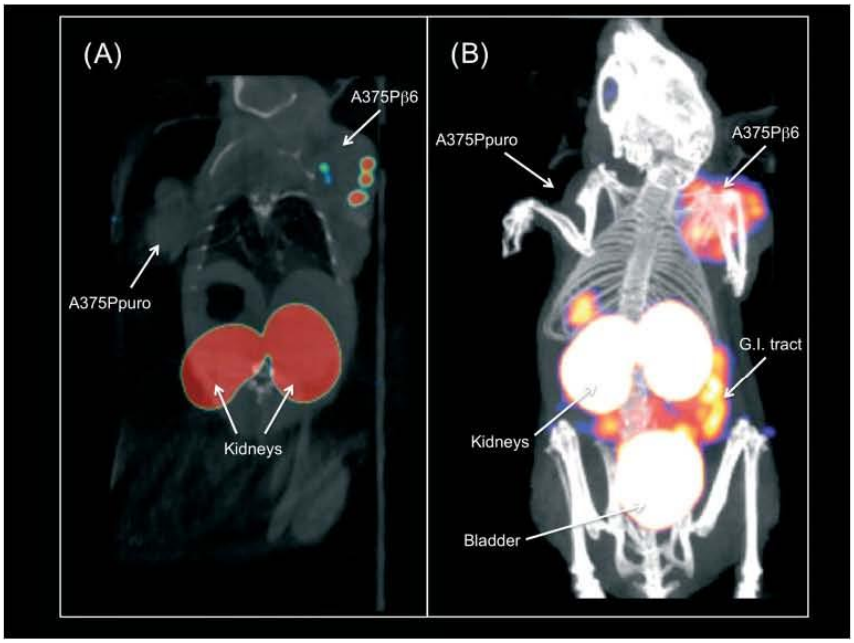

Figure 6. SPECT imaging of αvβ6 with ^{111}In-DTPA-A20FMDV2. 10 MBq of ^{111}In-DTPA-A20FMDV2 was injected intravenously into mice bearing A375Ppuro (left shoulder) and A375Pβ6 (right shoulder) tumours. After 1 h, the mice were anaesthetized and imaged on a NanoSPECT/CT small animal imaging machine. (A) Coronal slice showing that the radio-peptide has accumulated selectively in the A375Pβ6 tumour in discrete areas or 'hot-spots'. In contrast, the A375Ppuro tumour was negative. The kidneys are also labelled. (B) Maximum intensity projection (MIP) of images from a different mouse. The A375Pβ6 tumours are labelled strongly with radio-peptide, again showing that peptide does not distribute uniformly. The A375Ppuro tumours again were negative. The kidneys and bladder are labelled strongly, as is the lower GI tract.

our initial studies with fluorine-18 labelled A20FMDV2 [19], there was no significant kidney retention, suggesting that the exact formulation and radiolabelling strategy of the peptide also influence kidney retention.

We next determined the utility of ^{111}In-DTPA-A20FMDV2 as an imaging agent. Figure 6 shows high-resolution images, collected on a NanoSPECT/CT machine, of a mouse bearing A375Pβ6/A375Ppuro paired tumours. The combination of high retention of radio-peptide in the A375Pβ6 tumour and the high resolving power of the NanoSPECT/CT showed that distribution in tumours was not uniform; rather, there were regions 1–2 mm in diameter with higher radio-peptide retention. The reasons for this differential retention are not known but could, for example, relate to areas of increased angiogenesis. Figure 6B also shows minimal localization to the A375Ppuro tumour, correlating with biodistribution studies (observed more clearly in the Supporting information, Movie 1). Thus, we conclude that A20FMDV2 locates specifically to αvβ6-expressing tissues *in vivo* and can be used for efficient imaging of αvβ6-expressing cancers. Since such cancers often represent those associated with poorer survival [11–13], suggesting these cancers are more aggressive, imaging αvβ6 may have diagnostic value for patient management.

The ability of A20FMDV2 to be internalized in an αvβ6-specific manner (Figure 8) suggests that this may enhance its potential as an imaging agent, by accumulating radioligand in the target tumour, but also suggests that it could be used to deliver a therapeutic payload to αvβ6-expressing cancers. However, as ^{111}In-DTPA-A20FMDV2 is degraded in serum (Figure 2A), to increase its potential utility as a therapeutic vector it may be advantageous to generate serum-resistant variants.

Next we applied the same approaches to two αvβ6-expressing (data not shown) breast cancer models. Figure 7 shows that ^{111}In-DTPA-A20FMDV2 located specifically to MCF10A.DCIS.COM and MCF10A.CA1a xenografts, in a similar non-uniform distribution pattern to the A375Pβ6 tumour with 1–2 mm 'hot-spots' (see Supporting information, Movies 2 and 3 for whole body distribution). The specific retention for either tumour was greater than 2% ID/g of tumour tissue, similar to the A375Pβ6 model

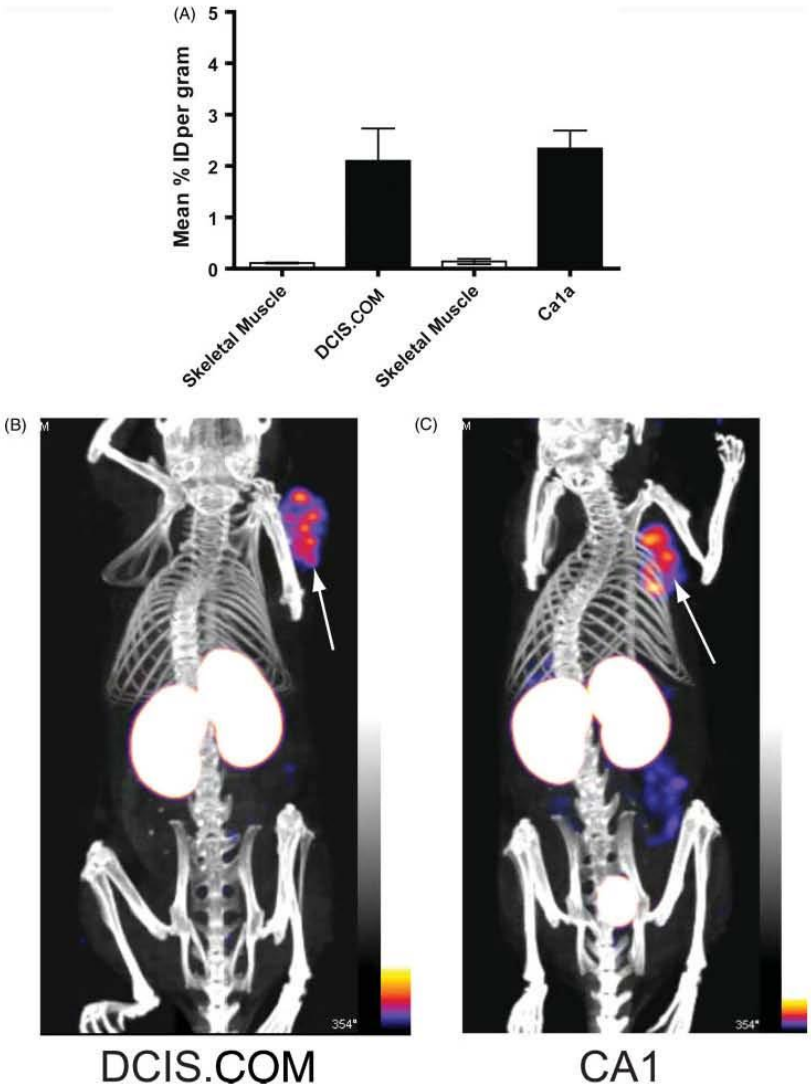

Figure 7. SPECT imaging of breast carcinoma by targeting endogenous αvβ6 with ^{111}In-DTPA-A20FMDV2. ^{111}In-DTPA-A20FMDV2 was injected intravenously into mice bearing either MCF10A.DCIS.COM or MCF10A.CA1a breast tumours. After 1 h, the mice were anaesthetized and imaged on a NanoSPECT/CT small animal imaging machine. (A) Data show that both breast tumours selectively uptake and retain significant amounts of radio-peptide, in contrast to the skeletal muscle control. Maximum intensity projection (MIP) of images from a mouse bearing (B) an MCF10A.DCIS.COM tumour or (C) an MCF10A.CA1a tumour on the right shoulder. Both tumours were labelled strongly with radio-peptide and again showed that the peptide does not distribute uniformly in the tumour. The kidneys and lower GI also retained radioactivity.

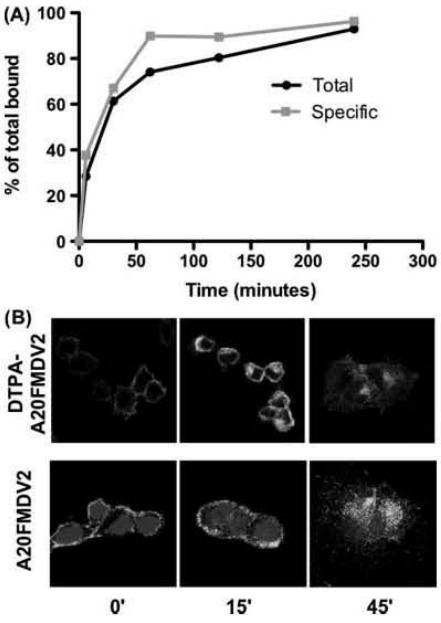

Figure 8. Internalization of DTPA-A20FMDV2. (A) A375Pβ6 cells were grown to confluency in six-well plates, washed, and incubated with DMEM/1% BSA supplemented with or without a molar excess (10 μM) of cold DTPA-A20FMDV2. ^{111}In-DTPA-A20FMDV2 (20 ng/ml) was added at ambient temperature and cells were incubated at 37 °C. At various time points, cells were transferred to ice and washed. Washes in DMEM/HCl (pH 4) removed the surface-bound radioactivity and the residual radioactivity, representing the internalized fraction, was collected by lysis with NaOH. 'Total' peptide internalized was calculated as the internalized fraction expressed as a percentage of the total radioactivity bound (membrane-bound fraction + internalized fraction). 'Specific' peptide internalized was similarly calculated after the non-specific bound radioactivity was subtracted. Results show that 50% of the bound peptide was internalized by 20 min. When the same internalization experiment was performed on A375Ppuro cells, there was no significant binding or internalization (data not shown). (B) The confocal images reveal that at 0 min, both the biotinylated DTPA-A20FMDV2 and the biotinylated A20FMDV2 peptides were located at the cell membrane. This was followed rapidly by translocation into the cytoplasm of A375Pβ6 cells. Peptides did not bind to, nor were they internalized by, A375Ppuro cells (data not shown).

and showing that the model fairly reflects the potential uptake of endogenous αvβ6-expressing tumours. The potential of targeting αvβ6 in breast cancer is highlighted by a recent report that 43% of breast cancers expressed significant levels of αvβ6 [25]. This translates in the UK, where the incidence of breast cancer is more than 45 000 per year (Cancer Research UK), to over 19 000 women annually who potentially could benefit from αvβ6-targeted imaging and therapy.

In summary, αvβ6 is a major new target for molecular-specific imaging and therapy of cancer. We have developed the first radio-peptide ligand, ^{111}In-DTPA-A20FMDV2, that permits high-resolution, αvβ6-specific imaging of cancers by SPECT. Our data suggest that A20FMDV2 can be developed not only to permit diagnostic imaging, but also to deliver anti-cancer therapy specifically to tumour cells while sparing local normal tissues.

Acknowledgment

We thank Drs Shelia Violette (Stromedix, Cambridge, MA, USA) and Paul Weinreb (Biogen Idec, Cambridge, MA, USA) for their continued support and supply of reagents. We thank Dr Nicola O'Reilly and staff at the Peptide Synthesis Laboratories, Cancer Research UK for supply of peptides and we also thank Dr Jane Sosabowski, Dr Julie Foster, and Ms Ciara Finucane for assistance with radio-imaging studies.

Author contribution statement

AS performed most of the studies; DE assisted in all experiments using radio-peptide; GJT performed the pathology; and SV assisted in all *in vivo* experiments. SJM provided expert guidance and experimental design on all radioactivity issues; IRH funded the study and co-wrote the manuscript; and JFM project-led the study and wrote the manuscript.

References

1. Hynes RO. Integrins: versatility, modulation, and signaling in cell adhesion. *Cell* 1992; **69**: 11–25.
2. Guo W, Giancotti FG. Integrin signalling during tumour progression. *Nature Rev Mol Cell Biol* 2004; **5**: 816–826.
3. Breuss JM, Gallo J, DeLisser JM, *et al*. Expression of the beta 6 integrin subunit in development, neoplasia and tissue repair suggests a role in epithelial remodelling. *J Cell Sci* 1995; **108**: 2241–2251.
4. Hakkinen L, Koivisto L, Gardner H, *et al*. Increased expression of beta6-integrin in skin leads to spontaneous development of chronic wounds. *Am J Pathol* 2004; **164**: 229–242.
5. Thomas GJ, Lewis MP, Whawell SA, *et al*. Expression of the alphavbeta6 integrin promotes migration and invasion in squamous carcinoma cells. *J Invest Dermatol* 2001; **117**: 67–73.
6. Thomas GJ, Nystrom ML, Marshall JF. Alphavbeta6 integrin in wound healing and cancer of the oral cavity. *J Oral Pathol Med* 2006; **35**: 1–10.
7. Thomas GJ, Lewis MP, Hart IR, *et al*. AlphaVbeta6 integrin promotes invasion of squamous carcinoma cells through up-regulation of matrix metalloproteinase-9. *Int J Cancer* 2001; **92**: 641–650.
8. Niu J, Gu X, Turton J, *et al*. Integrin-mediated signalling of gelatinase B secretion in colon cancer cells. *Biochem Biophys Res Commun* 1998; **249**: 287–291.
9. Nystrom ML, McCulloch D, Weinreb PH, *et al*. Cyclooxygenase-2 inhibition suppresses alphavbeta6 integrin-dependent oral squamous carcinoma invasion. *Cancer Res* 2006; **66**: 10833–10842.

10. Xue H, Atakilit A, Zhu W, *et al*. Role of the alpha(v)beta6 integrin in human oral squamous cell carcinoma growth *in vivo* and *in vitro*. *Biochem Biophys Res Commun* 2001; **288**: 610–618.
11. Bates RC, Bellovin DI, Brown C, *et al*. Transcriptional activation of integrin beta6 during the epithelial–mesenchymal transition defines a novel prognostic indicator of aggressive colon carcinoma. *J Clin Invest* 2005; **115**: 339–347.
12. Hazelbag S, Kentner GG, Gorter A, *et al*. Overexpression of the alpha v beta 6 integrin in cervical squamous cell carcinoma is a prognostic factor for decreased survival. *J Pathol* 2007; **212**: 316–324.
13. Elayadi AN, Samli KN, Prudkin L, *et al*. A peptide selected by biopanning identifies the integrin alphavbeta6 as a prognostic biomarker for nonsmall cell lung cancer. *Cancer Res* 2007; **67**: 5889–5895.
14. Ruoslahti E. RGD and other recognition sequences for integrins. *Annu Rev Cell Dev Biol* 1996; **12**: 697–715.
15. DiCara D, Rapisarda C, Sutcliffe JL, *et al*. Structure–function analysis of Arg-Gly-Asp helix motifs in alpha v beta 6 integrin ligands. *J Biol Chem* 2007; **282**: 9657–9665.
16. DiCara D, Burman A, Clark S, *et al* Foot-and-mouth-disease virus forms a highly stable, EDTA-resistant complex with its principal receptor, integrin αvβ6: implications for infectiousness? *J Virol* 2008; **82**: 1537–1546.
17. Kogelberg H, Tolner B, Thomas GJ, *et al*. Engineering a single-chain Fv antibody to alpha v beta 6 integrin using the specificity-determining loop of a foot-and-mouth disease virus. *J Mol Biol* 2008; **382**: 385–401.
18. Santner SJ, Dawson PJ, Tait L, *et al*. Malignant MCF10CA1 cell lines derived from premalignant human breast epithelial MCF10AT cells. *Breast Cancer Res Treat* 2001; **65**: 101–110.
19. Hausner SH, DiCara D, Marik J, *et al*. Use of a peptide derived from foot-and-mouth disease virus for the noninvasive imaging of human cancer: generation and evaluation of 4-[18F]fluorobenzoyl A20FMDV2 for *in vivo* imaging of integrin alphavbeta6 expression with positron emission tomography. *Cancer Res* 2007; **67**: 7833–7840.
20. O'Donnell V, Pacheco, Gregg D, *et al*. Analysis of foot-and-mouth disease virus integrin receptor expression in tissues from naive and infected cattle. *J Comp Pathol* 2009; **141**: 98–112.
21. Brown JK, McAleese SM, Thornton EM, *et al*. Integrin-alphavbeta6, a putative receptor for foot-and-mouth disease virus, is constitutively expressed in ruminant airways. *J Histochem Cytochem* 2006; **54**: 807–816.
22. Monaghan P, Gold S, Simpson J, *et al*. The alpha(v)beta6 integrin receptor for foot-and-mouth disease virus is expressed constitutively on the epithelial cells targeted in cattle. *J Gen Virol* 2005; **86**: 2769–2780.
23. Meyer T, Marshall JF, Hart IR. Expression of alphav integrins and vitronectin receptor identity in breast cancer cells. *Br J Cancer* 1998; **77**: 530–536.
24. Jackson T, Sheppard D, Denyer M, *et al*. The epithelial integrin alphavbeta6 is a receptor for foot-and-mouth disease virus. *J Virol* 2000; **74**: 4949–4956.
25. Van Aarsen LA, Leone DR, Ho S, *et al*. Antibody-mediated blockade of integrin alpha v beta 6 inhibits tumours progression *in vivo* by a transforming growth factor-beta-regulated mechanism. *Cancer Res* 2008; **68**: 561–570.
26. Janes SM, Watt FM. Switch from alphavbeta5 to alphavbeta6 integrin expression protects squamous cell carcinomas from anoikis. *J Cell Biol* 2004; **166**: 419–431.
27. Hahm K, Lukashev ME, Luo Y, *et al*. Alphav beta6 integrin regulates renal fibrosis and inflammation in Alport mouse. *Am J Pathol* 2007; **170**: 110–125.
28. Gotthardt, M, van Eerd-Vismale J, Oyen WJ, *et al*., Indication for different mechanisms of kidney uptake of radiolabeled peptides. *J Nucl Med* 2007; **48**: 596–601.

SUPPORTING INFORMATION ON THE INTERNET

The following supporting information may be found in the online version of this article.

Figure S1. Optimizing biodistribution studies.

Figure S2. Saturation binding assay.

Movie 1. Mice bearing A375Ppuro (left shoulder) and A375Pβ6 (right shoulder) tumours were given intravenous injections of In^{111}-DTPA-A20FMDV2 (10 MBq).

Movie 2. Mice bearing a MCF10A.DCIS.COM tumour (right shoulder) were given an intravenous injection of In^{111}-DTPA-A20FMDV2 (10 MBq).

Movie 3. Mice bearing a MCF10A.CA1a tumour (right shoulder) were given an intravenous injection of In^{111}-DTPA-A20FMDV2 (10 MBq).

Supplementary Methods.